Dissecting Neural Crest Ontogenesis and Axial Specification *in Vitro* Using Human Pluripotent Stem Cells

By :

Antigoni Gogolou

Submitted in partial fulfilment of the requirements
for the degree of Doctor of Philosophy

Centre for Stem Cell Biology
The University of Sheffield
Faculty of Science
School of Biosciences

December 2022

To my family

“It is the time you have wasted for your rose
that makes your rose so important.”
— Antoine de Saint-Exupéry, The Little Prince

M E R A K I
[may-rah-kee] (Greek)

(n.) to do something with soul, creativity or love;
to leave a part of yourself into your work

Acknowledgments

This PhD journey has truly been a challenge and there are so many friends and colleagues I'd like to thank for their constant support during this life-changing and greatly rewarding experience. I would not have been able to complete this without your help.

First of all, I'd like to thank my supervisor Dr Anestis Tsakiridis who gave me the opportunity to undertake this project in his laboratory. Anestis has been a great mentor during this journey offering me excellent scientific advice and his encouragement, optimism and guidance in moments of great despair, certainly kept me going. His enthusiasm for science has certainly influenced my work and it is a source of inspiration for my future scientific career. Next, I'd like to thank my co-supervisor Emeritus Prof. Peter Andrews and my advisor Dr Martin Zeidler. Their useful comments and suggestions during our advisory meetings have really kept me on the right track. I am also thankful to previous and present members of the Tsakiridis group who have really made the lab a fun place to work, even at times of crisis. Ingrid, Fay, Katy, Rebecca our endless conversations in the corridors about experiments not working or troubleshooting have surely been an integral part of this PhD. Also, I would be remiss If I did not thank Celine for all the help she offered in my project. Her positive attitude has made it great to work around her and without her contributions and the never ending qPCRs, the eLife paper would not have been finished by now. I'm also grateful to all the past and present members of the Centre For Stem Cell Biology for all the inspiring scientific and non-scientific discussions we had over the last few years and for making me feel part of the family from the very first moment. It's been a pleasure to work in this environment. Moreover, special thanks to Dylan and my gym buddy Chris P. for the long hours they spent with me sorting and for their experienced advice on technical matters. Moreover, special thanks to Paul Gokhale, who has been taking care of everyone in the office making sure we have enough coffee and snacks to keep up with the day's duties apart from giving us excellent scientific advice. This journey would not have been the same if it wasn't for my lab mates Tom and Matty. Thanks a lot Tom for teaching me cell culture, for all your support and encouragement when needed; the morning coffee meetings have definitely been a highlight while working together. Thanks a lot Matty for always making me smile and having me looking forward to our pub nights on Fridays after work.

Moreover, I'd like to acknowledge the funding body of my PhD, the Horizon 2020 program and our collaborators from the CONNECT project Dr Pieter Vanden Berghe and Yi-Ning for their input on the functional assessment of my cultures. I greatly enjoyed our conversations on ENS matters.

I thank my old school friends Eleni and Yannis for always cheering me up and offering me a nice getaway to Manchester for the weekend. I was so lucky to have you living so close to me all this time, especially away from home. I also thank my friends Margarita, Natalie and Fotis, who have always been a point of contact at the toughest times and for always putting a smile on my face.

To my wonderful parents, grandparents, my sister and my nephew, to whom this dissertation is dedicated, I could not have undertaken this journey without your constant support. Thanks for always believing in me.

Finally, I'd like to thank Jack who has been by my side throughout this PhD and for helping me in whatever way he could during this challenging time. His patience and calmness have been extremely helpful and his support, particularly in the long days of writing, has truly gave me the courage to complete this journey.

Abstract

Neural crest (NC) is a multipotent embryonic population integral to vertebrate development owing to its broad contribution to an array of derivatives including peripheral ganglia and the craniofacial skeleton. The NC cells originate from the dorsal tip of the neural tube along the anteroposterior axis and based on their positional identity, which is coupled with their ability to generate distinct cell types, are subdivided into cranial, cardiac and vagal, trunk and sacral NC in an order that corresponds to the adjacent regions of the spinal cord. The importance of NC integrity is demonstrated by the wide spectrum of NC-related pathologies including tumours, termed neurocristopathies, that predominantly arise from defects in the development of NC and their derivatives in multiple tissues. Our knowledge of NC ontogenesis and pathophysiology primarily comes from studies with animal models, however, the model organisms don't always recapitulate human development. Thus, human pluripotent stem cells (hPSCs) are an attractive platform to study NC ontogenesis and pathogenesis in human context *in vitro*. Several studies using directed differentiation have decoded the signalling requirements for cranial NC specification from hPSCs, but the signals and transcription factors that drive the acquisition of a posterior axial identity that corresponds to vagal and trunk levels in *in vitro*-derived NC have been less studied. Recently, it was demonstrated that vagal NC cells are derived from cranial crest through the action of the caudalising factor retinoic acid (RA), whereas their trunk counterparts are generated downstream of a neuromesodermal progenitor (NMP) population. The work presented here defines Wnt along with cell density as critical factors for vagal NC specification *in vitro* and demonstrates the ability of RA-induced vagal NC to give rise to their enteric nervous system (ENS) derivatives upon further differentiation using two different hPSC lines. It also shows that Notch pathway inhibition as part of the culture regimen enhances neural and glial differentiation in ENS cultures. Additionally, it reveals a previously unknown role of the pro-mesodermal factor TBXT together with Wnt signalling effectors in regulating, through chromatin remodelling, the adoption of posterior axial identity in NMP-derived trunk NC. We believe that these insights contribute to our knowledge of posterior patterning in post-otic NC and they can be applied in the future to optimise NC differentiation strategies with practical implications in biomedicine.

List of figures

List of tables

Abbreviations

Abbreviation	Meaning
(e)GFP	(enhanced) Green Fluorescent Protein
A-P	Anteroposterior
ALK	Activin Receptor-like Kinase
B27	B27 media supplement
BMP	Bone Morphogenetic Protein
cDNA	Complimentary DNA
CHIR	CHIR 99021, GSK3 antagonist which activates Wnt signalling pathway
CNS	Central Nervous System
Ct	Cycle Threshold
DAPT	N-[N-(3, 5-difluorophenacetyl)-l-alanyl]-s-phenylglycinet-butyl ester, a γ-secretase inhibitor that blocks the activity of Notch pathway
DMH1	Dorsomorphin 1, inhibitor of BMP type-I receptor ALK2
DMSO	Dimethyl sulfoxide
ECM	Extracellular Matrix proteins
ENS	Enteric Nervous System
FACS	Fluorescence Activated Cell Sorting
FGF	Fibroblast Growth Factor
FN	Fibronectin, coating solution
GRN	Gene Regulatory Network
GTX	Geltrex, basement membrane matrix
hESC	Human Embryonic Stem Cell
hiPSC	Human induced Pluripotent Stem Cell
hPSC	Human Pluripotent Stem Cell
HSCR	Hirschsprung's disease
LAM	Laminin, coating solution
N2	N2 media supplement
NC	Neural Crest
NE	Neuroectoderm
NMPs	Neuromesodermal Progenitors
NNE	Non-Neural Ectoderm
PDLO	Poly-dl-ornithine, adhesion promoter
PG	Paralog Group
PNS	Peripheral Nervous System
PO	Poly-l-ornithine, adhesion promoter
PPE	Pre-placodal Ectoderm
qRT-PCR	Quantitative Reverse-transcription Polymerase Chain Reaction
RA	Retinoic Acid
RQ	Relative Quantification of expression
SB 431542	Inhibitor of the TGF-β type I ALK4, ALK5 and ALK7 receptors
TGFβ	Transforming Growth Factor Beta
TSS	Transcription Start Site
VTN	Vitronectin, coating solution

Publications included in the thesis

Publication I

Retinoic acid accelerates the specification of enteric neural progenitors from in-vitro-derived neural crest.

Frith, T.J.R., **Gogolou, A.,** Hackland, J.O.S., Hewitt, Z.A., Moore, H.D., Barbaric, I., Thapar, N., Burns, A.J., Andrews, P.W., Tsakiridis, A. & McCann, C.J.

Stem Cell Reports (2020), vol. 15, no. 3, pp. 557-65.

Publication II

Generating Enteric Nervous System Progenitors from Human Pluripotent Stem Cells.

Gogolou, A., Frith, T.J.R. & Tsakiridis, A.

Current Protocols (2021), vol 1, e137.

Publication III

Early anteroposterior regionalisation of human neural crest is shaped by a pro-mesodermal factor.

Gogolou, A.*, Souilhol, C*., Granata, I., Wymeersch, F.J., Manipur, I., Wind, M., Frith, T.J.R., Guarini, M., Bertero, A., Bock C., Halbritter, F., Takasato, M., Mario R Guarracino, M.R., Tsakiridis, A. (* Equal contribution)

Elife (2022), vol. 11.

Declaration

I, the author, confirm that the Thesis is my own work. I am aware of the University's Guidance on the Use of Unfair Means (www.sheffield.ac.uk/ssid/unfair-means). This work has not been previously been presented for an award at this, or any other, university.

Chapter 1: Introduction

1.1. Neural crest specification

The neural crest (NC) is a transient, embryonic population that has the extraordinary ability to migrate extensively and differentiate into numerous derivatives that make up several tissues and organs as the embryo develops. NC cells are unique to vertebrates and due to their contribution to predatory features including the jaw, together with other craniofacial structures and paired sensory organs, they have played a profound role in the evolution of the vertebrates (Gans and Northcutt 1983).

The NC was first identified in the chicken embryo by Wilhelm His in 1868 (His 1868) and since then has been the subject of extensive research. Embryonic events such as induction, specification, migration and cell fate determination have been widely explored in the context of NC in multiple model systems, making these cells one of the best-studied progenitor populations of the vertebrate embryo (Simoes-Costa and Bronner 2015). Classical experimental embryology studies using tissue ablation, heterotopic transplantation, cell labelling dyes and genetic fate mapping have revealed an array of NC derivatives including cranial bones and cartilage, sensory, autonomic and enteric ganglia, smooth muscle and melanocytes as well as their contributions to the body plan (Dupin et al. 2006; Le Douarin 1973; Le Douarin et al. 2004; Le Douarin and Teillet 1973; Rothstein et al. 2018; Tang and Bronner 2020). Hence, owing to the great diversity of its progeny, the NC has been appositely called “the fourth germ layer” (Hall 2000).

According to the classical model of NC induction, NC cells are considered to be of ectodermal origin and their formation occurs in a series of sequential morphogenetic events that initiate during gastrulation. The development of NC begins with the specification of the neural plate border, a region that resides between the neural plate and the surface ectoderm, structures that will form the prospective central nervous system (CNS) and epidermis, respectively (Figure 1.1Ai, B). As the neurulation progresses and the neural plate bends to form the neural tube, the NC progenitor cells are specified and find place in the most dorsal lateral portions of the neural tube, termed neural folds (Figure 1.1Aii). After specification, NC cells lose connections with surrounding neuroepithelial cells, undergo epithelial to mesenchymal transition, delaminate from the neural tube and emigrate to various locations within the body following stereotypical migratory routes (Figure 1.1Aiii) (reviewed in Simoes-Costa and Bronner 2015). Although the series of events that lead to NC formation are quite well established, the multipotent nature of NC and its contribution to progeny of two germ layers, namely ectodermal (pigment cells, peripheral

neurons, glia) and ectomesenchymal (term adapted to distinguish the NC-derived mesenchyme from mesoderm-derived mesenchyme; Platt 1893) derivatives (cartilage, bone of the skull) have challenged the classical view of its ectodermal origin and the time of NC emergence (Prasad et al. 2019). Studies in avian (Basch et al. 2006; Patthey et al. 2008) and rabbit (Betters et al. 2018) embryos demonstrated that NC induction occurs early, at a pre-gastrula stage and prior to the formation of the three germ layers, suggesting an independent of neural and mesodermal origin. A recent report in *Xenopus* also proposed a pre-gastrula origin of NC and suggested that NC cells share stemness regulators with the blastula stage and these allow them to bypass the linage restriction taking place in the adjacent cells and maintain a broad developmental potential (Buitrago-Delgado et al. 2015). Evidence supporting an early and independent to neural origin onset of NC were also provided by a human pluripotent stem cell-(hPSC)-derived NC model study (Leung et al. 2016), which showed that NC first emerges from pre-neural border precursors, a finding that may in part explain the broad spectrum of NC derivatives.

Although numerous transcription factors as well as the inhibitory interactions between them taking place to establish the neural plate border, neural plate and surface ectoderm territories have revealed (Simoes-Costa and Bronner 2015), the common origin of the ectodermal domains, the mechanism and time of lineage segregation remain unclear. The presence of less cell-fate specific markers at the neural plate border (Tfap2a, Zic1, Msx1/2) in combination with data showing overlapping expression of multiple fate-specific transcription factors (Sox2, Msx1/2, Pax7, Tfap2a, Six1 for early placode) in individual cells during the early gastrula stage in the chicken embryo (Roellig et al. 2017), have challenged the classical model of “binary competence” which states that the ectoderm is subdivided into neural/NC and placode/epidermal competent domains (Pieper et al. 2012) and have proposed the “neural plate border” model instead (Roellig et al. 2017). According to this, the neural plate border until early neurulation consists of non-fate restricted precursors and when the expression of a specifier has exceeded a threshold level, cells start to commit to a certain lineage (Roellig et al. 2017). This plastic state consistent with a broad developmental potential is in line with data from the *Xenopus* embryo at which NC precursors are believed to retain stemness characteristics of the blastula stage (Buitrago-Delgado et al. 2015).

Conversely, a recent study using single cell transcriptomics integrated and expanded the previous models and suggested the “gradient border” model at which neural plate border cells do not exhibit discrete transcriptional profiles and the cell fate determination is linked to their spatiotemporal position (Thiery et al. 2022). However some lineages are more favoured than others and, cells located laterally are biased towards placode/non-neural fate, cells located

medially are biased towards NC/neural fate, while a subset of cells holds the potential to equally differentiate towards the four cell lineages (NC, neural, placode, epidermis) (Thiery et al. 2022).

The complex and timely controlled events that guide the formation of NC which are summarised as NC induction, specification and diversification are mediated by the interactions of signalling pathways, transcription factors and numerous effectors which comprise an extensive, highly sophisticated and evolutionary conserved gene regulatory network (GRN)(Prasad et al. 2019). The fibroblast growth factor (FGF), bone morphogenetic protein (BMP), Wnt and Notch signalling pathways together with neural plate border (Zic, Msx, Pax3/7, Tfap2, Dlx5/6, Gbx2) and NC (Sox5/8/9/10, Pax3/7, Tfap2, FoxD3, Snai1/2, Twist, Ets1) specifiers are some of the key components of the NC GRN (Figure 1.1A; boxes) (Simoes-Costa and Bronner 2015) and the contribution of some of them to the development of NC will be described below.

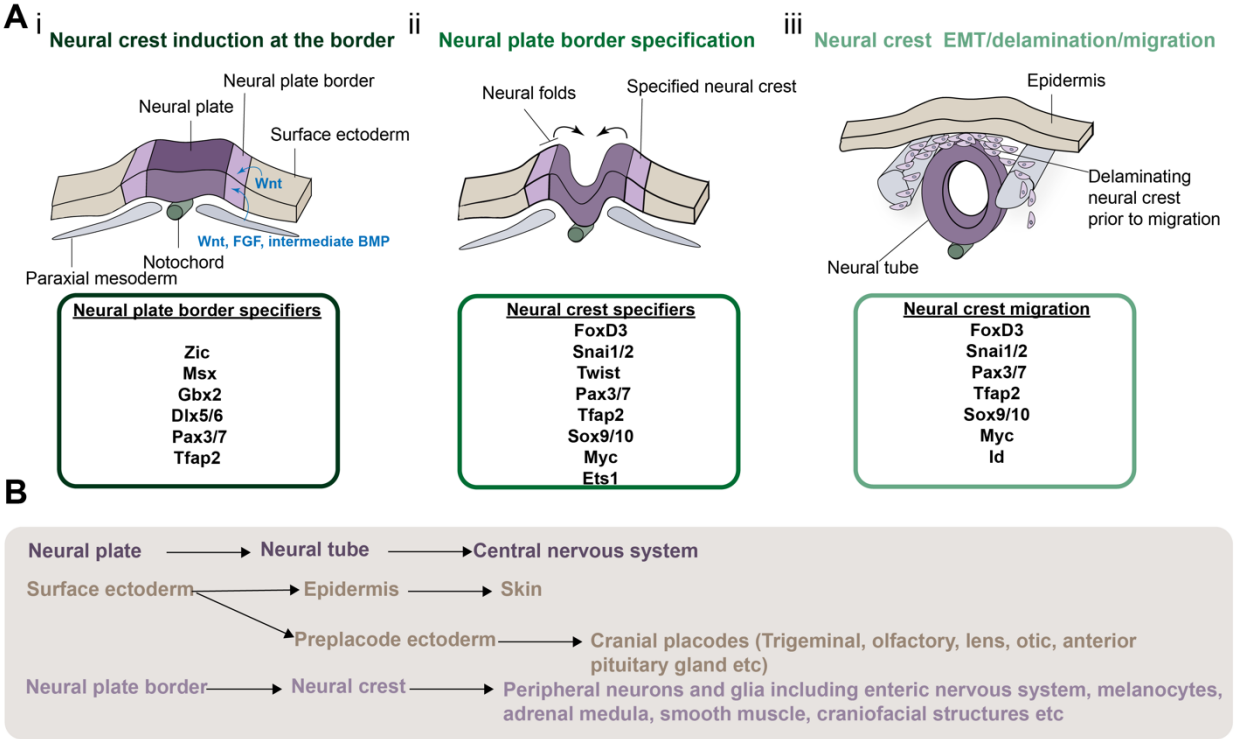

Figure 1.1. Schematic of the early events that lead to neural crest formation. (A) NC is first induced at the neural plate border (i), the neural plate border is subsequently specified (ii) and then NC cells originate in the dorsal part of the neural tube below the epidermis (iii). NC cells later undergo epithelial to mesenchymal transition (EMT), delaminate and migrate. Boxes include some indicative factors that regulate NC formation processes. This is just a representation and might not apply for all species. Pre-placodal ectoderm is not included for simplicity. (B) Derivatives of the different ectodermal domains including NC.

1.1.1. The role of BMP, Wnt, FGF and Notch signalling in the formation of neural crest

BMP signalling

BMPs are a group of proteins that belong to the transforming growth factor-β (TGF-β) superfamily of secreted ligands and play a profound role in embryogenesis and development as they are involved in several processes including the dorsoventral patterning and neural induction (Bier and De Robertis 2015; Streit and Stern 1999). The BMP signalling cascade is activated upon BMP binding to type 1 (ALK2, ALK3, ALK6) and type 2 (BMPR-2, ActR-2A, ActR-2B) serine/threonine kinase receptors (Wang et al. 2014; Wrana et al. 1994) which subsequently stimulates the phosphorylation of downstream substrates, the receptor-regulated Smads (R-Smads), Smad1/5/8. Phosphorylated Smads form a complex by associating with Smad4 and this translocates to the nucleus where it functions as a transcription factor to regulate gene expression (Figure 1.2) (Heldin et al. 1997).

BMPs behave as morphogens and regulate several developmental processes in a dose-dependent fashion (Bier and De Robertis 2015). Early work in the *Xenopus* embryo demonstrated that NC establishment relies on intermediate levels of BMP signalling, while high and low BMP activity induces epidermal and neural fate, respectively (Baker et al. 1999; LaBonne and Bronner-Fraser 1998; Marchant et al. 1998; Wilson and Hemmati-Brivanlou 1995). The BMP morphogen mediolateral gradient is achieved by the antagonistic interactions between BMPs which are initially expressed in the embryo laterally and BMP inhibitors, such as noggin, follistatin, chordin, which are secreted from medial regions in close vicinity to neural plate (Simoes-Costa and Bronner 2015) (Figure 1.1A). The requirement of intermediate BMP activity for NC induction has been demonstrated in other model organisms. In zebrafish, embryos with mutations in BMP signalling pathway components show different levels of BMP activity and NC expansion, supporting the notion that a BMP gradient determines the formation of NC (Nguyen et al. 1998; Schumacher et al. 2011). Consistent with the morphogen model are also the findings of Kwon et al. (2010) who demonstrated that high levels of the BMP pharmacological inhibitor dorsomorphin in zebrafish embryos led to NC extinction while low levels resulted in NC expansion. Although, some degree of BMP signalling is required at some point during NC formation, intermediate levels of BMP activity are not sufficient to induce NC and the input of other signalling pathways is indispensable (Figure 1.1A) (Alkobtawi et al. 2021; Garcia-Castro et al. 2002; LaBonne and Bronner-Fraser 1998; Patthey et al. 2009; Sasai et al. 2014).

In contrast to the gradient model, studies in *Xenopus* and chicken have suggested a two-step induction model at which FGF, Wnt and loss of BMP is required at the early gastrula stage to

induce NC, whereas intermediate levels of BMP activity downstream of Wnt in the neural plate border are critical to maintain NC induction (Patthey et al. 2009; Piacentino and Bronner 2018; Steventon et al. 2009). Moreover, BMP by interacting with Wnt and Notch signalling has also been shown to regulate delamination and early migration of NC cells in avian embryos emerging from the midbrain (Piacentino et al. 2021) and trunk (Burstyn-Cohen et al. 2004; Liu et al. 2013a) region. Specifically, stimulation of Wnt by BMP results in G1/S transition, a necessary step for NC delamination (Burstyn-Cohen et al. 2004), while BMP and Wnt induce phosphorylation of *Sox9* which subsequently cooperates with *Snai2* to initiate trunk NC delamination (Liu et al. 2013a). A requirement of BMP signalling in the development of NC has also been demonstrated in the mouse. Embryos lacking *Noggin (Nog*$^{-/-}$) or both *Chordin* and *Noggin* (*Chrd*$^{-/-}$;*Nog*$^{-/-or+/-}$) displayed increased levels of BMP signalling and this coincided with an expansion of NC cells and defects in NC migration, differentiation, particularly to craniofacial structures, and overall increased apoptosis (Anderson et al. 2006). These findings proposed a role of BMP antagonism in regulating the generation and survival of NC in mammalian development (Anderson et al. 2006). Additionally, genetic studies using a Cre-Lox system and conditional knockout of *Bmpr1a* (encodes a BMP receptor) in dorsal neural folds prior to neural tube closure revealed a reduction in NC cells accompanied with decreased expression of NC markers and defective contribution to peripheral nervous system (PNS) structures, consistent with a requirement of BMP activity in specification and early differentiation of NC (Stottmann and Klingensmith 2011).

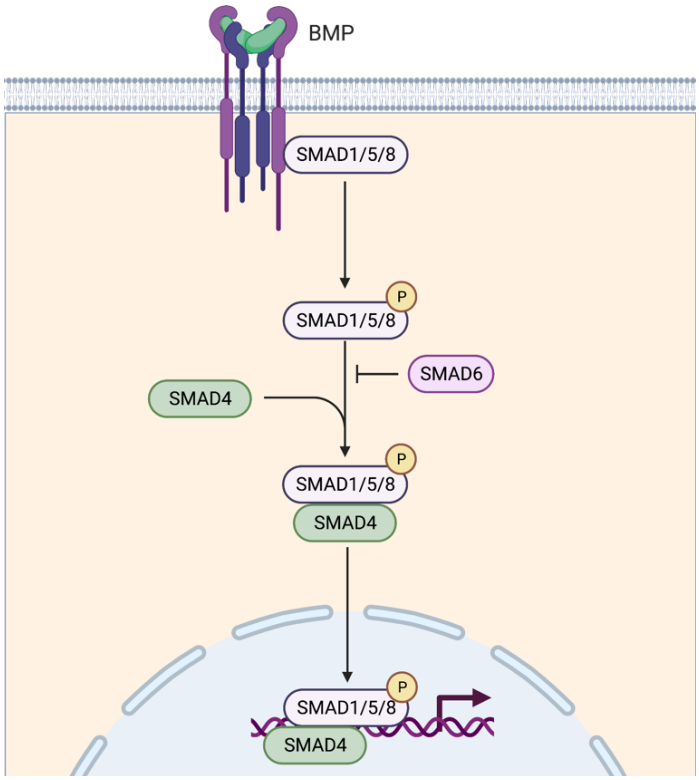

Figure 1.2. Overview of the BMP signalling pathway. BMP *ligands bind to* type 1 and type 2 serine/threonine kinase receptors *and form a heterotetrametric complex. The* active *type 2* receptor then transphosphorylates the type *1* receptor *which subsequently* phosphorylates the R-Smads (Smad1/5/8). Phosphorylated Smad1/5/8 *interacts* with the co-Smad (Smad4), and the complex translocates to the nucleus where it further associates with coactivators or corepressors to regulate gene expression. The illustration was created using the scientific image and illustration software, BioRender.

Wnt signalling

The Wnts are a family of secreted glycoproteins that signal through various routes and regulate key processes in development and tissue homeostasis. The best studied route is the canonical Wnt signalling pathway (Figure 1.3), which is activated when a Wnt ligand binds to frizzled receptor and its co-receptors LRP5 and LRP6. This binding initiates a cascade of events which result in inhibition of glycogen synthase kinase-3 (GSK3) and stabilisation of the cytoplasmic protein β-catenin, which otherwise in the absence of Wnt ligand is phosphorylated and marked for degradation by the activity of GSK3. When Wnt signalling is active, β-catenin translocates to the nucleus and cooperates with TCF/LEF transcription factors to regulate the expression of Wnt target genes (MacDonald et al. 2009).

The involvement of Wnt signalling in the formation of NC has been well documented in several vertebrates. In the *Xenopus* and chicken embryo stimulation of Wnt signalling by ectopic expression of Wnt ligands or other components of the Wnt signalling pathway, enhanced the formation of NC and NC marker expression, while inhibition of Wnt activity blocked NC formation (Deardorff et al. 2001; Garcia-Castro et al. 2002; LaBonne and Bronner-Fraser 1998; Saint-Jeannet et al. 1997; Wu et al. 2005). Similarly, loss of function experiments in zebrafish indicated that activation of canonical Wnt signalling is necessary for NC formation (Lewis et al. 2004). Although the role of Wnt in NC induction in *Xenopus*, chicken and zebrafish embryo is quite well established (Figure 1.1A), the contribution of Wnt in early NC formation in the mouse remains unclear (Prasad et al. 2019). Mouse embryos with *Wnt1*-driven loss of β-catenin downstream of Wnt pathway, fail to properly develop cranial ganglia and skeletal structures due to defective NC survival and differentiation, suggesting a requirement of β-catenin in normal NC development (Brault et al. 2001). Similarly, Wnt-1 and Wnt-3a mutants exhibit craniofacial malformations and loss in NC-derivatives, proposing a role of Wnt in NC expansion (Ikeya et al. 1997). Moreover, GSK-3β homozygous null mice have cleft palate, consistent with a crucial role of GSK3 in craniofacial development (Liu et al. 2007) and GSK3 as a substrate of the neuroblastoma related anaplastic lymphoma kinase (ALK) was later shown to regulate the early events of cranial NC migration through the formation of lamellipodia, cytoskeletal structures critical for cell migration (Gonzalez Malagon et al. 2018). Although several studies demonstrate an implication of Wnt and its components in NC survival, migration and cell fate determination in the mouse, many of them fail to address the role of Wnt in early events such as NC induction/formation. This may be in part due to functional redundancy in components of the Wnt pathway or due to unappreciated late Wnt1 expression following NC induction that does not allow the Wnt1-Cre drivers to capture this early event, as suggested previously (Barriga et al. 2015).

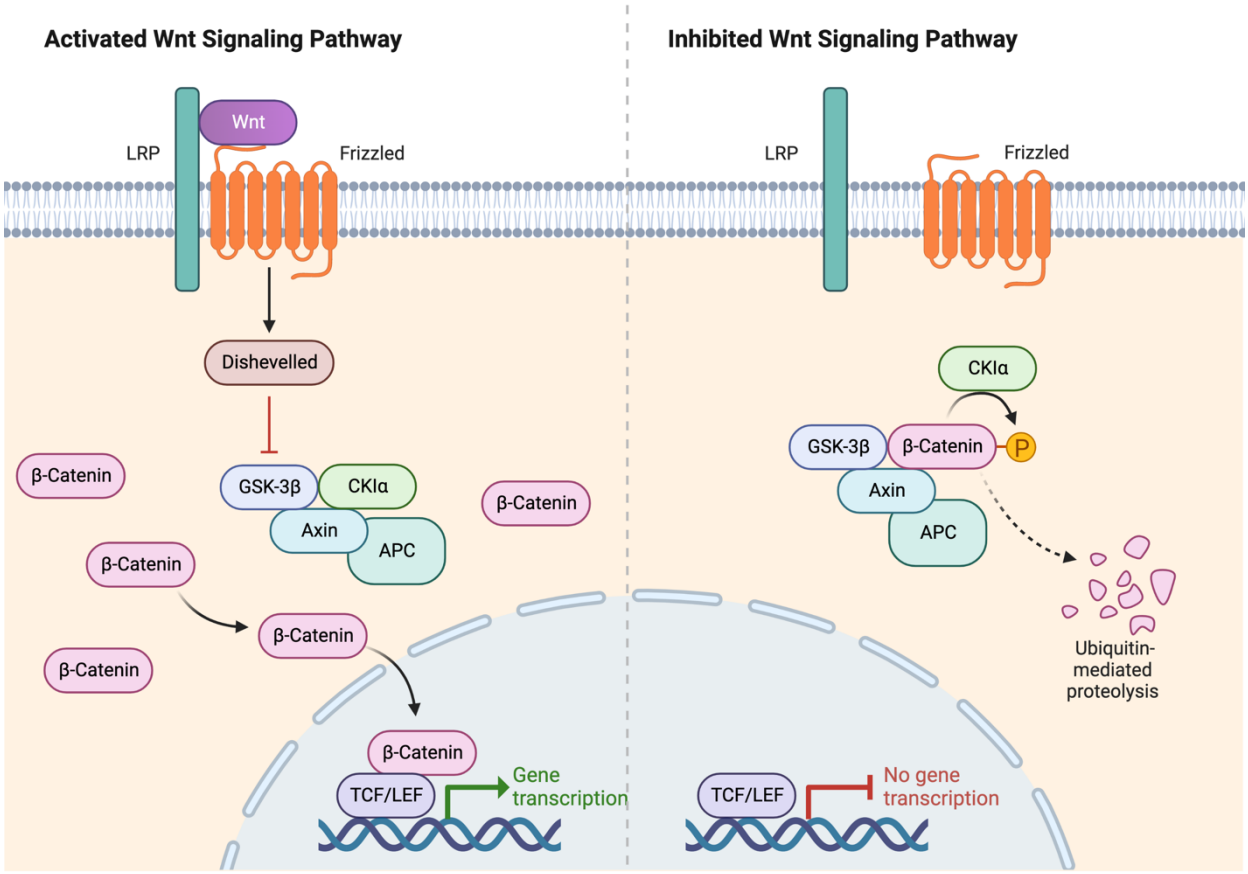

Figure 1.3. Overview of the canonical Wnt signalling pathway. In the absence of Wnt (right panel), cytoplasmic β-catenin is degraded by the destruction complex which includes Axin, adenomatosis polyposis coli (APC), glycogen synthase kinase 3 (GSK3) and casein kinase 1α (CK1α). β-catenin is marked for ubiquitination and subsequently proteasomal degradation. In the presence of Wnt ligand (left panel), a receptor complex between frizzled and its co-receptors LRP5 and LRP6 is formed which results in the recruitment of the scaffolding protein Dishevelled and the negative regulator of Wnt, Axin. This series of events leads to a disruption in the function of the Axin-mediated destruction complex, accumulation of β-catenin in the cytoplasm and its eventual translocation to the nucleus, where it cooperates with TCF/LEF family members to activate the transcription of target genes. The illustration was created using the scientific image and illustration software, BioRender.

FGF signalling

The FGF superfamily consists of eighteen secreted proteins which signal through binding and activating high-affinity tyrosine kinase receptors (FGFR1, FGFR2, FGFR3, and FGFR4). FGF activation leads through a cascade of phosphorylation events in the induction of multiple downstream signalling pathways such as Ras/Raf-MEK-MAPKs (mitogen-activated protein kinases), phosphatidylinositol-3 kinase/protein kinase B (PI3K/AKT), PLCγ, and Jak-STAT depending on the cellular context (Figure 1.4) (Xie et al. 2020).

The FGF signalling pathway has a wide range of cellular and developmental functions and is also implicated in the establishment of NC in various model organisms (Figure 1.1A). In *Xenopus*, FGF in the presence of BMP antagonism induces the formation of NC (LaBonne and Bronner-Fraser 1998; Mayor et al. 1997), while overexpression of a dominant negative Fgf receptor results in inhibition of NC marker expression (Mayor et al. 1997). Moreover, FGF8 derived from the paraxial mesoderm (the dorsal region of embryonic mesoderm that forms somites and musculoskeleton) is sufficient to induce NC transiently without the requirement of BMP antagonists (Monsoro-Burq et al. 2003). Similarly, studies in the chicken provide evidence that FGF activity in the ectoderm is necessary during gastrulation, as FGF chemical inhibition in neural plate border leads to reduced NC marker expression (Stuhlmiller and Garcia-Castro 2012b), while ectopic expression of FGF4 in the surface ectoderm is sufficient to induce NC marker expression (Yardley and Garcia-Castro 2012). Furthermore, a study published by Sasai et al. (2014) using chicken explants delineated the temporal requirement of FGF in NC induction in the caudal pre-neural tube and proposed a model at which FGF establishes a region of NC competence in cooperation with BMP and Wnt signals, which progressively diminishes as the axis elongates and FGF signals regress. This allows the generation of prospective neural cells in the more anterior domains. Recent work in the chicken embryo further highlighted the requirement of FGF in NC induction and specification and suggested that FGF levels are modulated via a post-transcriptional mechanism which involves miRNA-mediated gene silencing (Copeland and Simoes-Costa 2020). Similar to BMP and Wnt, the contribution of FGF signalling has mainly been studied in chicken and frog embryos and little is known about its role in mammalian NC formation. Loss of function experiments for *Fgf8* in mouse mutant lines suggest a crucial role of *Fgf8* gene function during gastrulation and early NC development, as mice mutants showed impaired brain development and exhibited craniofacial and cardiac malformations, in line with a faulty NC formation/development (Meyers et al. 1998). However, the precise role of *Fgf8* in the early morphogenetic events following gastrulation was not examined (Meyers et al. 1998).

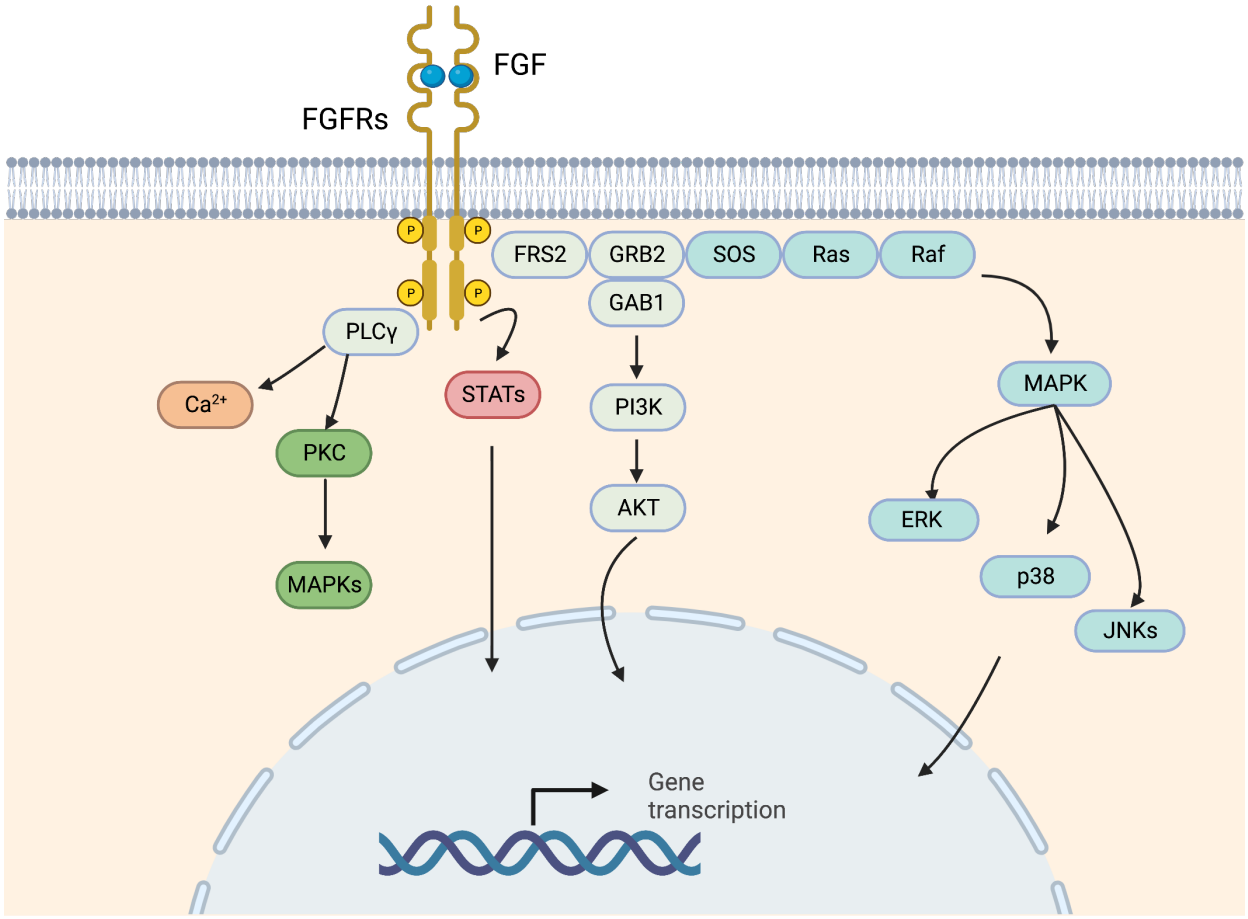

Figure 1.4. Overview of the classical FGF pathways. FGFs bind and activate tyrosine kinase receptors (FGFRs) leading to transphosphorylation of the tyrosine kinase domain in the intracellular compartment. Activated FGFRs further stimulate multiple downstream signalling pathways such as Ras-MAP kinase, PI-3 kinase/AKT, STAT and PLCγ. FRS2α, FGFR substrate 2α; GAB1, GRB2 associated binding protein 1; GRB2, growth factor receptor-bound 2; PKC, protein kinase C; SOS, son of sevenless. The illustration was created using the scientific image and illustration software, BioRender.

Notch signalling

The Notch signalling pathway is a fundamental and evolutionarily conserved pathway that governs almost every aspect of embryonic morphogenesis. Notch receptors and ligands are present throughout embryonic development and adult life and act in a pleiotropic way to modulate cell-fate determination between immediate neighbours in nearly every tissue and organ in the body by influencing proliferation, differentiation and apoptosis (Bray 2006). The Notch receptors and their ligands Delta and Serrate (Jagged in mammals) (the number of which varies between species) are transmembrane proteins located on the surface of adjacent interacting cells (Figure 1.5). Ligand-receptor binding triggers a series of proteolytic events which eventually result in the γ-secretase dependent release of the Notch intracellular domain (NICD) from the cell membrane. The NICD translocates to the nucleus where it cooperates with the Notch signalling effectors suppressor of hairless (CBF1/RBPjκ (mammalian homolog)) (a DNA-binding protein) and the nuclear protein mastermind to trigger the transcription of target genes, among them the basic helix–loop–helix hairy and enhancer of split (HES) proteins: HES1 and HES5 in mammals (Louvi and Artavanis-Tsakonas 2006).

As in many developmental processes, the Notch signalling pathway is implicated in NC formation. Studies in *Xenopus* and avian embryos have demonstrated a role of Notch pathway and Delta1-mediated activation in regulating *Bmp4* expression and thus, NC induction at the neural plate border during gastrulation (Endo et al. 2002; Glavic et al. 2004). In zebrafish, mutations in *deltaA* or reduced delta signalling leads to reduced NC marker expression in the trunk and to loss in trunk NC derivatives, while the cranial NC cells remained unaffected, suggesting 1) that distinct mechanisms regulate cranial and trunk NC development and 2) a role of Notch in trunk NC development, however, its implication in NC induction or cell fate determination remains unclear (Cornell and Eisen 2000). Consistent with a role of Notch in early cell fate diversification, Hernandez-Lagunas et al. (2011) using zebrafish model demonstrated a role of this pathway in determining the NC versus neural fate choices at the neural plate border by regulating the expression of mutual repressors, prdm1a and olig4. Moreover, gain or loss of function in components of Notch signalling in mouse embryos revealed a wide array of developmental defects associated with NC derivatives in the craniofacial skeleton, in heart structures and neurons of the enteric nervous system (Mead and Yutzey 2012). These findings highlight the importance of Notch in NC development in the mouse and suggest that Notch regulates migration, proliferation and differentiation (Mead and Yutzey 2012), however, the role of Notch in NC induction in the mouse still remains elusive.

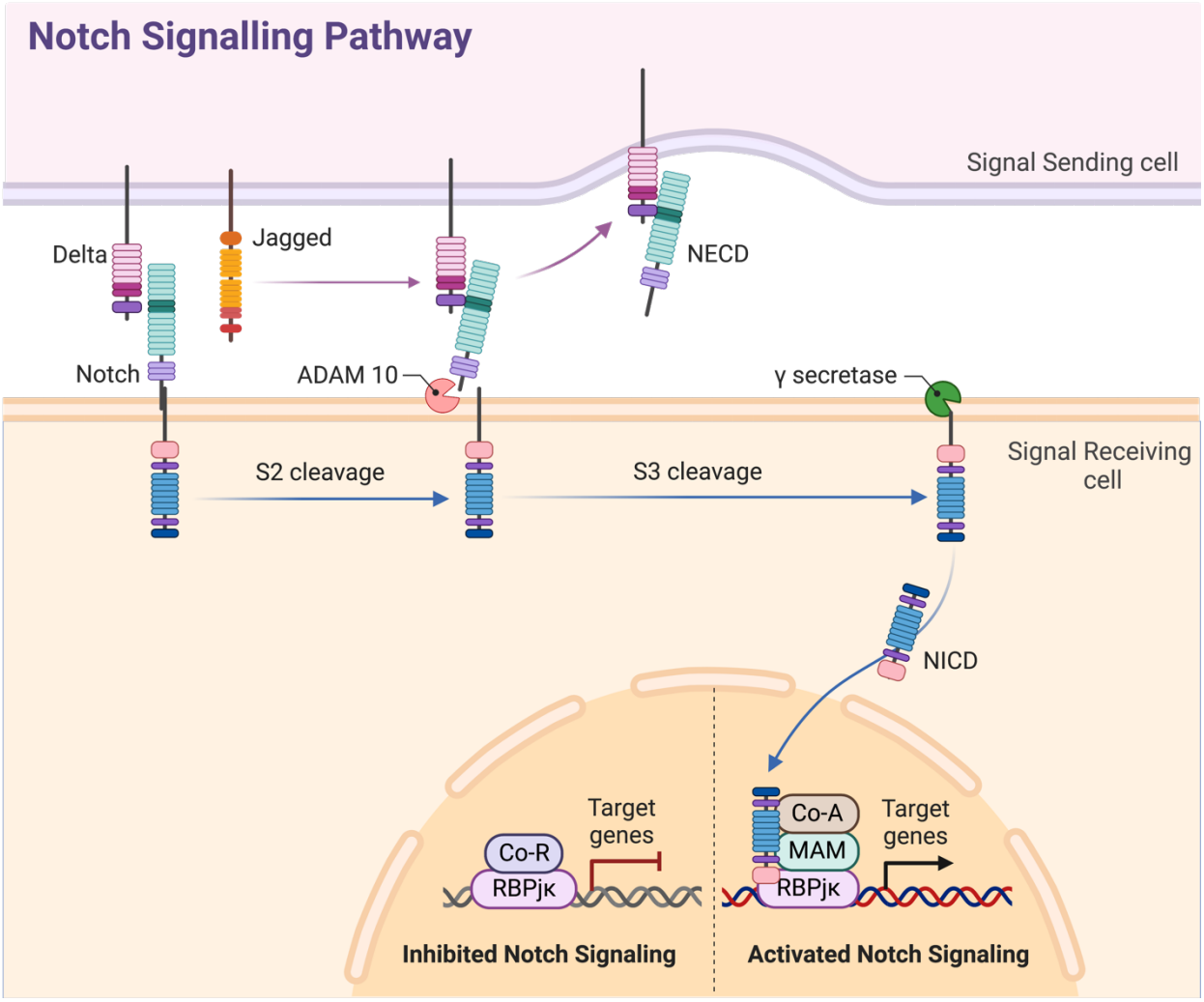

Figure 1.5. Overview of the canonical Notch signalling pathway in mammals. Activation of Notch signalling occurs upon interaction between Notch receptors (Notch 1-Notch 4) and Notch ligands (Jagged 1, Jagged 2, Delta-like 1, Delta-like 3, Delta-like 4) on the membrane of adjacent cells. Receptor-ligand binding triggers a series of proteolytic cleavages, mediated by ADAM10 metalloprotease and the γ-secretase complex. These events result in the release of the Notch intracellular domain (NICD) from the cell surface and its subsequent translocation into the nucleus, where it associates with the RPB-Jκ protein complex, displaces co-repressors and recruits transcriptional activators, including the co-activator protein mastermind (MAM) to initiate Notch target gene transcription. The illustration was created using the scientific image and illustration software, BioRender.

1.1.2.Transcription factors involved in neural crest development

Neural plate border specifiers

The combinatorial action of Wnt, BMP, FGF and Notch signals emerging from the surrounding tissues (paraxial mesoderm, neural plate, surface ectoderm) triggers the induction of the neural border domain at the interface of the neural plate, which is located medially, and the surface ectoderm, which is located laterally (Figure 1.1Ai). In response to these signals, neural plate border cells upregulate a set of transcription factors, termed neural plate border specifiers (Figure 1.1Ai), that allows the adoption of a NC competent transcriptional program and in turn activate the expression of NC specifiers (Sauka-Spengler and Bronner-Fraser 2008). The genes encoding these transcription factors are evolutionarily conserved among vertebrates. Studies in *Xenopus*, chicken, zebrafish, basal vertebrates such as lamprey, mouse and hPSCs have contributed to our knowledge about the expression patterns and regulation of these markers, which are considered to be the earliest modulators of NC formation (Prasad et al. 2019).

The “paired domain” *Pax* family members *Pax3* and *Pax7* are expressed in the neural plate border domain in most vertebrates (Hong and Saint-Jeannet 2007; Monsoro-Burq et al. 2005; Prasad et al. 2019) and are critical for NC induction as loss of their expression severely reduces NC marker expression, NC migration and impedes differentiation of NC to various derivatives (craniofacial structures and enteric ganglia) as it is shown in the chicken, mouse, lamprey and *Xenopus* embryos (Basch et al. 2006; Hong and Saint-Jeannet 2007; Lang et al. 2000; Mansouri et al. 1996; Monsoro-Burq et al. 2005; Nikitina et al. 2008). In particular, Pax7 is first detected in the chicken embryo as early as epiblast stage 4 and is considered to be induced by BMP and Wnt signals (Basch et al. 2006). As the NC induction progresses, Pax3 expression starts to overlap with Pax7 and the expression of the latter eventually localises to neural folds and later to migratory NC cells (Basch et al. 2006). In *Xenopus* embryos instead, *Pax3* is the first Pax paralog expressed in response to Wnt and FGF8 signals (Maczkowiak et al. 2010; Monsoro-Burq et al. 2005; Sato et al. 2005) and in turn positively regulates *Pax7* expression in addition to Wnt, FGF8 and retinoic acid (RA) (Maczkowiak et al. 2010). Moreover, Pax3 modulates its own expression as part of an autoregulatory feedback loop (Plouhinec et al. 2014). Notably, *Pax3* expression is not only confined in the neural plate border and neural folds during early development but it continues to be expressed in migratory NC precursors with functional implication in enteric neuron and melanocyte development (Bondurand et al. 2000; Lang et al. 2000; Lang and Epstein 2003).

Zic1 is another neural plate border specifier that cooperates with *Pax3* in the dorsolateral ectoderm to induce NC formation in the *Xenopus* embryo (Sato et al. 2005). *Zic1* induces the

expression of downstream NC specifiers *foxd3* and *snai2 (slug)* (Sato et al. 2005). This is likely to happen via direct binding to *snai1/2* promoters (Plouhinec et al. 2014). Additionally, the NC specifiers *twist1* and *tfap2b* are also induced by Pax3 and Zic1 to promote a NC fate (Plouhinec et al. 2014). A combined and balanced activity between Pax3 and Zic1 is necessary to induce NC as a variation in their levels is shown to shift the cell fate towards the identity of neighbouring domains. Particularly, an increase in the levels of Pax3 favors the formation of hatching gland, while Zic1 upregulation promotes pre-placodal ectoderm fate (PPE) (Hong and Saint-Jeannet 2007).

Msx genes also play a key role in neural plate border specification. In *Xenopus* and zebrafish, Wnt signalling and intermediate levels of BMP activate *msx1* which, in turn, induces the expression of its downstream targets *snai1, snai2, foxd3* that confer cells competence to induce a NC identity (Sato et al. 2005; Tribulo et al. 2003). FGF8-mediated activation of *msx1* is also shown to promote *snai2* expression via activating *pax3* and *zic1*, revealing that *msx1* is located upstream of *pax3* and *zic1* in the cascade of NC specification and further highlighting the existence of multiple regulatory steps/factors towards NC specification (Monsoro-Burq et al. 2005). Zebrafish with mutations in *msxB, msxC* and *msxE* (Phillips et al. 2006) and mice double mutants for *Msx1* and *Msx2* (Satokata et al. 2000) develop cranial bone malformations due to impaired NC differentiation and proliferation of NC progeny, in line with a role of *Msx* family members in the development of NC.

Members of the Transcription Factor AP-2 (*Tfap2*) family are also key regulators in the NC GRN (de Croze et al. 2011; Nikitina et al. 2008). *Tfap2* genes are highly conserved among chordates and in vertebrates are implicated in NC and surface ectoderm/PPE development (Hoffman et al. 2007). The *tfap2a* gene is detected in the ectoderm during gastrulation and its expression spans between the neural plate border and the surface ectoderm until it becomes confined to pre-migratory NC in the dorsal neural tube (de Croze et al. 2011). *The Tfap2a gene* in lamprey shows a similar expression pattern and functions upstream of *Pax3/7* and *Zic1* to promote their activation (Nikitina et al. 2008; Sauka-Spengler et al. 2007). Similarly in *Xenopus*, Tfap2a which is induced by FGF, BMP and Wnt signals mediates neural plate border specification via direct binding and transcriptional activation of *pax3* in cooperation with Wnt (de Croze et al. 2011). In mouse, loss of Tfap2 is lethal and mice die perinatally having severe craniofacial defects due to Tfap2-associated failure in neural tube closure (Schorle et al. 1996; Zhang et al. 1996), in line with the crucial role of *Tfap2* in morphogenesis (Mitchell et al. 1991). In addition to its role in neural plate border specification, Tfap2a also functions as a NC specifier in a mechanism that is independent from its former action in the neural plate border (de Croze et al. 2011; Sauka-Spengler et al. 2007). Tfap2a in this case, acts downstream of *pax3* and *zic1* to mediate the

activation of NC bona fide genes such as *sox9, sox10, snai2, foxd3* (de Croze et al. 2011). The transcription factor TFAP2A is likely to modulate transcription via direct binding to key NC enhancers and promoting an open/permissive chromatin landscape that will allow other transcriptional regulators such as MSX1, ZIC1 or PAX3/7 to bind and activate NC target genes as it was shown during hPSC differentiation to NC (Rada-Iglesias et al. 2012; Simoes-Costa and Bronner 2015).

Neural crest specifiers

Shortly after neural plate border specification, NC specifier genes are upregulated in the presumptive NC population by the coordinated action of border specifiers and integrated signals (Figure 1.1Aii). NC specifiers regulate critical processes such as proliferation, delamination and the onset of migration and in contrast to border specifiers, they retain their expression in the migratory NC population (Sauka-Spengler and Bronner-Fraser 2008). However, border specifiers such as Pax3/7 and Tfap2a have reiterative functions in NC formation and diversification and their expression persists during all the stages of NC development including induction, specification, delamination.

SoxE (Sox8, Sox9, Sox10) family of transcription factors are key regulators of NC specification and downstream differentiation, as mutations in their expression have been associated with many developmental disorders dubbed SOXopathies which are characterised, among others, by severe defects in NC derivatives (Angelozzi and Lefebvre 2019). The onset and temporal sequence of SoxE protein expression varies between species. In the chicken Sox9 expression precedes the expression of Sox8 and Sox10 in premigratory NC (Cheung and Briscoe 2003), whereas in *Xenopus* Sox8 expression is followed by Sox9 and Sox10 (Hong and Saint-Jeannet 2005). In *Xenopus*, as NC specification progresses Sox9 expression is restricted in migrating cranial NC towards the pharyngeal arches, whereas Sox10 mainly persists in NC from the trunk region (Aoki et al. 2003; Spokony et al. 2002). In chicken, Sox9 expression is mainly maintained in migrating cells that will generate structures of the heart, while Sox10 persists in NC cells of cranial and trunk regions that will form peripheral ganglia (Cheng et al. 2000; Montero et al. 2002). In humans, premigratory and migratory NC cells express SOX9 and SOX10 and in contrast to the findings in the *Xenopus* and chicken, SOX9- and SOX10-expressing cells are observed in the cranial ganglia and mesenchyme along with other anatomical domains in the periphery (Betters et al. 2010).

The importance of Sox genes in NC specification is demonstrated by functional analysis studies. Ectopic expression of Sox8/9/10 in neural tube of chicken embryos induces NC differentiation at the expense of neural fate and Sox9 promotes the expression of other NC markers including

Sox10 (Cheung and Briscoe 2003). Additionally, forced expression of Sox10 in the trunk region of the neural tube at a later stage induces NC migration, while sustained Sox10 expression inhibits differentiation, suggesting a role of Sox10 in controlling these events (McKeown et al. 2005). A similar role of *Sox10* in maintaining multipotency while inhibiting differentiation to neuronal linages is also demonstrated in mouse NC stem cells (Kim et al. 2003). Overexpression of SOX10 has also been demonstrated to convert fibroblasts to NC cells *in vitro* (Kim et al. 2014; Motohashi et al. 2016). Depletion of Sox9 in mouse embryo does not impair trunk NC specification, however, NC cells in Sox9 mutants undergo apoptosis (Cheung et al. 2005).

The forkhead box transcriptional repressor foxD3 is another key regulator during NC specification. It is one of the earliest markers of the NC lineage and its expression precedes the expression of Sox10 in the chicken embryo (Simoes-Costa et al. 2012). FoxD3 is sequentially expressed from anterior to posterior in premigratory and migratory NC of all axial levels before being restricted to NC-derivatives in peripheral ganglia (Kos et al. 2001; Simoes-Costa et al. 2012). Overexpression of FoxD3 in the chicken neural tube and *Xenopus* embryo results in an increase in NC marker expression which coincides with enhanced migration (Dottori et al. 2001; Kos et al. 2001; Sasai et al. 2001). On the contrary, loss of function of FoxD3 in *Xenopus* embryos supresses NC markers such as *Snai2, Twist, Ets-1*, highlighting a requirement of FoxD3 for NC specification (Sasai et al. 2001). Moreover, work in the mouse demonstrated a role of *Foxd3* in maintaining the NC-derived progenitor pool (Teng et al. 2008). *Foxd3* mutant embryos were characterised by cranial skeletal abnormalities, loss of peripheral ganglia and strikingly, their enteric nervous system was missing (Teng et al. 2008). Additionally, FoxD3 controls the expression of cell adhesion molecules and hence is considered to be involved in NC delamination (Cheung et al. 2005).

1.2. Neural crest differentiation

1.2.1. Neural crest subtypes

The NC is formed along the anteroposterior axis of the developing embryo, spanning from the posterior diencephalon to lumbosacral region and can be divided into distinct subpopulations (cranial, cardiac, vagal, trunk, sacral) that arise sequentially in time and in space as the embryo elongates (Rothstein et al. 2018) (Figure 1.6B). NC cells from distinct axial levels exhibit discrete migratory behaviours and are equipped with the ability to generate axial level-specific derivatives throughout the body (Figure 1.6C). Each NC subpopulation reflects a certain axial location and

is further defined by the expression of *Hox* gene paralogous groups (PGs), which function as regional identity specifiers (Hunt et al. 1991).

The *Hox* gene family encodes a set of transcription factors that are crucial for the anteroposterior patterning of the embryo during development. *Hox* genes are evolutionary conserved between species and in vertebrates are grouped in 4 discrete clusters (HoxA, HoxB, HoxC, HoxD) on different chromosomes. Each cluster contains a set of *Hox* genes which are organised in a numerical order (1-13) and genes of different clusters are termed paralogs (Figure 1.6A) (Deschamps and Duboule 2017; Deschamps and van Nes 2005). These are activated in a spatiotemporal fashion according to their genomic order in each chromosomal cluster, a process known as "temporal co-linearity" (Kmita and Duboule 2003). Thus, the expression of 3' *Hox* genes precedes the expression of more 5' *Hox* genes, with the latter being induced sequentially as the axis elongates (Deschamps and Duboule 2017). *Hox* genes encode positional information as they specify tissues along the anteroposterior axis and therefore, they are widely used as a readout of axial identity. In the NC, *Hox* genes are implicated in axial specification and are critical in defining subpopulations that emerge from different axial levels.

Cranial NC displays an anterior *Hox*-negative and posterior *Hox* PG (*1-3*)-positive domain, while the vagal is characterised by the expression of *Hox* PG (*3-5*). NC cells from the trunk region are marked by the expression of *Hox* PG (*5-9*) and posterior to them, sacral NC exhibits a *Hox* PG (*10-13*)-positive domain (Cooper and Tsakiridis 2022a; Le Douarin et al. 2004) (Figure 1.6A). *Hox* gene expression starts in NC located in the hindbrain region, posterior to rhombomeres r2-3 (reviewed in Parker et al. 2018). The absence of *Hox* genes from the anterior cranial NC population has been associated with the ectomesenchymal potential of cranial NC, as targeted expression of *Hoxa2*, *Hoxa3*, *Hoxb4* in the *Hox*-negative anterior cranial NC domain restricted the ability of these cells to form skeletal structures (Creuzet et al. 2002). Notably, ectopic expression of *Hoxb1* in the chicken neural tube at trunk axial levels was sufficient to induce a NC-like identity and promote epithelial to mesenchymal transition through activation of key transcriptional regulators Snai2 and Msx1/2 (Gouti et al. 2011), highlighting the implication of anterior *Hox* genes in NC specification. *Hox* genes expressed in the posterior NC domains are also crucial for NC development and differentiation (Kam and Lui 2015). In particular, *Hoxb5* expression is maintained in migratory vagal NC/ENS progenitors in zebrafish, chicken, mouse and human gut (Fu et al. 2003; Howard et al. 2021; Kuratani and Kirby 1992; Kuratani and Wall 1992), where it has been shown to function in controlling the size of the progenitor pool (Howard et al. 2021) and regulating migration and enteric neural differentiation through activation of Ret (Lui et al. 2008).

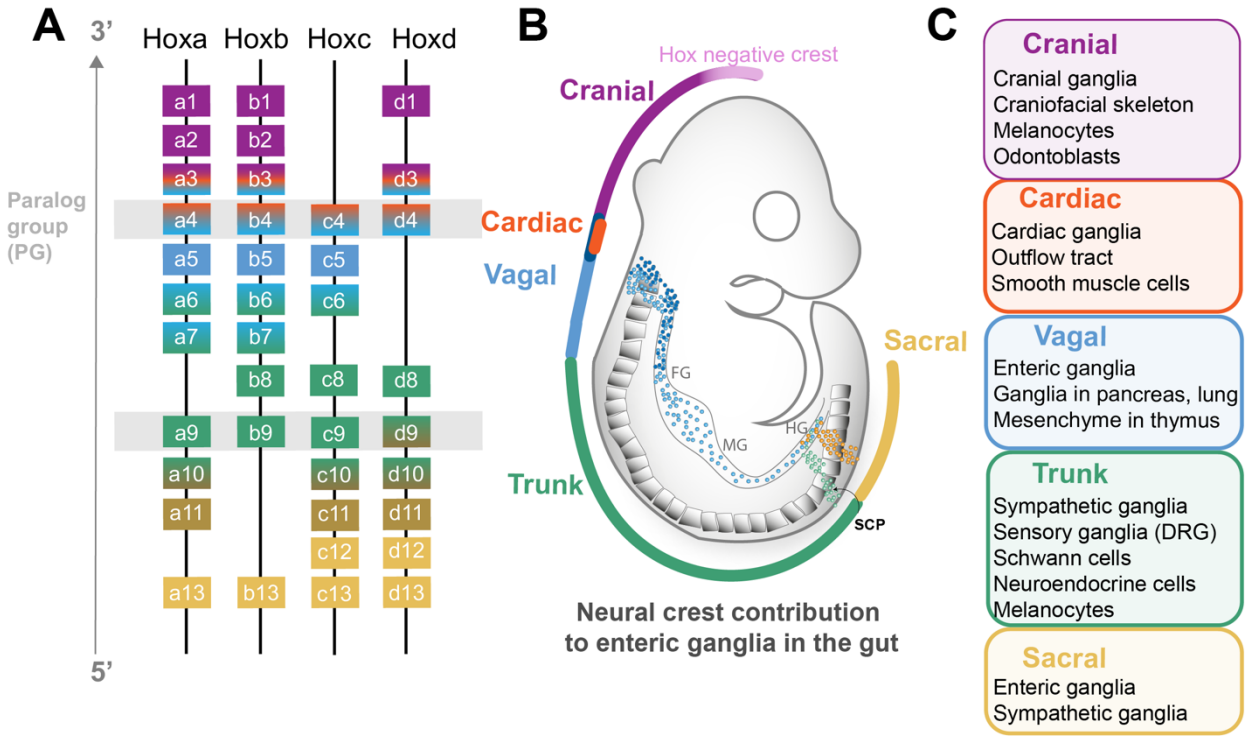

Figure 1.6. Overview of neural crest populations and their contributions along the anteroposterior axis. (A) *Hox* gene organisation in 4 chromosomal clusters. (B) NC subdivisions and contributions to ENS. Vagal NC from somites1-2 migrate like Schwann cell precursors (SCP) to the foregut and generate neurons in the oesophagus, whereas the rest vagal NC populate the entire gastrointestinal tract. Sacral NC contribute to the distal gut, while SCP derived from the trunk NC emigrate to the hindgut later in development and contribute to enteric ganglia. (C) List of NC derivatives based on axial identity. FG; foregut, MG; midgut, HG; hindgut, DRG; dorsal root ganglia.

Cranial neural crest

The cranial NC arise in the rostral part of the neural tube, anterior to the otic vesicle and is the first population to delaminate and leave the neural tube (Bronner and LeDouarin 2012). It produces ectomesenchymal structures of the face such as bones, cartilage and connective tissue, melanocytes, neurons and glia of the cranial ganglia (D'Amico-Martel and Noden 1983; Le Lievre 1978; Le Lievre and Le Douarin 1975; Platt 1893). The cranial NC collectively migrate dorsolaterally beneath the ectoderm to reach their destination (reviewed in Minoux and Rijli 2010). Cranial NC arising from the anterior domains (forebrain, midbrain) follow a dorsal pathway to generate the fronto-nasal structures in the head, whereas NC from the posterior/hindbrain region migrate laterally and ventrally in defined streams along the hindbrain rhombomeres to populate the pharyngeal arches (Couly et al. 1993; Kontges and Lumsden 1996; Lumsden and Guthrie 1991; Osumi-Yamashita et al. 1994). Cranial NC streams have also been shown to provide the tracks for the migration of placodal neuroblasts, precursors of cranial sensory neurons, from the placodal epithelium towards the hindbrain in chicken and mouse embryos and consequently contributing in addition to forming neurons in the proximal cranial ganglia to the structural organisation of their distal counterparts (Freter et al. 2013).

Vagal/Cardiac neural crest

The vagal NC is located posteriorly to cranial NC and emerges in the post-otic hindbrain region adjacent to somites 1-7. It generates numerous specialised derivatives with main contributions to the enteric nervous system (ENS; neurons and glia of the gastrointestinal tract) (Le Douarin and Teillet 1973; Yntema and Hammond 1954), to ganglia in the pancreas and lung and to mesenchyme and pericytes in the thymus (Hutchins et al. 2018). Vagal NC that generate enteric neurons and glia predominantly follow the ventral pathway and travel through the somitic mesoderm towards the gut (Kuo and Erickson 2011; Nagy and Goldstein 2017) (Figure 1.6B). In addition to this, it was recently proposed that NC emerging next to somites 1-2 take an alternative route to the foregut along the descending fibres of the vagus nerve (Espinosa-Medina et al. 2017). According to this, NC from these levels give rise to Schwann cell precursors which are guided through the vagus nerve to the oesophagus and stomach and populate these regions with enteric neurons, highlighting the complex and heterogeneous behaviour of NC that belong to the same subdivision nevertheless, hold different axial position (Espinosa-Medina et al. 2017) (Figure 1.6B). A detailed description of the ENS is included in chapter 4.

In addition to vagal population, NC cells emerging from somites 1-3 follow the dorsolateral pathway to the heart and contribute to various derivatives of the cardiovascular system, including the outflow tract septation complex, cardiac ganglia and the smooth muscle layer of the dorsal aorta and aortic arch arteries (George et al. 2020; Kirby et al. 1983). Because of their essential role in the formation of the heart, this NC subpopulation is named cardiac. Similar to cranial, NC cells that correspond to vagal axial levels generate melanocytes (Reedy et al. 1998).

Trunk neural crest

The trunk NC arise in the posterior part of the embryo at the region that corresponds to cervical and thoracic axial levels, spanning from somite 8 to 24 in the mouse or to 28 in avian embryos (Le Douarin and Teillet 1973; Rothstein et al. 2018). These cells participate in the formation of the PNS as they give rise to sensory and sympathetic ganglia, Schwann cells in addition to endocrine cells of the adrenal gland and melanocytes (reviewed in Le Douarin et al. 2004; Le Douarin and Teillet 1973; 1974; Serbedzija et al. 1994; Teillet et al. 1987). Although the aforementioned are considered to be direct derivatives of the trunk NC, recent studies have suggested the additional contribution of a NC-derived glial progenitor, termed Schwann cell precursor, to their emergence (Furlan and Adameyko 2018). Schwann cell precursors are multipotent like the NC population they originate from and have been shown to share a transcriptional profile with late migratory NC even though they demonstrate a fate bias towards

discrete NC derivatives (Kastriti et al. 2022). They migrate along the developing nerves of the PNS to various locations and differentiate towards diverse cell types including melanocytes (Adameyko et al. 2009), neuroendocrine cells (Furlan et al. 2017; Kastriti et al. 2019), parasympathetic (Dyachuk et al. 2014) and enteric neurons (El-Nachef and Bronner 2020; Uesaka et al. 2015). Notably, Uesaka et al. (2015) revealed that trunk NC-derived Schwann cell precursors invade the gut via extrinsic nerves and generate ~20% of the neurons in the large intestine postnatally (Figure 1.6B), a seminal work expanding our understanding about the origin of the ENS beyond the vagal NC contribution.

Non-neuronal cell types including mesenchymal derivatives in mice (e.g. myofibroblasts and bone marrow mesenchymal stem cells) in addition to Schwann cells are also derived by peripheral glial cells (Isern et al. 2014; Joseph et al. 2004). The mesenchymal potential of trunk NC has been also explored in the avian embryo, where trunk NC were reported to be capable of differentiating into skeletal elements *in vitro* and *in vivo* when cultured in appropriate conditions and following transplantation into the developing head in chicken embryos, respectively (McGonnell and Graham 2002).

In order to reach their destination and generate the various derivatives, trunk NC cells upon delamination, follow three stereotypic pathways (Vega-Lopez et al. 2017). Cells that migrate dorsolaterally, beneath the ectoderm, give rise to melanocytes (Reedy et al. 1998), while cells that contribute to sensory neurons and glia of the dorsal root ganglion and sympathetic neurons travel via a ventrolateral (through somites)/ventromedial (between the neural tube and sclerotome) route (reviewed in Kuo and Erickson 2010; Vega-Lopez et al. 2017). NC that will generate secretory cells migrate ventrally (Polak et al. 1971). Notably, the pathways and the timing that NC cells migrate varies between species (Vega-Lopez et al. 2017).

Sacral neural crest

The Sacral NC emerge in the developing embryo caudally to trunk NC subdivision and posterior to somite 24, from the region that corresponds to lumbosacral levels of the spinal cord (Bronner and LeDouarin 2012). Sacral together with vagal NC generate the majority of enteric neurons and glia of the gastrointestinal tract, however, the contribution of the former is much smaller (~20%) and restricted to the hindgut (Figure 1.6B)(Burns and Douarin 1998; Kapur 2000; Le Douarin and Teillet 1973; Tang et al. 2022).

1.2.2. Neural crest fate decisions and transitions to their derivatives

How NC cells decide between alternative fates and whether they represent multipotent progenitors or a mixed population of lineage restricted precursors are some of the key long lasting questions in the field of developmental biology (Dupin et al. 2018) and recently single cell mutli-omics combined with mathematical modelling studies have provided important insights into NC cell lineage separation in the avian and mouse model (Lignell et al. 2017; Soldatov et al. 2019; Williams et al. 2019). Williams et al. (2019) looking at transcriptome and chromatin profiling at single cell level in the chicken embryo revealed the existence of various populations with distinct transcriptional and epigenetic profiles within premigratory cranial crest cells. The authors proposed that the heterogeneity in cis-regulatory elements including enhancers and super-enhancers and their interactions with novel, in addition to core, NC transcription factors drives lineage segregation downstream of NC. They also showed that an epigenetic and transcriptional neural-specific program primes pre-migratory NC towards neural fate and suggested the early segregation of NC cells associated with the neural from the mesenchymal lineage (Williams et al. 2019). A fate bias linked to spatial organisation within the heterogeneous premigratory cranial NC in the dorsal neural tube in the chicken embryo was also described by Lignell et al. (2017). The authors, using fluorescent probes and an image analysis pipeline that enables spatial transcriptional profiling, identified spatially confined NC subpopulations with distinct transcriptional profiles characterised by the concurrent expression of multiple linage specific and pluripotency markers as well as a subpopulation predominantly expressing a marker of cartilage fate, *Col2a1* (Lignell et al. 2017).

Moreover, a recent study from the Adameyko and Kharchenko groups (Soldatov et al. 2019) using single-cell RNA sequencing and spatial transcriptomics provided valuable insights into fate transitions during cranial and trunk NC differentiation in the mouse embryo. This study proposed that NC diversification occurs via sequentially binary fate splits mediated by the co-activation and subsequent mutual repression of transcriptional programs driving alternative fates within heterogeneous progenitors in early migratory NC. While cranial NC showed a mesenchymal fate bias demonstrated by the activation of *Twist1*, *Prrx2* and *Dlx2*, delaminating trunk NC cells were predisposed towards sensory neuronal lineage with expression profile characterised by an upregulation of *Neurog1, Pou4f1* and *Nkx2.1* genes. Within migratory trunk NC cells, the authors demonstrated that the first bifurcation separates the sensory lineage, whereas the second one, diverges the autonomic from the mesenchymal fate (Soldatov et al. 2019). A similar mechanism for cell fate specification via activation and inhibition of opposing transcriptional programs was shown to govern the segregation of sympathoadrenal progenitors and immature Schwan cells or enteric glia and immature Schwan cells in trunk NC-derived Schwann cell precursors following

NC migration in the chicken embryo (Kastriti et al. 2022). Similarly, sequential branching points resulting from transcriptional changes in NC-progeny of the sensory (Faure et al. 2020) and ENS lineage (Morarach et al. 2021) have been shown to construct neural subtype diversity in the developing PNS, findings underlying that a common mechanism for cell-fate specification persists from early the early steps of NC differentiation until terminal differentiation of NC derivatives.

1.3. Neurocristopathies

The faulty development of NC due to defects in specification, proliferation, migration, differentiation and survival leads to a large number of rare syndromes and diseases, which are collectively known as neurocristopathies (Bolande 1974; Vega-Lopez et al. 2018). These pathologies affect a great number of infants and constitute congenital malformations associated with pigmentation, cardiac and craniofacial abnormalities, thyroid and hearing disorders as well as defects in the ENS (Vega-Lopez et al. 2018). Some examples of neurocristopathies are Waardenburg, CHARGE, DiGeorge, Treacher Collins syndromes (McDonald-McGinn and Sullivan 2011; Sato et al. 2019; Trainor 2010) and Hirschsprung's disease (HSCR; Heanue and Pachnis 2007). In addition to congenital malformations, NC-derived tumours such as neuroblastoma, melanoma, pheochromocytoma and Schwann cell-associated tumours also fall under the umbrella of neurocristopathies (Vega-Lopez et al. 2018). The primary cause of neurocristopathies is chromosomal aberration and/or gene mutations in NC-associated genes that perturb the NC GRN or dysregulate epigenetic mechanisms that control gene activity and formation of gene products. However, non-genetic factors such as alcohol consumption and imbalance in the levels of vitamin A, linked to the maternal diet, have also been implicated in NC-derived developmental disorders (Pilon 2021; Vega-Lopez et al. 2018).

For instance, neuroblastoma, the most common childhood malignancy associated with increased catecholamine production, affects the sympathoadrenal lineage which developmentally arises from the trunk NC and is characterised by clinical and molecular heterogeneity (Maguire et al. 2015). Amplification of the *MYCN* gene, loss of 1p and 11q, gain of 17q, mutations in *ALK* and *PHOX2B* are among the most frequent genetic aberrations reported in neuroblastoma (Johnsen et al. 2019). These genetic abnormalities appear to disrupt normal NC development and drive neuroblastoma tumorigenesis in sympathoadrenal progenitors (Gonzalez Malagon and Liu 2022).

HSCR, a birth defect characterised by the lack of enteric ganglia in the distal colon and as a consequence severe gut dysmotility, has a strong genetic basis with main etiology being

mutations in signalling components crucial for normal ENS development including *RET, GDNF, SOX10, PHOX2B, EDNRB, EDN3* (Heanue and Pachnis 2007; Sergi et al. 2017). Thus, ENS progenitors fail to migrate, proliferate, differentiate as well as survive in the developing ENS resulting in inadequate colonisation (Barlow et al. 2008; Young et al. 2004) and subsequently aganglionosis. This pathology is lethal unless the aganglionic part of the intestine is surgically removed (Tam 2016). Several animal models up to date carrying known mutations in ENS signature genes have expanded our current understanding on the pathophysiology of HSCR or in general, neurocristopathies and have further paved the way towards improvising molecular and cellular approaches to treat these disorders, which up to date lack curative treatment.

1.4. Anteroposterior patterning of neural crest *in vivo*

1.4.1. Axial-specific gene regulatory networks

Although the early events of NC induction and specification in amniotes and anamniotes have been studied extensively over the past decades, the molecular mechanisms establishing axial level-specific NC populations have been largely unexplored (Rothstein et al. 2018). Experimental embryology with elegant heterotopic grafting of NC from and to distinct axial levels have been extremely informative about the intrinsic features of each NC subpopulation that confer a specific developmental potential; for instance the contribution to ectomesenchymal derivates in the head is an attribute of cranial and not trunk NC and the role of the environmental cues in directing cell fate decisions (Rocha et al. 2020). The establishment of distinct NC populations along the anteroposterior axis as well as their intrinsic properties is considered to be a result of the coordinated action of axial level-specific genes and GRN (Rothstein et al. 2018). The cranial-specific transcription factor Ets1 is expressed in NC in avian embryos (Tahtakran and Selleck 2003) and is a key regulator for cranial NC specification as it activates cranial-specific regulatory elements (Simoes-Costa and Bronner 2015) and promotes NC delamination even when it's ectopically expressed (Theveneau et al. 2007). Similarly, *Twist1*, a mesenchymal gene expressed in mouse and chicken cranial NC is one of the main drivers of the cranial NC-mesenchymal program (Soldatov et al. 2019). Loss of Twist1 function in chicken cranial NC leads to a reduction in mesenchymal derivatives, while forced expression of Twist1 in the trunk, promotes a cranial migratory behaviour and a shift towards mesenchymal fate (Soldatov et al. 2019).

In addition to axial level-specific transcription factors, region-specific enhancers regulating the transcription of pan-NC genes (*Sox10*, *FoxD3*) have also been identified in cranial and post-otic

NC (Betancur et al. 2010; Murko and Bronner 2017; Simoes-Costa et al. 2012). In the case of *Sox10*, SOX10E2 enhancer mediates its expression in cranial NC upon activation by Sox9, Ets1 and cMyb transcriptional regulators, while SOX10E1 drives Sox10 expression in migrating vagal and trunk NC (Betancur et al. 2010; Murko and Bronner 2017). In a similar manner, *FoxD3* expression in early cranial NC is controlled by the NC1 enhancer, whereas *FoXD3* activation in vagal, trunk and late migrating cranial NC is mediated upon activation of the NC2 enhancer (Simoes-Costa et al. 2012). A differential regulation of *foxd3* by different sets of autoregulatory enhancers along the anteroposterior patterning of NC in zebrafish embryo has also been demonstrated recently (Lukoseviciute et al. 2021). The presence of axial level-specific modes regulating pan-NC genes, reflects the existence of distinct transcriptional programs that confer cells the ability to activate the same genes in response to different environmental signals (Rothstein et al. 2018).

The existence of axial level-specific genetic programs is further supported by the findings of recent transcriptomic analysis studies (Gandhi et al. 2020; Simoes-Costa and Bronner 2016). Simoes-Costa and Bronner (2016) using cranial-specific enhancers identified a subset of genes enriched in the cranial NC compartment (*Tfap2b, Sox8*, and *Ets1*) and demonstrated that their ectopic expression in trunk NC is sufficient to reprogram cells to cranial identity and confer them the ability to generate ectopic cartilage in the head. A similar approach followed by Gandhi et al. (2020) revealed that forced expression of cardiac NC-specific battery of genes *Sox8, Tgif1* and *Ets1* redirects trunk NC to adopt a cardiac NC-like identity and cardiac-crest developmental potential, which is further demonstrated by their ability to rescue heart defects in chicken embryos that cardiac NC was removed. Finally, these studies highlight that axial level-specific regulatory programs are tightly coupled with axial level-specific NC fates.

1.4.2. Neuromesodermal axial progenitors generate posterior neural crest

The notion that posterior tissue and, specifically the tail bud, contributes to NC derivatives in caudal parts of avian embryos was first introduced by Schoenwolf (1977); Schoenwolf et al. (1985) in a series of transplantation experiments followed by analysis of donor derivatives and was later supported by the findings of a fate-mapping study, which in a similar way by using quail-chicken chimaeras showed that trunk NC along with caudal spinal cord and posterior mesodermal derivatives arise from the tail bud (Catala et al. 1995). More recently, clonal analysis, multiple linage tracing studies and single-cell transcriptomic data (Javali et al. 2017; Lukoseviciute et al. 2021; Rodrigo Albors et al. 2018; Tzouanacou et al. 2009; Wymeersch et al. 2016) further revealed that trunk NC cells (and potentially sacral) and their neural derivatives (e.g. the DRG) (Shaker et al. 2021) originate from neuromesodermal-potent (Binagui-Casas et

al. 2021) progenitors residing in the caudal lateral epiblast/tailbud, termed NMPs. The NMPs are axial progenitors with stem cell-like properties that supply the elongating axis with spinal cord as well as presomitic/paraxial mesoderm descendants (reviewed in Wymeersch et al. 2021). They first appear just before the start of somitogenesis (Wymeersch et al. 2016) in the caudal lateral epiblast (CLE) and the node-streak border (NSB) and later in the chordoneural hinge in the tail bud (Wymeersch et al. 2021). Their induction as well as maintenance relies predominantly on the synergistic action of FGF and Wnt signalling inputs emanating from the primitive streak and CLE (Henrique et al. 2015; Wymeersch et al. 2021). The NMPs are characterised by the co-expression of the neural progenitor marker Sox2 and the mesodermal marker Brachyury (T) (Henrique et al. 2015; Tsakiridis et al. 2014) and they also upregulate a battery of genes consistent with a caudal regional identity, including *Nkx1.2, Cdx2, Tbx6* and posterior *Hox* genes (Gouti et al. 2017; Guillot et al. 2021; Javali et al. 2017; Rodrigo Albors et al. 2018; Wymeersch et al. 2019).

1.5. hPSC-based models of neural crest development

The recent advances in transcriptomics that enable to obtain information at high resolution and single cell level, together with very sophisticated lineage tracing, fate mapping and functional genetic studies have expanded our understanding on NC ontogenesis, development and related pathologies in animal models. Despite the tremendous progress that has been made, particularly over the last 2 decades (reviewed in Etchevers et al. 2019), our knowledge regarding the cellular and molecular mechanisms that govern NC development in humans is still poor. The restricted access to human embryos due to ethical and technical limitations renders hPSCs an invaluable tool to study the early, unreachable events of human NC induction/specification *in vitro*. hPSCs (human embryonic stem cells; hESCs or reprogrammed, human induced pluripotent stem cells; hiPSCs), owing to their capacity to self-renew and produce almost any cell type of interest, offer an excellent, infinite cellular source to study human development.

To date, several efforts have been made to model NC development using hPSCs, particularly via manipulation of BMP, Wnt and FGF signals (Figure 1.7, 1.8) due to their role in driving NC induction *in vivo*. With regards to BMP signalling, hPSC-based studies have demonstrated that a careful regulation of BMP activity at distinct time points and precise levels is a prerequisite for the generation of NC *in vitro* (Figure 1.7) (Hackland et al. 2017; Leung et al. 2016; Mica et al. 2013). While low-endogenous BMP activity is sufficient for NC derivation (Leung et al. 2016), blocking or activating BMP signalling pathway was found to stimulate neural and epidermal differentiation, respectively, in agreement with the role of BMP in neuroectodermal patterning

and surface ectoderm specification *in vivo* (Chambers et al. 2009; Metallo et al. 2008). Moreover, BMP-Smad signalling triggered by changes in cell shape and morphogenetic cues at the colony edge was shown to regulate the spatial organisation of neural plate border-like cells in a hPSC-based neuroectoderm patterning model (Xue et al. 2018). In line with the role of Wnt in inducing NC in vertebrates *in vivo*, activation of Wnt signalling is also used to derive hPSC-derived NC cells *in vitro* (Frith et al. 2020; Hackland et al. 2017; Leung et al. 2016; Menendez et al. 2011). Wnt stimulation in combination with low Smad signalling yields NC cells at the expense of neuroectoderm (Menendez et al. 2011) and promotes the acquisition of NC by supressing the surface ectoderm and PPE fate (Leung et al. 2016). Similarly, Wnt stimulation after a pulse of BMP signalling following an initial ectoderm induction using Nodal inhibition was shown to derive NC cells in a hPSC-based platform of micropatterned ectoderm (Britton et al. 2019). Furthermore, Wnt activation was required for the establishment of a NC domain at the expense of neural and placodal lineage as inhibition of endogenous Wnt resulted in loss of NC and expansion of neural, placodal and epidermal fate (Britton et al. 2019).

In addition to NC specification, Wnt signalling pathway is involved in axial patterning of NC cells *in vitro,* with low levels of Wnt activity promoting a rostral NC axial identity while high levels of Wnt with input from FGF signalling inducing NC cells that correspond to a more caudal region (Frith et al. 2018; Gomez et al. 2019b). The implication of FGF signalling in mammalian NC induction has also been studied in *in vitro* NC models from hPSCs (Frith et al. 2018; Gomez et al. 2019b; Hackland et al. 2019; Leung et al. 2016). According to these studies, the endogenous FGF signalling is essential for the derivation of hPSC-NC cells (Leung et al. 2016) and FGF activity is required to modulate NC anteroposterior patterning towards more posterior/trunk axial levels (Figure 1.7) (Frith et al. 2018; Gomez et al. 2019b; Hackland et al. 2019). Inhibition of FGF during NC differentiation impairs *HOX* gene induction and slightly reduces CDX2 expression, while SOX10 remains unaffected (Gomez et al. 2019b; Hackland et al. 2019). On the contrary, increased levels of FGF signalling result in an upregulation of sacral *HOX* genes (*HOXA10, HOXA11, HOXD13*) but SOX10 expression is severely compromised (Hackland et al. 2019), suggesting along with the other reports that precise levels of FGF signalling are required to induce posterior/ trunk NC identity. Induction of sacral *HOX* genes in *in vitro* NMP-derived cultures is likely to rely on GDF11 activity (Figure 1.7) (Cooper et al. 2022; Lippmann et al. 2015), a finding that could facilitate the generation of sacral NC from hPSCs (Cooper et al. 2022), which requires further attention.

In addition to BMP, Wnt and FGF, Notch stimulation was also shown to influence NC differentiation from hPSCs and to have 2 distinct functions; the first, being essential for NC

induction, while its inhibition results in neural differentiation and the second, maintaining NC cells at a premigratory state by suppressing downstream neural differentiation (Noisa et al. 2014).

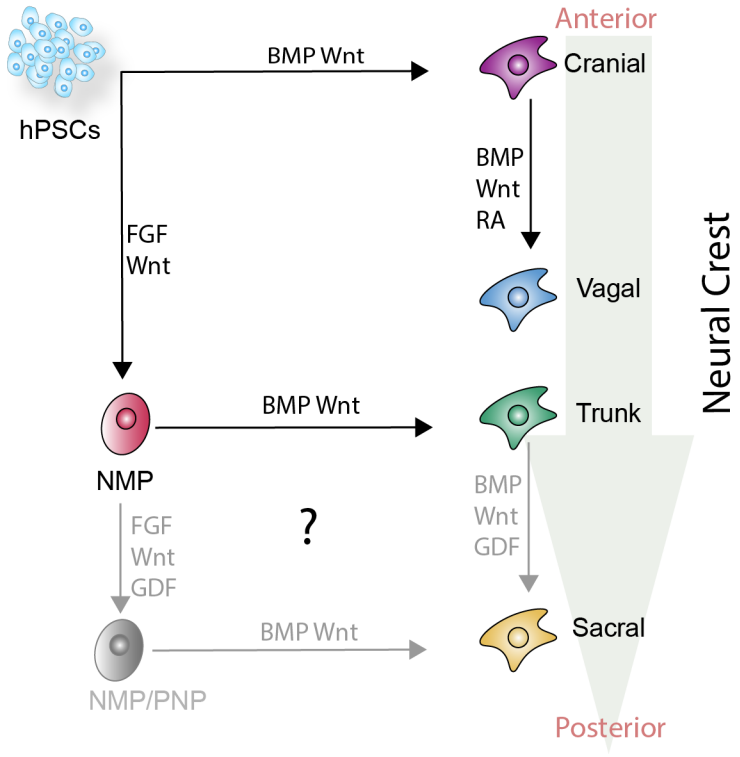

Figure 1.7. Overview of the current approaches and signalling combinations used to derive neural crest cells from human pluripotent stem cells. The generation of hPSC-derived sacral NC has not been described in detail and further work is required for the derivation of this lineage *in vitro*. NMP; neuromesodermal progenitors, PNP; pre-neural progenitors. Source/Modified (Cooper and Tsakiridis 2022a)

Using various signalling combinations, several research groups up to date have devised protocols for the generation of human NC cells with transcriptional and functional properties indicative of *in vivo* NC from different axial levels (Figure 1.7) (reviewed in Cooper and Tsakiridis 2022a). Cranial, vagal and trunk NC have been successfully generated *in vitro* and notably, have been shown to be capable of differentiating towards their immediate derivatives: osteocytes, chondrocytes, peripheral neurons and glia from the cranial (Hackland et al. 2017; Leung et al. 2016), enteric neurons and glia from the vagal (Figure 1.8) (Fattahi et al. 2016; Frith et al. 2020; Gogolou et al. 2021) and sympathoadrenal progenitor cells and sympathetic neurons from the trunk (Frith et al. 2018; Frith and Tsakiridis 2019; Hackland et al. 2019). An overview of the existing protocols for the generation of vagal NC and subsequently cells of ENS lineage from hPSCs is included in Figure 1.8. These strategies will be discussed in more detail in chapter 4 which focuses on ENS differentiation.

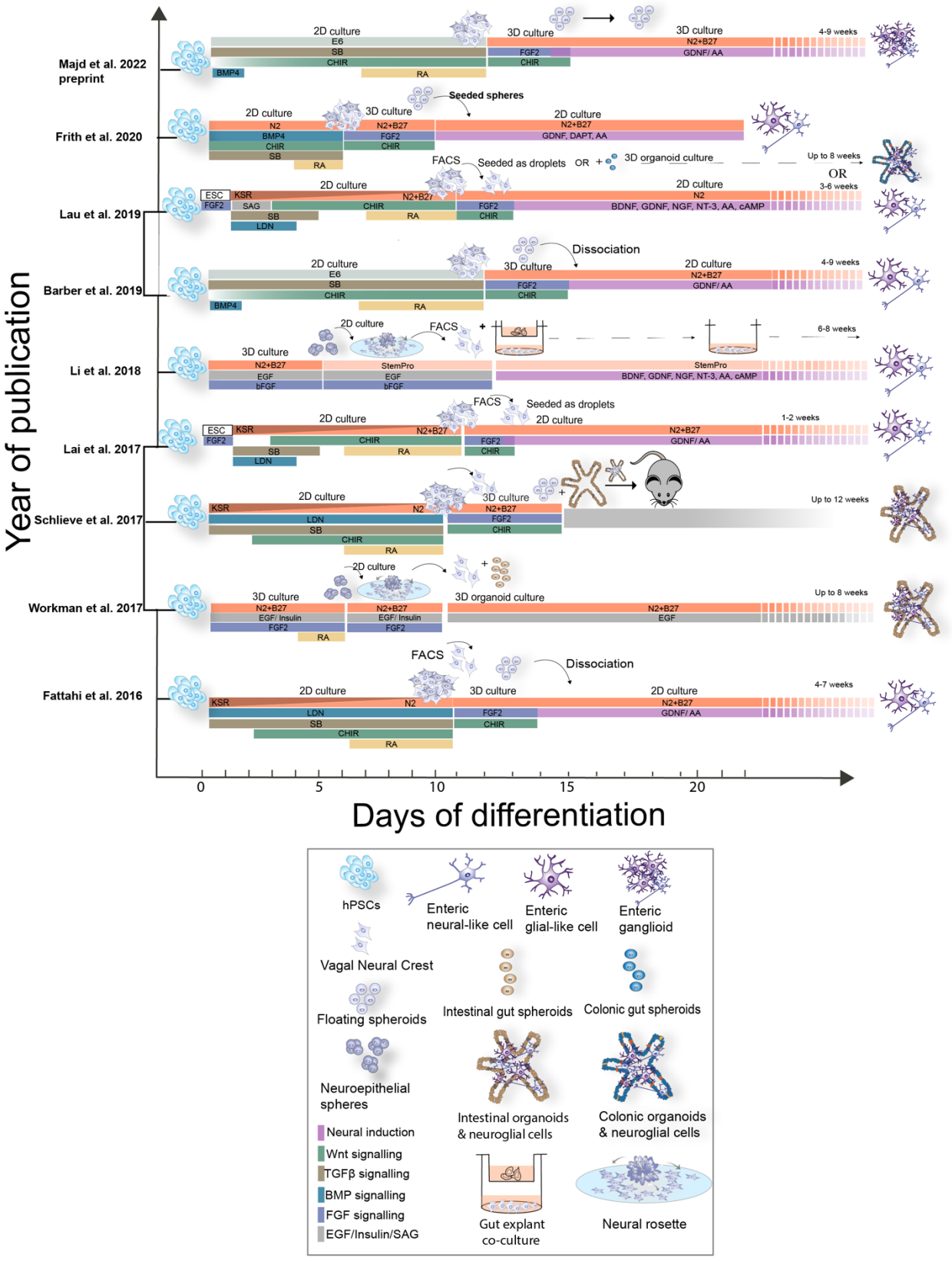

Figure 1.8. Illustration of the existing protocols for the generation of enteric nervous system cultures from human pluripotent stem cells via a vagal NC intermediate.

1.6. hPSC-derived neural crest: Applications to human disease

The potential of hPSC-derived NC cells is not only limited in studying human NC development but also expands in disease modelling of NC-associated disorders, drug screening and regenerative medicine. Our recent findings and work of others have demonstrated that hPSC-derived vagal NC cells have the ability to integrate, colonise and differentiate in the mouse, chicken, human adult gut (Fattahi et al. 2016; Frith et al. 2020; Li et al. 2018; Workman et al. 2017) as well as hPSC-derived intestinal and colonic organoids (Lau et al. 2019; Workman et al. 2017). Notably, *in vitro* derived vagal NC were able to engraft and rescue the fatality of HSCR mouse model *Ednrb*$^{s\text{-}l/s\text{-}l}$ (Fattahi et al. 2016) and more recently, their enriched in nitrergic (NO) neurons descendants were capable of colonising the colon of NO neuron-deficient mice (Nos1$^{-/-}$) (Majd et al. 2022). These studies illustrate the functional potency of human *in vitro* NC and hold promise for the development of cell-based therapeutic treatments for enteric neuropathies (Burns and Thapar 2014; Chng and Pachnis 2020; Stamp 2017).

Also, as part of the CONNECT consortium, a Horizon 2020 Project, we are currently aiming to connect hPSC-derived CNS and PNS (emerging from NC) components on a single platform to examine nervous system's connectivity (https://fet-proactive-connect.com/) using organ-on-chip technology and human stem cell research. This approach would be particularly useful to study and model diseases in which both parts of the nervous system are implicated, such as Parkinson's disease (Braak et al. 2006), and would be beneficial for drug discovery and personalised medicine by enabling high-throughput screening.

Moreover, Lai et al. (2017) using CRISPR/Cas9 gene editing were able to correct HSCR-associated mutations in patient derived iPSCs and further restore their function with respect to differentiation and migration, which had been impaired, following differentiation to ENS progenitors *in vitro*. This study indicates the importance of gene editing technology in identifying and correcting mutations associated with NC disorders in patient derived reprogrammed cells and moreover, the application of iPSC-derived NC in disease modelling. In line with this, a recent study using hiPSCs derived from patients with Bardet-Biedl Syndrome, a ciliopathy characterised among others by craniofacial dysmorphology, demonstrated impaired cranial NC induction and differentiation of patient-derived lines carrying mutations in *BBS10* compared to healthy controls (Barrell et al. 2019). The inefficient differentiation of mutant lines to NC, which could be attributed to a reduced response to WNT and BMP instructive signals, indicated the importance of *BBS10* in human NC development and illustrated the feasibility of using such platform to model and explore the cellular and molecular mechanisms that underlie NC-related disease (Barrell et al. 2019). Similarly, hPSCs harbouring chromosomal aberrations prevalent in the childhood tumour,

neuroblastoma, failed to differentiate into trunk NC and sympathoadrenal progenitors, the presumptive precursors of adrenal glands, where the neuroblastoma develops, and exhibited tumourigenic hallmarks (Saldana-Guerrero et al. 2022). The authors nicely demonstrated that hPSC-derived NC cells offer a suitable platform to model human embryonic tumourigenesis, like neuroblastoma.

Collectively, the above represent only a few examples of the broad potential applications of hPSC-derived NC cells in biomedical research and highlight the very promising opportunities they offer to transfer the current knowledge into clinical practice, an avenue we just started to explore (Cooper and Tsakiridis 2022b).

1.7. Hypothesis and aims

The existing hPSC-based differentiation protocols until recently had focused on the induction and early specification of NC and predominantly gave rise to cranial/anterior HOX-negative NC and their direct derivatives. The lack of protocols generating NC of a more caudal axial identity has been an obstacle to the study of anteroposterior patterning of NC and in particular of the specification of posterior (post-otic) NC cells and their products, namely vagal and trunk NC. Our group and others have recently described protocols for the generation of these cell types and have shown their developmental potential by differentiating them towards their downstream derivatives.

Utilisation of such *in vitro* differentiation systems towards understanding the signalling environment being experienced by the cells during posterior NC patterning will enable a higher degree of control over the morphogenetic cues that they receive and lead to refinement of the current differentiation approaches for the generation of axial level-specific NC populations with greater efficiency. Such a level of control is critical for the derivation of posterior NC cells where many signals might function, in a dose-dependent manner, to induce a NC identity and/or pattern the cells towards more caudal axial levels. Additionally, deciphering the role of key signals during NC differentiation is particularly important for the generation of clinically relevant axial specific NC cells and their specialised derivatives for cell therapy purposes. The hypothesis underlying this study was that the temporal and dose control of key NC inducing signals, centred around Wnt, FGF, BMP and RA, influence the generation and axial specification of posterior NC. In order to examine this, I generated NC cells following our previously devised vagal and trunk NC protocols, challenged different signalling pathways using agonist/antagonist treatments or shRNA mediated knockdown and assessed the transcriptional profile of the cells over the period of differentiation.

Overall using this approach, I set out to investigate the signalling and transcriptional basis of posterior patterning in hPSC-derived NC and determine factors/parameters crucial for their downstream differentiation towards neural derivatives. Specifically, this thesis aimed to:

1) Define the role of critical candidate signals in guiding the specification of vagal NC cells and their downstream derivatives
2) Determine key signals/transcriptional regulators necessary for trunk NC induction and differentiation

Chapter 2: Methods and Materials

2.1. Cell culture and differentiations

2.1.1. Cell lines

H9 (WA09), hES cell line published in Thomson et al. (1998). Employed for vagal, trunk NC and ENS differentiation.

H9:SOX10GFP, hES cell reporter line, kindly provided by Mark Tomishima to Peter Andrews. It was generated in H9 hES cell line using bacterial artificial chromosome (BAC) transgenesis and utilises multiple promoter and enhancer elements of the *SOX10* gene upstream of the green fluorescent protein (GFP) (Mica et al. 2013). This reporter cell line was employed to monitor *SOX10* expression levels during vagal NC and ENS differentiation.

MasterShef7, hES cell line derived at the University of Sheffield, Centre for Stem Cell Biology as described in Aflatoonian et al. (2010). It was used to demonstrate the generation of vagal NC from multiple cell lines.

WTC11 (UCSFi001-A), hiPS cell line derived from adult skin (leg) fibroblasts (Conklin Lab, Gladstone Institute). A gift from Femke de Vrij, Erasmus Medical Center, The Netherlands. The WTC11 line was employed for vagal NC and ENS differentiation.

WTC11:GFP, enhanced GFP (eGFP) expressing reporter cell line cloned from the rainbow cell reporter WTC11 hiPS cell line by Rebecca Lea at the University of Sheffield. The rainbow reporter prior to FACS isolation was treated with recombinant cell-permeant Cre to initiate permanent recombination of the rainbow cassette containing GFP, RFP and FRFP. In brief, hiPSCs were passaged 1:6 using TrypLE and cultured overnight in cell culture medium in the presence of 10μM Y-27632 2HCl. The following day, Y-27632 2HCl was removed from the culture medium and cells were treated with TAT-CRE Recombinase (100 units/ml ~ 90 μg of TAT-CRE) (Merck, # SCR508) for 6 hours in mTeSR. Upon TAT-CRE treatment, cells were washed with 1XPBS and expanded in culture using mTeSR medium. The expression of different fluorescent proteins and hues as a result of different recombination events was confirmed using fluorescence microscopy. The Cre-mediated conversion of the rainbow hiPS cell line was performed by Fay Cooper at the University of Sheffield. The rainbow cell reporter was acquired from Jennifer Davis, University of Washington (El-Nachef et al. 2020). The eGFP clone was used to track ENS progenitor migration in time-lapse videos in chapter 4.

TBXT and B2M shRNA sOPTiKD, hESC lines engineered to exhibit shRNA-mediated, tetracycline (Tet)-inducible knockdown of *TBXT* and *B2M* (control) expression, respectively. The cell lines were developed in the H9 cell line as described in Bertero et al. (2016) and were provided by Prof. Ludovic Vallier, University of Cambridge. The TBXT and B2M shRNA sOPTiKD cell lines were employed for all TBXT loss-of- function and sequencing experiments.

Table 2.1. hPSC lines used in the study

Name	Type	Sex	Reference
H9 (WA09)	hES	Female	Thomson et al. (1998)
H9:SOX10GFP	hES	Female	Mica et al. (2013)
MasterShef7	hES	Male	Aflatoonian et al. (2010)
WTC11 (UCSFi001-A)	hiPS	Male	Kreitzer et al. (2013)
WTC11:GFP cloned from rainbow reporter (WTC11)	hiPS	Male	El-Nachef et al. (2020)
TBXT and B2M shRNA sOPTiKD (H9)	hES	Female	Bertero et al. (2016)

2.1.2. Pluripotent Stem Cell culture

Feeder free culture

Human pluripotent stem cells (hPSCs) were grown in feeder-free conditions and maintained at 37ºC under humidified atmosphere and 5% CO_2 levels. Cell culture was carried out on 12.5 cm^2 tissue culture flask (VWR, #734-2309) coated with Geltrex (GTX) and incubated for an 1hour at 37ºC/5% CO_2 prior to use. hPSCs were grown in mTeSR (Stem Cell Technologies, #85850; Ludwig et al. (2006)) and the media was replenished daily. Cell lines were routinely cultured for a maximum of 12-15 passages to prevent accumulation of genetic abnormalities following long-term passaging. Passaging was carried out every 3-5 days and when the cells reached approximately 80 to 90% confluency, using an EDTA-based dissociation solution ((Invitrogen, #15575020; Beers et al. (2012)) or ReleSR (Stem Cell Technologies, #05872).

For EDTA based passaging, cultures were washed briefly with 1X PBS (Merck, #D1408; diluted 1:10 in ddH2O and sterilised using an autoclave) and 0.5 mM EDTA solution was added to the cells prior to incubation for 3-5 min at 37ºC. When cells began to separate from each other uniformly, EDTA solution was aspirated and fresh media was added to the cells. Efficient colony detachment was ensured by thorough mixing and small aggregates with size between 50-200 µm were obtained by pipetting the cell mixture using a serological pipette. Following that, cell aggregate suspension was dispensed at the appropriate dilution (1:6 or 1:12) in a new coated flask.

For ReleSR based passaging, media was aspirated and cells were incubated with ReLeSR for 30 seconds at room temperature. Following that, ReLeSR was removed and the flask was incubated for additional 3-4 minutes at room temperature and until hPSC colonies started to lift off of the cultureware. Media was subsequently added to the flask and by gentle tapping hPSC colonies fully detached. Colonies were broken up into optimally-sized aggregates (50-200 μm) following pipetting and cells were transferred to freshly coated culture flasks at the desired dilution (1:6 or 1:12). Cell culture was carried out using a horizontal laminar-flow clean bench and aseptic technique.

hPSC thawing

A frozen vial of hPSCs was removed from liquid nitrogen or -80^{o}C and placed in 37 ^{o}C water bath until most, but not all, cells were thawed. The content of the vial was next resuspended in mTeSR media for a quick wash. Cells were centrifuged at 1200rpm for 4min and cell pellet was resuspended in 3ml of mTeSR media supplemented with 10μM Y-27632 2HCl (AdooQ Bioscience, #A11001), a Rho-associated coil kinase (ROCK) inhibitor. Cell suspension was transferred to a freshly coated GTX flask and incubated at 37^{o}C. Flasks were not disturbed for 24h after thawing to allow cells settle. Media was changed daily and ROCK inhibitor was withdrawn the following day.

hPSC freezing

Medium was aspirated from a 12.5 cm^{2} culture flask and ReLeSR was added for 30 seconds at room temperature. ReLeSR was removed and the empty flask was next incubated for 3-4 minutes at room temperature and until cell contacts became loose. After the short incubation period, 1ml of freezing medium STEM-CELLBANKER (Amsbio) was added to the flask and cells were dissociated into small aggregates following gentle pipetting. The cell suspension was divided into 2 cryovials, placed in a freezing container (Mr frosty) in -80 ^{o}C freezer overnight before being transferred to liquid nitrogen for long-term storage. Prior to freezing hPSCs and creating master cell banks, a sister flask was sent for karyotype analysis or a qPCR assay was performed as described in Laing et al. (2019) to detect common copy number changes that occur in hPSCs.

Cultureware preparation

a. Geltrex

GTX LDEV-Free Reduced Growth Factor Basement Membrane Matrix (Thermo Fisher, #A1413202) was diluted 1:100 in cold DMEM/F12 (Merck Life Science, #D6421) and transferred to each flask/plate. Coated cultureware were incubated for 1hour at 37^{o}C prior to use. For longer storage following dilution, GTX aliquots were kept at 4^{o}C for up to 10 days.

b. Vitronectin

Vitronectin (VTN-N) Recombinant Human Protein, Truncated (Thermo Fisher, #A31804) was diluted 1:100 (working concentration 5µg/ml) in 1X PBS and used to coat the plates following a minimum 40min incubation period at room temperature prior to use.

c. Laminin 521

Laminin 521 (LN521, Biolamina, #LN521-05) was diluted in DPSB with calcium, magnesium (Thermo Fisher, #14040117) at 5µg/ml and used to coat 12.5 cm^2 culture flasks for a minimum of 1h at 37^{o}C.

TBTX inducible knockdown in the TBXT shRNA sOPTiKD hESC line

The TBXT and B2M shRNA sOPTiKD hESC lines (Bertero et al. 2016) were employed for the loss-of-function and sequencing experiments in D3 NMPs and their posterior derivatives. Stem cells were maintained in mTeSR medium, grown on LN521 or GTX and passaged twice a week using EDTA (0.5mM).

TBXT knockdown was carried out using tetracycline hydrochloride (Merck Life Science, # T7660) at 1µg/ml as described previously (Bertero et al. 2016). For efficient TBXT knockdown, tetracycline hydrochloride treatment was initiated 2 days before the differentiation. Stem cells were cultured in mTeSR medium supplemented with 1µg/ml tetracycline hydrochloride 2 days prior to differentiation and tetracycline treatment was maintained throughout the differentiation for the periods of time indicated in the results section.

2.1.3. *In vitro* differentiation

2.1.3.1. Vagal neural crest differentiation

GTX coated plates were prepared (as described in 2.1.2) and hPSC cultures at 80-90% confluency were firstly washed with PBS and then dissociated into a single cell suspension following treatment with Accutase solution (Merck Life Science, #A6964) for 5-7 minutes at 37^{o}C. Dissociation was monitored under the microscope to ensure cells had fully detached. After incubation time, the remaining cell aggregates were subsequently broken up by pipetting and DMEM/F12 media was added for neutralization. Culture suspension was then transferred into a conical tube and viable cells were counted using a hemocytometer. Cells were centrifuged at 1200 rpm for 4 minutes and the pellet was then resuspended in NC media (see Table 2.2) supplemented with Y-27632 2HCl to obtain a final concentration of 1 x 10^{6} cells/ml. Cell suspension was subsequently plated at an optimal density of 30 ± 20,000 cells/ cm^{2}, depending on the cell line, onto GTX-coated plates containing NC media supplemented with 10 μM Y-27632 2HCl and incubated at 37^{o}C. The day of plating is considered as day 0 of the differentiation.

At day 2, 48 hours post plating, small colonies started to emerge and NC media was refreshed without Y-27632 2HCl. Cells were incubated for 48 hours. At day 4, when cultures have reached 90% of confluency-an indicator of protocol's efficiency- old media was changed to NC media containing 1 μM all-trans Retinoic acid (RA; Merck Life Science, #R2625) and plates were incubated at 37^{o}C, protected from light. Stock solution of 10^{-2} M RA was prepared in DMSO and stored at −80°C. Working stock of 10^{-3} M RA was prepared and stored at -20^{o}C in light protected vials for a short period (up to 3 months). Cultures treated with RA displayed increased cell death and acquired a spiky morphology. For representative images of cells' morphology please refer to Figure 3.1. The day after, day 5 of differentiation, media was fully changed with fresh NC media supplemented with 1 μM all-trans RA and cells were incubated at 37^{o}C for an additional day. At day 6 of the protocol, cells displayed a characteristic NC morphology (stellate morphology, please refer to Figure 3.1) and were either harvested for analysis or plated for subsequent differentiation. A detailed version of the protocol is published in current protocols (Gogolou et al. 2021).

Table 2.2. Neural crest induction media

Component	Stock Conc.	Volume for 50ml	Final Conc.	Company	Cat #
DMEM/F12	1X	48.5ml	N/A	Merck	D6421
N2 Supplement	100X	0.5ml	1x	Thermo Fisher	17502048
NEAA	100X	0.5ml	1x	Thermo Fisher	11140050
GlutaMAX	100X	0.5ml	1x	Thermo Fisher	35050061
CHIR99021†	10mM	5μl	1μM	Tocris	4423
SB431542	10mM	10μl	2μM	Tocris	1614/1
BMP4	50μg/ml	20μl	20ng/ml	Thermo Fisher	PHC9533
DMH-1	10mM	5μl	1μM	Tocris	4126/10
All-trans RA	1mM	50μl (**ADDED D4)**	1μM	Merck	R2625

*Penicillin-Streptomycin (5,000 U/ml; Thermo Fisher, #15070063) at 1:100 was added to media (optional)

† An alternative CHIR99021 from Selleck Chemicals (Cat # S2924) was used in 3.4.1 to compare it with the standard Tocris

2.1.3.2. Enteric nervous system differentiation

The *in vitro* generation of ENS derivatives takes place into 2 successive steps which include the derivation of NC/ENS progenitor spheres and the induction of enteric neurons and glia.

Step 1: Generating neural crest spheres

Day 6 vagal NC cells were re-plated into non-adherent conditions to form free floating spheroids, using the Corning Ultra-Low attachment plates (Corning, #3471). To this end, cells were enzymatically dissociated following treatment with Accutase for 7 minutes at 37°C, neutralised with DMEM/F12 and centrifuged for 4 min at 1200 rpm. Supernatant was then removed and cell pellet was re-suspended in sphere media, (see Table 2.3) supplemented with 10 μM Y-27632 2HCl, in the appropriate volume so that cells grown on a well of an adhesion 6 well plate were transferred to a well of a 6 well Ultra-Low attachment plate (ratio 1:1). Cells were then incubated at 37°C for 2 days. After a day in non-adherent conditions, cell aggregates were formed and small spheroids were present. At day 8, 48 hours post plating, spheres of different sizes were formed and sphere media was half changed, carefully, using a serological pipette to avoid excessive cell loss. Cells were then incubated until day 9 or 10 at 37°C. When spheres were joint and long tube like structures were formed, mainly at day 9, cell suspension was transferred to a 50 ml conical tube and sphere clumps were triturated up and down, using a 5ml serological

pipette, to break up into smaller aggregates. The mechanical dissociation was performed very gentle to avoid over-trituration of spheres. Spheres were then distributed equally back to each well and kept at 37^{o}C until day 9/10 for analysis and re-plating in ENS induction conditions. Sphere media was supplemented with 1 μM all-trans RA throughout the sphere stage as indicated in the results section in chapter 4.

Table 2.3. Sphere media

Component	Stock Conc.	Volume for 50ml	Final Conc.	Company	Cat #
Neurobasal	1x	23.75ml	0.5X	Thermo Fisher	21103049
DMEM/F12	1x	23.75ml	0.5X	Merck	D6421
NEAA	100x	0.5ml	1X	Thermo Fisher	11140050
GlutaMAX	100x	0.5ml	1X	Thermo Fisher	35050061
N2	100x	0.5ml	1X	Thermo Fisher	17502048
B27	50x	1ml	1X	Thermo Fisher	17504044
CHIR99021	10 mM	15 μl	3μM	Tocris	4423
FGF2	10 μg/ml	50 μl	10 ng/ml	R&D Systems	233-FB/CF
Y-27632 2HCl	10 mM	50 μl	10 μM	AdooQ Bioscience	A11001

*Penicillin-Streptomycin (5,000 U/ml; Thermo Fisher, #15070063) at 1:100 was added to media (optional)

Step 2: Enteric neuronal differentiation

Day 9/10 spheres were collected using a 10 ml serological pipette into a 50 ml conical tube and were let to sediment for 3 minutes. Old media was then carefully and manually removed to avoid disturbing spheres collected at the bottom of the tube. Spheres collected from one well of the low attachment plate were resuspended in 3-4 ml (optimised for each cell line) of ENS induction media (without 10 μM Y-27632 2HCl; see Table 2.4) and gently mixed using a 5 ml serological pipette. When big aggregates were present, excessive pipetting was used to break them up into smaller clumps. For plating, 0.5 ml and 1 ml of sphere suspension was transferred onto GTX-coated 24 and 12 well plates, respectively. To ensure that cell aggregates were equally distributed, plates were monitored under the microscope. ENS media was changed every other day (half medium change) and supplemented with Vitronectin at 1:100 to facilitate attachment of axons for long periods of culture and when cells started detaching from the periphery. Two to three days post plating, cells started migrating out of the spheres and neural-like projections became apparent (Figure 4.1). A detailed description of the protocol was published in current protocols (Gogolou et al. 2021).

Table 2.4. Enteric nervous system induction media

Component	Stock Conc.	Volume for 50ml	Final Conc.	Company	Cat #
BrainPhys	1x	47.5 ml	N/A	StemCell Tech	05790
NEAA	100x	0.5 ml	1X	Thermo Fisher	11140050
GlutaMAX	100x	0.5 ml	1X	Thermo Fisher	35050061
N2	100x	0.5 ml	1X	Thermo Fisher	17502048
B27	50x	1 ml	1X	Thermo Fisher	17504044
GDNF	10 µg/ml	50 µl	10 ng/ml	Peprotech	450-10
DAPT	10 mM	50 µl	10µM	Tocris	2634
Ascorbic Acid	200 mM	50 µl	200 µM	Sigma-Aldrich	A8960

*Penicillin-Streptomycin (5,000 U/ml; Thermo Fisher, #15070063) at 1:100 was added to media (optional)

Replating enteric neurons

Substrate preparation

Glass coverslips were sterilised with 70% ethanol, washed and left to dry prior to incubation with the cell adhesion promoters PDLO or PO. PDLO or PO solution was added on top of each coverslip and plates were incubated at 37°C overnight. Solutions then were removed, wells were washed three times with double-distilled water and left to dry. Following that, coverslips were coated with different combinations of substrates as shown in Table 2.5 and incubated at 37°C for at least 2 hours or overnight.

Table 2.5. Substrate combinations for replating enteric neurons

Sub-strate	Components	Final conc.	Company	Cat#
1	GTX	150µg/ml in DMEM (1:100)	Thermo Fisher	A1413202
2	poly-dl-ornithine (PDLO) GTX	50µg/ml in borate buffer 150µg/ml in DMEM (1:100)	Sigma-Aldrich	P0671
3	Mouse Laminin I (LAM)	10µg/ml in PBS	Cultrex	3400-010-02
4	Poly-dl-ornithine (PDLO) Mouse Laminin I (LAM)	50µg/ml in borate buffer 10µg/ml in PBS	-	-
5	VTN	5µg/ml in PBS	Thermo Fisher	A31804
6	Poly-l-ornithine (PO) Mouse Laminin I (LAM) Fibronectin (FN)	50µg/ml in PBS 2µg/ml in PBS 2µg/ml in PBS	Sigma-Aldrich R&D Systems	P4957 1918-FN

The replating of ENS cultures was performed at the indicated time points (see results in 4.3.3) and when the cells had created robust neural networks. The earliest and latest time points replating was attempted was at day 15 and 60, respectively. ENS medium was first carefully removed using a pipette to avoid disturbing the monolayer with the suction force of a vacuum aspirator, cells were subsequently washed twice using PBS and then incubated with accutase

for 15-20 min at 37°C. Following that, ENS media in a ratio 1:5 of the accutase solution (without 10 µM Y-27632 2HCl) was added directly to the wells, cultures were lifted as flat sheets from the bottom of the culture vessel and subsequently transferred using a 5ml serological pipette (wide opening is required) into a 50ml falcon tube to settle down for 2-3 minutes. Long incubation time was avoided to prevent debris from sinking to the bottom of the tube together with the neurons. When cells formed a pellet, media was carefully removed and the pellet was resuspended 1:5-1:6 in fresh ENS media without 10 µM Y-27632 2HCl. Flat sheets of neurons were broken up into smaller aggregates by gentle pipetting, cell suspension was mixed thoroughly and transferred into coated plates. Replated cultures were incubated at 37 °C and medium was changed after 2 days.

2.1.3.3. Neuromesodermal progenitor differentiation

The NMP differentiation was performed on VTN-coated plates, prepared as described in 2.1.2. At the first day of the differentiation (day 0), hPSCs that had reached 80% confluency were dissociated into singe cell suspension following Accutase treatment for 7 min at 37 °C. Cell numbers were counted manually using a hemocytometer, samples were centrifuged at 1200 rpm for 4 min and resuspended in NMP medium (Table 2.6) supplemented with 10 µM Y-27632 2HCl to obtain a final concentration of 1 x 10^6 cells/ml. Following that, cells were seeded at 50,000 cells/cm^2 on VNT-coated multiwell plate and incubated at 37 °C. Medium (without Y-27632 2HCl) was replenished after 24 hours (day 1) and cells were analysed or proceeded to downstream differentiation 72 hours after the initial plating (day 3).

For signalling pathway activation/inhibition, N2B27 (NMP basal medium) containing 0.5X Neurobasal, 0.5X DMEM/F12, 1X NEAA, 1X GlutaMAX, 1X N2 supplement, 1X B27, 50 µM 2-Mercaptoethanol was supplemented with the agonist/antagonist (Table 2.7) combinations for the periods indicated in the results section (see section 5.4.1).

For tet-mediated inducible TBXT knockdown, the TBXT shRNA sOPTiKD hESC line was employed and the differentiation was performed following the protocol described above in the constant presence of 1µg/ml tetracycline hydrochloride. Plates following tetracycline administration were kept in dark.

Table 2.6. Neuromesodermal progenitor differentiation media

	Component	Stock Conc.	Volume for 50ml	Final Conc.	Company	Cat #
N2B27 media	Neurobasal	1x	23.75ml	0.5X	Thermo Fisher	21103049
	DMEM/F12	1x	23.75ml	0.5X	Merck	D6421
	NEAA	100x	0.5ml	1X	Thermo Fisher	11140050
	GlutaMAX	100x	0.5ml	1X	Thermo Fisher	35050061
	N2	100x	0.5ml	1X	Thermo Fisher	17502048
	B27	50x	1ml	1X	Thermo Fisher	17504044
	2-Mercaptoethanol	50 mM	50 µl	50 µM	Thermo Fisher	31350010
	CHIR99021	10 mM	15 µl	3 µM	Tocris	4423
	FGF2	10 µg/ml	100 µl	20 ng/ml	R&D Systems	233-FB/CF

Table 2.7. List of agonists/antagonists used during the neuromesodermal progenitor differentiation

Conditions	Component	Stock Conc.	Final Conc.	Company	Cat #
1. WNT, FGF	CHIR99021	10 mM	3 µM	Tocris	4423
	FGF2	10 µg/ml	20 ng/ml	R&D Systems	233-FB/CF
2. WNTi, FGF	XAV 939	10mM	1 µM	Tocris	3748
	FGF2	10 µg/ml	20 ng/ml	R&D Systems	233-FB/CF
3. WNT, FGFi	CHIR99021	10 mM	3 µM	Tocris	4423
	PD0325901	10mM	1 µM	Merck	PZ0162
4. WNT, FGF, RA	CHIR99021	10 mM	3 µM	Tocris	4423
	FGF2	10 µg/ml	20 ng/ml	R&D Systems	233-FB/CF
	All-trans RA	1mM	0.1 µM	Merck	R2625
5. WNTi, FGF, RA	XAV 939	10 mM	1 µM	Tocris	3748
	FGF2	10 µg/ml	20 ng/ml	R&D Systems	233-FB/CF
	All-trans RA	1mM	0.1 µM	Merck	R2625
6. WNT, FGFi, RA	CHIR99021	10 mM	3 µM	Tocris	4423
	PD0325901	10 mM	1 µM	Merck	PZ0162
	All-trans RA	1mM	0.1 µM	Merck	R2625

2.1.3.4. Trunk neural crest differentiation

For trunk NC differentiation, day 3 NMPs were harvested using Accutase solution, counted and plated at a density of 50,000 cells/cm^2 onto GTX-coated plates in NC induction medium (Table 2.2) (supplemented with 15ng/ml BMP4 instead of 20ng/ml) in the presence of 10 µM Y-27632 2HCl for the first 48 hours. Medium was replenished every 2 days.

For signalling inhibition during trunk NC differentiation, the protocol was followed as described above and the medium was supplemented with the agonist/antagonist combinations indicated in

the corresponding figures in the results section 5.4.2, using the concentrations listed in Table 2.8.

For Tet-mediated inducible TBXT knockdown, the TBXT shRNA sOPTiKD hESC line was employed and the differentiation was performed following the protocol described above in the constant presence of 1µg/ml tetracycline hydrochloride. Cells were kept in dark upon tetracycline treatment.

Table 2.8. List of agonists/antagonists used during the trunk neural crest differentiation

Conditions	Component	Stock Conc.	Final Conc.	Vendor	Cat #
1. WNT, BMP	CHIR99021	10 mM	1 μM	Tocris	4423
	BMP4	50 μg/ml	15 ng/ml	Thermo Fisher	PHC9533
	DMH-1	10 mM	1 μM	Tocris	4126/10
	SB431542	10 mM	2 μM	Tocris	1614/1
2. WNTi, BMP	XAV 939	10 mM	1 μM	Tocris	3748
	BMP4	50 μg/ml	15 ng/ml	Thermo Fisher	PHC9533
	DMH-1	10 mM	1 μM	Tocris	4126/10
	SB431542	10 mM	2 μM	Tocris	1614/1
3. WNT, BMPi	CHIR99021	10 mM	1 μM	Tocris	4423
	LDN-193189	10 mM	100 nM	Tocris	6053
	SB431542	10 mM	2 μM	Tocris	1614/1
4. WNT, BMP, FGFi	CHIR99021	10 mM	1 μM	Tocris	4423
	BMP4	50 μg/ml	15 ng/ml	Thermo Fisher	PHC9533
	DMH-1	10 mM	1 μM	Tocris	4126/10
	SB431542	10 mM	2 μM	Tocris	1614/1
	PD0325901	10 mM	1μM	Merck	PZ0162

For neutral conditions and in order to eliminate the effect of extrinsic signals on NMP downstream differentiation, day 3 TBXT shRNA sOPTiKD NMPs generated in the presence/absence of 1µg/ml tetracycline hydrochloride were dissociated following Accutase treatment and plated at 50,000 cell/cm^2 on GTX-coated multiwell plates in basal medium (N2B27) (Table 2.6) supplemented with 10 µM Y-27632 2HCl in the presence/absence of 1µg/ml tetracycline hydrochloride. Media was replenished every 2 days and Y-27632 2HCl was withdrawn after 48 hours. The differentiation was terminated at day 7 and cells were fixed/harvested for analysis.

2.1.3.5. Early spinal cord progenitor differentiation

For early spinal cord progenitor differentiation, day 3 hPSC-derived NMPs were dissociated using Accutase solution and plated at 37,500 cells/cm^2 on GTX-coated plates in early spinal cord progenitor induction medium (Table 2.9) in the presence/absence of 1µg/ml tetracycline

hydrochloride and supplemented with 10 μM Y-27632 2HCl (for the first day only). Medium was replenished every 2 days and the differentiation was terminated at day 7 for subsequent analysis.

Table 2.9. Early spinal cord progenitor induction medium

	Component	Stock Conc.	Volume for 50ml	Final Conc.	Vendor	Cat #
N2B27 media	Neurobasal	1x	23.75ml	0.5X	Thermo Fisher	21103049
	DMEM/F12	1x	23.75ml	0.5X	Merck	D6421
	NEAA	100x	0.5ml	1X	Thermo Fisher	11140050
	GlutaMAX	100x	0.5ml	1X	Thermo Fisher	35050061
	N2	100x	0.5ml	1X	Thermo Fisher	17502048
	B27	50x	1ml	1X	Thermo Fisher	17504044
	2-Mercaptoethanol	50 mM	50 μl	50 μM	Thermo Fisher	31350010
	CHIR99021	10 mM	15 μl	3 μM	Tocris	4423
	FGF2	10 μg/ml	500 μl	100 ng/ml	R&D Systems	233-FB/CF

2.1.3.6. Paraxial mesoderm differentiation

For paraxial mesoderm differentiation, day 3 hPSC-derived NMPs were dislodged into single cells following Accutase treatment and re-plated at a density of 45,000 cells/cm^2 on GTX-coated plates in paraxial mesoderm induction medium (Table 2.10) including 10 μM Y-27632 2HCl (for the first day only). Medium was replenished the day after plating (day 4) and cells were fixed/collected for analysis the following day (day 5).

Table 2.10. Paraxial mesoderm induction medium

	Component	Stock Conc.	Volume for 50ml	Final Conc.	Vendor	Cat #
N2B27 media	Neurobasal	1x	23.75ml	0.5X	ThermoFisher	21103049
	DMEM/F12	1x	23.75ml	0.5X	Merck	D6421
	NEAA	100x	0.5ml	1X	ThermoFisher	11140050
	GlutaMAX	100x	0.5ml	1X	ThermoFisher	35050061
	N2	100x	0.5ml	1X	ThermoFisher	17502048
	B27	50x	1ml	1X	ThermoFisher	17504044
	2-Mercaptoethanol	50 mM	50 μl	50 μM	ThermoFisher	31350010
	CHIR99021	10 mM	40 μl	8 μM	Tocris	4423
	FGF2	10 μg/ml	200 μl	40 ng/ml	R&D Systems	233-FB/CF

2.2. Molecular techniques

2.2.1. Real-time Polymerase Chain Reaction (qPCR)

RNA extraction

Cell pellets stored either at -80^{o}C or at room temperature after cell harvesting were proceeded for RNA extraction using total RNA purification plus kit (Norgen BioTek, #48200). Up to 3 x 10^{6} cells were lysed in a mixture of 350 µl Buffer RL and 1:10 of 2- Mercaptoethanol and sufficient lysis was achieved by swirling sample. Lysate was next transferred to a gDNA Removal Column assembled with a collection tube and centrifuged at 14,000 x g for 1 minute. After centrifugation, the flow through containing the RNA was retained and kept on ice to avoid degradation until the protocol was carried out. Next, 100% ethanol was added into the collection tube (60 µl of 100% ethanol to every 100 µl of RNA sample) and sample was mixed by vortexing. Following that, the lysate with ethanol was transferred to an RNA Purification Column with one of the provided collection tubes attached and centrifuged for a second time at 4,000 x g for 1 minute at 4^{o}C. After centrifugation, the RNA was bound to the column and washed by applying 400 µl of Wash solution A to the column and spun at 14,000 x g for 1 minute at 4^{o}C. The washing step was repeated three times and the flow through was discarded prior to every washing. When the successive washing steps were completed the flow through was again discarded and the column was centrifuged for a final time at 14,000 x g for 2 minute at 4^{o}C to dry thoroughly. The column was then placed into a new 1.7 ml Elution tube before 30 µl of Elution Solution A was applied directly onto the centre of the column. The sample then was centrifuged at 200 x g for 2 minute and this was followed by a second spin at 14,000 x g for 1 minute at 4^{o}C. To achieve a maximum RNA recovery, the eluted sample was passed again through the column and centrifuged for 2 successive rounds as described above.

Purified RNA concentration was measured using Nanodrop Lite Spectrophotometer (Thermo Fisher) by determining the absorbance at 260 nm, and RNA purity was evaluated based on a ratio of the absorbance reading at 260 nm and 280 nm (A260/280). RNA sample with ratio ranging from 2,0 ± 0,2 was considered pure. The isolated RNA was stored at -80^{o}C until cDNA synthesis (next step).

Reverse Transcription

CDNA synthesis was performed using the High-Capacity cDNA Reverse Transcription Kit (Thermo Fisher, #4368813) according to manufacturer instructions. Each reaction was carried out at a final volume of 20 µl and 2 µg of total RNA was converted to 2 µg of single-stranded cDNA per 20- µl reaction. All kit components apart from the enzyme (MultiScribe™ Reverse

Transcriptase) were fully thawed on ice before use. First, the RT master mix was prepared in a sterile tube by pipetting, after adequate vortexing, kit components as follows: 2 µl of 10X RT buffer, 0.8 µl of 25X dNTP Mix (100mM), 2 µl 10X RT Random Primers and 1 µl of MultiScribe™ Reverse Transcriptase used straight from -20 °C. The above volumes account for a single reaction and these numbers were adjusted to the total number of reactions taking place by multiplying the volumes with the amount of samples used. Also, additional reactions were included in the calculations to ensure adequate volume following reagent transfer loss. For example, for 3 samples a RT master mix for 5 reactions (3+2) was prepared by mixing 10 µl of 10X RT buffer, 4 µl of 25X dNTP Mix (100mM), 10 µl 10X RT Random Primers and 5 µl of MultiScribe™ Reverse Transcriptase. The RT master mix then was mixed gently and stored on ice until used. Following that, 2 µg of total RNA per sample was transferred into 200 µl PCR tubes and RNAse free water was subsequently added to a final volume of 14.2 µl. Then, 5.8 µl of the RT master mix was transferred into each tube containing the RNA sample, the content was thoroughly mixed by pipetting and samples were quickly spun down to eliminate any air bubbles left. After cDNA RT reaction preparation, 20- µl reaction tubes were loaded into a thermal cycler with conditions programmed as shown in Table 2.11 and the reverse transcription was set to run. When the full thermal cycles were completed, the cDNA RT tubes were stored at -20°C or used directly for quantitative PCR.

Table 2.11. Thermal cycler settings for reverse transcription

	Step 1	Step 2	Step3	Step 4
Temperature °C	25	37	85	4
Time	10 min	120 min	5 min	∞

Quantitative Polymerase Chain Reaction (qPCR)

RT-qPCR was performed using the Applied Biosystems QuantStudio™ 12K Flex thermocycler in combination with the Roche Universal Probe Library system* and the TaqMan™ Fast Universal PCR Master Mix no AmpErase™ UNG (Applied Biosystems, #4366072) following manufacturer instructions. Amplification was carried out in 384 well plates (LW2960) provided by Alpha Laboratories.

For each primer set, a gene specific master mix was prepared in 1.5 ml Eppendorf by adding the following volumes per reaction: 5 µl Taqman Mix, 0.2 µl Primer Mixture Forward-Reverse (100 µM), 2.7 µl Nuclease free water and 0.1 µl of the appropriate probe. Primers (Table 2.13) were designed using the Universal Probe Library Assay Design Centre* and oligonucleotides were ordered from Integrated DNA Technologies (https://eu.idtdna.com/site/order/oligoentry). The

oligonucleotides of forward and reverse primers were resuspended in TE buffer to a recommended 100 µM stock concentration as per IDT instructions.

The stock solution of cDNA for each sample was diluted 1:20 to obtain a concentration of 5 ng/µl for the qPCR working stock. Amplification was performed in triplicates by transferring 8 µl of gene specific master mix and 2 µl of qPCR cDNA solution in a well of a 384 well plate. To identify contaminating sequences, nuclease free water was used instead of cDNA solution per gene specific master mix as a negative control. For each sample, mainly GAPDH or occasionally TBP housekeeping genes were used in triplicates as a positive amplification control and reference gene for relative quantification normalization (see qPCR data processing section below). After plating, qPCR well plates were sealed, centrifuged briefly to bring components to the bottom of the well and loaded into the thermocycler before a "fast" qPCR cycle was set.

Table 2.12. Instrument's settings for qPCR

Step	Enzyme activation	Denaturation	Annealing/ Elongation
Temperature °C	95	95	60
Time	20 sec	1 sec	20 sec
Cycles	1	40	

**The Roche Universal Probe Library system was discontinued during the course of my PhD and predesigned primers/probe mixtures from the PrimeTime qPCR Probe assay from IDT were also employed.*

For PrimeTime qPCR Probe Assay

Predesigned primers/probes (Table 2.14) were resuspended in TE buffer as 20X stocks and each reaction was performed by combining: 5 µl Taqman mix, 0.5 µl PrimeTime assay Mix, 2.5 µl Nuclease free water and 2 µl of CDNA (5 ng/µl).

qPCR data processing

Analysis of qPCR data was performed using the relative quantification method normalized to a reference gene (GAPDH or TBP). For multiple sample comparison, one untreated or baseline sample served as control and the relative amount of mRNA in all samples was expressed as an increase or decrease relative to the control.

The amount of template present at the start of the amplification reaction, known as threshold cycle C_T, was measured for all genes across samples and was subsequently used to determine the expression level of a target gene using the Livak method, also known as the $2^{-\Delta\Delta CT}$ formula (Livak and Schmittgen 2001), in 4 steps.

Step 1: The expression of a target (TAR) gene was normalised to reference (REF) gene expression levels within the same sample, for both treated (TR) and control (CTL) sample per each technical repeat (replicate n), to determine the ΔC_T:

$$\Delta C_{T(TR,\ replicate\ n)} = C_{T(TAR,\ TR,\ replicate\ n)} - C_{T(REF,\ TR,\ replicate\ n)}$$
$$\Delta C_{T(CTL,\ replicate\ n)} = C_{T(TAR,\ CTL,\ replicate\ n)} - C_{T(REF,\ CTL,\ replicate\ n)}$$

Step 2: The ΔC_T of the treated sample was normalised to the ΔC_T of the control, following calculation of the average of the technical replicates for the target gene in the control:

$$\Delta C_T\ average_{(TAR,\ CTL)} = Sum\ [\Delta C_{T\ (replicate\ n)}] / number\ of\ technical\ replicates$$
$$\Delta\Delta C_{T\ (replicate\ n)} = \Delta C_{T(TR,\ replicate\ n)} - \Delta C_T\ average_{(TAR,\ CTL)}$$

Step 3: The relative quantity (RQ) of a target gene normalised to a reference gene and relative to the control sample was measured as follows:

$$RQ_{\ (replicate\ n)} = 2^{-\Delta\Delta C_T\ (replicate\ n)}$$

Step 4: The average from the technical replicates for the relative amount of a target gene relative to control sample was calculated per biological experiment:

$$Mean\ RQ = Sum\ [RQ_{\ (replicate\ n)}] / number\ of\ technical\ replicates$$

The mean RQ values from technical replicates (3 technical replicates were run at all times) per biological experiment are plotted in each graph in the results chapters.

Table 2.13. List of qPCR primer sets compatible with the Universal Probe Library system used for qPCR analysis

Gene	Forward primer	Reverse primer	Roche UPL Probe
GAPDH	5'-agccacatcgctcagacac-3'	5'-gcccaatacgaccaaatcc-3'	#60†
GAPDH	5'-ccccggtttctataaaattgagc-3'	5'-cttccccatggtgtctgag-3'	#63†
TBP	5'- gaacatcatggatcagaacaaca-3'	5'-atagggattccgggagtcat-3'	#87†
NANOG	5'-agatgcctcacacggagact-3'	5'-ggactggtggaagaatcagg-3'	#69
OCT4	5'-gtggagagcaactccgatg-3'	5'- tgcagagctttgatgtcctg-3'	#78
HOXA1	5'- gacgaccgcttcctagtgg-3'	5'- tcccggaagtctggtaggta-3'	#9
HOXA2	5'-caagaaaaccgcacttctgc-3'	5'-tgtgttggtgtaagcagttctca-3'	#5
HOXA3	5'-gacagctcatgaaacggtctg-3'	5'-ggtttgacacccgtgagg-3'	#70
HOXA4	5'-gttgccacccaagagagaac-3'	5'-ccaagtagtccttctcaggtatcc-3'	#20
HOXA5	5'-gcgcaagctgcacataag-3'	5'-cggttgaagtggaactcctt-3'	#1
HOXA6	5'-ggaaaacaagctcatcaattcc-3'	5'-cctgcccaggcatctactc-3'	#26
HOXB1	5'-ccagctaggggcttgtc-3'	5'-atgctgcggaggatatgg-3'	#39
HOXB2	5'-aatccgccacgtctcctt-3'	5'-gctgcgtgttggtgtaagc-3'	# 70
HOXB3	5'-agctgctgaactgtccgttt-3'	5'-ccaggtccacgatgattttt-3'	#3
HOXB4	5'-aaaccaggccccttcctac-3'	5'-gcacacagatattcacacatacga-3'	#45
HOXB4	5'-ctggatgcgcaaagttcac-3'	5'-agcggttgtagtgaaattcctt-3'	#62
HOXB5	5'-aagcttcacatcagccatga-3'	5'-cggttgaagtggaactccttt-3'	#1
HOXB6	5'-tggaagctgaagaagaaactgaa-3'	5'-gccgggtttatgatttgttg-3'	#12
HOXB7	5'-ctacccctggatgcgaag-3'	5'-caggtagcgattgtagtgaaattct-3'	#1
HOXB8	5'-agctcttcccctggatgc-3'	5'-atagggattaaataggaactccttctc-3'	#1
HOXB9	5'-ccgccccttgtagaaaaat-3'	5'-tgtctacagtggggttgacct-3'	#39
HOXC4	5'-agccaattctcatccttctcc-3'	5'-caatgcaaaaggcctaagga-3'	#12
HOXC5	5'-cccgggatgtacagtcagaa-3'	5'-gcctgctcctctttgatctc-3'	#25
HOXC6	5'-tgaattcctacttcactaacccttc-3'	5'-atcataggcggtggaattga-3'	#87
HOXC8	5'-tcccagcctcatgtttcc-3'	5'-tgataccggctgtaagtttgc-3'	#86

HOXC9	5’-tcctagcgtccaggtttcc-3’	5’-gctacagtccggcaccaa-3’	#70†
HOXC9	5’-gcagcaagcacaaagagga-3’	5’-cgtctggtacttggtgtaggg-3’	#85†
HOXC10	5’-aggagagggccaaagctg-3’	5’-agccaatttcctgtggtgtt-3’	#19
HOXD1	5’-caccctggtgctttccag-3’	5’-agagacggacttggggtagg-3’	#57
HOXD3	5’-tcaagaaaacacacacatacataattg-3’	5’-tgctgaatcctgagagagctg-3’	#1
HOXD8	5’-cccttgtaatcgcctgaaat-3’	5’-ctactgaaaataacggaacacagc-3’	#83
SOX9	5’-gtacccgcacttgcacaac-3’	5’-tctcgctctcgttcagaag-3’	#61
SOX10	5’-ggctcccccatgtcagat-3’	5’-ctgtcttcggggtggttg-3’	#21
PAX3	5’-aggaggccgacttggaga-3’	5’-cttcatctgattggggtgct-3’	#13
PAX7	5’-gaaaacccaggcatgttcag-3’	5’-gcggctaatcgaactcactaa-3’	#66
ASCL1	5’-cgacttcaccaactggttctg-3’	5’-atgcaggttgtgcgatca-3’	#38
PHOX2B	5’-ctaccccgacatctacactcg-3’	5’-ctcctgcttgcgaaacttg-3’	#17
TFAP2A	5’-aacatgctcctggctacaaaa-3’	5’-aggggagatcggtcctga-3’	# 62
PAX6	5’- gcacacacacattaacacacttg-3’	5’-ggtgtgtgagagcaattctcag-3’	#9
CDX2	5’-atcaccatccggaggaaag-3’	5’-tgcggttctgaaaccagatt-3’	#34
OTX2	5’-ccatctccccactgtcagat-3’	5’-ggtcatgggataggacctctg-3’	#4
ETS1	5’-gcagaatgagctactttgtgga-3’	5’-ttgctaggtccttgcctca-3’	#3
TCF1	5’-cagagactcttcccggacaa-3’	5’-agcagattgaaggcggagta-3’	#65
LEF1	5’-cgacacttccatgtccaggt-3’	5’-atgagggatgccagttgtgt-3’	#79
SOX1	5’-gaagcccagatggaaatacg-3’	5’-ggacaaggaagggtgttgag-3’	#66
SOX2	5’- ttgctgcctctttaagactagga-3’	5’- taagcctggggctcaaact-3’	#35†
SOX2	5’-atgggttcggtggtcaagt-3’	5’-ggaggaagaggtaaccacagg-3’	#19†
AXIN2	5’-gatatccagtgatgcgctga-3’	5’-actgcccacacgataaggag-3’	#56
SPRY4	5’-ccccggcttcaggattta-3’	5’-ctgcaaaccgctcaatacag-3’	#17
TBXT	5’-aggtacccaaccctgagga-3’	5’-gcaggtgagttgtcagaataggt-3’	#23
NKX1-2	5’-gtcgaagcggggaaagat-3’	5’-gatcctccgcatcctcct-3’	#78
CALB2	5’-gcgatcttcacattttacgaca-3’	5’-tcatttccttttgtttttctcg-3’	#42
SST	5’-accccagactccgtcagttt-3’	5’-acagcagctctgccaagaag-3’	#38

CHAT	5'-cagccctgatgccttcat-3'	5'-cagtcttcgatggagcctgt-3'	#78
TH	5'-acgccaaggacaagctca-3'	5'-agcgtgtacgggtcgaact-3'	#42
HTR2A	5'- tgatgtcacttgccatagctg-3'	5'- caggtaaatccagactgcacaa3'-	#3
S100B	5'-gagctttcccatttcttagagga-3'	5'- gaagtcacattcgccgtctc-3'	#47
S100B	5'-ggaaggggtgagacaagga	5'- ggtggaaaacgtcgatgag-3'	#78
PRPH	5'-aagacgactgtgcctgaggt-3'	5'- tgctccttctgggactctgt-3'	#10
cRET	5'-catcaggggtagcgaggtt-3'	5'- gggaaaggatgtgaaaaca-3'	#17
TRKC	5'- ccgtacgagagggtgacaat-3'	5'- tggtccagttcagattggtct-3'	#21
GFRA1	5'- caccattgccctgaaagaat-3'	5'- cgcttttaggggttcaggtc-3'	#36

†Alternative primer sets were used for some genes due to shortage in fluorescent probes as The ROCHE UPL system was discontinued in December 2021.

Table 2.14. Pre-validated IDT PrimeTime qPCR primers used for qPCR analysis

Gene	Assay ID
GAPDH	Hs.PT.39a.22214836
NOTCH1	Hs.PT.58.23074795
NOTCH2	Hs.PT.58.28296019
HES1	Hs.PT.58.4181121
HES5	Hs.PT.58.14966721.gs
HES6	Hs.PT.58.4357258.g
JAG1	Hs.PT.56a.4972610
JAG2	Hs.PT.58.3493191
DLL1	Hs.PT.58.41063402
DLL3	Hs.PT.58.21516515
DLL4	Hs.PT.58.3416363

2.2.2. RNA-seq

Day 3 NMPs derived from TBXT shRNA sOPTiKD hESC line treated with or without tetracycline for Tet-mediated knock down were harvested and proceeded for RNA purification using the method described above (2.2.1). Samples from three biological replicates per condition were used for RNA-seq and quality control. Library construction and sequencing were carried out by

Novogene (http://en.novogene.com) as described in materials and methods section of Gogolou et al. (2022).

In brief, library preparation was carried out using the NEB Next Ultra RNA Library Prep Kit and sequencing was performed on an Illumina NoveSeq platform (PE150). Reads were processed through FastQCv0.11.2 (https://www.bioinformatics.babraham.ac.uk/projects/fastqc/) and Trim Galore (https://www.bioinformatics.babraham.ac.uk/projects/trim_galore/). Reads were aligned to the human reference genome assembly GRCh38 (Ensembl Build 79) in the two-pass mode using STAR v2.4.2a (Dobin et al. 2013). The RSEM v1.3.0 (Li and Dewey 2011) was used to extract expected gene counts, where genes expressed in <3 samples or with total counts ≤5 among all samples were excluded. Genes showing significant differential expression were identified with DESeq2 (Love et al. 2014), with log2FoldChange>|0.5| and Benjamini–Hochberg-adjusted p<0.05. Data were deposited to GEO (Accession number: GSE184620).

2.2.3. ChIP-seq

Sample preparation was performed according to Active Motif protocol (www.activemotif.com). Day 3 NMPs derived from TBXT shRNA sOPTiKD hESCs without tetracycline treatment and undifferentiated counterparts (10 million cells/sample; three pooled replicates per sample) were fixed with 1:10 formaldehyde solution (11% formaldehyde, 0.1M NaCl, 1mM EDTA (pH 8.0), 50mM HEPES (pH 7.9)) for 15 minutes at room temperature on a shaking apparatus. Fixation was stopped by adding 1:20 volume glycine solution (2.5 M glycine) for 5 minutes at room temperature and cell colonies were obtained in suspension by scraping the culture vessel's surface. Cells were spun down for 10 min at 800 x g at 4^{o}C and pellets were resuspended in 10 ml chilled PBS-Igepal (1X PBS (pH 7.4), 0.5% Igepal CA-630, (Merck, #I-8896)). The wash step was repeated and pellets were resuspended in 10 ml chilled PBS-Igepal and 1mM PMSF (Merck, #P-7626). Samples were spun down for a third time, pellets were snap-frozen and stored at -80 ^{o}C until they were shipped to Active Motif (Carlsbad, CA) for downstream sample preparation, library construction and sequencing as described in Gogolou et al. (2022).

In brief, cells were lysed and sonicated using Active Motif's EpiShear probe sonicator (cat# 53051) to obtain 300–500 bp DNA fragments. Genomic DNA was subjected to RNase, proteinase K treatment, heat for de-crosslinking and was cleaned using SPRI beads (Beckman Coulter) prior to quantitation. The genomic DNA was used as input control and extrapolation to the original chromatin volume allowed the determination of the total chromatin yield. Chromatin (50 µg) was precleared with protein G agarose beads (Invitrogen) and genomic DNA regions of interest were isolated using 4 µg of antibody against Brachyury (R&D Systems, cat# AF2085, lot#

KQP0719121). Complexes were washed, eluted from the beads with SDS buffer, and treated with RNase and proteinase K. Protein-DNA complexes were reverse-crosslinked at 65 °C overnight and ChIP DNA was purified by phenol-chloroform extraction and ethanol precipitation. qPCR reactions were performed on genomic regions of interest using SYBR Green Supermix (Bio-Rad). Illumina sequencing libraries were prepared from the ChIP and Input DNAs following the enzymatic steps of end-polishing, dA-addition, and adaptor ligation on an automated system (Apollo 342, Wafergen Biosystems/Takara). After a final PCR amplification step, the resulting DNA libraries were quantified and sequenced on Illumina's NextSeq 500 (75 nt reads, single end). Reads were aligned to the human genome (hg38) using the BWA algorithm (default settings; Li and Durbin 2009). Only uniquely mapped reads (mapping quality >25) were used for further analysis and multiple reads mapped to the same location were removed. Alignments were extended in silico at their 3'-ends to a length of 200 bp, which is the average genomic fragment length in the size-selected library, and assigned to 32-nt bins along the genome. Peak locations were determined using the MACS algorithm (v2.1.0) (Zhang et al. 2008) with a cut-off of p-value= 1e–7 and further analysis was performed using Active Motifs proprietary analysis program. Motif analysis was carried out using the Homer software (Heinz et al. 2010). Regions of 200 bp surrounding the summit of the top 2500 peaks (based on MACS2 p-values) were analysed. Data were deposited to GEO (Accession number: GSE184622).

2.2.4. ATAC-seq

Day 3 NMPs and day 8 trunk NC cells (50,000 cells/sample) derived from TBXT shRNA sOPTiKD hESCs with or without tetracycline treatment (three biological replicates per condition/time point) were harvested, counted aiming for viability >85-90% and processed for tagmentation using the Illumina Tagment DNA Enzyme and Buffer Small Kit (Illumina, #20034197), 1% Digitonin (Promega, #G9441) and EDTA-free Protease Inhibitor cocktail (Roche, #11873580001) according to manufacturer instructions. Differentiation and preparation of day 3 NMP samples was carried out by Celine Souilhol. DNA was purified using Qiagen MinElute kit (#28004) and samples were eluted in 12 µl EB buffer in 1.5 ml Eppendorf DNA LoBind tubes (Merck, # EP0030108051). DNA samples were stored for short period at -20 ^{o}C and were sent to the Biomedical Sequencing Facility at CeMM (Research Center for Molecular Medicine of the Austrian Academy of Sciences, Vienna) for library preparation, sequencing and downstream analysis as described in Gogolou et al. (2022).

In short, 1 µl of eluted DNA was used in a qPCR reaction to determine the optimal number of amplification cycles and following that, the rest 11 µl of DNA were amplified in a second round of qPCR. The total amplified DNA was selected for fragments of size between 150 bp and 1200 bp

using AMPure beads (Beckman Coulter). Library amplification was performed using custom Nextera primers. DNA concentration was measured with a Qubit fluorometer (Life Technologies) and library profile was checked with Bioanalyzer High Sensitivity assay (Agilent Technologies). Libraries were sequenced by the Biomedical Sequencing Facility at CeMM (Research Center for Molecular Medicine of the Austrian Academy of Sciences, Vienna) using the Illumina HiSeq 3000/4000 platform and the 50 bp single-end configuration. Base calling was performed by Illumina Real Time Analysis (v2.7.7) software and the base calls were converted to short reads using the IlluminaBasecallsToSam tool from the Picard toolkit (v2.19.2) ('Picard Toolkit' 2019. Broad Institute, GitHub Repository. http://broadinstitute.github.io/picard/; Broad Institute). Sequencing adapters were removed, and the low-quality reads were filtered using the fastp software (v 0.20.1) (Chen et al. 2018) . Alignment of the short reads on GRCh38 was performed using Bowtie2 (v2.4.1) (Langmead and Salzberg 2012) with the '-very-sensitive' parameter. The PCR duplicates were marked using samblaster (v0.1.24) (Faust and Hall 2014), and the reads mapped to the ENCODE black-listed (Amemiya et al. 2019) regions were discarded prior to peak calling. To detect the open chromatin regions, peak calling was performed using the MACS2 (v2.2.7.1) (Zhang et al. 2008) software. Peaks in the format of bed files were analysed for differential analysis to compare signals corresponding to the + vs –Tet samples using the GUAVA software. Differential peaks with a distance from TSS ranging from –1–1 kb, log2FC cutoff = 1 and p-value< 0.05 were extracted. Finally, HOMER findMotifs (v4.11) (Heinz et al. 2010) was used for motif enrichment analysis over the detected open chromatin regions. Data were deposited to GEO (Accession number: GSE184227).

2.2.5. Immunofluorescence microscopy and flow cytometry

2.2.5.1. Immunocytochemistry (adherent cultures)

Plates that were to be immunostained were firstly fixed, incubated with permeabilisation buffer, blocked and lastly, proceeded for intracellular staining.

Fixation

Plates were washed once with PBS (without Ca^{2+}, Mg^{2+}) before 4% of PFA (Merck, #P6148; made according to manufacturer's instructions) was added to fix cells. Plates were incubated for 10 minutes at room temperature before PFA was removed. Following that, an additional wash with PBS was performed before cell permeabilisation. Plates that were not to be immunostained directly, were stored with excess PBS, sealed thoroughly with parafilm to prevent sample from drying and stored at 4°C for long periods (up to 12 months).

Permeabilisation

For intracellular marker staining, cells were subsequently permeabilised with permeabilisation buffer containing 10% (v/v) Fetal Calf Serum (FCS), 0.1% (w/v) Bovine Serum Albumin (BSA) and 0.5% (v/v) Triton X-100 in 1X PBS and incubated for 15 minutes at room temperature. After incubation, cells were washed with PBS.

Blocking

Following permeabilisation, cells were incubated in blocking buffer consisted of 10% FCS and 0.1% BSA in 1X PBS for 1 hour at room temperature or alternatively kept overnight at 4°C. After blocking, cells were washed with PBS and were either stored at 4°C or proceeded directly for staining.

Antibody staining

Primary and secondary antibodies were diluted separately in blocking buffer at a working concentration following manufacturer instructions or after performing a series of dilutions in a titration experiment for optimal signal detection (Table 2.15).

Diluted primary antibody was added to wells and plates were incubated on a rocking platform for 24-48 hours at 4°C. Following primary antibody incubation, a minimum of three 5-minute washes with PBS were performed and fluorophore-conjugated secondary antibody solution was added to the stained samples. Secondary antibody solution was prepared by mixing secondary antibody at an optimal concentration with nuclear counterstain solution Hoechst 33342 (Thermo Fisher Scientific, #H3570) at 1:5000 in blocking buffer. Cells were incubated for 1-2 hours at room temperature or overnight at 4°C in a dark environment. After secondary antibody incubation, three 5-minute washes with PBS were performed and samples were proceeded for analysis. A well incubated with secondary antibody solution was used at all times as a negative control.

In case the secondary antibody and the nuclear stain solution were prepared separately, cells were incubated with secondary antibody for 1 hour at room temperature or overnight at 4°C in dark, washed twice with PBS before nuclear stain solution was added to wells (1:1000 or 1:5000). Samples were incubated for 10 minutes at room temperature in dark and subsequently washed twice with PBS. When washing steps were completed, plates were filled with PBS, sealed thoroughly to avoid liquid evaporation, covered with aluminium foil and stored at 4°C until visualisation. Fluorescent images were acquired using the InCell Analyser 2200 system (GE Healthcare).

For ENS culture characterisation, stained cells grown on coverslips were mounted on 75x25 mm glass slides (VWR, Menzel Gläser, SuperFrost® Plus) using 8-12 µl of VECTASHIELD mounting media (2B Scientific, #H-1700-10) and left to dry in dark before imaging or before storing them at 4°C. Mounting of coverslips was performed carefully to avoid introducing bubbles in the samples to be analysed. Fluorescent images were acquired using a LSM800 confocal system with Airyscan detectors (Zeiss) and data were processed using the available Zeiss software.

2.2.5.2. Flow cytometry analysis

Antibody staining for cell surface markers (live cells)

Cells were washed with PBS and detached in a single cell suspension following incubation with Accutase at 37 °C for 5-7 minutes. After incubation period, cell suspension was neutralised using FACS buffer (PBS/10% FCS) and centrifuged at 1100 rpm for 4 minutes. Samples obtained from late stages of differentiation and that were not completely dissociated were passed through a 70 µm strainer (Miltenyi Biotec, #130-110-916) to ensure adequate single cell dissociation. In the meantime, cells were counted and cell pellet was re-suspended at a concentration $2x10^6$ cells/ ml. For flow cytometry analysis, 100 µl of cell solution was transferred into a falcon 5mL round bottom test tube (SLS, # 352053) and primary antibody was added at the appropriate dilution as shown on Table 2.16. Cell suspension/antibody mixture was incubated for 20 minutes at 4°C and subsequently washed with 4 ml of FACS buffer. Following centrifugation at 1100 rpm for 4 minutes, supernatant was aspirated leaving around 100 µl of media into the tube. Then, 100 µl of secondary antibody solution was added at the appropriate dilution into each tube and cell suspension/antibody mixture was incubated for 20 minutes at 4°C protected from light. After the incubation period, samples were washed, cell pellets were resuspended in 0.2 ml of FACS buffer and proceeded for analysis. A separate negative control stained with secondary antibody only or an isotype control (P3X) were used to set the baseline fluorescence. In particular, P3X is an antibody secreted from the parent myeloma used for the derivation of all in house hybridomas (Table 2.16) and it was used to determine non-specific binding due to its minimal reactivity to human cells (Kohler and Milstein 1975).

Antibody staining for intracellular markers (fixed cells)

Cells to be analysed were first washed with PBS, detached into single cell suspension following accutase treatment, counted and fixed in suspension with 4% PFA for 10 minutes at room temperature. After fixation, samples were washed with blocking buffer and resuspended in permeabilisation buffer for 10 minutes at room temperature. Following that, a quick wash was performed and samples were incubated with primary antibody diluted in blocking buffer on a rocking platform overnight at 4°C. After the incubation period and a wash, secondary antibody diluted in blocking buffer was added and samples were incubated again for 1 hour on a rocking platform at room temperature and protected from light. Primary and secondary antibodies were diluted in 200 µl and staining was performed in samples containing 10^5-10^6 cells. Following that, a final wash was performed, cell pellets were resuspended in 0.2 ml blocking buffer and proceeded for analysis. A separate negative control stained with secondary antibody only was used to set the baseline fluorescence in all channels.

Flow cytometry analysis was performed with FACSJazz™ Cell Sorter instrument (BD Biosciences) and data were analysed/visualised using the software package FlowJo™ v10.8 (BD Life Sciences).

2.2.5.3. Fluorescence Activated Cell Sorting (FACS)

Day 6 vagal NC cells derived from the H9SOX10:GFP reporter cell line were harvested into single cells and stained for the cell surface marker CD49d following the protocol described above. Following laser alignment and setting the drop delay for sorting with the use of Accudrop beads, samples were run through the machine for analysis and in order to set the sorting gates. The baseline fluorescence for the GFP channel was set using undifferentiated unlabelled cells of the parental cell line (H9), while for the far-red channel the baseline fluorescence was set using undifferentiated unlabelled cells (H9) and/or day 6 SOX10:GFP differentiated cells stained with the isotype control P3X. TRA-1-85, a pan-human antibody was used as positive control. Cell sorting was performed using the FACSJazz™ Cell Sorter instrument (BD Biosciences). Sorted samples were collected in falcon tubes and processed for RNA extraction. After cell sorting, a small sample of the isolated populations was reanalysed in the machine for purity control (>95% purity).

Table 2.15. List of primary antibodies used for immunocytochemistry

Antibody	Company	Cat #	Species	Class	Dilution
Anti-SOX10	CST	89356	Rabbit	mAb	1:500
Anti-SOX10	R&D systems	AF2864	Goat	pAb	1:200
Anti-beta III Tubulin(TuJ1)	Abcam	ab78078	Mouse	mAb	1:1000
Anti-beta III Tubulin(TuJ1)	BioLegend	PRB-435P	Rabbit	pAb	1:1000
Anti-TrkC	CST	3376	Rabbit	mAb	1:500-1000
Anti-peripherin	Millipore Sigma	AB1530	Rabbit	pAb	1:60-1:100
Anti-peripherin	Novus Biolog.	NBP1-05423	Chicken	pAb	1:200
Anti-PGP9.5	Abcam	ab108986	Rabbit	mAb	1:1000
Anti-S100 (β-Subunit)	Millipore Sigma	S2532	Mouse	mAb	1:1000
Anti-S100	Dako Omnis	Z0311	Rabbit	pAb	1:50-1:250
Anti-Phox2b	Santa Cruz	sc-376997	Mouse	mAb	1:50
Anti-HuC/HuD	Invitrogen	A-21271	Mouse	mAb	1:60-1:100
Anti-neurofilament heavy polypeptide (NF-H)	Abcam	ab8135	Rabbit	pAb	1:1000
Anti-Choline Acetyltransferase (ChAT)	Millipore Sigma	AB144P	Goat	pAb	1:200
Anti-Tyrosine Hydroxylase (TH)	Millipore Sigma	T1299	Mouse	mAb	1:500
Anti-Substance P	R&D Systems	MAB4375	Mouse	mAb	1:100
Anti-Calretinin	Abcam	ab16694	Rabbit	mAb	1:100
Anti-MASH1/Achaete-scute homolog 1	Abcam	ab211327	Rabbit	mAb	1:100
Anti-Pax6	Abcam	ab195045	Rabbit	mAb	1:200
Anti-CD49d	BioLegend	304302	Mouse	mAb	1:1000
Anti-p75NTR	CST	8238	Rabbit	mAb	1:1000
Anti-Ki67	Abcam	ab238020	Mouse	mAb	1:100
Anti- Alpha-Smooth Muscle Actin (SMA)	Invitrogen	14-9760-82	Mouse	mAb	1:500
Anti-SOX1	R&D systems	AF3369	Goat	pAb	1:100
Anti-SOX2	Abcam	ab92494	Rabbit	mAb	1:400
Anti-Brachyury	Abcam	ab209665	Rabbit	mAb	1:1000
Anti-HOXC9	Abcam	ab50839	Mouse	mAb	1:50

Table 2.16. List of primary antibodies used for flow cytometry

Antibody	Antigen	Species	Dilution	Source	Reference
ME20.4	p75NTR	Mouse	1:20	In House Hybridoma	Ross et al. (1984)
Anti-CD49d	CD49d	Mouse	1:1000	BioLegend (#304302)	-
63-AG8	P3X	Mouse	1:10	In-House Hybridoma	Kohler and Milstein (1975)
TRA-1-85	TRA-1-85	Mouse	1:50	In-House Hybridoma	Williams et al. (1988)

Table 2.17. List of secondary antibodies used for immunocytochemistry or flow cytometry analysis

Antibody	Conjugate	Company (Cat #)	Dilution	Application
Donkey anti-Goat IgG (H+L)	AF488	Invitrogen (A-11055)	1:1000	ICC, Flow
Donkey anti-Goat IgG (H+L)	AF594	Invitrogen (A-11058)	1:1000	ICC
Donkey anti-Goat IgG(H+L)	AF647	Invitrogen (A-21447)	1:1000	ICC
Donkey anti-Rabbit IgG (H+L)	AF488	Invitrogen (A-21206)	1:1000	ICC, Flow
Donkey anti-Rabbit IgG (H+L)	AF555	Invitrogen (A-31572)	1:1000	ICC
Donkey anti-Rabbit IgG (H+L)	AF594	Invitrogen (A-21207)	1:1000	ICC
Donkey anti-Mouse IgG (H+L)	AFPlus405	Invitrogen (A-11058)	1:1000	Flow
Donkey anti-Mouse IgG (H+L)	AF488	Invitrogen (A-21202)	1:1000	ICC, Flow
Donkey anti-Mouse IgG (H+L)	AF647	Invitrogen (A-31571)	1:1000	ICC, Flow
Donkey anti-Chicken IgY (H+L)	FITC	Invitrogen (SA1-72000)	1:200	ICC
Rat anti-Mouse IgG1	BV421	BioLegend (406615)	5µl/10^6 cells	Flow
Goat anti-Rabbit IgG	BV421	BD Biosc. (565014)	1:500	Flow
Donkey anti-rabbit IgG	BV421	BioLegend (406415)	1:500	Flow

2.3. Image analysis

Fluorescent images acquired either from InCell Analyser 2200 or LSM800 confocal system were processed in Fiji (Schindelin et al. 2012) using identical brightness/contrast settings to allow comparison between different treatments. A sample incubated with secondary antibody solution only was used at all times to set a threshold for the positive signal, minimising labelling artefacts introduced by fluorophore-conjugated secondary antibodies. A positive and negative control sample, whenever it was possible, were included in the analysis for antibody validation. Representative immunofluorescence analysis images showing signal in positive and negative controls together with samples incubated with secondary antibody only are shown in Appendix S6-S7.

2.3.1. Quantification using CellProfiler

Quantification was performed using the image analysis software CellProfiler (Carpenter et al. 2006) and custom made pipelines. Nuclei segmentation was first performed to identify cells and the resulting nuclei were subsequently mapped onto the other fluorescent channels for single-cell fluorescence intensity quantification. A sample stained with secondary antibody solution only was used to set a threshold for the positive signal and cells with fluorescence levels higher than that were classified as positive. Histograms and bar charts were created using FlowJo™ v10.8 Software (BD Life Sciences) and GraphPad Prism (GraphPad Software), respectively.

2.3.2. Quantification using Fiji

Quantification of neural/glial cultures was performed in Fiji, using custom made macros to automate batch processing. The macros used for the analysis are attached in the Appendix. The morphology of the neural cultures (formation of big neural clusters-aggregates, excessive debris and areas of high density) restrains the application of nuclear segmentation tools and reduces the credibility of the acquired data. For this reason, the quantification was performed using the available feature in Fiji after applying a suitable segmentation method (thresholding) and by measuring the area occupied by positive fluorescence signal over the area consisting of total cellular material calculated following nuclear staining.

For HUCD staining:

$$HUCD\%\ of\ Total\ Area = \frac{area\ occupied\ by\ green\ fluorescent\ signal\ (HUCDpos\ cells)}{area\ occupied\ by\ green\ fluorescent\ signal\ (HUCDpos) + area\ occupied\ by\ Hoechst\ pos\ cells}\ x100$$

For SOX10 staining:

$$SOX10\%\ of\ Total\ Area\ = \frac{area\ occupied\ by\ red\ fluorescent\ signal\ (SOX10pos\ cells)}{area\ occupied\ by\ red\ fluorescent\ signal\ (SOX10pos) + area\ occupied\ by\ Hoechst\ pos\ cells}\ x100$$

For S100 staining:

To score the glial population (S100+ cells) we made the assumption that all S100+ cells should be SOX10+. SOX10 expressing cells were first identified using the “Li dark” segmentation method, 30.00-280.00 μm size threshold and their total number was calculated. To score the S100+ cells, for each identified object (SOX10+ cell-nuclear signal), a band of 2 μm expanding into the cytoplasm was created and the intensity of the fluorescent signal within the expanded area was measured in the channel stained for S100. Since the S100 protein is located primarily in the cytoplasm, the expansion of each nucleus identified by nuclear staining for the transcription factor SOX10 was required to allow sufficient calculation of S100 signal falling within the cytoplasmic area. Cells with mean fluorescent intensity greater than in the negative control (secondary only sample) or than the background signal were scored as S100 positive.

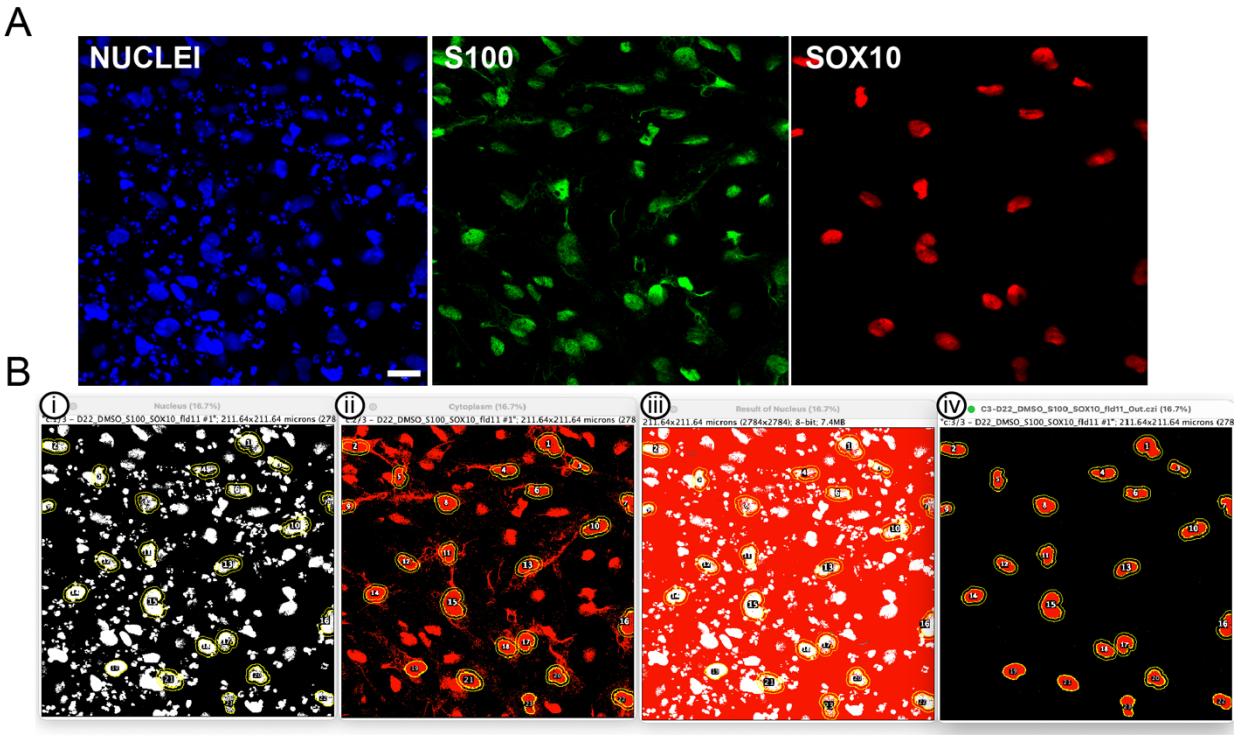

Figure 2.1. Example of the pipeline followed for the quantification of glial cells in hPSC-derived enteric nervous system cultures. (A) Representative immunofluorescence image showing S100 (green) and SOX10 (red) expression in ENS cultures. (B) Snapshots of the analysis performed for the quantification of glia (SOX10+/S1000+) in the image displayed in A. The total cellular material was initially calculated using the "Li dark" thresholding method to identify/mask nuclei stained with Hoechst (white mask) (i), cells emitting green fluorescent cytoplasmic signal (red mask) were identified (ii) and subsequently merged with the previous mask (iii). SOX10+ cells (30.00-280.00 µm) were identified using the "Li dark" thresholding method (iv) and the area occupied by them as well as their numbers were calculated. For measuring the expression of S100, a band of 2 µm was created around each SOX10+ identified nuclei and the fluorescent signal within the expanded area was measured in the green channel.

2.4. Statistical analysis

2.4.1. Imaging

Statistical significance was calculated using GraphPad Prism (GraphPad Software). For all samples the normality of the distribution was examined to decide between parametric or non-parametric test to be performed. When the normality test was not feasible (small sample size/number of subjects), an assumption that the data follow a Gaussian distribution was made (parametric test).

For all immunocytochemistry experiments, unless otherwise stated, the average value from all the fields scored was calculated per biological experiment and the mean values of different biological experiments were plotted in a bar chart. Statistical analysis was performed using the mean values and the appropriate statistical tests provided in GraphPad Prism.

2.4.2. RT-qPCR

For gene expression analysis from RT-qPCR, statistical analysis was performed using GraphPad Prism. This was done by comparing the mean -ΔΔCt values of all biological repeats, calculated by averaging the values of 3 technical replicates and following analysis, the significance was demonstrated in graphs presenting mean RQ values.

Chapter 3: Dissecting human vagal neural crest specification *in vitro*

3.1. Introduction

In vivo, NC development is a step-wise process characterised by a succession of inductive events, activation of discrete sets of transcription factors, tissue specification, migration and eventual differentiation (Stuhlmiller and Garcia-Castro 2012a). This process is tightly modulated by a combination of signals, most notably the BMP, FGF, and Wnt signalling pathway, acting on the neuroepithelium to establish a NC fate (Stuhlmiller and Garcia-Castro 2012a). Several studies have utilised agonist/antagonist combinations of known NC induction cues in order to generate NC cells from *hPSCs in vitro*. TGF-β inhibition, Wnt signalling pathway activation or FGF stimulation combined with moderate levels of BMP have been previously shown to induce NC cells, marked by the expression of HNK1 and/or p75 and SOX10 with various yields (Chambers et al. 2012; Hackland et al. 2017; Lee et al. 2010; Lee et al. 2007; Li et al. 2018; Menendez et al. 2011; Mica et al. 2013). The resulting NC cells, however, lack the expression of *HOX* genes or exhibit expression of the most anterior *HOX* PG e.g. *HOXA2* (Lee et al. 2007) and they are perceived to reflect the cranial subdivision. Commitment to a more caudal/postotic NC population is typically achieved through the addition of caudalising factors, such as retinoic acid (RA) and/or further Wnt activation within a narrow time window (Denham et al. 2015; Fattahi et al. 2016; Frith et al. 2018; Huang et al. 2016; Workman et al. 2017). The aforementioned strategies result in the upregulation of *HOX* genes belonging to anterior-central *HOX* PG (*1-5*), a key feature denoting a vagal regional signature.

Even though such approaches have successfully generated postotic NC cells, the combination/duration of signalling cues used (outlined in Figure 1.8; vagal NC induction takes place up to the first 10-12 days) as well as the methods followed, vary considerably. For instance, some protocols employ neural rosette formation in combination with EGF and FGF signalling cues (Li et al. 2018; Workman et al. 2017), whereas others adopt a monolayer differentiation strategy including the coordinated activity of TGF-β signalling suppression together with BMP activation/inhibition depending on the absence or presence of serum replacement factors, a formulation called knockout serum replacement (KSR) media, respectively, and WNT activation/GSK3 inhibition using CHIR99021 (Barber et al. 2019; Fattahi et al. 2016; Frith et al. 2020; Gogolou et al. 2021; Lau et al. 2019; Schlieve et al. 2017). Additionally, the caudalisation cues and the time window they are added to promote a vagal regional signature are also different between protocols. While RA is required for posterior patterning in most approaches (Barber et al. 2019; Fattahi et al. 2016; Lai et al. 2017; Lau et al. 2019; Schlieve et al. 2017; Workman et al. 2017), no additional factors were used to obtain a caudal NC identity in the study of Li et al.

(2018). The NC efficiency also displays great variability among different reports (40-60% SOX10+ (Frith et al. 2020; Gogolou et al. 2021); 60% SOX10+ (Fattahi et al. 2016); 80% SOX10+ (Barber et al. 2019); 40% HNK1+/p75+ (Lau et al. 2019); 20% HNK1+/p75+ (Lai et al. 2017)) and some of the studies highlight the requirement for additional FACS-based purification of selected progenitor subpopulations (Fattahi et al. 2016; Li et al. 2018; Lai et al. 2017; Lau et al. 2019). Thus, the differences between the existing protocols, reflected to a great extent in the differentiation yield, underlie the need to clearly define critical parameters or signalling cues that will allow fine-tuning vagal NC specification *in vitro*.

3.2. Aims

The existing protocols for the generation of vagal NC from hPSCs although predominantly rely on the same combination of signals, vary in the duration of treatments and yield. In this chapter, using a differentiation protocol we recently established (Frith et al. 2020; Gogolou et al. 2021), I sought to determine the effect of different parameters and signals on differentiation and anteroposterior patterning during the derivation of vagal NC from hPSCs. Therefore, in this chapter I aimed to:

1. Characterise the *in vitro* generation of vagal NC from hPSCs
2. Define critical parameters and signals that modulate cell fate specification during the transition of hPSCs to vagal NC

3.3. Generation of vagal neural crest from hPSCs

3.3.1. Characterisation of *in vitro*-derived vagal neural crest cells

In the first part of this chapter, I sought to characterise thoroughly a protocol, previously developed by our group (Frith et al. 2020), for the *in vitro* generation of vagal NC and early ENS progenitor cells from hPSCs.

The derivation of vagal NC from hPSCs was performed using the culture regime depicted in Figure 3.1A, in a process which lasts 6 days. Wnt stimulation using the GSK3 antagonist CHIR99021 (CHIR), TGF-β pathway suppression using the ALK receptor inhibitor SB431542 and precise levels of BMP4, achieved through the introduction of saturating levels of exogenous BMP and the antagonistic action of BMP type-I receptor inhibitor DMH-1, were the signals implemented for NC induction (Frith et al. 2020; Hackland et al. 2017). Manipulation of BMP pathway using this strategy, called top-down inhibition (Hackland et al. 2017), was performed to counteract the variation in endogenous BMP expression which was previously shown to have adverse effect on protocol's efficiency and reproducibility. Cells grown under the influence of these signals progressively differentiated, phenotypically changed acquiring the characteristic NC morphology and simultaneously proliferated, reaching 90-95% of their confluency by day 4 (Figure 3.1B). On day 5 of the protocol and following 24 hours treatment with all-trans RA, cells rounded up becoming less closely associated with the culture vessel and exhibited a more elongated, darker appearance which became more distinguishable by the end of the differentiation (Figure 3.1B).

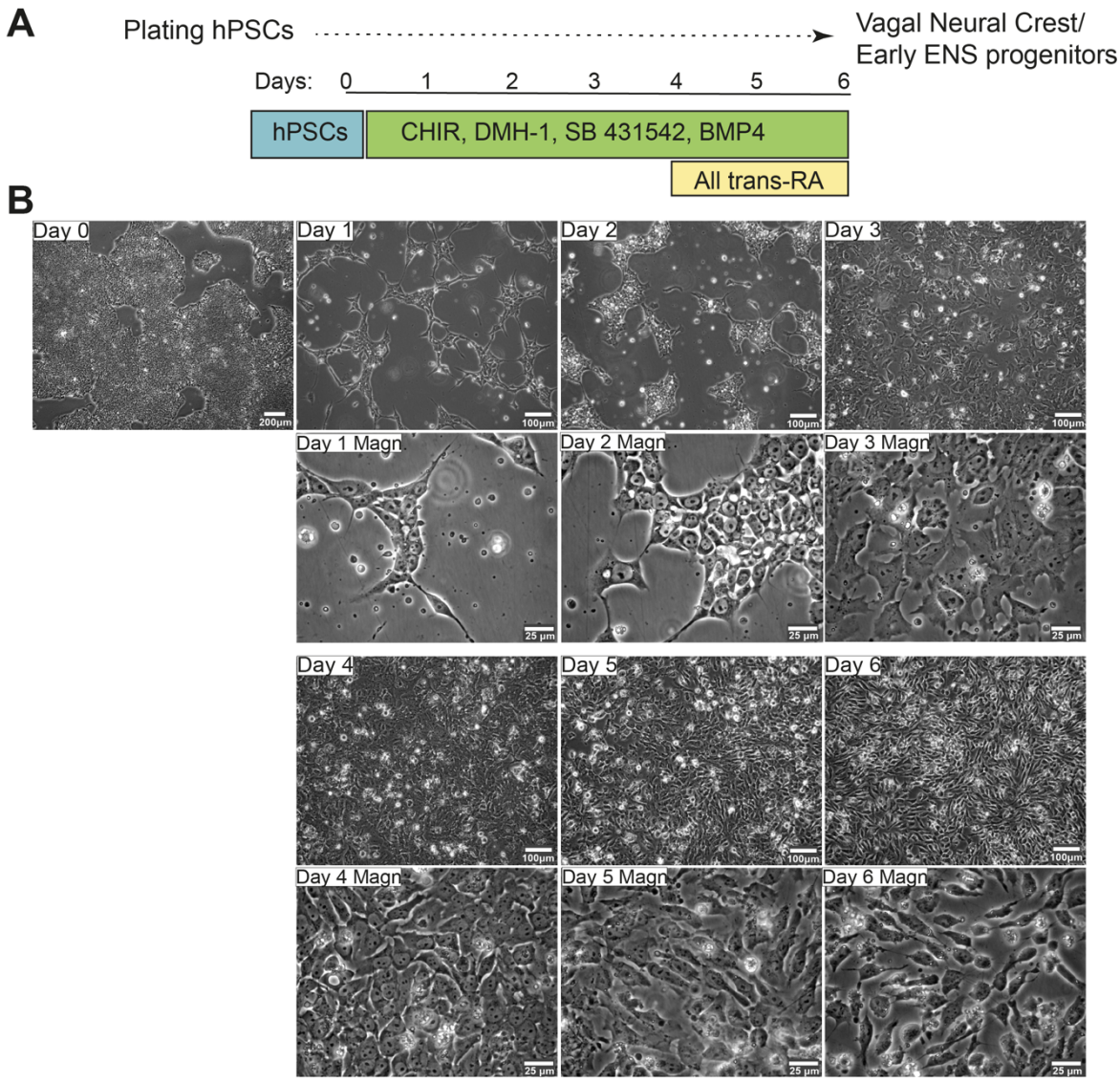

Figure 3.1. Overview of the protocol for vagal neural crest/enteric nervous system progenitor differentiation. (A) Schematic showing the culture conditions and timeline of vagal NC differentiation. (B) Representative low power and high power (magnified) images demonstrating cell morphology on a day-to-day basis throughout the protocol. Images were acquired using a H9SOX10:GFP reporter line. Scale bars are indicated at the bottom of each image (Day 0:200μm, Day 1-6: 100μm (low magnification), 25μm (high magnification)). ENS, enteric nervous system; Magn, magnified. Images were obtained from Gogolou et al. (2021).

To assess the efficiency of our differentiation method in NC formation, RT-qPCR was performed for NC associated genes in day 6 cultures derived using two different hES cell lines (H9 carrying a SOX10:GFP reporter, Mica et al. (2013); MasterShef7, Aflatoonian et al. (2010)) and one hiPS cell line (WTC-11, Kreitzer et al. (2013)) (Figure 3.2). The analysis revealed a significant upregulation (>100-fold) in the neural plate border/NC markers *PAX3*, *PAX7*, *TFAP2A* relative to hPSCs. Expression of the definitive NC marker *SOX10* showed an approximately 100-fold increase compared to control in all lines examined, further indicating the acquisition of a NC fate (Figure 3.2). Additionally, this expression profile was accompanied by significant loss in

pluripotency markers *SOX2*, *OCT4, NANOG* a result reflecting the exit from the undifferentiated state while cells commit to NC lineage (Figure 3.2).

To further assess the regional identity of our hPSC-derived RA-treated NC cultures, I next looked at the expression of *HOX* genes corresponding to the cervical/vagal axial location, *HOX* PG (1-5) (Figure 3.2). The mRNA levels of all *HOX* genes examined (*HOXB1-B5*) were significantly induced compared to control, in accordance with our previous observations and the well-established role of RA on promoting a vagal NC transcriptional signature (Frith et al. 2020). In contrast, RA treatment did not trigger the expression of more posterior *HOX* genes indicative of posterior brachial/thoracic axial levels *HOXB7*, *HOXC9*, (Figure 3.2C), a result consistent with previous findings showing that the *in vitro* generation of trunk NC relies on a FGF/Wnt induced NMP intermediate (Cooper et al. 2022; Faustino Martins et al. 2020; Frith et al. 2018; Hackland et al. 2019). The trunk NC specification via NMPs will be discussed in chapter 5.

Our group previously showed that RA-mediated patterning of vagal NC coincides with an early specification towards ENS lineage demonstrated by the expression of transcriptional regulators/ENS specifiers *ASCL1* and *PHOX2B* (Frith et al. 2020). To confirm this, I first examined A*SCL1, PHOX2B* transcript levels following RT-qPCR. I found a 20-fold increase in the expression *of ASCL1* relative to control in the MasterShef7 line and a more robust 100-1000 fold increase relative to control in the H9 and WTC-11 cell lines (Figure 3.2). The expression levels of *PHOX2B* were also found to be greatly increased (100-fold induction relative to control) in the H9 and WTC-11 cell lines while its levels were undetectable in MasteShef7 (Figure 3.2). The discrepancy in the transcription of *ASCL1* and *PHOX2B* between the three cell lines examined, suggests that there might be a cell line dependent differential response to RA, highlighting the need for adaptation of RA concentration for each cell line. Additionally, the moderate increase in *ASCL1* and in most *HOX* genes in MasterShef7 compared to the H9 and WTC-11 could suggest inefficient RA levels considering its decreased stability (Maltman et al. 2009), a point I further investigated in section 3.4.3.

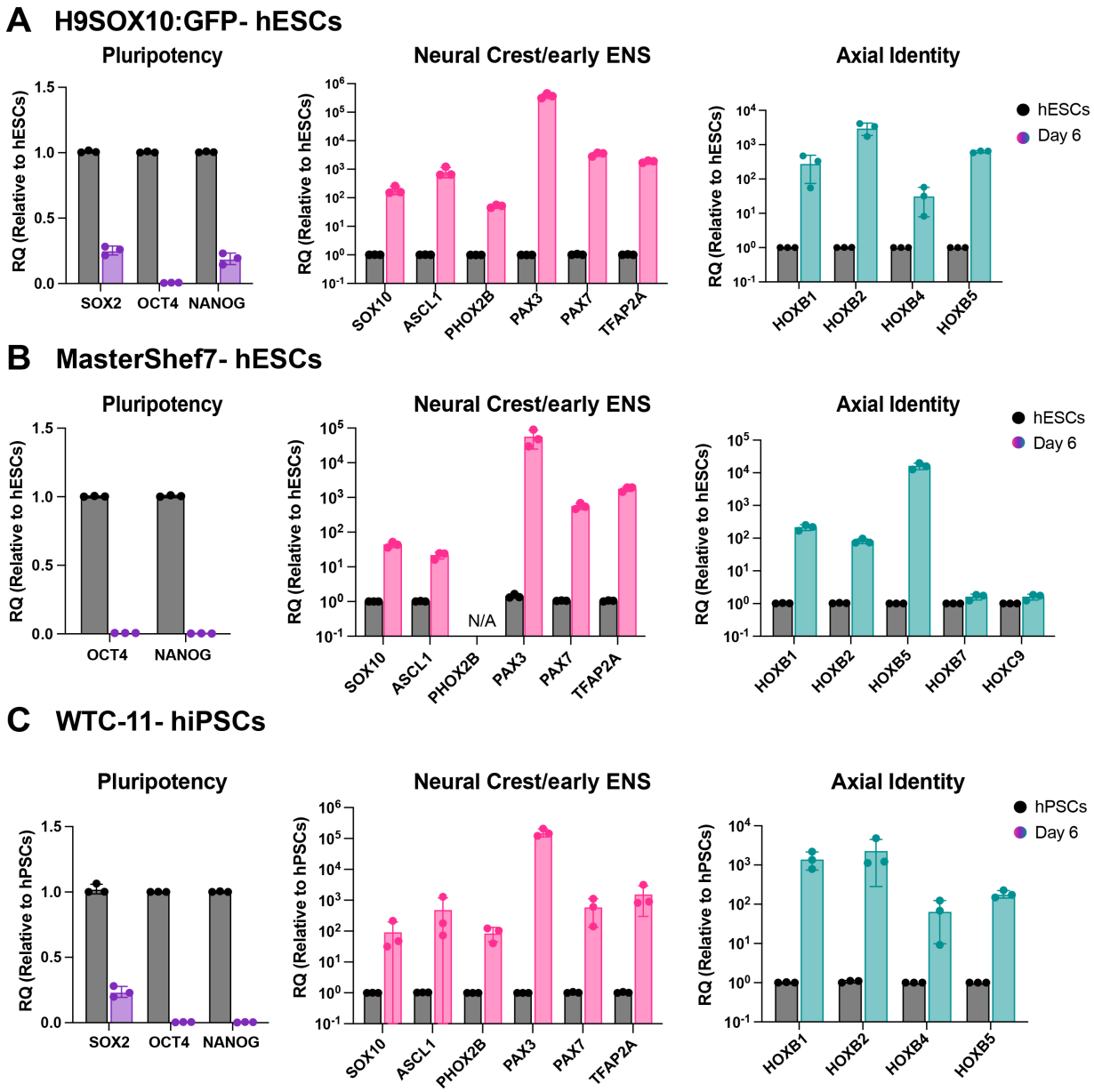

Figure 3.2. Gene expression profile of hPSC-derived vagal neural crest/early enteric nervous system progenitors on day 6 of the differentiation. RT-qPCR expression analysis of indicated pluripotency (left column-purple), NC/early ENS (middle column-magenta) and axial identity (right column-green) markers in day 6 NC cells derived from 3 different hPS cell lines (A, H9SOX10:GFP; B, MasterShef7; C, WTC-11). Data shown are the mean of mean values from 3 independent experiments with three replicates in each experiment and error bars represent SD.

To further assess ENS progenitor specification following RA treatment, I next examined protein expression of ASCL1, PHOX2B and SOX10 in our day 6 cultures and at single cell level using immunocytochemistry (Figure 3.3A).These triple labelling experiments revealed heterogenous expression of all three markers and at different levels with SOX10 being the most abundant antigen observed. While SOX10 was present in a relatively big subset of cells, PHOX2B immunoreactivity was limited to a minor fraction, negative for SOX10 either representing a more advanced enteric neural committed progenitor that has switched off SOX10 expression (Young et al. 2003) or a contaminating, CNS progenitor of cranial motor neurons (Pattyn et al. 2000) (Figure 3.3A). On the contrary, ASCL1 expression was more variable and confined in three subpopulations: (i) Cells expressing relatively low levels of ASCL1 ($ASCL1^{low}$) co-expressed PHOX2B (ASCL1+/PHOX2B+; red arrowhead) possibly marking a more committed/enteric neural progenitor (Kim et al. 2003) or a CNS entity (Pla et al. 2008) (ii) a major fraction of $ASCL1^{high}$ cells that were positive for SOX10 (ASCL1+/SOX10+; white arrowhead), a subpopulation likely to represent an ENS progenitor (Lo et al. 1991) and (iii) a small number of cells appeared single positive for ASCL1 ($ASCL1^{low/high}$/PHOX2B-/SOX10-; asterisk) (Figure 3.3A). The absence of a progenitor defined by the parallel expression of the canonical ENS progenitor markers SOX10, ASCL1, PHOX2B, albeit the increased mRNA levels in the bulk population may in part be explained by a delayed translation during protein synthesis of the transcription factor PHOX2B, potentially due to post-transcriptional modification.

As part of the molecular characterisation of day 6 vagal NC cultures, I next sought to determine whether hPSC-derived NC cells represent a putative progenitor population. To this end, I looked at the proliferation capacity of day 6 vagal NC cells using the proliferation marker Ki67 along with antibody staining against SOX10 to specifically mark the NC entity (Figure 3.3B-C). Overall, I found that around 70% and 30% of cells expressed SOX10 while 90% and 80% showed the typical Ki67 punctate pattern in the SOX10:GFP reporter and WTC-11 cell lines, respectively (Figure 3.3B-C). Interestingly, the data in the reporter cell line showed that the vast majority of SOX10+ cells were highly proliferative as nearly all cells were positive for Ki67 (66 ± 12.8%). In contrast, only a small fraction of SOX10+ cells appeared to be negative for KI67 (5 ± 3%), reflecting a population that has undergone cell cycle exit (Figure 3.3B). A similar trend was observed in the WTC-11 line (Figure 3.3C) at which the majority of SOX10+ cells co-expressed Ki67 (28 ± 8%), while a minor population was negative for it (3.6 ± 1.3%). However in both cases, the double negative (KI67-/SOX10-) and single positive (KI67+/SOX10-) groups are likely to represent cells of non-NC lineage and the particularly high percentage of KI67+/SOX10- in the WTC-11 cell line denotes the emergence of a proliferating/progenitor contaminant resulting from of a sub-optimal NC differentiation (30% SOX10+ cells as opposed to 70% under optimal conditions).

I next sought to explore further the heterogeneity of our vagal NC cultures in order to identify potential contaminant cell entities. I first examined the neuroectodermal lineage and the expression of the definitive neuroectoderm marker, PAX6 (Zhang et al. 2010) (Figure 3.3D-E). PAX6+ cells have formerly been found to occasionally emerge in NC cultures, supporting the notion that some cells differentiate along the neural pathway instead of committing to NC lineage (Hackland et al. 2017; Leung et al. 2016; Menendez et al. 2011). Together with PAX6, I also examined the expression of *SOX1*, another neural progenitor marker (Wood and Episkopou 1999). Surprisingly, PAX6+ cells were rarely detected in our differentiating cultures and represented ~2% of the total population (Figure 3.3E). These cells, were detected within clusters in high-density areas and the majority of them were primarily surrounded by SOX10:GFP expressing cells (Figure 3.3D). On the contrary, SOX1+ cells were not detected in day 6 cultures, a result suggesting that is probably relatively early for SOX1 expression (Zhang et al. 2010). In summary, these data demonstrate the generation of proliferative vagal NC/early ENS progenitor cells from three independent hPSC cell lines using our previously published protocol. Moreover, immunofluorescence analysis revealed the heterogeneity in day 6 vagal NC cultures and indicated the emergence of neural progenitors marked either by the expression of ASCL1, PHOX2B or PAX6. However, this population represented only a minor fraction of the cultures and further research is required to identify other contaminating cells that account for the rest of the heterogenous culture.

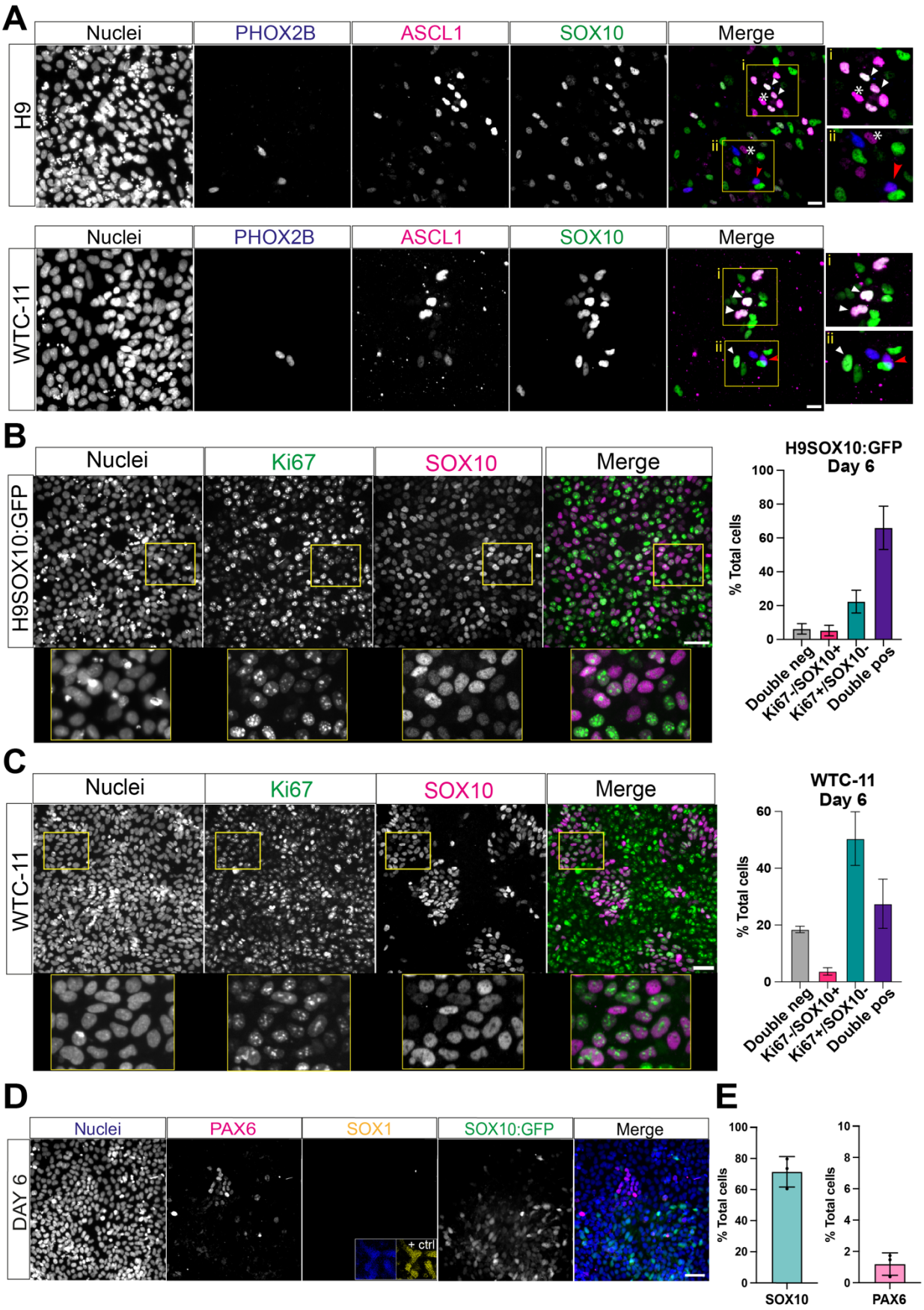

Figure 3.3. **Typical marker expression in hPSC-derived vagal neural crest cultures**. (A) Immunofluorescence analysis of the expression of PHOX2B, ASCL1 and SOX10 in day 6 vagal NC cultures derived from H9 and WTC-11 cell lines (magnified regions corresponding to the boxed areas are also shown). SOX10 and PHOX2B were present in mutually exclusive cells whereas ASCL1 was either expressed on its own (asterisk points to ASCL1+/PHOX2B-

/SOX10-), co-expressed with SOX10 (white arrowhead points to ASCL1+/SOX10+) or with PHOX2B (red arrowhead points to ASCL1+/PHOX2B+). No triple positive cells were observed at all times. Scale bars= 20 μm. (B-C) Immunofluorescence analysis and quantification of the expression of the NC marker SOX10 and the proliferation marker Ki67 following antibody staining in day 6 cultures generated using the reporter H9SOX10:GFP (B) and WTC-11 line (C). Scale bars= 50 μm. Insets indicate magnified areas. The data in the graphs were obtained after scoring ten random fields per experiment for the reporter cell line and twenty random fields per experiment for the WTC-11 cell line. Data indicate the mean of mean values of different biological experiments (n=3) and error bars represent SD (D) Immunofluorescence analysis for the neural markers PAX6 and SOX1 in day 6 cultures generated using the H9SOX10:GFP reporter cell line. The image was chosen on the basis of PAX6 expression for display and it is not representative of the field, as PAX6+ cells were rarely found in the culture. SOX1 protein was not detected. Insets show SOX1 positive staining in control sample to verify the validity of the antibody. (E) Quantification of SOX10 and PAX6 protein levels in vagal NC cultures presented in D. SOX10 protein levels were measured following antibody staining for SOX10. Data were derived after scoring 10 fields of view per experiment and are presented as the mean of mean values from 3 independent experiments. Error bars state SD (n=3).

To further characterise the resulting *in vitro*-derived vagal NC cell cultures, I looked at surface marker expression using flow cytometry. To this end, I utilised antibodies against the cell surface antigens p75 and CD49d (integrin subunit α4), markers which have been widely used to identify and isolate migrating NC cells *in vivo* and *in vitro* (Bixby et al. 2002; Fattahi et al. 2016; Lee et al. 2007; Morrison et al. 1999). In addition to these markers, a SOX10:GFP reporter H9 hES cell line was employed to allow simultaneous monitoring of *SOX10* transcriptional activity (Figure 3.4A,C). To ensure the accuracy of the analysis, the baseline fluorescence was set using the parental unlabelled H9 cell line and the P3X antibody (Kohler and Milstein 1975), which shows minimal reactivity to human cells, as negative controls (Figure 3.4A-B). TRA-1-85 antibody staining recognising human cells (Williams et al. 1988) was additionally employed as positive control (Figure 3.4A-B).

On day 6, flow cytometry analysis of the SOX10:GFP reporter cell line showed that all cells expressed p75 while 56% of them were also positive for SOX10:GFP. Interestingly, the expression of SOX10:GFP coincided with increased p75 levels (fluorescence intensity $>10^3$), classifying the double positive population as $p75^{high}$/SOX10:GFP+ (52%), whereas the fraction with low p75 expression (fluorescence intensity between 10^2 and $0.8x10^3$) was predominantly negative for SOX10:GFP, identifying a second population as $p75^{low}$/SOX10:GFP- (6%) (Figure 3.4A). The association between SOX10:GFP and increased p75 expression has been previously reported by other members of our group (Frith et al. 2020; Hackland et al. 2017) and by a previous study (Menendez et al. 2011), pointing to an expression profile typical for hPSC-derived putative NC cells. Specifically, Hackland et al. (2017) and Menendez et al. (2011) both showed following FACS isolation, enrichment for the neuroepithelial marker *PAX6* in the $p75^{low}$ fraction and upregulation of the NC markers *SOX10*, TF*AP2A* in the $p75^{high}$ population. These data indicate that the $p75^{high}$/SOX10:GFP+ and $p75^{low}$/SOX10:GFP- emerging in our cultures represent NC-like and neural progenitor cells, respectively. I also observed a third subpopulation exhibiting increased p75 levels and no SOX10:GFP expression ($p75^{high}$/SOX10:GFP-) (Figure 3.4A). This

population which accounts for around 32.5% of the culture, is likely to represent a delayed NC-like entity which has changed from a $p75^{low}$ to $p75^{high}$ expression profile, since p75 expression starts early on and increases throughout the differentiation (data not shown) and it is possibly transitioning at this stage from a $p75^{high}$/SOX10:GFP- to a $p75^{high}$/SOX10:GFP+ molecular identity. Moreover, we cannot rule out the possibility that the observed $p75^{high}$/SOX10:GFP- may result from an inefficiency of the reporter cell line to accurately reflect the transcriptional activity of the *SOX10* promoter, something which will be discussed subsequently. Given the inherent differences between different hPSC lines, I also assessed the efficiency of MasterShef7 hESCs to generate vagal NC cells using our protocol. Flow cytometry analysis revealed an increased yield with around 84% of cells expressing high levels of p75, a profile consistent with the formation of NC-like population (Figure 3.4B).

Since the p75 surface marker is also expressed by CNS neural progenitor cells, I next examined the presence of CD49d, a candidate NC marker that has been shown to mark postmigratory NC stem cells in the embryonic gut (Bixby et al. 2002). Similarly, all cells in the SOX10:GFP cell line were positive for CD49d, while 56% of them co-expressed SOX10:GFP and 84% of cells were immunoreactive to CD49d in the MasterShef7, displaying an expression pattern indistinguishable from p75 (Figure 3.4A-B). Collectively, these data suggest that our differentiation method within 6 days, yields a high percentage of NC-like cells (around 85%) marked by the expression of p75++ and CD49d and over half of the population has upregulated the definitive NC marker, SOX10 (~55% SOX10:GFP+).

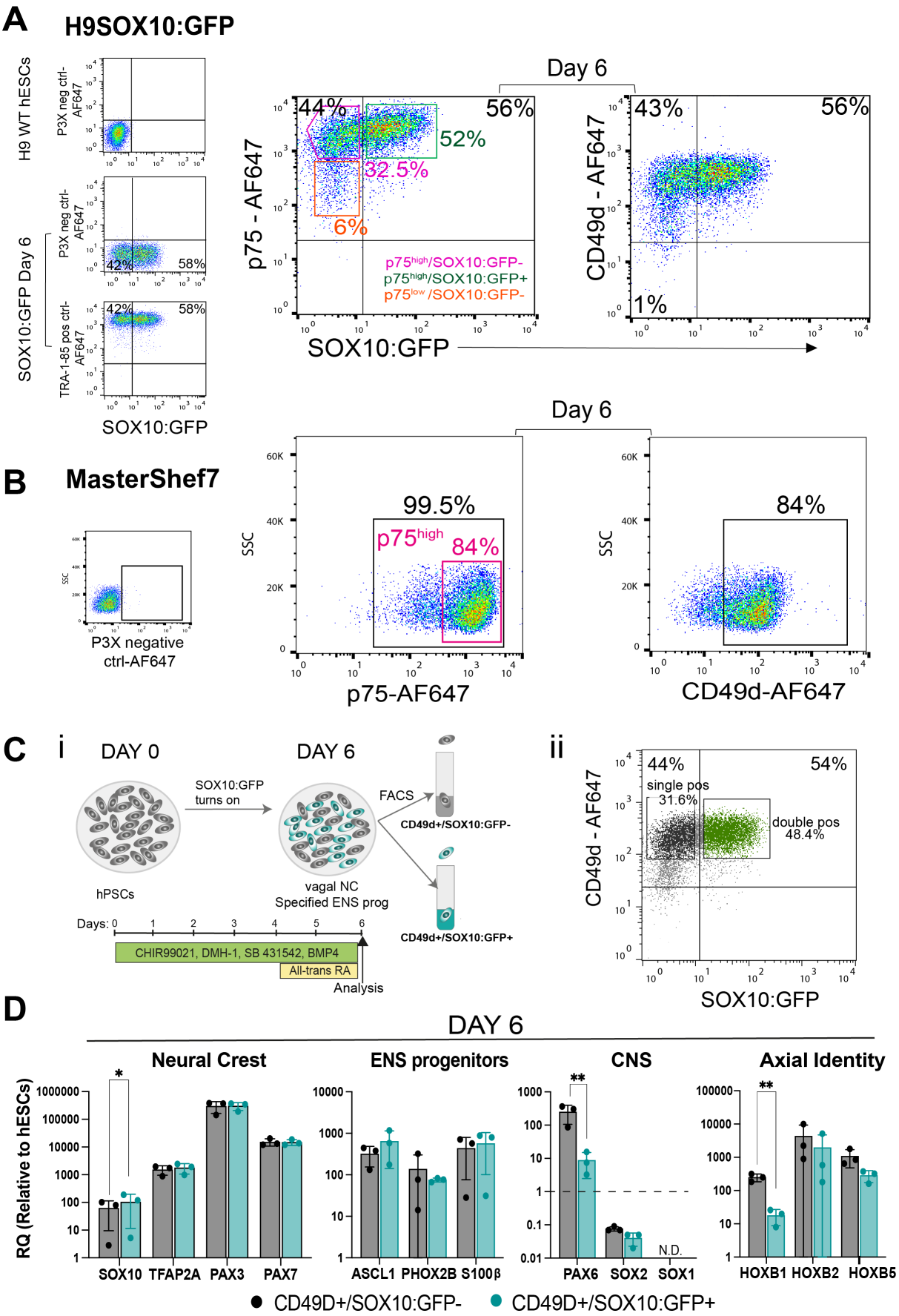
A
H9SOX10:GFP
H9 WT hESCs
P3X neg ctrl-AF647
SOX10:GFP Day 6
TRA-1-85 pos ctrl-AF647
42%
58%
SOX10:GFP
Day 6
44%
56%
52%
32.5%
6%
p75 - AF647
p75high/SOX10:GFP-
p75high/SOX10:GFP+
p75low /SOX10:GFP-
SOX10:GFP
43%
56%
CD49d - AF647
1%
B
MasterShef7
SSC
P3X negative ctrl-AF647
99.5%
p75high
84%
p75-AF647
CD49d-AF647
C
i
DAY 0
DAY 6
SOX10:GFP turns on
FACS
hPSCs
vagal NC
Specified ENS prog
CD49d+/SOX10:GFP-
CD49d+/SOX10:GFP+
Days: 0 1 2 3 4 5 6
CHIR99021, DMH-1, SB 431542, BMP4
All-trans RA
Analysis
ii
44%
54%
single pos
31.6%
double pos
48.4%
CD49d - AF647
SOX10:GFP
D
DAY 6
Neural Crest
ENS progenitors
CNS
Axial Identity
RQ (Relative to hESCs)
SOX10 TFAP2A PAX3 PAX7
ASCL1 PHOX2B S100β
PAX6 SOX2 SOX1
N.D.
HOXB1 HOXB2 HOXB5
CD49D+/SOX10:GFP-
CD49D+/SOX10:GFP+

Figure 3.4. Analysis of the expression of p75 and CD49d in hPSC-derived vagal neural crest cultures. (A-B) Representative flow cytometry analysis profiles showing co-expression of the NC markers p75, CD49d and SOX10:GFP in the indicated cell lines at day 6 of the differentiation. The baseline fluorescence for the green channel was set using a GFP negative cell line and for the far-red channel using the isotype control P3X. TRA-1-85 staining was utilised as positive control (left panels). Subpopulations are colour-coded to match the percentages in the FACS plot. (C) Schematic depicting the experimental conditions and the strategy followed (i) for the isolation of CD49d+ cells on the basis of SOX10:GFP expression as presented in the FACS plot (ii). (D) RT-qPCR analysis for the indicated genes in CD49D+/SOX10:GFP- (grey bar) and CD49+/SOX10:GFP+ (green bar) sorted cells (from Cii). Dashed line denotes the expression levels in control hESCs. Data shown are the mean of mean values ± SD, n=3 independent experiments with three replicates in each experiment. **P* ≤0.05, ***P* ≤0.01, paired t-test. N.D., not determined

Next I sought to examine the identity of CD49d+ cells, and thus I generated vagal NC using the H9SOX10:GFP cell line following our standard protocol (Figure 3.4Ci) and sorted CD49d+ cells on the basis of SOX10:GFP expression as depicted in Figure 3.4Cii. RT-qPCR analysis revealed a slight but statistically significant increase in *SOX10* transcripts in the GFP+ compared to GFP- population, confirming the validity of isolation based on SOX10:GFP expression (Figure 3.4D). On the contrary, no differences in mRNA levels for the rest NC/ENS progenitor related genes between the two groups were observed (Figure 3.4D). Interestingly, expression of the CNS neurectoderm marker *PAX6 ,* was significantly higher in the GFP- population, a finding supporting the idea that CD49d+/SOX10:GFP- represents a CNS entity emerging in the NC culture. To examine this further, I looked at the expression of other neural genes such as *SOX2* and *SOX1* in the two sorted populations. *SOX2* expression was similar in both groups, albeit reduced compared to hESCs (10-fold decrease relative to hESC expression indicated by dashed line) verifying the exit from pluripotent state, while *SOX1* transcripts were not detected (Figure 3.4D).

Moreover, I looked at the anteroposterior regional signature of CD49d+/SOX10:GFP- and CD49d+/SOX10:GFP+ cells by examining *HOX* gene expression. *HOXB2*, *HOXB5* transcript levels were comparable between the two groups, despite some inter-experimental variability, while *HOXB1* expression was significantly induced in the GFP- group (Figure 3.4D). Given the ability of PAX6 and HOXB1 to interact (Mikkola et al. 2001), the latter finding suggests that a positive feedback loop signalling from *PAX6* to *HOXB1* and vice versa may occur, specifying this population to a cranial motor neural progenitor (Osumi et al. 1997). Based on these data, we conclude that CD49d+/SOX10:GFP- represents a putative CNS progenitor subpopulation whereas the CD49d+/SOX10:GFP+ fraction reflects a NC/ENS specified progenitor. The characterisation of CD49d+/SOX10:GFP- and CD49d+/SOX10:GFP+ at the NC stage shows similarities with the findings regarding $p75^{low}$ and $p75^{high}$ groups, respectively, (Hackland et al. 2017; Menendez et al. 2011) and this prompted me to explore whether CD49d and p75 mark the same prospective NC-like cells. To this end, I performed immunocytochemistry for these two markers in day 6 cultures either expressing SOX10:GFP (H9SOX10:GFP; Figure 3.5A) or stained with an antibody against SOX10 (WTC11; Figure 3.5B). The analysis revealed a

corelation in the expression of CD49d, p75 and SOX10 (or SOX10:GFP) as these markers predominantly labelled the same cells within day 6 cultures (Figure 3.5A-B). However, it is noteworthy that none of the aforementioned markers (p75 and CD49d) is specific to the NC lineage, unless a special gating approach is adopted or double labelling is employed and screening for candidate NC surface makers would be beneficial to identify new, more specific and reliable targets.

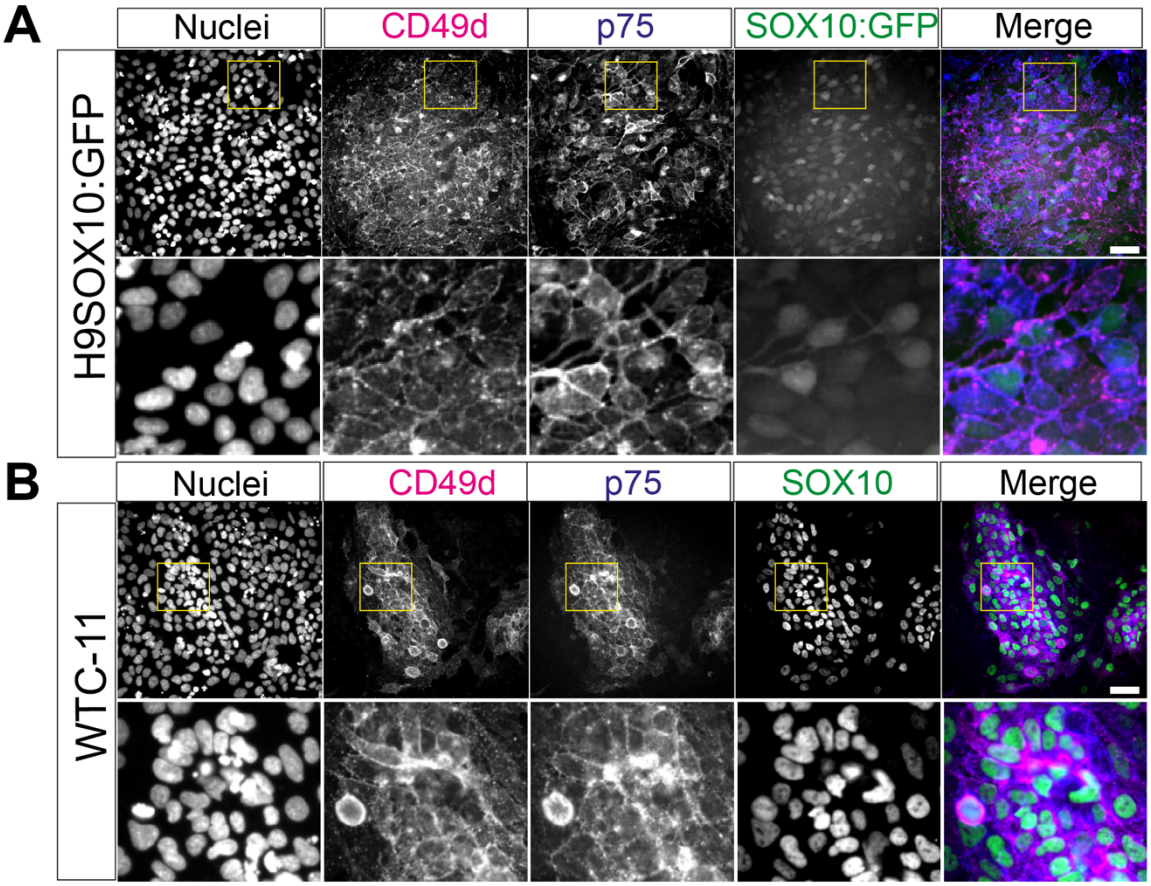

Figure 3.5. Typical cell surface marker expression in hPSC-derived vagal neural crest cultures. Immunofluorescence analysis and visualisation of the expression of CD49D, p75 and SOX10 in day 6 vagal NC cultures derived from H9SOX10:GFP (A) and WTC-11 (B) cell lines (magnified regions corresponding to the boxed areas are also shown). Scale bars= 50 μm.

3.3.2. SOX10:GFP reporter validation

The H9SOX10:GFP reporter cell line is arguably a powerful tool to our research since it allows us to monitor and visualise SOX10 expression while cells commit to NC fate. The reporter cell line, which has been extensively used in the literature to mark prospective NC cells and their SOX10 expressing progeny (Barber et al. 2019; Chambers et al. 2012; Fattahi et al. 2016; Frith et al. 2020; Hackland et al. 2017; Mica et al. 2013) was provided by Lorenz Studer and it was

created using bacterial artificial chromosome (BAC) transgenesis and engineered to express GFP under the control of SOX10 promoter (Mica et al. 2013).

I previously showed that the SOX10:GFP hES cell line efficiently differentiates towards NC (Figure 3.2A) and enriches for NC markers in the GFP+ fraction (*SOX10* vs *PAX6*) (Figure 3.4D). Despite the increased *SOX10* expression in the GFP+ population, elevated *SOX10* transcript levels were also observed in the GFP- fraction (Figure 3.4D). This result, which has been repeatedly observed amongst three independent experiments, suggests either a failure of the cell line to report accurately or a delayed response in GFP expression following SOX10 activation. To further validate the reporter, I FACS-purified SOX10:GFP positive and negative cells obtained following differentiation of early passage SOX10:GFP hESCs (Figure 3.6A). Gene expression analysis in nearly pure GFP+ and GFP- fractions (95% purity after FACS isolation; Figure 3.6A), revealed an expression profile similar to the one shown in Figure 3.4D. Although *PAX6* was highly expressed in GFP- (50-fold increase relative to GFP+), *SOX10* transcripts (50-fold increase relative to hESCs) were also detected in the GFP- fraction (Figure 3.6B). This result was further verified by flow cytometry analysis and following antibody staining for the intracellular SOX10. The analysis showed the presence of a SOX10- population (Q3; blue) residing in the GFP+ fraction of SOX10:GFP+ sorted cells and SOX10+ (Q1; green) emerging within the GFP- fraction of SOX10:GFP- sorted cells (Figure 3.6C). Moreover, antibody staining against SOX10 in day 6 bulk NC (Figure 3.6C lower panel-D) demonstrated substantial overlap in SOX10 and SOX10:GFP expression (~36% of the population in Q2; magenta) as well as single positive SOX10 (~21% of the population in Q1; green) and SOX10:GFP (~23% of the population in Q3; blue) fractions (Figure 3.6C). Collectively, these data suggest that the SOX10:GFP reporter cell line does not report accurately the number of SOX10 expressing cells, and thus it is not a reliable tool to evaluate NC efficiency per se.

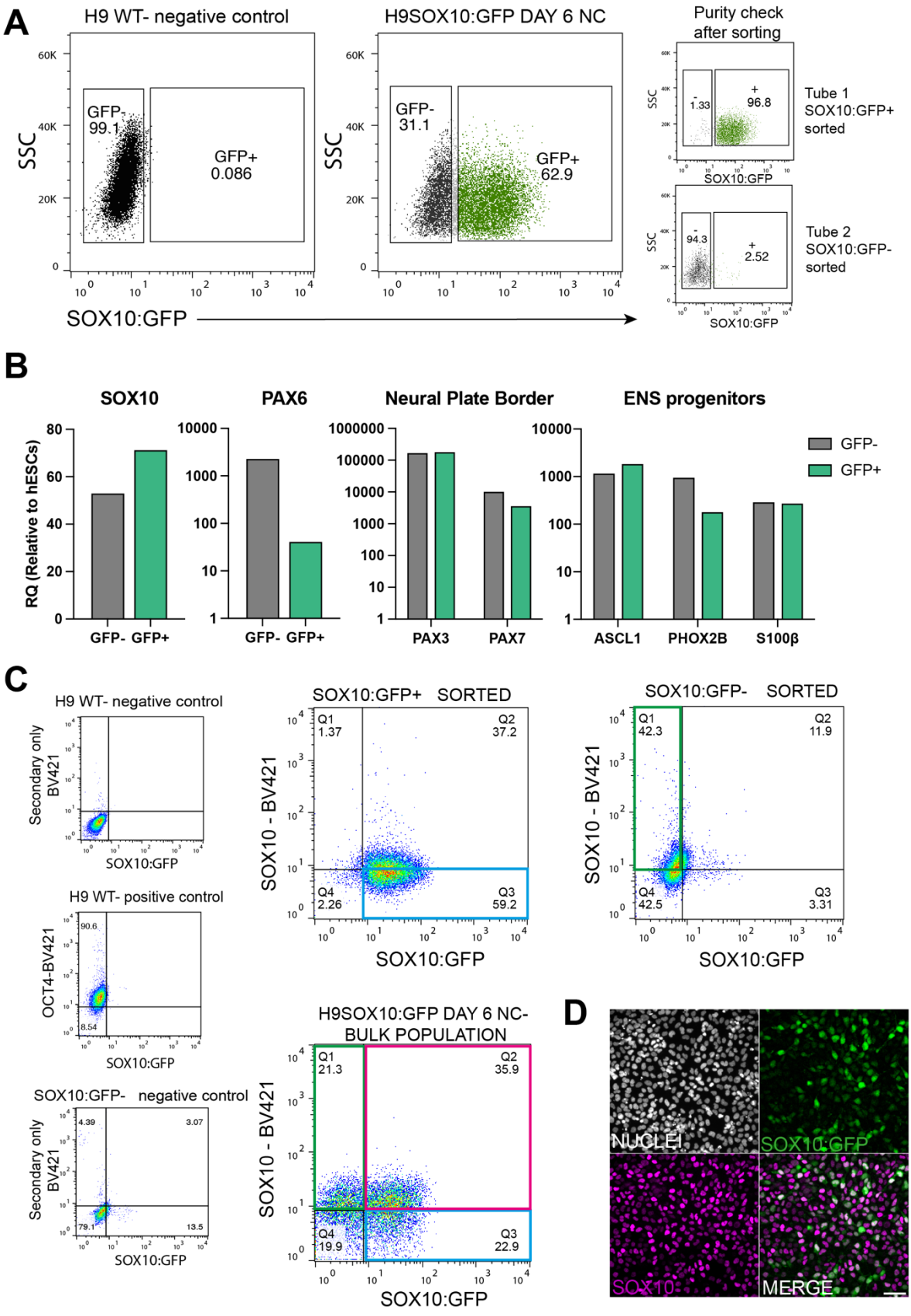

Figure 3.6. SOX10:GFP reporter cell line does not accurately report SOX10 levels. (A) Flow cytometry analysis plots of day 6 vagal NC generated using the H9SOX10:GFP reporter cell line and isolated by FACS on the basis of GFP expression. Plots on the right depict purity levels of the isolated populations. (B) RT-qPCR analysis for neural plate border/NC-/ENS-related genes and the neural marker *PAX6* in sorted GFP- and GFP+ cells. Each bar represents the mean value of three technical replicates (n=1). (C) Validation of SOX10:GFP expression following staining with an

antibody against SOX10. Day 6 sorted SOX10:GFP+, SOX10:GFP- cells and SOX10:GFP bulk populations were used for the analysis. Plots on the left depict the controls used including antibody staining for OCT4 that positively marks hPSCs to set the gates. (D) Immunofluorescence analysis of SOX10 protein expression following antibody staining and SOX10:GFP in day 6 NC cultures derived from the reporter cell line. Scale bar=50 μm. WT; wild type unlabelled and undifferentiated cells from the parental cell line.

3.4. Critical parameters for vagal neural crest specification

The intra and inter-experimental variability observed in our protocol's efficiency, reflected in the heterogeneous SOX10 expression and emergence of PAX6+ cells (Figure 3.7A-C), prompted me to examine candidate cues and parameters influencing vagal NC specification *in vitro*.

3.4.1. Examining the role of WNT signalling on vagal neural crest specification

Given the instrumental role of canonical Wnt signalling in NC formation *in vivo* (Garcia-Castro et al. 2002; Wilson et al. 2001) and the influence of Wnt pathway activation on the specification of NC from hPSCs *in vitro* (Leung et al. 2016; Menendez et al. 2011), I first focused on this pathway. It has been previously shown that Wnt pharmacological activation in combination with BMP and Activin A/Nodal signalling inhibition shifts neuroectoderm cells towards a NC lineage while diminishing the occurrence of PAX6 expressing cells (Menendez et al. 2011). Therefore, I hypothesized that sub-optimal Wnt signalling levels may account for the generation of neuroepithelial over NC cells in low NC yield cultures.

Our standard vagal NC differentiation protocol employs 1 μM of CHIR (CHIR 99021), a selective inhibitor of GSK-3 which acts as Wnt activator (An et al. 2010). To enable a clearer analysis and to exclude technical issues that might account for the inefficient differentiation, after performing CHIR batch testing (data not shown), I compared CHIR supplied from 2 independent sources (Tocris vs Selleck chemicals) (Figure 3.7D-F). Overall, no significant changes in *SOX10*, *PAX3* and *PAX6* gene expression were observed between the standard, Tocris (T) and alternative supplier, Selleck chemicals (S) (Figure 3.7E). However, *SOX10* expression appeared slightly higher in control cultures (Figure 3.7E). Immunofluorescence analysis showed a greater but more variable number of SOX10+ cells (32 ± 14%) in cultures treated with CHIR from Selleck and a considerably lower number of PAX6+ cells (7 ± 4%) compared to control. Cultures treated with CHIR from Tocris showed moderate SOX10 protein expression (31 ± 4%) and increased, albeit variable, PAX6 protein levels (33 ± 13%) (Figure 3.7F). Taken together, this comparison suggests that GSK3 antagonist batch and supplier differences may contribute to inter-experimental variability.

The higher levels of PAX6 protein expression in cultures treated with Tocris CHIR might reflect lower Wnt activity. In turn this suggests that a higher Tocris CHIR dose might be required for more efficient Wnt pathway activation and Wnt-mediated NC specification. To investigate this in more detail, I treated hPSCs during NC induction with a slightly elevated concentration of Tocris CHIR (1.5 μM) and examined its effect on NC formation by looking at the expression of a panel of NC markers (Figure 3.7G). Transcriptional analysis revealed a statistically significant increase in the expression of *SOX10* and *PHOX2B* in cultures treated with 1.5 μM CHIR relative to control, 1 μM CHIR treated cultures (P <0.05 and P <0.01, respectively; paired t-test) (Figure 3.7H). On the contrary, higher CHIR concentration resulted in significant downregulation in the expression of *ASCL1* (10-fold reduction, P <0.01; paired t-test) relative to control, while the levels of *PAX3* transcripts appeared unaffected (Figure 3.7H). Treatment with higher CHIR led to robust induction of *PAX6* transcripts (P <0.01, ratio paired t-test; Figure 3.7H), suggesting a link between Wnt pathway activity and *PAX6* upregulation in hPSC-derived NC cultures. This contrasts the findings of Menendez et al. (2011), who showed that Wnt administration favors the formation of NC over neural progenitor cells in a dose-dependent manner. The discrepancy between their findings and our observations may be due to differences in the protocols, in the combination of signals involved and particularly for BMP, as the effect of Wnt on NC specification was examined in combination with minimal or absent BMP activity (Menendez et al. 2011). This is further supported by the fact that BMP activation is a prerequisite in our protocol while they report an antagonistic action of BMP on Wnt-mediated NC specification (Menendez et al. 2011).

The effect of higher Wnt agonist concentration on axial identity specification was also examined by assessing the expression of *HOX* genes. The mRNA levels of *HOXB1*, *HOXB2* and *HOXB4* were considerably increased in 1.5 μM CHIR treated cultures, however, *HOXB5* transcript remained unaffected (Figure 3.7H). The reported increase in the expression of *HOX* genes in response to higher Wnt stimulation may be an indication of synergistic action of Wnt signalling and RA in *HOX* induction as the latter is part of the culture regime and essential for axial specification (Figure 3.7H).

Altogether, these data suggest that GSK3 inhibition enhances the induction of posterior cranial/vagal axial identity *HOX* genes and promotes *PHOX2B* upregulation while it represses *ASCL1* expression. They also show an increase in *SOX10* transcript levels, a result consistent with the role of Wnt in promoting NC specification. The unexpected upregulation in *PAX6* transcripts though, in response to elevated Wnt activity, indicates that Wnt signalling pathway may be involved in regulating PAX6 transcription.

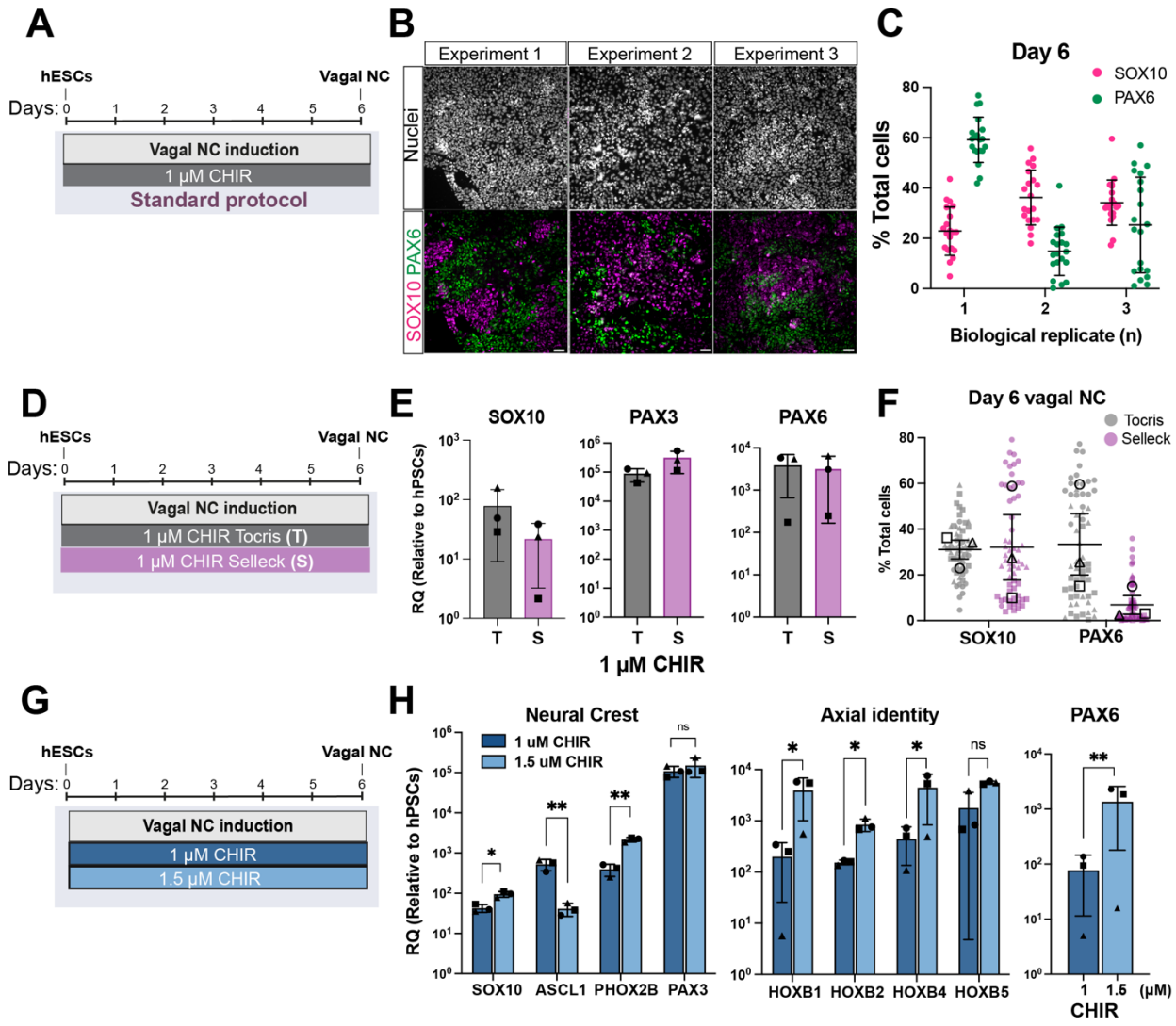

Figure 3.7. Role of Wnt signalling pathway on neural crest specification. (A) Diagram demonstrating standard conditions for vagal NC differentiation. (B-C) Representative images (B) and quantification (C) of SOX10 and PAX6 protein expression in cultures generated using the standard protocol depicted in A, in three independent experiments. For the analysis, twenty random fields per experiment were selected. Data shown are the mean ± SD of different fields of view (n=20) per biological experiment. (D) Schematic showing the experimental design to compare CHIR 99021 (CHIR; GSK3 antagonist) bought from two different suppliers, Tocris (used in the standard protocol) and Selleck chemicals. For direct comparison, same concentration of the compound was used. (E) Gene expression analysis in vagal NC cultures generated using 1 µM CHIR supplied from Tocris or Selleck. Data shown are the mean of mean values ± SD, n=3 independent experiments with three replicates in each experiment. Each biological replicate is represented by a unique shape. (F) Quantification of SOX10 and PAX6 protein expression in vagal NC cultures generated using 1 µM CHIR supplied from Tocris or Selleck. SuperPlots show pooled data from 3 independent experiments (20 fields scored/condition for each experiment). Each independent experiment is represented by a unique shape. Large symbols denote the means of different experiments (n=3) and error bars indicate SEM. (G-H) Schematic showing WNT pathway manipulation during vagal NC induction and the effect of a slightly higher concentration of CHIR (1.5 µM) on the expression of the indicated genes. Data shown are the mean of mean values ± SD, n=3 independent experiments with three replicates in each experiment. Each independent experiment is represented by a unique shape, **P* ≤0.05, ***P* ≤0.01, paired t-test and ratio paired t-test for PAX6. ns=not significant. Scale bars= 50 µm.

I next sought to further investigate the relationship between elevated Wnt signalling and *PAX6* induction. Seeding density of hESCs has been proposed to have a critical role on *in vitro*

differentiation. In particular, previous studies have reported a requirement of high plating cell density for efficient neuroepithelial differentiation through neural rosette formation (Lippmann et al. 2014) and that increased plating density impairs NC formation favoring neural differentiation (Chambers et al. 2009). Specifically, the latter study has shown that cell density determines the ratio of CNS and PNS by enriching for PAX6+ neural cells over PAX6- NC cells in cultures plated at a higher density and under the influence of the same inductive signals (dual-SMAD-inhibition protocol) (Chambers et al. 2009). This observation is also supported by my empirical observations for PAX6+ spatial organisation and emergence of such cells in very dense areas that are present in our day 6 NC cultures (Figure 3.8A). Moreover, cell density has been previously reported to influence the levels of β-catenin and hence, canonical Wnt activation in cancer (Kim et al. 2019) and during mESC differentiation and at hPSC state (LeBlanc et al. 2022; Massey et al. 2019).

Based on these findings I explored the effect of cell density in our vagal NC differentiation system and its links to Wnt signalling. I initially examined the influence of cell density on *SOX10* and *PAX6* transcripts after subjecting hPSCs plated at three different plating cell densities (30-50 x 10^3 cells/cm^2) to NC differentiation. I found that increasing cell density did not significantly affect *SOX10* transcriptional levels although there was a lower induction of *SOX10* when cells were plated at 50 x 10^3/cm^2, the highest cell density examined (Figure 3.8B). In contrast, *PAX6* expression levels were dramatically increased (5- to 10-fold upregulation, P <0.05) when hPSCs were plated at higher density, confirming a positive correlation between high plating density and PAX6 induction (Figure 3.8B). Since higher Wnt signalling and increased plating density resulted in *PAX6* upregulation (Figure 3.7H, 3.8.B, respectively), I next examined the response of Wnt activity to cell density changes by measuring the transcriptional levels of canonical Wnt target genes, *TCF1* (van de Wetering et al. 1997) and *AXIN2* (Jho et al. 2002). Gene expression analysis showed that *TCF1* maintained its expression levels relatively high and at a similar level to pluripotent stem cells (from Ct 27 in hPSCs to 26 in NC) across all densities examined (Figure 3.8C). On the other hand, increased cell density resulted in upregulation of *AXIN2*, suggesting that Wnt signalling activity and plating density are to some extent correlated (Figure 3.8C). In summary, these results support our hypothesis that in NC cultures generated under the influence of the same inductive signals, cell density dictates the balance between SOX10 and PAX6 expression. They also indicate the existence of a dynamic interplay between cell density and Wnt activity that could be critical for NC specification *in vitro*, however, further research is required to dissect the links between cell density, Wnt activity and SOX10 vs PAX6 upregulation.

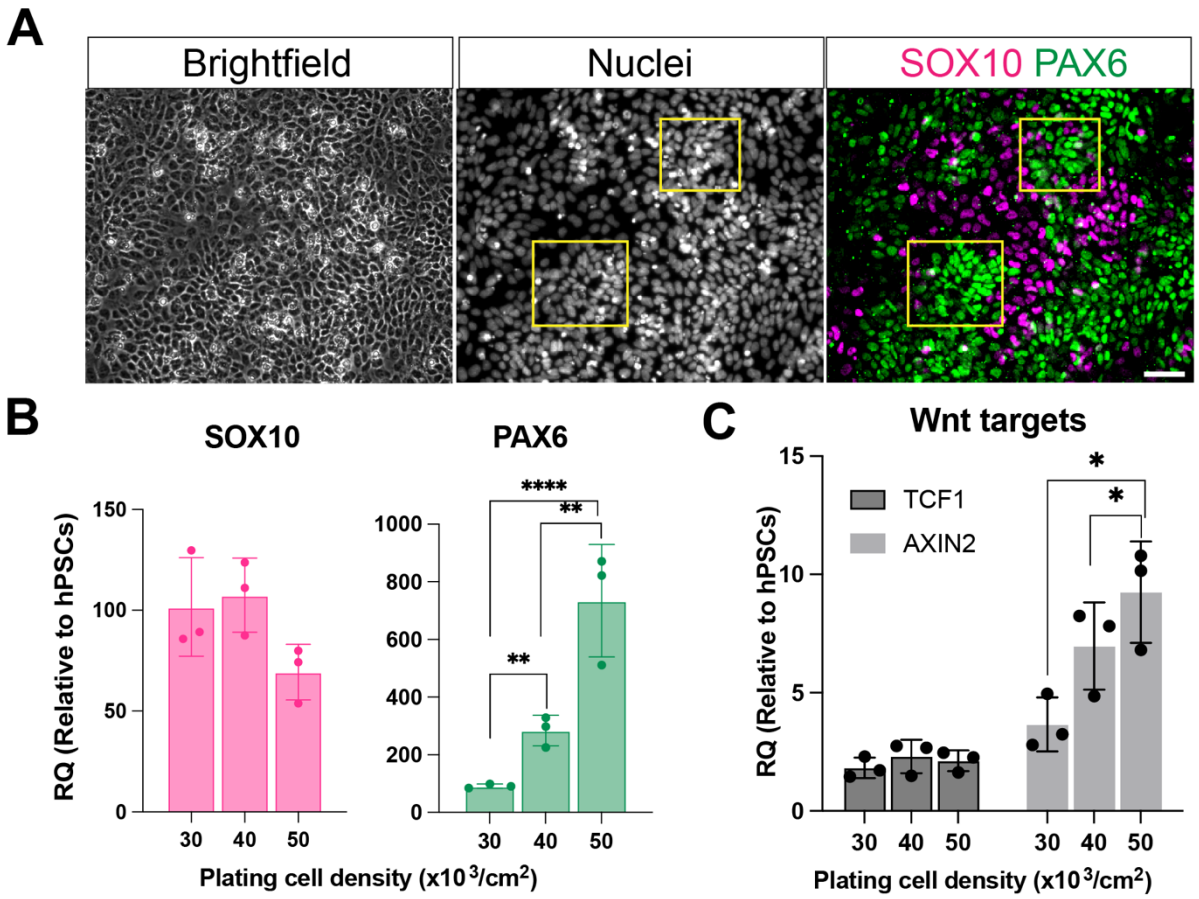

Figure 3.8. High plating density leads to *PAX6* upregulation in hPSC-derived neural crest cultures. (A) Representative bright field and immunofluorescence analysis images of day 6 vagal NC cultures showing the spatial relationship between PAX6+ and SOX10+ cells. Highlighted regions indicate PAX6+ cells emerging in very dense areas. Scale bar=50 μM. (B) RT-qPCR analysis for *SOX10* and *PAX6* transcripts in day 6 vagal NC cultures derived after plating hPSCs in three different densities. ***P* ≤0.01, *****P* ≤0.0001, one-way ANOVA followed by Tukey's post-hoc multiple comparisons test. (C) RT-qPCR analysis for Wnt target genes in day 6 vagal NC cultures derived after plating hPSCs in three different densities. **P* ≤0.05, one-way ANOVA followed by Holm-Sidak's post-hoc multiple comparisons test. For all graphs, data shown are the mean of mean values ± SD, n=3 independent experiments with three replicates in each experiment.

3.4.2. Cell density influences vagal neural crest protocol's efficiency

To investigate further the impact of cell density on NC differentiation, I plated two hES (H9:SOX10GFP and H9 WT) and one hiPS cell line (WTC-11) at different densities in NC-inducing media and examined the expression levels of SOX10 in combination with p75, CD49d or alone, as a means to evaluate protocol's efficiency (Figure 3.9). Flow cytometry analysis revealed that NC differentiation efficiency in H9:SOX10GFP hESCs is influenced by plating density and a progressive reduction in the number of cells expressing SOX10:GFP/p75 was observed with increasing plating density (from 58.3 ± 3.6% at the lowest density to 6.6 ± 2.4% at the highest density; Figure 3.9A). The greatest NC yield was achieved when cells were plated at the lowest density, 30 x 10^3 cells/cm^2 (Figure 3.9A). Similar results were obtained in differentiating cells from the parental H9 cell line, as high density correlated with a progressive

decrease in the number of cells expressing $p75^{high}$ (a fraction enriched for SOX10 is depicted within the pink gate) or CD49d (Figure 3.9B). In addition to surface antigen analysis, I assessed the effect of cell density on SOX10 protein expression in the H9 unlabelled cell line using immunocytochemistry (Figure 3.9Ci). I found that approximately 37 ± 8 % cells were positive for SOX10 in cultures plated at intermediate seeding densities (40-50 x 10^3 cells/cm^2) and this number decreased to 23 ± 4% and 30 ± 12.6% when cells were plated at the lowest (30 x10^3 cells/cm^2) and highest density (60 x10^3 cells/cm^2), respectively (Figure 3.9Cii). Together, these data demonstrate that in the H9 a slightly higher plating density compared to the reporter cell line (40 x 10^3 in the H9 compared to 30 x 10^3 cells/cm^2 in the reporter cell line) is required for optimal differentiation efficiency. This analysis was also carried out in the WTC-11 hiPS cell line. Similar to the hES cell lines, differentiating WTC-11 showed a negative correlation between SOX10 protein levels and increasing plating density (Figure 3.9D). Specifically, SOX10 expression reached a peak of 55 ± 24% of cells being positive for it in cultures initiated with the lowest plating density (30 x 10^3 cells/cm^2) and this number was reduced to 32 ± 3.5% when cells were plated at the highest density (50 x 10^3 cells/cm^2) (Figure 3.9D).

Collectively, these data demonstrate the progressive decline in SOX10 expression with increasing cell density and highlight the role of cell density as a critical determinant for optimal NC differentiation. A low plating cell density results in increased number of SOX10+ cells, while a high plating density leads to a considerably lower SOX10+ population and higher numbers of PAX6+ contaminating cells (Figures 3.8, 3.9E).

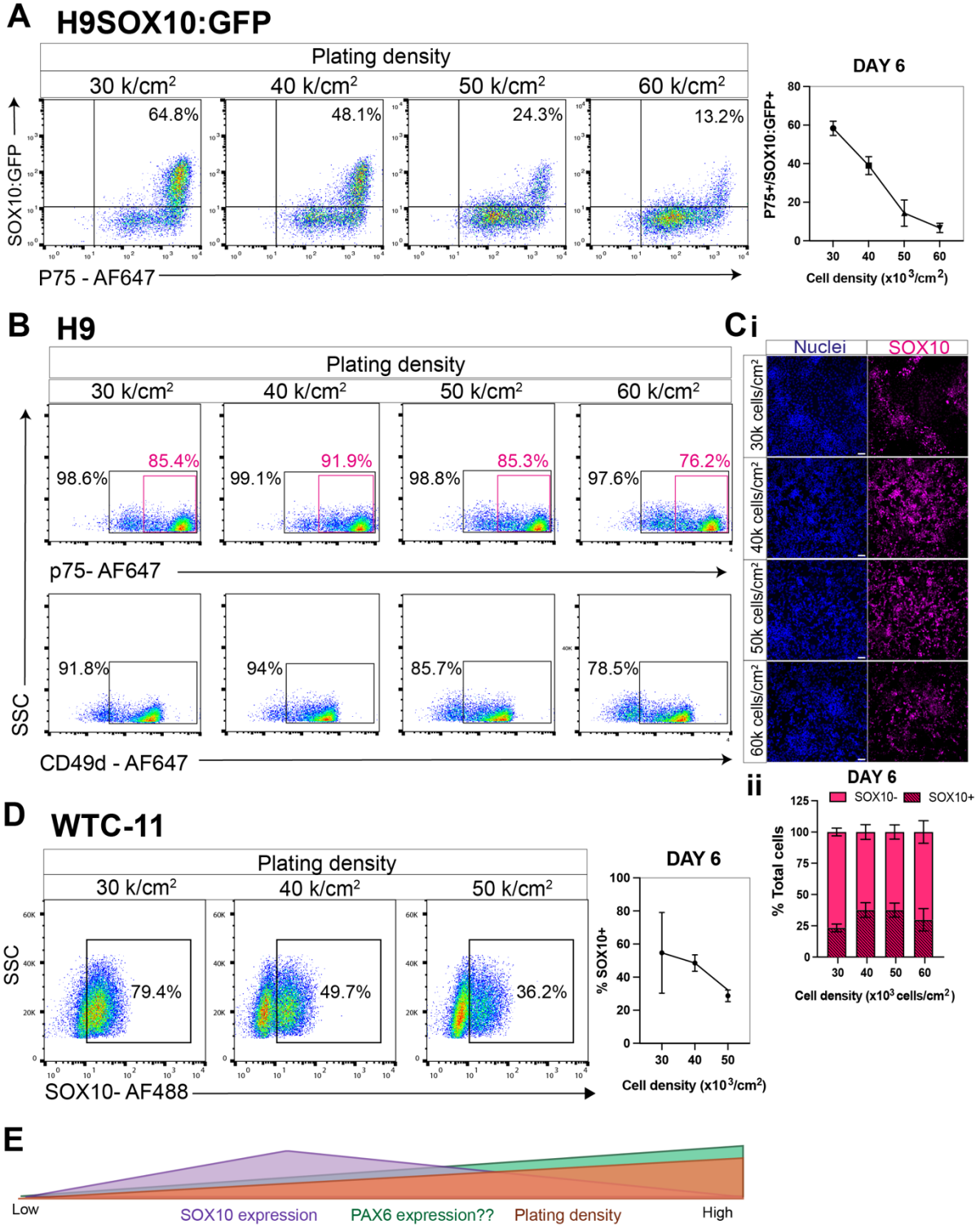

Figure 3.9. Lower plating density improves neural crest protocol's efficiency. (A) Representative flow cytometry analysis plots showing the effect of 4 different plating densities on NC efficiency on day 6 of the protocol using the SOX10:GFP reporter cell line. The line graph on the right summarises the quantification data for p75+/SOX10:GFP+ across all densities. Error bars indicate SD (n=3 independent experiments). (B) Representative day 6 flow cytometry profiles from H9 hESCs plated at 4 different densities demonstrating the percentage of cells expressing $p75^{high}$ (pink gates, upper panel) and CD49d (lower panel). (C) Immunofluorescence analysis (i) and quantification (ii) of SOX10 protein expression in H9-derived day 6 NC cells initially plated at 4 different densities. Scale bars= 50µm. Data in the graph were derived after scoring ten random fields per experiment. Data shown are the mean of mean values ± SD (n=2 independent experiments). (D) Representative flow cytometry analysis plots showing the percentage of SOX10+ cells in WTC-11 hiPSC-derived day 6 cultures initially plated at 3 different densities. The line graph on the right shows the quantification of flow cytometry data. Error bars indicate SD (n=3 independent experiments). (E) Illustration

demonstrating the dynamics of SOX10 and PAX6 expression in association with increasing plating density. SOX10 expression reaches a peak in low plating density and while cell density increases SOX10 expression decreases and PAX6 takes over the culture.

3.4.3. Efficient induction of ENS-associated genes in vagal neural crest cultures requires daily media change

Previous studies have shown that addition of all-trans RA in cranial NC cultures is required for patterning the cells towards the vagal subdivision which is reflected by the upregulation of corresponding *HOX* genes transcripts *HOX* PG (*1-5*) (Fattahi et al. 2016; Frith et al. 2018; Workman et al. 2017). Recently published work from our group has demonstrated an additional role of all-trans RA in guiding vagal NC cells towards an early ENS progenitor identity, exemplified by the upregulation of ENS progenitor specification genes, *ASCL1* and *PHOX2B* (Frith et al. 2020). Despite the relatively high induction of these two genes in NC cultures relative to undifferentiated control, their expression levels appeared substantially variable between various independent experiments we performed. Several lines of evidence suggest a high propensity of RA towards isomerisation and degradation when exposed to light or heat, emphasizing its reduced stability in culture (Maltman et al. 2009). Hence, I asked whether RA scarcity could be the source of variation in *ASCL1* and *PHOX2B* expression in day 6 differentiated cultures. To address this question, I differentiated hESCs into cranial NC and added all-trans RA to promote vagal axial patterning and ENS specification as described in Figure 3.10A. To examine whether the decreased RA stability and its high susceptibility in the environmental conditions influence gene expression, I replenished culture medium with fresh RA daily and compared the expression profile of cultures fed daily with control “media changed D4” cultures (Figure 3.10A). Interestingly, RT-qPCR analysis revealed that daily medium change (media changed D4,D5) resulted in a significant increase in the levels of *ASCL1* (~10-fold, P <0.01) and *PHOX2B* (~5-fold, P <0.01) transcripts compared to control, while SOX10 expression remained unaffected (Figure 3.10B). This finding supports a role of RA in upregulation and maintained expression of *ASCL1* and *PHOX2B*. Gene expression analysis for *HOX* genes did not show any differences between the two groups (Figure 3.10C), suggesting that *HOX* genes are less sensitive to RA reduced stability than *ASCL1*, *PHOX2B.*

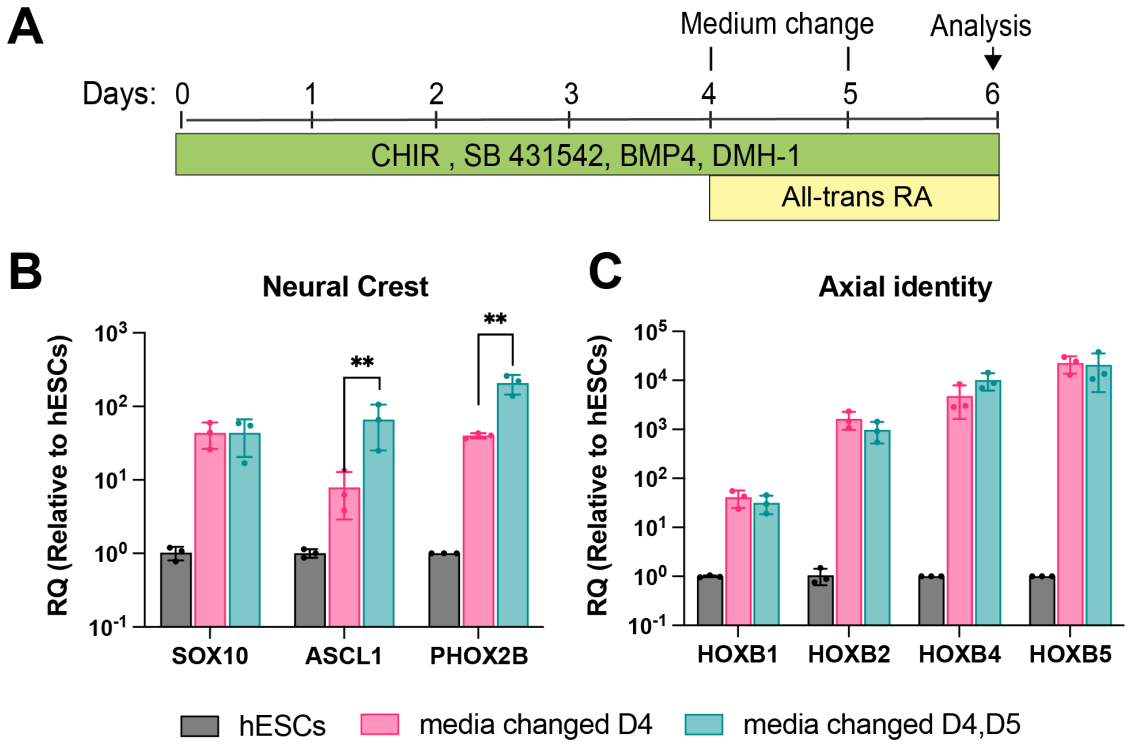

Figure 3.10. Induction of enteric nervous system progenitor-associated genes in vagal neural crest requires daily medium change. (A) Diagram presenting the experimental approach. (B-C) RT-qPCR expression analysis of genes associated with ENS specification (B) and axial patterning (C) in vagal NC after refreshing culture medium once (D4=day 4) and in two subsequent days (D4,D5= day 4 and day 5) as described in A. Data shown are the mean of mean values ± SD, n=3 independent experiments with three replicates in each experiment. ***P* ≤0.01, paired t-test. Only statistically significant changes are indicated.

3.5. Discussion

3.5.1. Understanding the heterogeneity in hPSC-derived vagal neural crest cultures

Gene expression analysis for a battery of NC genes (*SOX10*, *PAX3*, *PAX7*, *TFAP2A*) in day 6 hPSC-derived vagal NC cultures revealed transcriptional changes consistent with adoption of a NC identity *in vitro*. In this population, a fraction of 50-70% is found to be immunoreactive to SOX10 (Figures 3.2,3.3) while the identity of the remaining population, which accounts for the 30-50% of the total, to a great extent is yet to be identified.

Several studies examining the early steps of NC formation/neural plate border specification *in vitro* (Leung et al. 2016; Menendez et al. 2011) and a growing body of single cell transcriptomic data (Ling and Sauka-Spengler 2019; Soldatov et al. 2019) providing information about NC lineage segregation *in vivo* have shed light to early events of NC specification and have provided us with large lists of candidate markers representative of distinct lineages that might account for the heterogeneity observed in our culture. A few of these proposed markers representative of

different linages were employed in this study to explore the heterogeneity of day 6 vagal NC cultures.

Initially, I focused on the neuroectodermal lineage by examining the expression of the definitive neuroectoderm marker, *PAX6* in our cultures (Figure 3.3D-E). PAX6+ cells have been previously found to emerge in NC cultures (Hackland et al. 2017; Leung et al. 2016; Menendez et al. 2011) comprising a small fraction, which has been shown to arise independently of NC as *PAX6* knock down did not impair the efficacy of hPSCs to generate SOX10+ NC (Leung et al. 2016). In agreement to this, our analysis showed that a minor population is positive for PAX6 in day 6 cultures (Figure 3.3D-E) and this number increases, potentially at the expense of a sharp decrease in SOX10, when the efficiency of the protocol is low (Figure 3.7C). The presence of PAX6 and the lack in the expression of a later neural progenitor marker SOX1, at transcript and at the protein level (Gerrard et al. 2005; Zhang et al. 2010), denotes that this population is likely to represent an early neuroectodermal lineage.

Given the natural relationship between neural plate (neuroectoderm), neural plate border and surface ectoderm (non-neural ectoderm) territories during late gastrulation/early neurulation in the embryo (Figure 1.1) and the fact that lineage segregation is dictated by timely and spatially defined combinations of BMP, FGF and WNT signals (Thawani and Groves 2020), we can speculate that the contaminating cells emerging in our cultures may belong to non-neural ectoderm (NNE) and its derivatives, the pre-placodal ectoderm (PPE) and epidermis (EPI) which arose in response to NC inductive signals (Kwon et al. 2010; Leung et al. 2013; Pieper et al. 2012). This idea is further supported by the findings of a recent single-cell transcriptome analysis study which reported the occurrence of cells with transcriptional profile similar to NNE and PPE in vagal NC-derived ENS cultures (Majd et al. 2022; preprint). The emergence of NNE and its progeny could be linked to Wnt transcriptional regulation in NC cultures since Wnt activation has been shown to restrict NNE induction and promote the generation of NC in differentiating hESCs (Leung et al. 2016). The emergence of a NNE progenitor undergoing spontaneous ectodermal differentiation within our NC cultures could also be supported by the observed increase in the transcriptional levels of *TFAP2A*, a critical regulator of the differentiation of surface ectoderm cells (Luo et al. 2002). Since TFAP2A is a marker shared between the NC and NNE lineage and its expression levels in our differentiating cultures have only been observed on a population level by RT-qPCR, immunofluorescence analysis in combination with another NNE marker (i.e. GATA3 (Sheng and Stern 1999)) would further delineate the presence of a population differentiating along the surface ectoderm route. Additionally, *Pax6* apart from its established role as neuroectoderm specifier (Zhang et al. 2010), has been shown to mark the anterior region of the prospective placodal ectoderm during placode development in *Xenopus laevis* and its

expression is later confined in anterior placode derivatives (olfactory, lens and anterior pituitary gland) (Schlosser and Ahrens 2004). *In vitro*, NNE- and PPE- derivatives expressing PAX6 are derived following an initial phase of TGF-β inhibition and BMP treatment (Conti and Harschnitz 2022), signals that are also involved in our NC induction medium, reinforcing the notion that the contaminating cells might belong to the PPE lineage. Thus, analysis at single cell level for a panel of indicative NNE (*DLX5*, *GATA3*, *ECAD*), PPE (*SIX1*) and EPI (p63) genes as suggested by Leung et al. (2016) would facilitate the identification of "unwanted" cells that belong to the aforementioned lineages.

However, the heterogeneity of day 6 NC cultures is not restricted to non-NC lineage and might occur within the NC compartment. RA administration specifies NC cells towards more posterior axial levels as indicated by the increase of *HOX* genes corresponding to "post-otic" region but whether these cells represent a pure vagal population still remains to be defined. Cells belonging to other NC streams such as cranial or cardiac may also emerge in our day 6 cultures, particularly due to the natural relationship they have in the embryo, as they emerge from adjacent and to an extent, overlapping domains (Figure 1.6) (Kuo and Erickson 2011). However, my pilot data based on immunocytochemistry analysis of the expression of the cranial NC marker *ALX1* (Iyyanar et al. 2022; Pini et al. 2022), the early and late cardiac mesenchyme markers *PRRX1* (Doufexi and Mina 2008; Leussink et al. 1995) and *BARX1* (Gould and Walter 2000; Tissier-Seta et al. 1995) were inconclusive. Specifically, I found that day 6 vagal NC cultures were not immunoreactive to PRRX1 and the antibodies against ALX1 and BARX1 were disregarded due to non-specific binding, a finding verified by the homogeneous and false positive signal upon antibody incubation in hESCs (Appendix Figure S3). Therefore, the emergence of cardiac and cranial NC populations in day 6 cultures requires further investigation. The lack of specific and reliable antibodies against certain cell types as well as the limited access to tissues expressing the desired markers to validate the antibodies, inevitably challenges our research. Hence, the best approaches to answer this question and determine to a great extent the overt heterogeneity and cellular composition of the NC compartment would be single cell transcriptome analysis (single cell-RNA seq) or hybridization chain reaction-RNA-fluorescence in situ hybridization (HCR RNA-FISH).

I previously showed by RT-qPCR an increase in *PHOX2B* and *ASLC1* transcript levels in response to RA treatment (Figure 3.2), a finding consistent with the acquisition of ENS progenitor transcriptional profile in day 6 cultures. Despite the global increase in their transcripts compared to undifferentiated cells, immunofluorescence analysis along with SOX10 demonstrated heterogeneous expression of these markers and depicted their presence in different subpopulations, that were not marked by the concurrent expression of SOX10 and the proneural genes *ASCL1*, *PHOX2B* (Figure 3.3). Surprisingly, PHOX2B protein expression did

not overlap with SOX10 and it was occasionally observed in ASCL1+ cells. This expression profile is consistent with the emergence of an advanced/enteric neural restricted progenitor at which SOX10 expression is repressed by ASCL1 and PHOX2B potentially via a negative-feedback loop (Kim et al. 2003). Also, the lack of SOX10 positivity in PHOX2B+ cells denotes that SOX10 is not required to retain PHOX2B expression, in agreement to a previous report (Kim et al. 2003). Whether SOX10 preceded PHOX2B expression in this subpopulation is still an intriguing question and that could be possibly addressed by isolating NC progenitors on the basis of SOX10:GFP expression and monitoring PHOX2B levels following RA treatment in a time course. Also, we cannot rule out the possibility that the PHOX2B+ and/or ASCL1+ subpopulation could reflect the presence of hindbrain/branchial motor neuron which arises from the same anteroposterior region to vagal NC and is marked by the expression of PHOX2B, ASCL1 and not SOX10 (Pattyn et al. 2000). This could be due to RA administration given its role in branchial motor neuron differentiation (Linville et al. 2004). The effect of RA treatment either in neuralisation or in advancing the vagal NC/ENS progenitors in day 6 NC cultures is also supported by our findings and the concomitant decrease in SOX10:GFP/p75 and SOX10:GFP/CD49d expression levels following a time course analysis in the presence/absence of RA (Appendix Figure S1,S2). The reduction in the levels of SOX10:GFP compared to non-RA-treated counterparts, 24hours after RA addition, therefore, denotes either a change in the cell fate decision (commitment to cranial motor neurons) underlying the transient state of the presumptive progenitor population and the plasticity of the hPSC-derived cultures or progression along the ENS differentiation pathway and early neural differentiation. Given how temporally closed these events are since SOX10:GFP starts being expressed around day 3 in culture (data not shown) and RA is added to induce PHOX2B expression at day 4, we can also argue that RA does not act only a SOX10+ putative NC progenitor but exerts its effect on a contaminating non-NC progenitor emerging in the culture (as discussed above) and steers a part of the population towards alternative non-NC associated differentiation routes. Finally, to determine the identity of SOX10-/PHOX2B+ cells in our cultures and distinguish between a cranial motor neuron and ENS progenitor lineage, staining for the motor neuron progenitor marker ISL1 would be the best approach to address this question (Pattyn et al. 2000; Pfaff et al. 1996).

Overall, how the overt heterogeneity in NC cultures affects the functionality and subsequent differentiation down to different routes remains to be determined. This matter requires thorough examination particularly in light of cell therapy treatment and the potential use of hPSC-derived NC cells to treat neurocristopathies such as Hirschsprung's disease.

3.5.2. Interplay between cell density and Wnt signalling pathway controls neural crest differentiation

Our observations, in line with previous findings (Chambers et al. 2009), suggest that cell density is a critical regulator of NC differentiation *in vitro* and an initial low-plating density is required to obtain NC cells with high yield (Figure 3.8B, 3.9). By contrast, when an initial high density is employed, the efficiency of the differentiation is greatly reduced and this is accompanied by an upregulation of *PAX6* (Figure 3.8B). A similar increase in *PAX6* expression is also observed after treating the cultures with a higher concentration of the Wnt agonist, CHIR99021, a finding suggesting that cell density and Wnt activity might be linked. Cell density and Wnt/β-catenin signalling have been shown to synergistically affect cell fate determination *in vitro*, in particular in cardiomyocyte differentiation (Buikema et al. 2020; Kempf et al. 2016; Le et al. 2021). For example, cell density-mediated Wnt inhibition through paracrine signalling in densely cultures was found to enhance cardiomyocyte generation (Le et al. 2021), while low-density plating associated with cell-cell contact disruption in cooperation with Wnt pathway stimulation was used to promote cardiomyocyte proliferation and expansion (Buikema et al. 2020).

The data in this chapter propose that cell density and Wnt signalling are also coupled in the context of NC. Gene expression analysis of the Wnt target, *AXIN2* revealed an increase in its expression levels when cells are plated at high density, a finding consistent with elevated canonical Wnt activity. Although Wnt stimulation is required for the induction of NC *in vitro* (Gomez et al. 2019a; Leung et al. 2016; Menendez et al. 2011), increased Wnt activity, as a result of high-plating density, seemed to have an antagonistic effect in our system, demonstrated by the reduction in SOX10 expression (Figure 3.9). This, contrasts previous findings from Menendez et al. (2011), which showed that increasing amounts of two Wnt activators, the GSK3 inhibitor, BIO and Wnt3a enhanced NC formation in a dose-dependent fashion and points to the requirement of precise and controlled levels of canonical Wnt signalling for efficient NC differentiation. The findings presented in this chapter in combination with the regulatory role of AXIN2 in restraining Wnt signalling activity (Lustig et al. 2002), suggest that cell density and concomitant *AXIN2* transcriptional activation might determine *SOX10* and *PAX6* expression by regulating Wnt signalling activity. According to this, I propose a model at which AXIN2 following its induction by high-plating density, may act in return to supress Wnt signalling as part of a negative feedback loop and as a result, impair NC differentiation by upregulating the expression of PAX6 (Figure 3.11).Under low-plating density and in the presence of the same Wnt inductive signals, we can speculate that AXIN2 expression is moderate, and therefore not sufficient to inhibit CHIR-mediated Wnt activation. Thus, Wnt pathway is active and allows for NC specification. Moreover, the findings summarised in this model highlight that cell density in

combination with Wnt agonist titration should be employed as a way to define the amount of Wnt activity required to obtain NC cells with high yield. Hence, we can speculate that higher concentration of CHIR might compensate for the negative feedback loop mediated by AXIN2 when cells are plated at a high density.

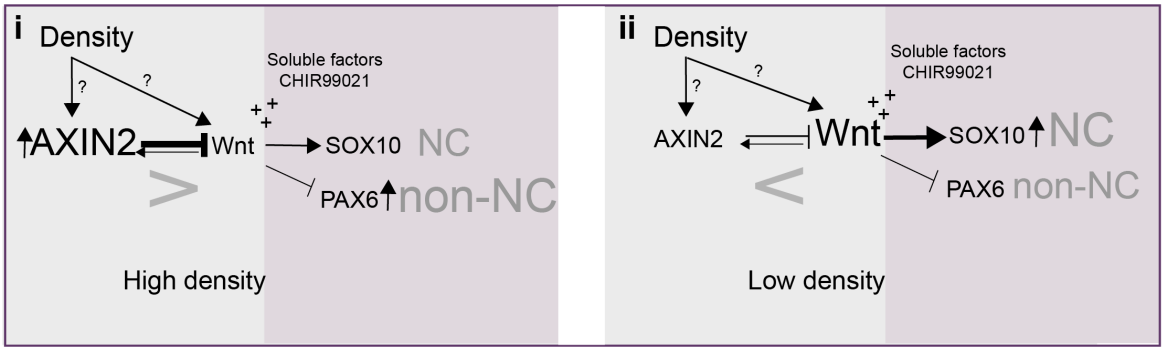

Figure 3.11. Schematic representation of the proposed model for the role of Wnt during neural crest induction: Wnt signalling pathway determines a NC or non-NC lineage in the case of (i) high and (ii) low plating density during hPSC-based NC differentiation. NC; neural crest.

The mechanism of action of cell density in our model though, still remains elusive and further work is required in order to dissect the links between low/high-plating density and Wnt/β-catenin pathway activity during NC differentiation. The use of a Wnt pathway luciferase reporter (TOPFlash (Korinek et al. 1997), SuperTOPFlash (Veeman et al. 2003), HAL (Yamaguchi et al. 2017) luciferase reporter constructs) would be a useful and more direct strategy for monitoring Wnt activity and measuring Wnt responses in cultures plated in increasing cell densities. This could be done in combination with AXIN2 knockdown to further evaluate the role of this gene in controlling Wnt pathway activity in response to high-plating density, possibly as part of a negative feedback loop.

Moreover, it is not clear to us how cell density stimulates Wnt signalling, and if paracrine or cell-cell contact mediated signalling is taking place. Several studies have previously shown that Wnt pathway could be equally activated by auto/paracrine factors and mechanical forces generated by cell-cell and cell-extracellular matrix contact signals in hES cell culture systems (Le et al. 2021; Muncie et al. 2020; Przybyla et al. 2016). For example, high cell-adhesion tension in hESCs (Muncie et al. 2020) and low-plating density (decreased cell-cell contact) in mESCs (LeBlanc et al. 2022) were found to promote release of β-catenin from cell-to cell junctions, β-catenin nuclear translocation and Wnt-mediated differentiation in response to external signals. It is possible then, that during NC differentiation, Wnt pathway could be stimulated by mechanical cues due to increased cell-cell contact, in a similar way to the previously mentioned systems. Moreover, we

can speculate that increased cell density could also regulate Wnt activity via ephrin–Eph or Notch-delta signalling, activated upon cell-cell contact. EfnB1 has been previously shown to inhibit canonical Wnt pathway during cranial NC induction in *Xenopus tropicalis* embryos (Wei et al. 2010), while Notch-Wnt molecular crosstalk has been implicated in many developmental processes (reviewed in Collu et al. 2014). Thus, examining the former signal transduction pathways (ephrin and Notch) in low- and high-plating density cultures in relation to Wnt activity can be used to determine if cell density exerts its effect on Wnt activity via juxtracrine interactions. On the other hand, a conditioned media transfer approach in compartmentalised cultures of low- and high-density cells and/or ELISA for Wnt regulators could be performed to evaluate the role of cell-secreted signals from high-plating density cultures on Wnt activation and NC formation through paracrine signalling. Collectively, the findings presented in this chapter propose a link between cell density, Wnt signalling activity and NC specification *in vitro*, however, further research is required to address the precise interactions and to provide a better insight into the underlying mechanism of high cell density and Wnt inhibition molecular interplay.

Chapter 4: Defining critical signals for human enteric nervous system specification *in vitro*

4.1. Introduction

The ENS is a complex and highly interconnected network of neurons and glia located within the wall of the gastrointestinal tract. It controls several vital processes including bowel motility, nutrients' absorption and digestion, secretion of water, electrolytes, hormones and regulates the blood flow (Furness 2012). The ENS is the largest branch of the PNS as it contains around 500 million neurons in humans (Furness 2006) and along with the sympathetic and parasympathetic divisions consists the autonomous nervous system. Although sympathetic and parasympathetic fibres provide the extrinsic innervation of the gut, the majority of the enteric neurons lack direct input from the CNS, and hence the ENS is able to mediate contractile reflex activity and peristalsis in an autonomous manner (Furness 2006). As mentioned earlier, the ENS originates from NC. The NC contribution to neurons and glia in the gastrointestinal tract was first described in 1954 in the avian embryo, by Yntema and Hammond, who demonstrated the absence of enteric ganglia in the gut upon resection of the dorsal neural tube in the caudal hindbrain region (Yntema and Hammond 1954). This notion, was further refined by Nicole Le Douarin and colleagues who pioneered cross-species transplantation and fate mapping experiments and revealed the axial-specific contribution of vagal and sacral NC-derivatives to the developing gut (Burns and Douarin 1998; Burns and Le Douarin 2001; Le Douarin and Teillet 1973). Within the vagal region, crest cells adjacent to somites 1-2, migrate along the vagus nerve as Schwann cell precursors and provide the oesophageal neurons, whereas cells close to somite levels 3-7 (posterior vagal/rostral trunk) follow the ventral pathway, contribute to the sympathetic chain and colonize the entire GI tract (Figure 1.6B). The sacral input, unlike the vagal, is mainly restricted to the pos-umbilical gut and was shown to expand the repertoire of enteric neurons by enriching for adrenergic/dopaminergic and serotonergic subtypes as opposed to secretomotor neurons derived from the vagal region (Tang et al. 2022). In addition to the vagal and sacral NC origin, Uesaka et al. (2015) using genetic fate mapping in mice proposed recently the ENS contribution of crest-derived Schwann cell precursors with thoracolumbar regional identity which migrate to the gut via extrinsic nerves and give rise to 20% of the ganglia, and predominantly calretinin-expressing neurons, in the colon after birth (Figure 1.6B). A similar contribution of trunk NC-derived Schwann cell precursors has been later demonstrated in post-embryonic gut in zebrafish (El-Nachef and Bronner 2020).

The colonisation of the gut starts around day 9-9.5 (E9-9.5) in mouse embryonic development and after week 4 of gestation in humans, when vagal NC/ENS precursors enter the foregut and

start migrating in a rostrocaudal fashion to populate its entire length (Heanue and Pachnis 2007). Once ENS precursors reach the hindgut, sacral NC invade the gut wall and migrate in the opposite direction to generate neurons and glia in the distal gut (Burns and Douarin 1998). Around E15 in mouse or week 7 of gestation in humans, the gut colonisation is complete (Heanue and Pachnis 2007). The generation of the right ENS derivatives in time and space requires the coordinated action and controlled balance between migration, proliferation and differentiation of ENS precursors within the bowel (Lake and Heuckeroth 2013).

NC cells migrating within the gut are molecularly identified by the expression of the pan-NC markers Sox10 (Southard-Smith et al. 1998), the low affinity neurotrophin receptor p75 (Chalazonitis et al. 1994) and the endothelin receptor type B, EDNRB (Nataf et al. 1996) as well as the ENS progenitor genes that encode the transcriptional regulators Phox2b (Pattyn et al. 1999), the mammalian achaete-scute homologue 1, Ascl1 (known as MASH1; Blaugrund et al. 1996) and the receptor tyrosine kinase, Ret (Pachnis et al. 1993). As ENS development progresses, ENS progenitors diverge along the neurogenic or gliogenic fate with neurons emerging prior to glia (Young et al. 2003). Progenitors destined to become neurons, downregulate Sox10 and p75, maintain the expression of Phox2b and Ret (Rao and Gershon 2016; Sasselli et al. 2012) and start expressing an array of pan-neuronal markers including PGP9.5 (Young et al. 2003), TUBB3 (Heanue and Pachnis 2006), neurofilament protein (NF) and HuC/D (Young et al. 2005). On the contrary, progenitors differentiating into glia retain the expression of p75 and Sox10, downregulate Ret and initiate the expression of glial markers like B-FABP, S100b and later, the terminal differentiation marker glial fibrillary acidic protein, GFAP (Young et al. 2003). A list with some of the aforementioned markers that are used in this study to characterise the ENS cultures is included in Table 4.1.

Although, numerous lineage-specific markers have revealed, the mechanism underlying cell fate determination in the ENS remains elusive. A recent study conducted by Laddach et al. (2022) attempted to decipher the mechanism of neural-glial diversification in the developing mouse small intestine using single cell transcriptomics and advanced bioinformatics. In contrast to the conventional bifurcation model at which ENS progenitors commit to neurogenic or gliogenic program, the authors propose the branching model, which, according to their findings suggests that the enteric neurons emerge sequentially upon committing to neurogenic fate and divert from the default gliogenic program (Laddach et al. 2022). During development, progenitors progressively lose the neurogenic bias and stick to the gliogenic transcriptional program (Laddach et al. 2022).

Several signals with gut origin guide the development of the ENS and presumably progenitors cell fate decisions. Among them, the glial-derived neurotrophic factor (GDNF) and endothelin-3 (ET3), which are both derived from the gut mesenchyme, are fundamental in controlling ENS progenitor's migration, proliferation and differentiation (Kang et al. 2021). GDNF, which acts through the RET/GFRα1 receptor complex expressed on the surface of migrating progenitor cells, promotes rostrocaudal migration and gut colonisation (Natarajan et al. 2002), survival and proliferation of ENS progenitors (Heuckeroth et al. 1998; Taraviras et al. 1999) as well as neuronal differentiation *in vitro* (Chalazonitis et al. 1998; Uesaka et al. 2013). Defects in GDNF signalling components (RET, GDNF or GFRα1) result in lack of enteric ganglia in the small and large intestine, highlighting the requirement of GDNF signalling in normal ENS development (Enomoto et al. 1998; Pichel et al. 1996; Schuchardt et al. 1994). Mutations in RET gene are amongst the most common cases in patients with HSCR (Amiel et al. 2008; Heanue and Pachnis 2007). Additionally, ET3 which is highly expressed in the caecum (Leibl et al. 1999), acts through its receptor EDNRB on the surface of migrating ENS progenitors to promote proliferation, to inhibit neural differentiation (Hearn et al. 1998; Nagy and Goldstein 2006) and maintain precursors in an uncommitted state (Hearn et al. 1998; Nagy and Goldstein 2017). Loss of EDNRB signalling is associated with aganglionosis in the distal colon (Gariepy et al. 1996; Hosoda et al. 1994) and mutations in genes of this pathway have been identified in HSCR (Amiel et al. 2008; Bhave et al. 2022) .

During ENS neurogenesis, progenitor cells acquire distinct neural phenotypes which differ in neurochemical content, electrophysiology, morphology and function. The ENS is mainly comprised of four types of neurons: 1) sensory neurons (also known as intrinsic primary afferent neurons, IPANs) which respond to environmental, mechanical and chemical cues, 2) interneurons, 3) excitatory and 4) inhibitory motor neurons controlling muscle activity (Fung and Vanden Berghe 2020; Furness 2012). Several classes of neurons have been identified in model organisms particularly in the guinea-pig and mouse. A recent study using sc-RNA sequencing identified 12 neuron classes in the mouse small intestine consisting of the aforementioned functional classes (Morarach et al. 2021). Although the subtype of neurons present in the human ENS have not been thoroughly catalogued (Hao and Young 2009), recent pioneering work using advanced single cell transcriptomics has described the neural cell populations emerging in distinct regions of the human ENS from fetal and adult intestines (Drokhlyansky et al. 2020; Elmentaite et al. 2021), elucidated the neuronal diversity as well as revealed conserved and species-specific transcriptional programs for major neuron classes.

As vagal NC cells predominantly generate the majority of the enteric ganglia *in vivo* (Le Douarin and Teillet 1973), we and others have tried to derive ENS components from a hPSC-derived

vagal NC intermediate *in vitro* (Figure 1.8) (Barber et al. 2019; Fattahi et al. 2016; Frith et al. 2020; Gogolou et al. 2021; Lai et al. 2017; Lau et al. 2019; Li et al. 2018; Majd et al. 2022; Schlieve et al. 2017; Workman et al. 2017). The protocols developed, in addition to the variation in the initial NC induction and presumably in the heterogeneity of the NC progeny, show a great degree of variation in the subsequent ENS differentiation, making it hard to compare and evaluate the success of each method. Tissue-engineering approaches (Fattahi et al. 2016; Schlieve et al. 2017), co-culture with intestinal and colonic organoids (Lau et al. 2019; Workman et al. 2017), gut explant culture (Li et al. 2018) and *in vivo* grafting into mouse/chicken gut (Fattahi et al. 2016; Frith et al. 2020; Li et al. 2018; Workman et al. 2017) are some of the strategies employed to show the ENS potential of hPSC-derived NC cells and their ability to form enteric neurons and glia (Figure 1.8). Among these studies, only a few of the protocols including ours (Gogolou et al. 2021; Barber, Studer & Fattahi 2019; Frith et al. 2020; Lai et al. 2017; Lau et al. 2019, Majd et al. 2022) explore the ENS potential of hPSC-derived vagal NC cells solely *in vitro*, without providing an *in vivo* physical niche or gut-derived instructive signals.

Even though these approaches share similarities regarding NC induction, the successive steps of ENS specification vary considerably. GDNF (Young et al. 2001) and the antioxidant, ascorbic acid (Rharass et al. 2017) are the main signals applied for the enteric neuronal induction in adherent cultures (Barber, Studer & Fattahi 2019; Fattahi et al. 2016; Frith et al. 2020; Lai et al. 2017; Lau et al. 2019). However, the protocols developed by Lau et al. (2019) and Li et al. (2018) in the intestinal explant culture, utilise a neural induction cocktail supplemented with additional small molecules such as BDNF, NT3, NGF, c-AMP, while Frith et al. (2020) use DAPT-mediated pharmacological inhibition of Notch signalling pathway to enrich for enteric neurons *in vitro*. The discrepancies in the small molecules used and the signalling cascades manipulated raise questions regarding the effect of these additional factors on ENS efficiency, neuron and glia diversification and downward neuronal subtype specification. There is, therefore, a requirement to define signals that ascribe NC cells an ENS signature in order to optimise current differentiation protocols and understand better the ENS ontogenesis *in vitro*. There is also need to characterise the molecular and electrophysiological properties of the cells generated throughout the differentiation to confirm peripheral, enteric neuron and glial identity. Identification and evaluation of such parameters will allow optimisation and standardisation of the current method and will be beneficial for translational research and potentially manufacturing clinically relevant progenitor cells for cell therapy treatment of enteric neuropathies.

Table 4.1. Markers used in this study to characterise vagal neural crest cells and their enteric nervous system derivatives.

Cell types	Markers
NC	PAX3/PAX7, SOX10, p75, CD49d
Vagal NC/early ENS progenitors	PAX3/PAX7, SOX10, p75, CD49d, ASCL1, PHOX2B, HOXB1-5, (S100β), RET, GFRA1
Enteric neurons	HuC/D, TuJ1, PGP9.5, PERIPHERIN, NF-H, PHOX2B, NOS, CHAT, TH, Calretinin (CALB2), HRT2A, SST, RET, TRKC
Enteric glia	SOX10, S100β, CD49d

4.2. Aims

The great variability between the existing culture regimes to generate ENS derivatives from hPSCs *in vitro*, the labour and skill-intensive approaches followed which last approximately 30-60 days make the direct comparison between the existing protocols impracticable. To circumvent these issues and to examine ENS ontogenesis *in vitro*, this chapter focuses on our previously published protocol (Frith et al. 2020; Gogolou, Frith & Tsakiridis 2021) as a means to define critical signals/parameters for ENS differentiation *in vitro.* Specifically, the work presented here aims at addressing the following:

1. Characterise the *in vitro* hPSC-derived ENS progenitors and neurons
2. Identify signals that influence cell fate specification during the transition from vagal NC to ENS progenitors and their derivatives, enteric neurons and glia

4.3. Derivation of enteric nervous system components

4.3.1. Molecular characterisation of *in vitro*-derived enteric nervous system components

Following the generation and characterisation of the vagal NC population, I aimed to derive and further characterise enteric neurons and glial cells downstream of vagal NC differentiation. This involves the expansion of vagal NC/ENS progenitors in non-adherent conditions for 3 days under the presence of FGF/Wnt/RA signals before plating them into neurotrophic media to induce an enteric neuron/glial cell identity (Frith et al. 2020; Gogolou et al. 2021) (Figure 4.1A).

To this end, I differentiated both the H9SOX10:GFP and the WTC-11 cell lines under standard vagal NC differentiation conditions to yield a vagal NC/early ENS progenitor identity by day 6 and following that, I subjected the progenitor cells in culture regime that promotes formation of 3D

cell sphere aggregates (Figure 4.1B; Day 9). These were subsequently grown for a short, 3-day period under the influence of FGF2, CHIR and RA instructive signals and then plated into ENS induction medium containing GDNF, ascorbic acid (AA) and DAPT (N-[N-(3, 5-difluorophenacetyl)-l-alanyl]-s-phenylglycinet-butyl ester), a γ-secretase inhibitor that indirectly blocks the activity of Notch pathway (Dovey et al. 2001), to promote enteric neuron and glial identity (as shown in Figure 4.1A). At day 10 of the differentiation (one day after plating into ENS induction conditions), cells started migrating out of the spheres and differentiating into neurons (Figure 4.1B; Day 10). At day 22, neurons were clustered together forming small ganglia-like structures (Figure 4.1B; Day 22), which progressively became highly interconnected with neighbouring clusters creating extended neural networks that were maintained *in vitro* for up to 100 days (Figure 4.1B; Day 60,100).

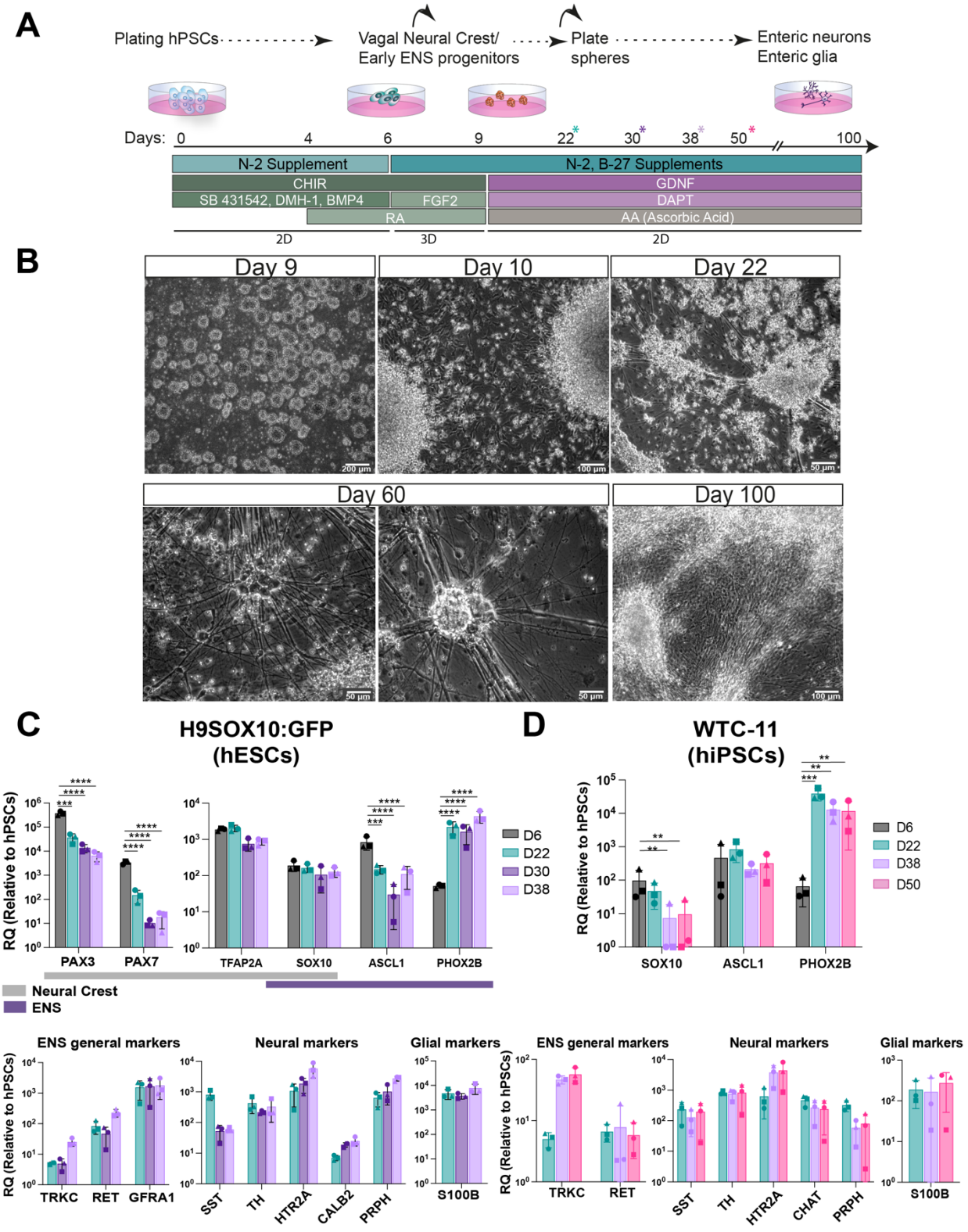

Figure 4.1. *In vitro* generation of enteric nervous system progenitors, enteric neurons and glia from hPSCs. (A) Schematic of the protocol depicting the time points and culture regimen employed for the generation of ENS components *in vitro*. Colour-coded asterisks indicate the time points of gene expression analysis and correspond to coloured bars in chart bars (C,D). (B) Representative brightfield images of differentiated cultures derived from the H9SOX10:GFP reporter cell line at the indicated time points. Scale bars are indicated. (C-D) Upper panel: Gene expression analysis of NC and ENS progenitor genes in H9SOX10:GFP (C) and WTC-11 (D) cell lines at the indicated time points. Lower panel: Gene expression analysis of ENS general, neural and glial markers in H9SOX10:GFP (C) and WTC-11 (D) cell lines at the indicated time points. Data shown are the mean of mean values ± SD, n=3 independent experiments with three technical replicates in each experiment. Each biological replicate is represented

by a unique shape, **P <0.01, *** P ≤0.001, ****P <0.0001 by one-way repeated measures ANOVA Dunnett's post-hoc multiple comparisons test with control "Day 6" group. Only statistically significant comparisons are indicated in C-D (upper panel).

To determine gene expression changes as vagal NC cells differentiated along the ENS pathway, RT-qPCR was performed for a panel of NC, ENS progenitor, neural and glial markers at distinct time points within a period of 38-50 days from the beginning of the protocol. Gene expression analysis for the neural plate border/NC-associated genes *PAX3*, *PAX7* revealed that they were highly induced at day 6 and following that, their transcript levels showed a steady and significant decline as cells differentiated along the ENS trajectory (Figure 4.1C; upper panel). In contrast, the NC specifier *TFAP2A* was upregulated at day 6 and its expression levels were maintained throughout differentiation (Figure 4.1C; upper panel). Similarly, *SOX10* was constantly expressed at all time points examined in the H9SOX10:GFP, however, its transcripts were greatly reduced/almost extinct at day 38 and day 50 of the protocol (~10-fold reduction) in the WTC-11 cell line (Figure 4.1D; upper panel). *ASCL1* transcripts in the H9SOX10:GFP were highly induced at day 6, marking early ENS progenitors and decreased at day 22 onwards, as cells differentiated towards enteric neurons (Figure 4.1C; upper panel) though no significant changes were observed in *ASCL1* levels between day 22-50 in the WTC-11 (Figure 4.1D; upper panel). The ENS progenitor/enteric neural marker *PHOX2B* was also upregulated following day 6, in response to ENS induction signals in both cells lines (Figure 4.1C-D; upper panel). The acquisition of an enteric neural signature was as well accompanied by an increase at day 22 and maintained expression throughout differentiation of the glial gene *S100B* (Young et al. 2003) (Figure 4.1C-D; lower panel).

The downregulation of NC- and upregulation of ENS-associated transcripts suggested that cells differentiated along the ENS lineage and acquired a more developmentally advanced phenotype. To further examine this and assess the ENS identity of the differentiated cultures, I looked at the expression of a set of ENS receptor, neural and glial markers at three distinct time points. In H9SOX10:GFP cell line, the transcript levels of *RET* and *GFRA1*, genes encoding the subunits of GDNF receptor complex in the developing ENS (Taraviras et al. 1999; Treanor et al. 1996), were highly induced throughout differentiation and *RET* expression reached its highest levels at day 38 of the protocol (RET: ~250-fold increase vs hPSCs, GFRA1: ~1000-fold increase vs hPSCs; Figure 4.1C; lower panel). Similarly, the transcript levels of *TRKC*, the transducing receptor for neurotrophin-3 (NT-3), a factor linked with ENS development and maintenance (Chalazonitis et al. 2001; Chalazonitis et al. 1994), were induced but to a lesser extend at day 38 of the differentiation (~25-fold increase vs hPSCs; Figure 4.1C; lower panel).

Gene expression analysis for a battery of neural markers revealed significant upregulation of *PRPH*, a protein coding gene widely expressed in PNS neurons (Escurat et al. 1990), *SST* (Somatostatin; encodes somatostatin, an hormone expressed in subclasses of enteric neurons (Kustermann et al. 2011; Qu et al. 2008)), *TH* (tyrosine hydroxylase; encodes the catecholamine synthetic enzyme- marker of dopaminergic neurons (Li et al. 2004)) and *HTR2A* (5-Hydroxytryptamine (Serotonin) Receptor 2A; encodes a receptor for serotonin-marker of serotonergic neurons (Li et al. 2011)) at day 22 of the differentiation (Figure 4.1C; lower panel). At later stages (day 30 and 38), the majority of neural markers showed a moderate increase while *SST* transcript levels dropped, denoting transient gene expression occurring in day 22 ENS cultures (Figure 4.1C; lower panel). Moreover, *CALB2* (encodes the calcium-binding protein, calretinin (Walters et al. 1993)) was slightly induced at day 22 and its expression increased steadily during ENS differentiation (~25-fold increase vs hPSCs; Figure 4.1C; lower panel). Differentiation of the WTC-11 cell line also resulted in upregulation of neural (*SST*, *TH*, *HTR2A*, *CHAT*, *PRPH*) transcripts on day 22 and their expression was sustained to a great extent, until the end of the protocol (Figure 4.1D; lower panel). Notably, *CHAT,* which encodes the synthetic enzyme of acetylcholine, (Choline O-Acetyltransferase; present in cholinergic enteric neurons (Hao et al. 2013; Qu et al. 2008)) was expressed throughout the differentiation (~400 fold increase vs hPSCs) in WTC-11 differentiated cells and unlike the H9SOX10:GFP cell line, *CALB2* transcripts were not observed during differentiation of the WTC-11 cell line (Figure 4.1D; lower panel). In addition to that, *TRKC* transcript levels were highly induced after day 22 of the protocol (~50-fold increase vs hPSCs) whereas *RET* expression showed only a minor upregulation between day 22 and 50 (Figure 4.1D; lower panel).

Collectively, the temporal expression of NC/ENS progenitor, enteric neuron and glial genes at the transcript level, indicates that this protocol promotes the progressive induction of ENS progenitors and enteric neurons/glia starting from a vagal NC intermediate, in a process that resembles the sequence of events occurring *in vivo*.

To verify the identity of the differentiated cells at the protein level, I next carried out immunofluorescence analysis at an early (Day 22; Figures 4.2-4.3) and late stage (Day 38-55; Figures 4.5-4.6) in differentiated cells from H9 (or H9SOX10:GFP) and WTC-11 cell lines. A battery of antibodies was used to define neurons by the their size, shape and neurochemical content. Antibodies against pan-neuronal markers (HUCD, PGP9.5, PERIPHERIN, TUJ1, NF-H) were employed at all times to visualise neural cell bodies and/or their projections and the main neural subtypes were identified in relation to the HUCD- or PGP9- positive neurons following antibody staining. At day 22, H9 and WTC-11 differentiated neurons showed strong immunoreactivity for HUCD, the ELAV-like neuronal RNA-binding proteins (De Giorgio et al.

2003) which have been shown to mark myenteric neurons in the mouse small intestine and the human colon (Murphy et al. 2007; Qu et al. 2008) (Figure 4.2A). HUCD signal was confined within neuronal somata, localised in the cytoplasm and to some extent in the nuclei and was found to label PERIPHERIN-positive neurons (Figure 4.2A). Neuron class III tubulin (TUJ1) immunoreactivity labelling neural projections was also detected in day 22 ENS cultures demonstrating the dense neural networks that have formed at this early stage (Figure 4.2B). SOX10 positivity following antibody staining (WTC-11) or using the reporter H9SOX10:GFP indicated the presence of progenitor and/or glial cells, as SOX10 at this stage likely marks both populations, growing in close vicinity to neural clusters (Figure 4.2B). To determine the identity of SOX10-positive cells and whether they represent glia, I performed immunostaining of H9SOX10:GFP-derived ENS cultures with the glial marker S100β (Figure 4.3). The analysis showed colocalization of SOX10:GFP and S100β signal, a finding that indicates the presence of glia in day 22 cultures (Figure 4.3; arrows). Glial cells were found close to Neurofilament-H (NF-H)-positive neural clusters and fibres, location that reflects their supporting role to neurons as well as potential neuron-glial crosstalk (Boesmans et al. 2019) (Figure 4.3). PHOX2B, a transcription factor shared between ENS progenitors and enteric neurons, was detected in the majority of PERIPHERIN-positive neurons located in low density areas (Figure 4.2Ci) and in very dense/3D clusters, and in mutually exclusive cells in relation to ASCL1 immunostaining (Figure 4.2Cii). The lack of strong PERIPHERIN signal in 3D clusters and the expression of ASCL1, which potentially marks remaining neuroblasts transitioning into the neurogenesis phase (Morarach et al. 2021) suggest that PHOX2B+/PERIPHERIN- cells located in 3D clusters represent ENS progenitor cells. This hypothesis is also supported by data acquired from live imaging of ENS cultures showing that neurons emerge and migrate out of the 3D clusters (Figure 4.4).

In this series of experiments, eGFP-labelled day 6 vagal NC cells were mixed in 1:10 ratio with stage of differentiation matched unlabelled cells derived from the parental cell line and subjected to sphere formation for 3 days prior to replating into ENS inducing conditions for single cell tracking (4.4A). A few hours after plating (6-9h), cells were observed to migrate out of the spheres, to elaborate axons and cells continued to move extensively for approximately 75h. Progressive cell death which reached its highest point after 48h, caused by a reagent that was found to be faulty, prevented downstream analysis and quantification of eGFP+ cell migration. Nonetheless, this approach showed that single cell tracking is feasible using this culture system and this assay could be readily exploited to extract information regarding progenitor cell migration directionality, speed and overall behaviour in these very dense and greatly hard to image cultures.

To define the major neural subpopulations emerging in day 22 cultures, I next examined the expression of the neural subtype markers TH, nNOS and ChAT. At day 22 cultures, a small proportion of neurons labelled with the pan-neural marker PGP9.5 was immunoreactive to TH (Figure 4.2.D; arrows) demonstrating the existence of catecholaminergic cells in *in vitro* derived ENS cultures, a subpopulation occurring in the mouse embryonic and human fetal gut (Baetge and Gershon 1989; Rauch et al. 2006; Young et al. 1999), while a bigger proportion of cells expressed ChAT (Figure 4.2E), a marker of cholinergic neurons, previously shown to mark nearly 50% of myenteric neurons in human colon (Murphy et al. 2007). Also at day 22, a fraction of HUCD-positive cells showed immunoreactivity to neuronal nitric oxide synthase (nNOS), the synthetic enzyme of nitric oxide, possibly marking inhibitory motor neurons and interneurons (Murphy et al. 2007) (Figure 4.2F).

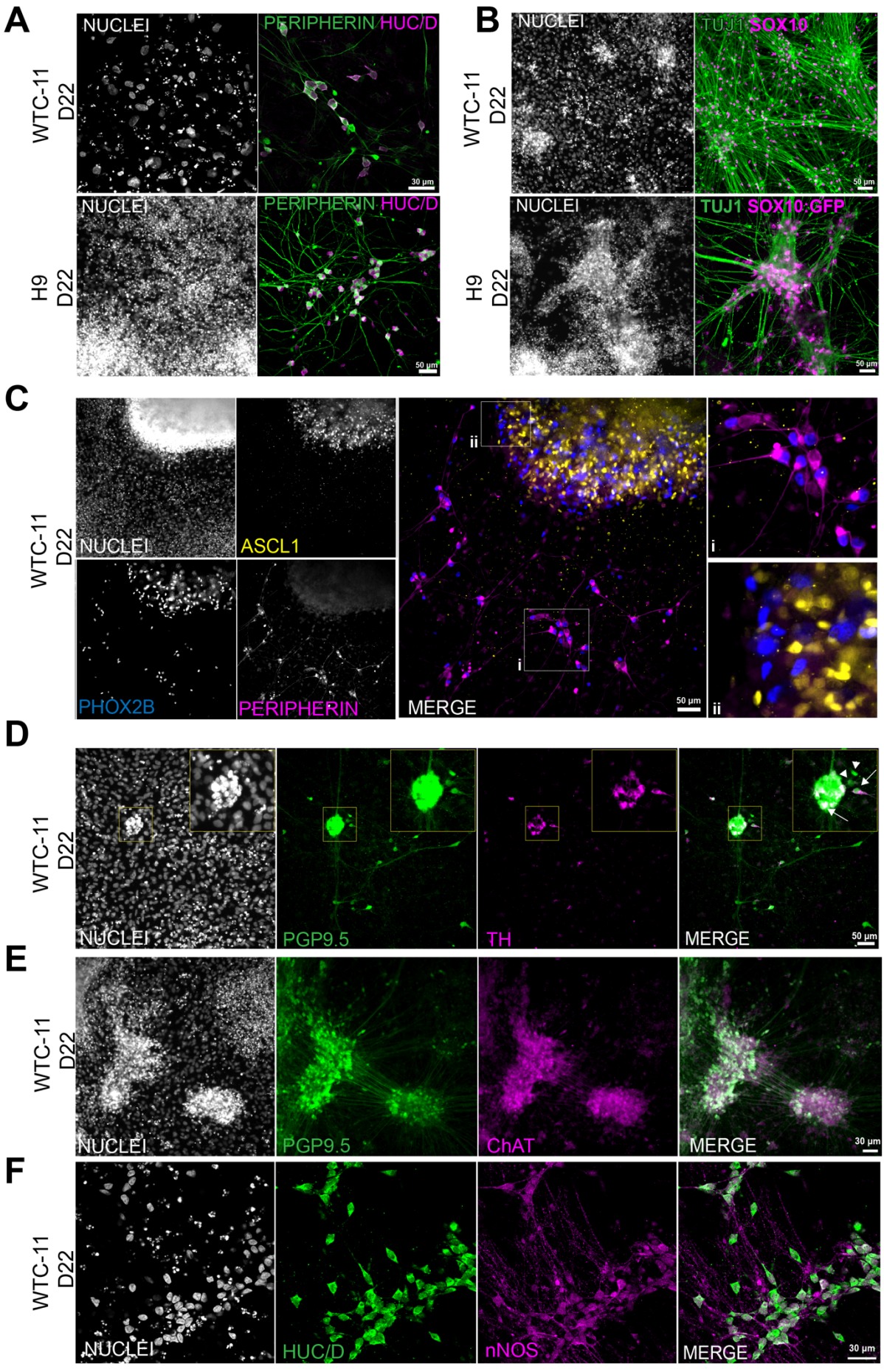
A
WTC-11 D22
NUCLEI
PERIPHERIN HUC/D
30 µm
H9 D22
NUCLEI
PERIPHERIN HUC/D
50 µm
B
WTC-11 D22
NUCLEI
TUJ1 SOX10
50 µm
H9 D22
NUCLEI
TUJ1 SOX10:GFP
50 µm
C
WTC-11 D22
NUCLEI
ASCL1
PHOX2B
PERIPHERIN
ii
i
MERGE
50 µm
i
ii
D
WTC-11 D22
NUCLEI
PGP9.5
TH
MERGE
50 µm
E
WTC-11 D22
NUCLEI
PGP9.5
ChAT
MERGE
30 µm
F
WTC-11 D22
NUCLEI
HUC/D
nNOS
MERGE
30 µm

Figure 4.2. Immunofluorescence analysis of day 22 hPSC-derived enteric nervous system cultures. (A-B) Expression of PERIPHERIN, HUCD (A) and TUJ1, SOX10 or SOX10:GFP (B) in day 22 cultures derived from WTC-11 and H9SOX10:GFP cell lines. (C) Immunofluorescence analysis of the expression of ASCL1, PHOX2B and PERIPHERIN in day 22 ENS cultures generated using the WTC-11 cell line. Insets show magnified regions of cells co-expressing PERIPHERIN and PHOX2B (i) and single positive cells for ASCL1 and PHOX2B(ii). (D) Expression of the neural subtype marker TH together with the pan-neural marker PGP9.5 in day 22 cultures generated using the WTC-11 cell line. Arrowheads in the magnified region indicate TH- neurons while arrows show TH+ neurons. (E) Expression of the neural subtype marker ChAT together with PGP9.5 in day 22 cultures generated using the WTC-11 cell line. (F) High power images showing the expression of the neural subtype marker nNOS together with the pan-neural marker HUCD in day 22 cultures generated using the WTC-11 cell line

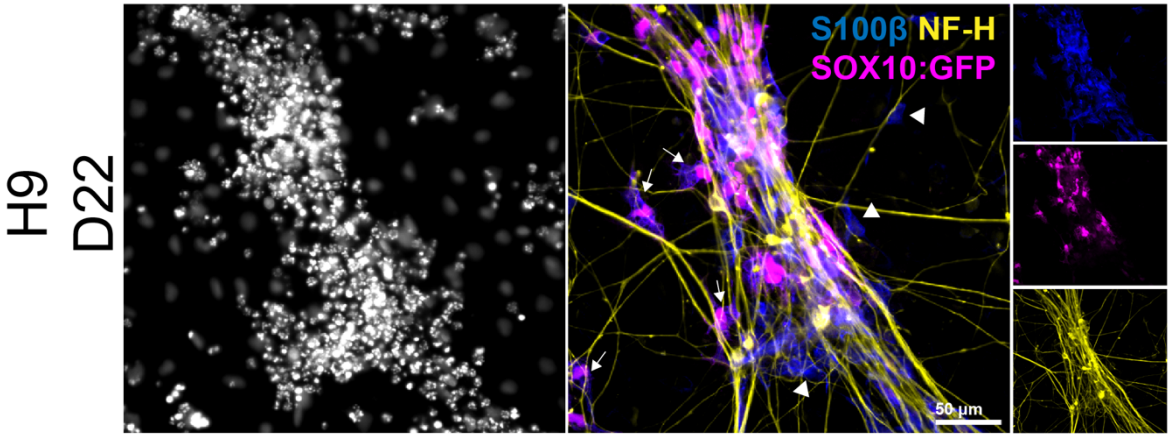

Figure 4.3. Day 22 cultures contain neurons and glial cells. Immunofluorescence analysis of the expression of the glial markers S100β, SOX10:GFP and the neural marker NF-H in day 22 cultures derived from the H9SOX10:GFP reporter cell line. Arrows indicate double-positive cells while arrowheads show S100+ cells.

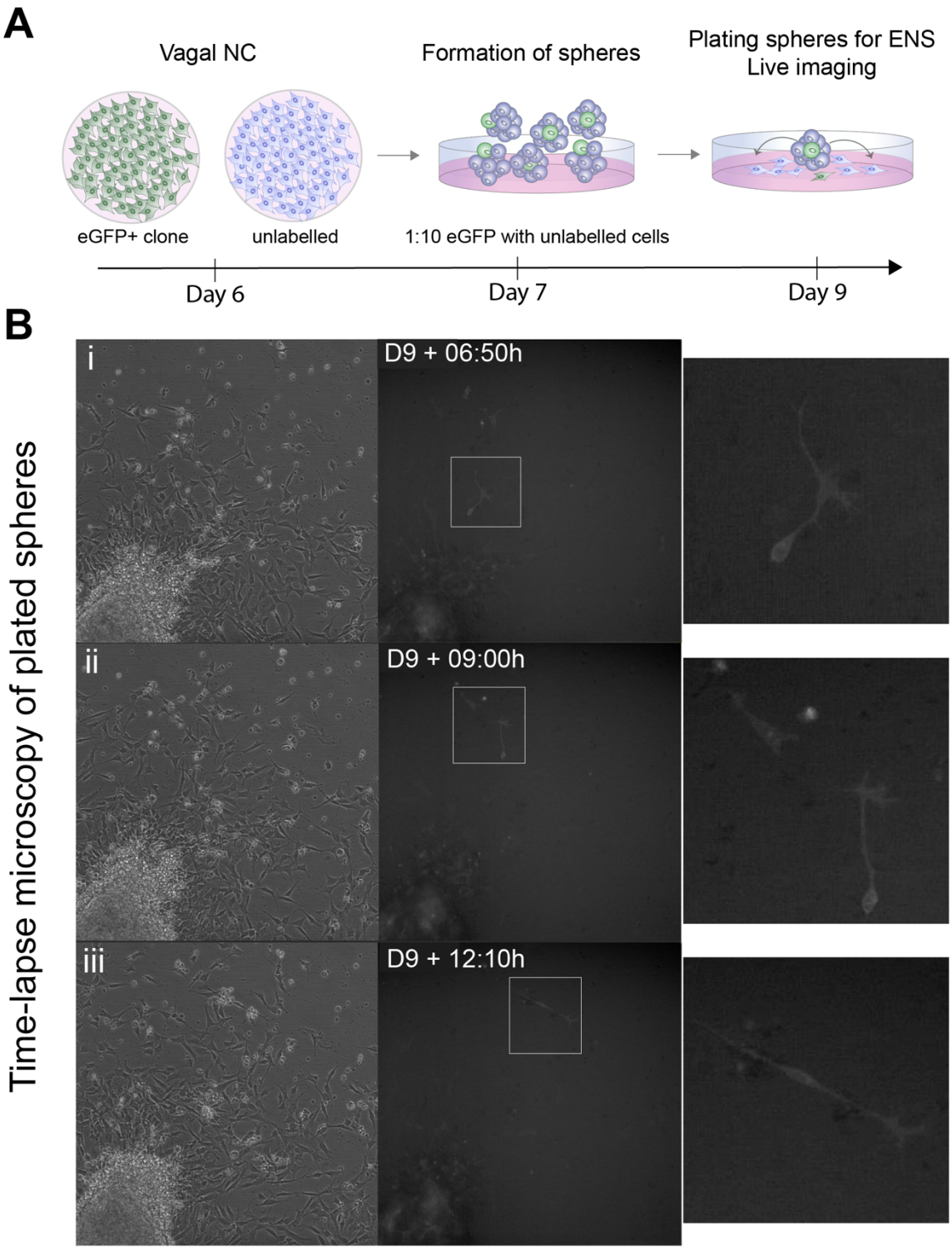

Figure 4.4. Neurons migrate out of the spheres a few hours after plating. (A) Schematic showing the experimental strategy. eGFP-expressing (WTC-11) and unlabelled cells from the parental line were differentiated to vagal NC and mixed 1:10 prior to sphere formation. Spheres were subjected to ENS differentiation (day 9) and were live imaged to track eGFP+ progenitor cells' migration. (B) Snapshots from time-lapse microscopy videos (brightfield and fluorescence imaging) showing neurons migrating out of the spheres at the indicated hours (h) after plating on day 9 (D9). Insets show magnified areas. The growth cone at the end of the axon is visible in all cases. eGFP-WTC-11 clone was provided by Rebecca Lea after sorting for the eGFP+ in the WTC-11 rainbow reporter cell line containing a modified Brainbow cassette. The rainbow reporter cell line was made in Jennifer Davi's group (El-Nachef et al. 2020). Live imaging was performed with the help of Chris Price in Nikon Biostation CT every 10 min for 75h.

At day 38 of the differentiation in H9SOX10:GFP-derived cultures, neural cells were organised into big clusters positive for PERIPHERIN and HUCD that surrounded SOX10:GFP expressing glia (Figure 4.5Ai). Antibody staining against RET (Heanue and Pachnis 2008; Pachnis et al. 1993) in d38 cultures revealed expression of the receptor in cells negative for the glial markers SOX10 and S100 (Figure 4.5Aii), possibly labelling cells of enteric neural lineage, in line with previous findings that suggest maintained expression of RET in differentiated neurons (Young et al. 2003). In contrast, antibody staining for the receptor TRKC showed positive signal in SOX10:GFP+ and SOX10:GFP- with a neural morphology cells (Figure 4.5Aiii), suggesting that TRKC expression is not restricted to a specific lineage. This is not the case in cultures of crest-derived cells isolated from fetal rat gut, where TRKC is predominantly expressed in a subset of enteric neurons (Chalazonitis et al. 2001), and therefore we can speculate that this is an *in vitro*-culture artefact, a technical error due to false reporting of the SOX10:GFP or that the double positive population (SOX10:GFP+/TRKC+) represents a differentiating progenitor transitioning into neuron (Figure 4.5Aiii). At day 55 of the differentiation in H9SOX10:GFP-derived cultures, peripheral neurons continued to be present (Figure 4.5Bii) and expressed enteric neural subtype markers such as CALRETININ (Figure 4.5Bi), TH (Figure 4.5Biii) and ChAT (Figure 4.5Biv).

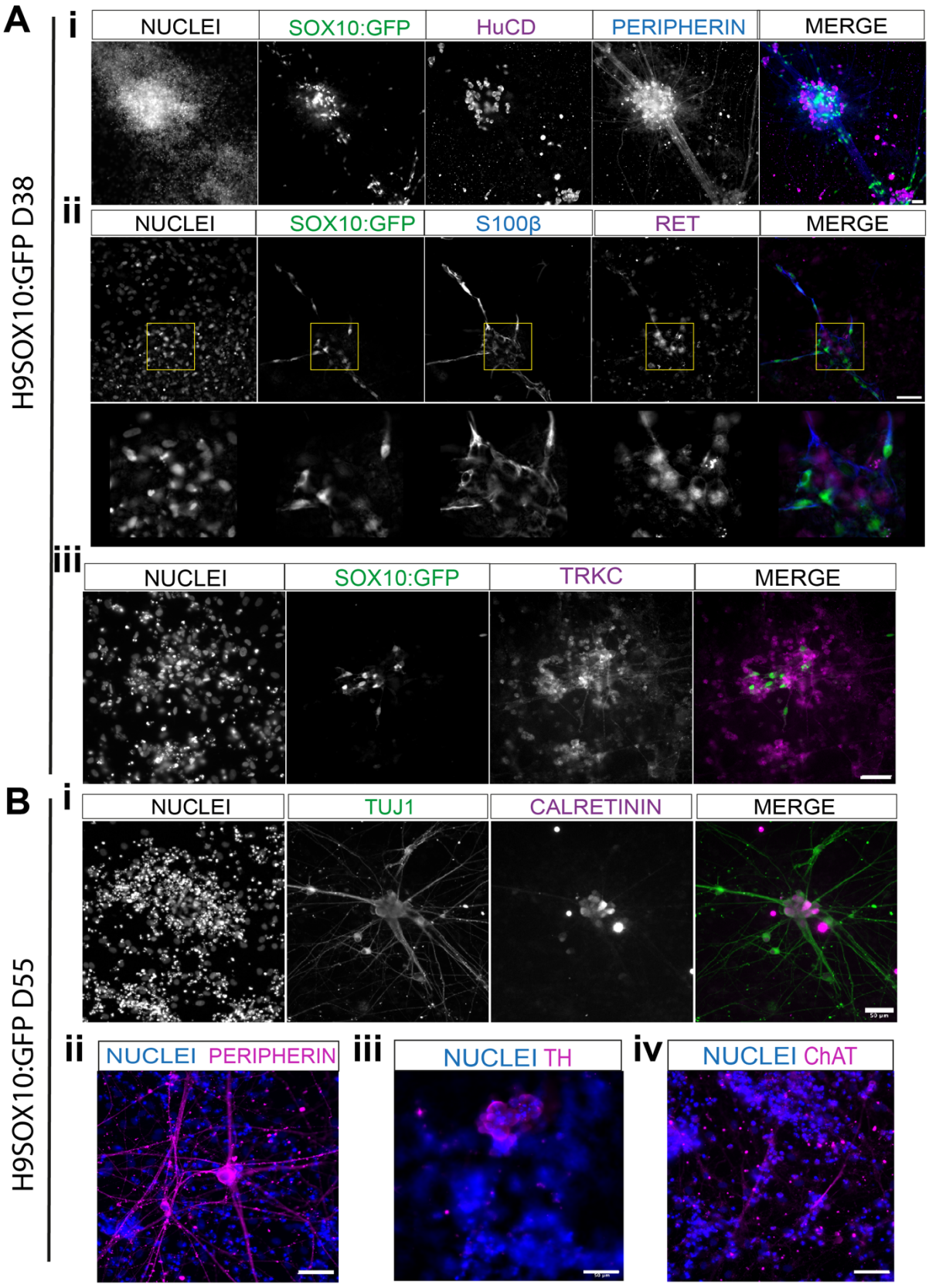

Figure 4.5. Immunofluorescence analysis of the expression of neural and glial markers in day 38 and 55 enteric nervous system cultures generated using the H9SOX10:GFP reporter cell line. (A) Expression of the neural markers PERIPHERIN, HUCD (i), RET (ii), the NT-3 growth factor receptor TRKC (iii) and the progenitor/glial markers SOX10 (SOX10:GFP) and S100β (i-iii) in day 38 ENS cultures. Insets show magnified regions. (B) Expression

of the neural subtype markers CALRETININ (i), TH (iii), ChAT (iv) and the pan-neural markers TUJ1 (i) and PERIPHERIN (ii) in day 55 ENS cultures. Scale bars=50 μm.

In day 50 ENS cultures derived from WTC-11 cell line, glial cells positive for SOX10, S100β (Figure 4.6A) and neural cells positive for TUJ1 (Figure 4.6A,F) or co-expressing PERIPHERIN, PHOX2B and infrequently ASCL1 (arrow, Figure 4.6B), were also observed. A subset of these neurons was stained positive for TH (Figure 4.6C), nNOS (Figure 4.6D), ChAT (Figure 4.6E), similar to day 22 cultures (Figure 4.2D-F). Immunofluorescence analysis of the expression of TRKC, showed homogenous staining in a large number of cells, possibly marking cells of neural lineage (Figure 4.6H), while a few cells positive for substance P, a neuropeptide expressed in subpopulations of excitatory neurons in the human ENS (Wattchow et al. 1988) were rarely observed (Figure 4.6G). These data demonstrate that our protocol generates enteric neural and glial cultures from hES and hiPS cell lines, they are labelled with markers expressed in the human ENS *in vivo* and these cultures could be maintained *in vitro* for at least 50-55 days.

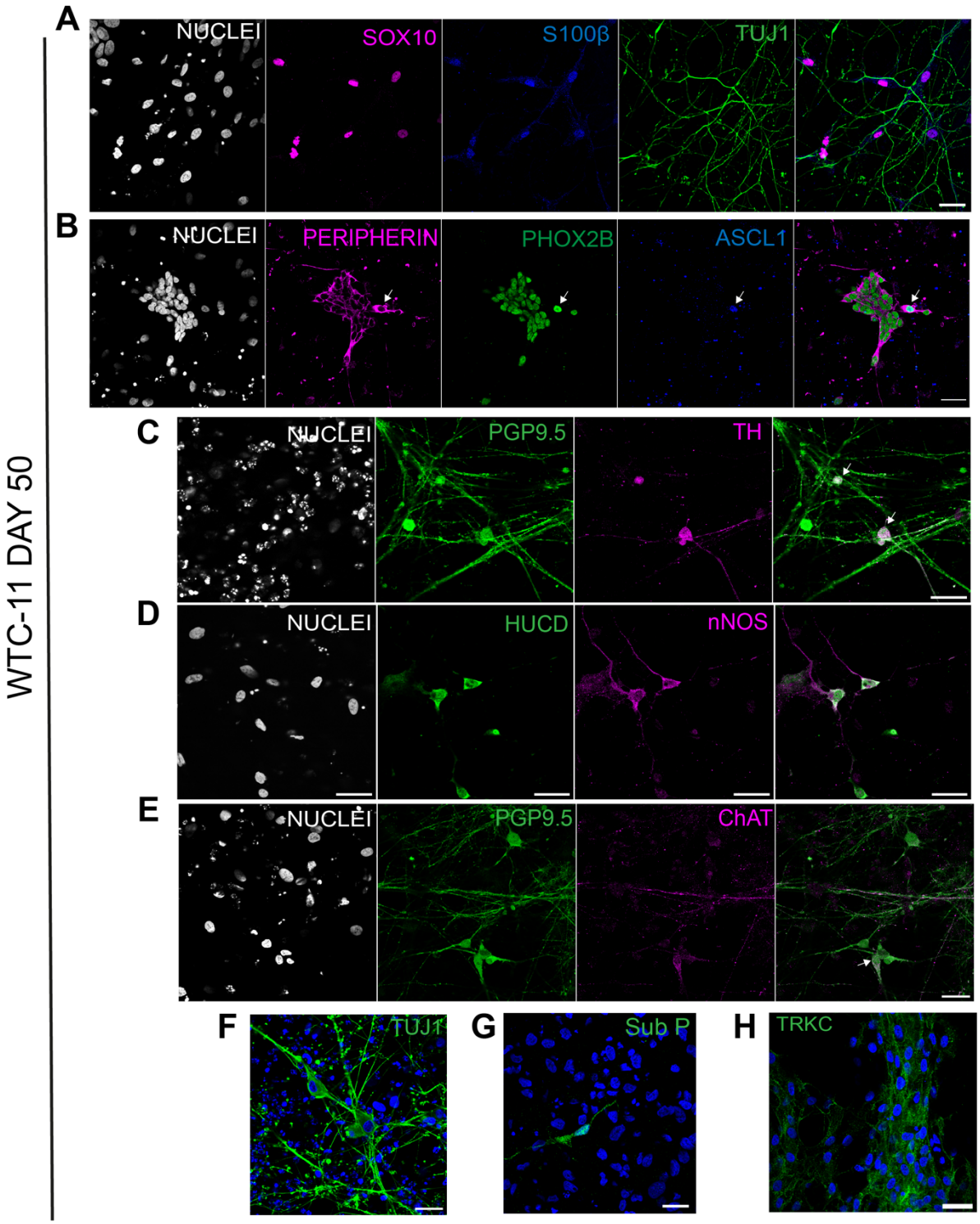

Figure 4.6. Immunofluorescence analysis of the expression of neural and glial markers in day 50 enteric nervous system cultures generated using the WTC-11 cell line. (A) Expression of the neural marker TUJ1 and the progenitor/glial markers SOX10 and S100β in day 50 ENS cultures. (B) Immunofluorescence analysis of the expression of ASCL1, PHOX2B and PERIPHERIN in day 50 ENS cultures. The arrow indicates the presence of a triple positive cell. (C-E) Expression of the neural subtype markers TH (C), nNOS (D), ChAT (E) together with the pan-neural marker PGP9.5 or HUCD in late ENS cultures. Arrows demonstrate double positive cells. (F-H) Expression of the neural markers TUJ1 (F), Substance P (Sub P) (G) and TRKC (H) in day 50 ENS cultures. Scale bars=30 μm.

In chapter 3 (3.3.1), I showed that CD49d expression is co-localised with p75 and SOX10 in day 6 NC/early ENS cultures marking presumptive ENS progenitor cells (Figure 3.5). To determine whether its expression persists during ENS differentiation and if it is fate-restricted following lineage segregation, in a similar manner to the expression of SOX10, I next examined CD49d immunoreactivity in differentiating ENS cultures in a time course analysis and in relation to progenitors/glia (SOX10+; Figure 4.7A, Figure 4.8) and neurons (PGP9.5+; Figure 4.7B). Immunofluorescence analysis revealed that CD49d marked predominantly SOX10 expressing cells at all time points examined and its expression was not detected in neurons (Figure 4.7). At day 11 of the differentiation, a time point the first neurons emerged, CD49d was restricted to SOX10+ ENS progenitors. The loss of CD49d expression in emerging neurons by day 11 indicates that its extinction coincides with neural differentiation (Figure 4.7; D11). As differentiation progressed (day 13-15), the fluorescence intensity of CD49d increased and its signal became more defined and strictly localised in SOX10+ cells (Figure 4.7; D13,D15). Concurrently, the number of neurons increased as more cells committed to neural lineage and these neurons continued to be negative for CD49d. At day 22 of the differentiation (Figure 4.7; D22), a similar pattern in CD49d expression was observed, while triple labelling experiment with the glial marker S100β revealed co-expression of SOX10, S100β and CD49d (Figure 4.8). This finding along with the previous observations suggests that CD49d expression in ENS differentiated cultures progressively becomes restricted from ENS progenitors to glial cells.

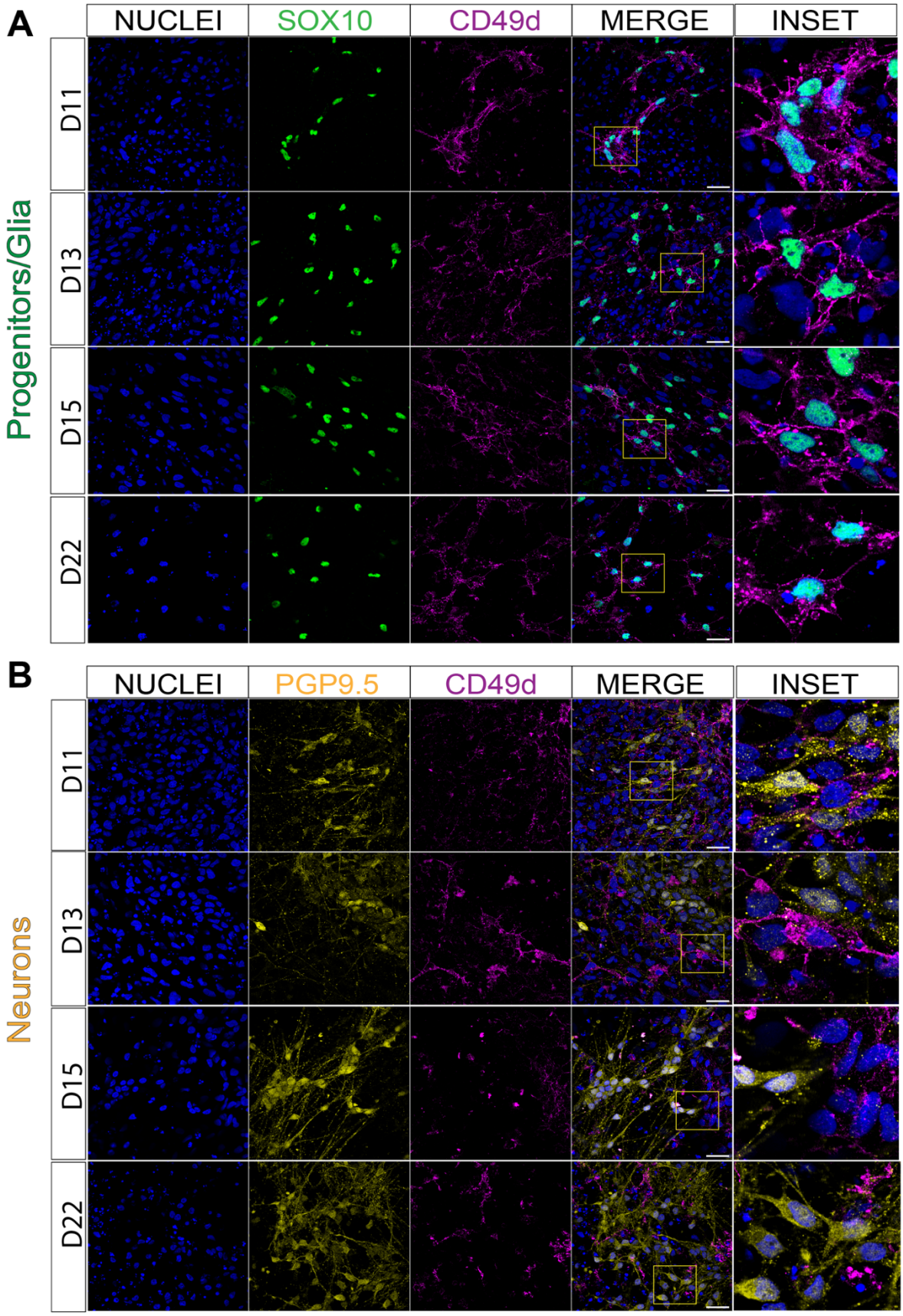

Figure 4.7. Characterisation of CD49d expression in enteric nervous system differentiating cultures over time. Immunofluorescence analysis of the expression of CD49D together with the ENS progenitor/glial marker SOX10 (A) or the neural marker PGP9.5 (B) at the indicated time points. Insets show magnified areas. Data were acquired using the WTC-11 cell line. Scale bars=30 µm.

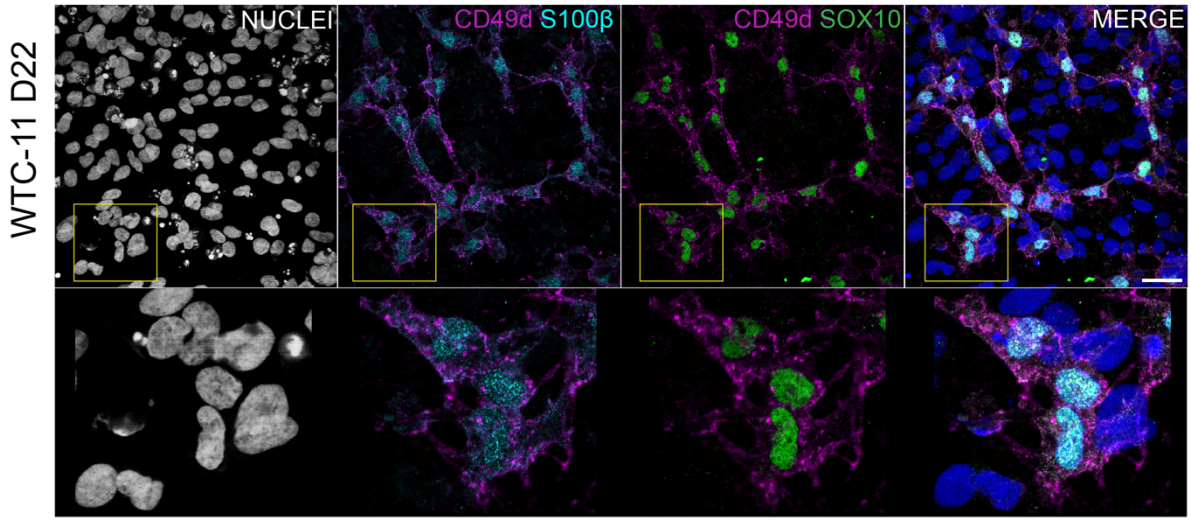

Figure 4.8. CD49d is expressed in glial cells in day 22 cultures. Immunofluorescence analysis of the expression of CD49d together with the glial markers SOX10 and S100β in day 22 cultures. Magnified regions of the indicated areas as shown in the lower panel. Scale bars=30 μm.

4.3.2. Electrophysiological characterisation of *in vitro*-derived enteric neurons

To characterise the functionality of the *in vitro*-derived ENS cultures with respect to synaptic transmission and neuronal activity, I generated enteric neurons and glial cells from hPSCs and shipped the cells to our collaborators (Pieter Vanden Berghe group) in KU Leuven to perform Ca^{2+} imaging and axonal transport measurements. For Ca^{2+} imaging, the Fluo-4 Ca^{2+} indicator was used to monitor changes in Ca^{2+} transients following chemical or electrical stimulation, to derive the response of neurons, and hence neuronal activity (Figure 4.9A-C). Application of high K^+ solution resulted in neural depolarisation in day 50 cultures at which individual cell bodies and axons were recorded to fire action potentials (Figure 4.9A). Stimulation of nicotinic acetylcholine receptors (nAChRs), a major mediator of excitatory neurotransmission in enteric ganglia (Galligan et al. 2000), using the synthetic agonist DMPP (Tapper and Lewand 1981) also elicited Ca^{2+} transients in day 50 hPSC-derived neurons (Figure 4.9B). This finding demonstrates the functional expression of acetylcholine receptors in *in vitro*-derived neurons, in line with their early and throughout development expression in the ENS *in vivo* (Foong et al. 2015). Similar to chemical depolarisation, stimulation of day 50 neurons in electric field evoked Ca^{2+} transients (Figure 4.9C), further demonstrating the neuronal activity of the *in vitro* generated enteric neurons. Given the key role of axonal transport in neuron development, function and survival (Guillaud et al. 2020), the hPSC-derived ENS cultures were next incubated with a fluorescent dye (Mito Tracker Red) to label mitochondria and were next assessed for mitochondrial movement. Time-lapse movies generated at an early (day 22, Figure 4.9D) and a late stage (day 36, Figure 4.9E) recorded mitochondrial movements which are visualised in the kymographs in

Figure 4.9D-E. During the time-lapse imaging, mitochondria were found to move anterograde and retrograde (diagonal lines in the kymograph), while some showed no displacement (vertical lines in the kymograph) (Figure 4.9D-E). At day 36, an increase in mitochondria movement compared to day 22 was observed, potentially denoting maturation of the cultures with time. Taken together, the activity measurement experiments revealed that hPSC-derived neurons are responsive to electrical and chemical stimuli, they have active nicotinic cholinergic neurotransmission and show active axonal transport at an early and late stage of the differentiation.

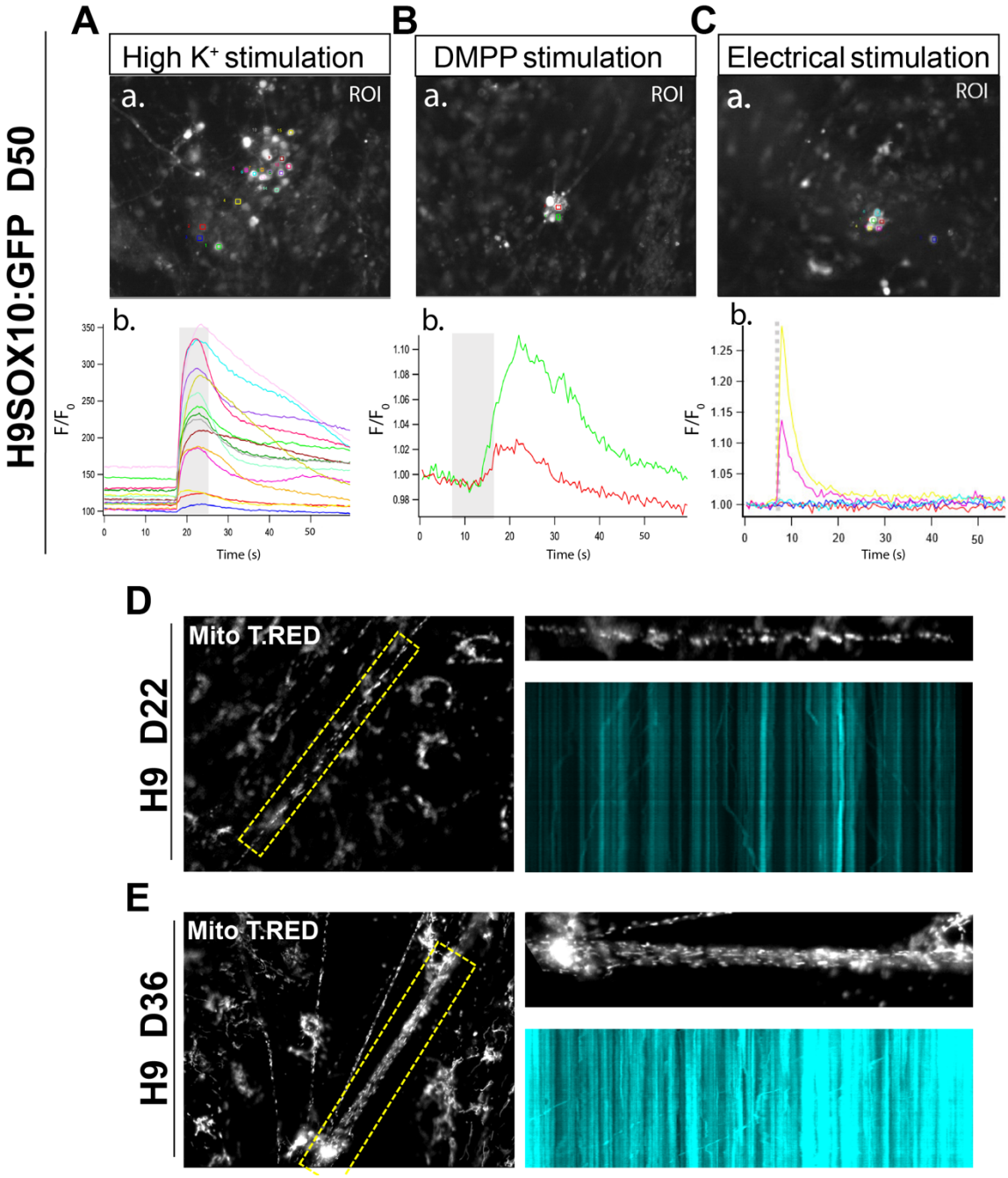

Figure 4.9. Measurement of electrical activity and axonal transport in hPSC-derived enteric neurons. (A-C). Activity measurements following high K+ (A), DMPP (10-5 M)(B) and electrical (2 sec at 20Hz) (C) stimulation in day 50 enteric neurons using the Ca2+ indicator, Fluo-4. (a) Image showing the regions of interest (ROI), (b) line traces depicting Ca2+ transients of neurons highlighted in a, as a change in the fluorescence intensity over time (F/F0, F0=

baseline fluorescence). The application of the stimulation is depicted with the gray bar. (D-E) Axonal transport imaging using the red-fluorescent dye, Mito Tracker Red in day 22 (D) and day 36 (E) ENS cultures. Snap shots of the time-lapse movie at the indicated time points (left), magnified areas (upper right) and kymographs generated from the movie showing mitochondria movement (lower right). Cultures were generated in Sheffield by me with the help of Tom Frith and neuronal activity measurements, axonal transport imaging were performed in KU Leuven by our collaborator Pieter Vanden Berghe and his student, Yi-Ning Kang.

4.3.3. Replating of enteric neurons as a means to obtain purified cultures

A major challenge in the molecular and electrophysiological characterisation as well as the long-term culture of the *in vitro* ENS has been the presence of unwanted, contaminating cells growing in most cases, underneath neurons (Figure 4.10A-B). These cells predominately show a flat morphology and a fraction of them are immunoreactive to alpha-smooth muscle actin (α-SMA) (Figure 4.10C) suggesting a myofibroblast identity, in agreement with previous observations (Barber et al. 2019). Although these cells do not seem to impede neural and glial differentiation at early stages, their continuous presence and potential expansion in culture has a detrimental effect on enteric neuron and glial survival.

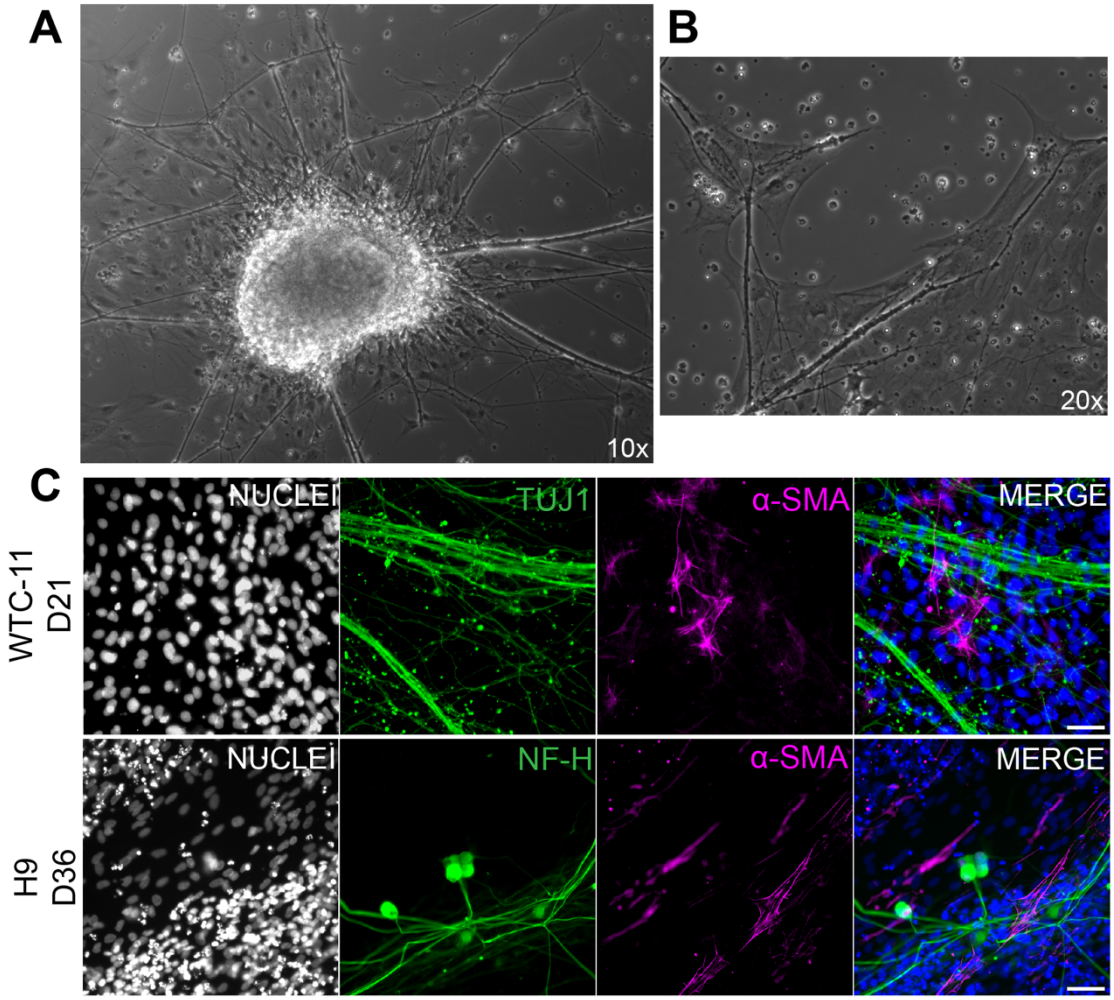

Figure 4.10. Representative images of enteric nervous system cultures demonstrating a spatial relationship between neural and non-neural cells. Low power (A) and high power (B) brightfield images of day 30 ENS cultures replated on Laminin 1 on day 15 of the differentiation showing neurons growing in close vicinity to myofibroblast-like cells. (C) Immunofluorescence analysis of the expression of alpha-smooth muscle actin (α-SMA) and neural markers. (TUJ1, NF-H) in day 21 and day 36 cultures derived from the WTC-11 and H9 cell lines, respectively. Scale bars= 50 μm.

To minimise the number of unwanted cells, I next examined whether clump passaging would result in obtaining purified ENS cultures. Cell selection via passaging is widely used in the field and this approach has been demonstrated before to yield >95% pure neural cultures from NTera2, a human teratocarcinoma cell line (Pleasure et al. 1992). To this end, late ENS neurons with established connections (day 28) were enzymatically detached, collected and replated as clumps in various ratios on Geltrex (GTX)-coated plastic plates (Figure 4.11Ai). Neurons in most cases survived replating and started forming networks with neighbouring cells within the first 6 days (Figure 4.11Aii). At 12 days after replating, robust neural networks with extensive projections were formed and cultures appeared "cleaner" devoid debris (Figure 4.11Aii). Contaminating cells of non-neural morphology were greatly eliminated from replated cultures 6 days post plating and were occasionally found to form small, spatially restricted colonies (Figure 4.11Aii). On day 12 following replating, the number of contaminating cells increased, a result suggesting that these cells are still cycling, however, their presence was again limited (Figure 4.11Aii). Replated neurons stained for TUJ1 and cells immunoreactive to α-SMA emerging in replated cultures are shown in Figure 4.11Aiii.

In vitro neural differentiation protocols use a variety of extracellular matrix (ECM) proteins to support neuron development and neurite axonal growth. Matrigel/GTX, laminin (LAM) and fibronectin (FN) have been previously reported to promote neurite outgrowth in neuronal cells from CNS, PNS and human teratocarcinoma cells *in vitro* (Manthorpe et al. 1983; Pleasure et al. 1992; Tonge et al. 2012), while vitronectin (VTN), a chemically defined and xeno-free substrate was proposed to efficiently promote and support derivation of forebrain neurons from hPSCs (Yuan et al. 2015). To determine whether different substrates can be used to increase the efficiency of the replating and promote neurite axonal growth, I replated late ENS cultures (day 40) on a variety of substrates as shown in Figure 4.11Bi and monitored the morphology of attached neurons over a 10-day period. In contrast to the experimental procedure that was discussed before (Figure 4.11A), cells were replated on pre-coated glass coverslips for immunostaining and to optimise replating conditions on glass as it is important for functional assays that we would like to carry out in the future. Two biochemical substrates poly-dl-ornithine (PDLO) and poly-l-ornithine (PO) were also used in combination with the ECM molecules to facilitate adhesion (Amin et al. 2016a). Microscopy analysis of replated cultures in different conditions after 10 days revealed that cell attachment and axonal outgrowth greatly depends on

the substrate (Figure 4.11Bii). Neural clusters replated on GTX, PDLO/GTX and PDLO/LAM re-extended elongated projections, while cells grown on VTN, PO/LAM/FN and LAM alone remained clustered and did not elaborate any processes (Figure 4.11Bii). The presence of PDLO as an adhesion promoter was critical in the replating process, due to the less efficient cell attachment on glass surface compared to plastic. This is further demonstrated by comparing replated cells grown on LAM and PDLO/LAM. Neurons replated on the former did not attach well and showed no projections (Figure 4.11Bii). To further confirm the neural identity of the observed cells I carried out antibody staining and fluorescence microscopy. Analysis of replated cultures in PDLO/GTX and PDLO/LAM at day 55 of the differentiation confirmed the survival of PERIPHERIN+/PGP9.5+ neurons (Figure 4.11Biii). Together, these data demonstrate that replating is an efficient strategy to obtain purified, low density and microscopy friendly enteric neural cultures. They also dictate that the substrate influences the axonal regrowth following replating.

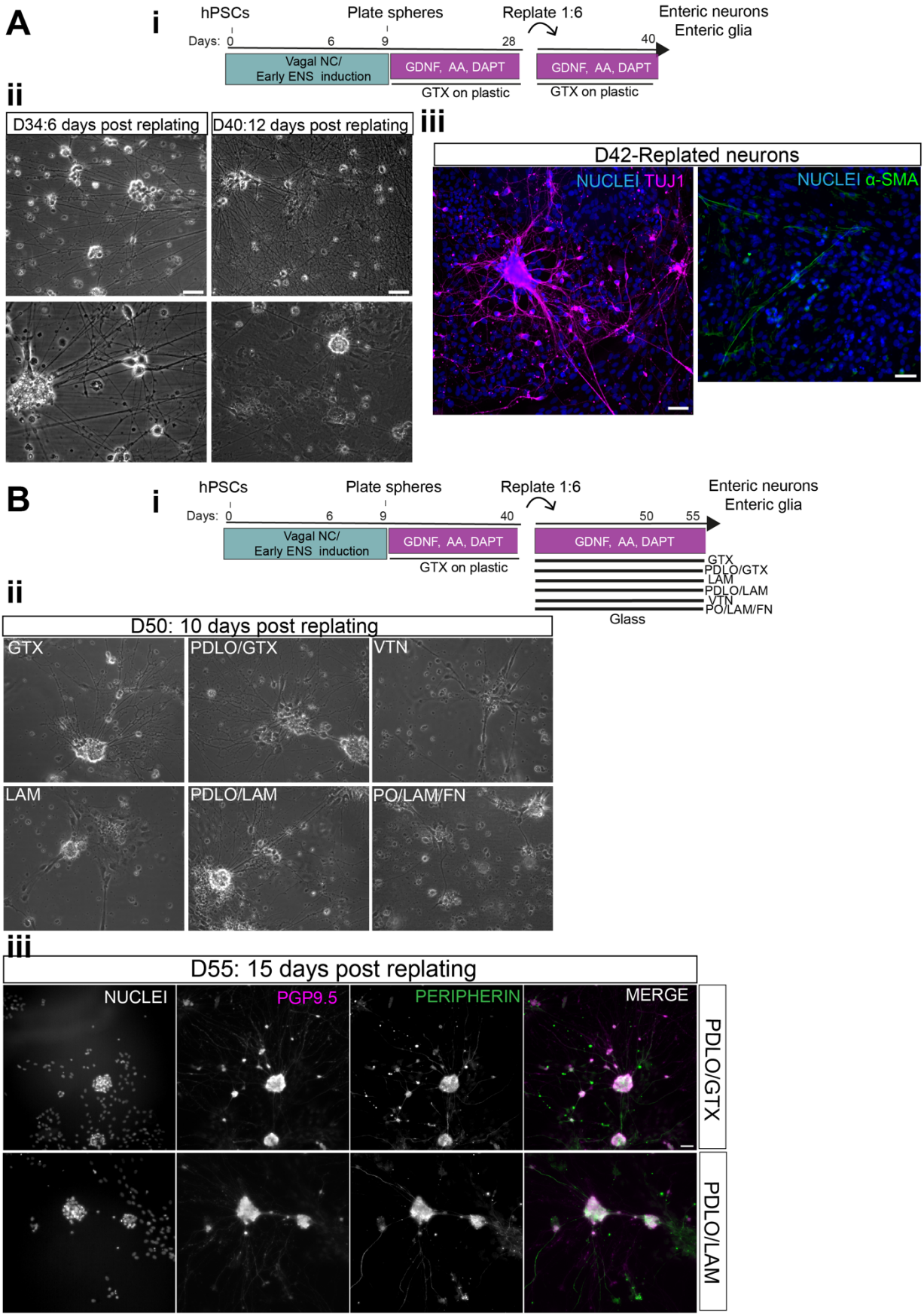

Figure 4.11. Replated hPSC-derived enteric neurons on plastic or glass surface. (A) Diagram depicting differentiation and replating approach of ENS cultures on GTX-coated plastic surface (i) and representative brightfield images demonstrating neurons 6 and 12 days after replating (ii). Immunofluorescence analysis of TUJ1 and α-SMA in

day 42 replated cultures demonstrating neural and myofibroblast-like cells, respectively (iii). (B) Diagram depicting differentiation and replating strategy of ENS cultures on glass surface on a variety of substrates (i) and representative brightfield images of neurons 10 days after replating (ii). Immunofluorescence analysis of the expression of PGP9.5 and PERIPHERIN in neurons from the best performing replated conditions (PDLO/GTX) and (PDLO/LAM). Scale bars= 50µm. GTX, Geltrex; LAM, Laminin, VTN, Vitronectin; FN, fibronectin; PDLO, poly-dl-ornithine; PO, poly-l-ornithine.

Given the effect of culture substrate on neurite development, I next sought to examine the influence of GTX and LAM on neurogenesis in ENS cultures *in vitro*. To this end, I plated day 9 ENS progenitors on GTX-coated and LAM-coated plates (Figure 4.12A). Cells were analysed at day 30 for a panel of ENS markers by RT-qPCR and immunostaining. Gene expression analysis revealed comparable induction between the 2 conditions for all genes examined (Figure 4.12B). Similarly, analysis of protein expression using neural (TUJ1, PGP9.5) and glial (SOX10, S100β) markers demonstrated equal expression among cells grown on GTX or LAM (Figure 4.12C). Notably, ENS cultures plated on LAM contained more myofibroblast-like cells, however, this is qualitative observation and further quantification is required (Figure 4.12C).

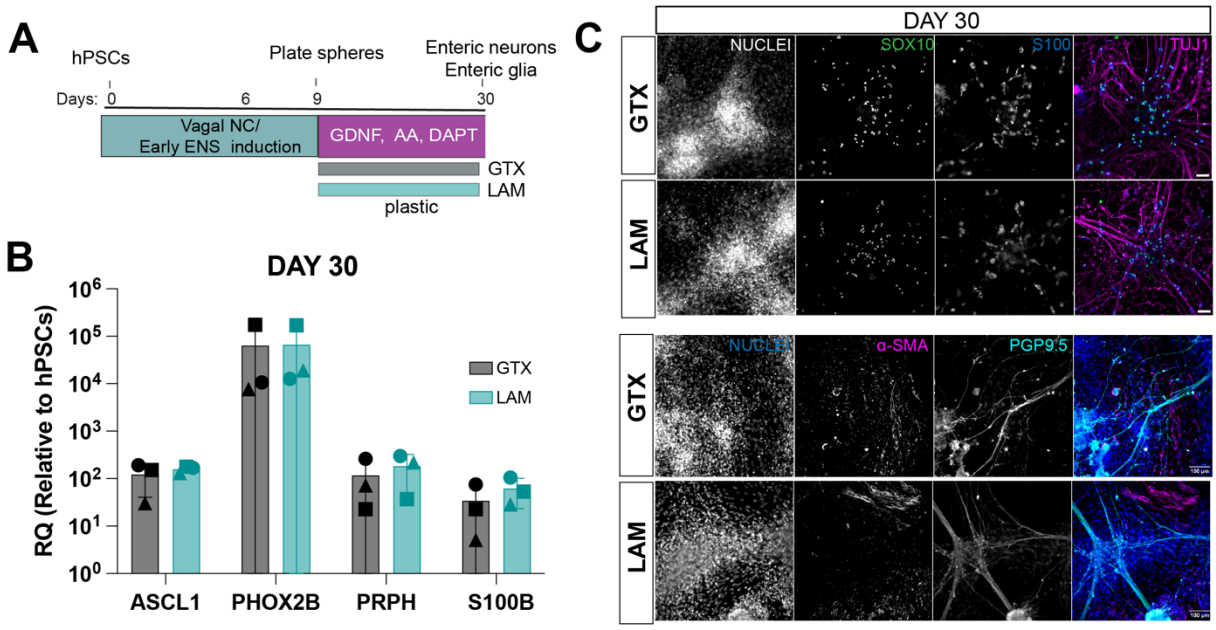

Figure 4.12. Comparison of enteric nervous system cultures grown on geltrex and laminin 1. (A) Schematic illustrating the culture conditions. (B) RT-qPCR analysis of ENS markers in day 30 ENS cultures grown on GTX or LAM. Data shown are the mean of mean values ± SD, n=3 independent experiments with three technical replicates in each experiment. Each independent experiment is represented by a unique shape. No statistically significant difference between the 2 conditions was observed (paired t-test). (C) Immunofluorescence analysis of the expression of indicated genes in day 30 ENS cultures grown on GTX or LAM. Scale bars= 50 µm. GTX; geltrex, LAM, laminin 1.

4.4. Critical signals for enteric nervous system specification *in vitro*

Although the events that lead to gut colonisation from vagal NC derivatives in the murine, avian, and zebrafish model system have been a subject of intensive research (Nagy and Goldstein 2017), the signals that orchestrate early cell fate decisions from vagal to ENS development, especially in mammalian/ human cells, are not well studied. Thus, I next employed my protocol for the *in vitro* generation of ENS cells in order to dissect the signalling basis of human ENS specification *in vitro*.

4.4.1. Wnt and FGF stimulation are not sufficient for enteric nervous system progenitor maintenance

I first examined whether the signals employed to expand vagal NC spheres are sufficient to maintain a vagal NC/ENS progenitor identity. Previous studies have demonstrated that avian cranial, trunk NC as well as hPSC-derived NC cells could be maintained in a pre-migratory state *in vitro* under appropriate culture conditions and as 3D aggregates, termed crestospheres, for several weeks without losing the ability to self-renew (Kerosuo et al. 2015; Mohlin et al. 2019). Thus, I generated vagal NC from the H9SOX10:GFP reporter cell line, I cultured them in neurosphere promoting conditions in the presence of FGF2 and CHIR for four weeks and passaged the spheres once a week (Figure 4.13A). During prolonged culture and following passaging, cell aggregates retained the ability to form spheres and proliferated, as the cell numbers increased and cultures became heavily crowded (Figure 4.13B). SOX10:GFP expression decreased gradually and hardly any cells positive for SOX10:GFP were present after four weeks (Figure 4.13B). In agreement with this, flow cytometry analysis revealed that the number of cells positive for the vagal NC/ENS progenitor markers SOX10:GFP/p75 started to decline after day 6 (10± 5% at week 1) and dropped to zero at the end of the third week (Figure 4.13C-D). Comparable results were also obtained from the analysis of SOX10:GFP/CD49D (Figure 4.13C-D).

Gene expression analysis showed a significant reduction in *PAX3* and *PAX7* transcript levels particularly at the end of the second week, while *ASCL1* levels were maintained moderate throughout the differentiation (Figure 4.13E). In contrast, *SOX10* transcripts remained considerably high for the first three weeks and dropped dramatically on the fourth week (Figure 4.13E). The reduced transcript and protein levels of NC and ENS-associated genes, a profile incompatible with an ENS progenitor identity suggests that the cells have either started differentiating to potential NC derivatives or that a cell population emerging in the heterogeneous cultures has taken over and expanded at the expense of ENS progenitors, reducing their presence until they became extinct. This is also supported by the observed reduction in $p75^{high}$

fraction and the shift towards a $p75^{low}$ population, an expression profile that does not match a NC identity (Figure 4.13C). On the contrary, the number of CD49d+/SOX10:GFP- increased with time, potentially marking differentiated NC derivatives (Figure 4.13C).

I next looked at the effect of prolonged FGF/Wnt signals on the axial identity of these cells. Expression of *HOXB1* and *HOXB2* was maintained throughout the sphere period although there was a significant decrease within the first three weeks (Figure 4.13F). *HOXB4* transcript levels were markedly increased over time and showed over a 10-fold increase compared to day 6, at the end of the fourth week (Figure 4.13F). Similarly, I observed an upregulation of more caudal *HOX* genes (*HOXB7*, *HOXC9*) in agreement with the role of FGF and Wnt to induce a more posterior axial identity (Cooper and Tsakiridis 2022a; Wymeersch et al. 2021), whereas *HOXB5* transcript levels showed an approximately 8-fold decrease compared to day 6 (Figure 4.13F). Together, these data indicate that ENS progenitors could not be maintained for extended period in culture and keep the characteristic vagal NC gene expression profile and axial identity following Wnt and FGF2 activation. However, this finding does not exclude the possibility that other signals might be more efficient in directing the maintenance and long term culture of SOX10+ ENS progenitors.

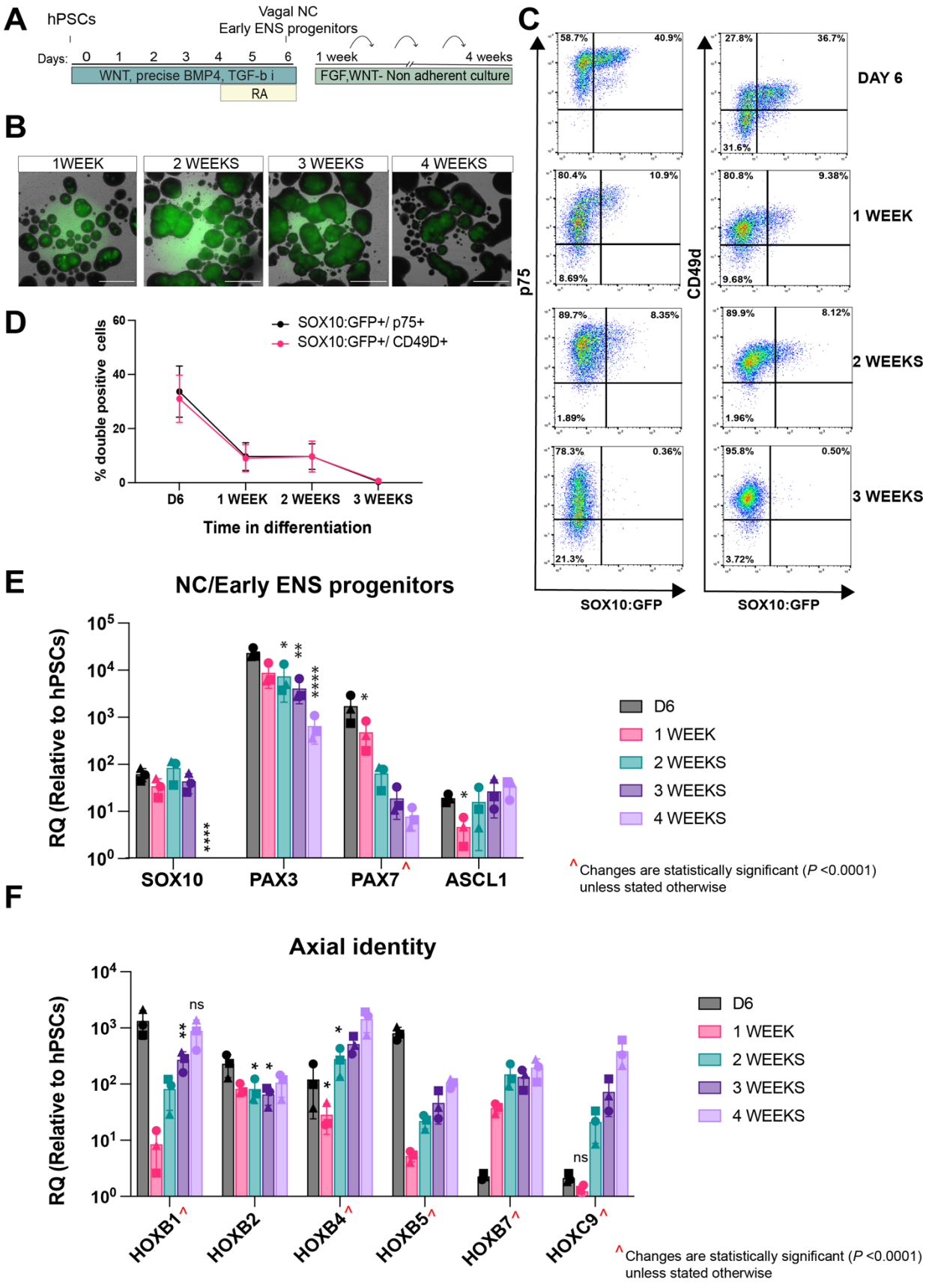

Figure 4.13. Early enteric neural progenitors cannot be maintained as 3D aggregates over prolonged culture period. (A) Diagram depicting culture conditions and experimental strategy followed. (B) Representative images of GFP expression in 3D cultures derived from the SOX10:GFP reporter cell line at the indicated time points. Scale bar=

1mm. (C-D) Representative flow cytometry analysis profiles showing co-expression of SOX10:GFP with p75 (left) and CD49d (right) at the indicated time points (C) and pooled data of the percentage of SOX10:GFP+/p75+ and SOX10:GFP+/CD49D+ from three biological replicates (D). The percentage of double positive cells decreases dramatically with time. Error bars= S.D. (n=3). (E-F) RT-qPCR gene expression analysis of indicated NC/Early ENS progenitor (E) and *HOX* (F) genes over 4-week culture period. Data state the mean of mean values ± SD, n=3 independent experiments with three replicates in each experiment, **P* <0.05, ***P* <0.005, *****P* <0.0001 by mixed model ANOVA Dunnett's post-hoc multiple comparisons test with control "D6" group. All data shown were derived from SOX10:GFP cell line. Each independent experiment is represented by a unique shape. ^Changes in *PAX7, HOXB1, HOXB4, HOXB5, HOXB7, HOXC9* expression were statistically significant (*P* <0.0001) unless otherwise stated.

4.4.2. Examining the role of retinoic acid in maintaining enteric neural progenitor identity

The inability of FGF/Wnt signals to maintain a vagal NC/ENS progenitor identity and the significant reduction in transcript levels of *ASCL1* and *HOX* genes observed at day 10 of the culture (magenta colour; Figure 4.14C) or after the first week as discussed in 4.4.1, prompted me to further define appropriate culture conditions that would maintain the expression of the aforementioned genes. Given the requirement of RA to induce and maintain the expression of *ASCL1* and *PHOX2B* in NC (discussed in 3.4.3 in chapter 3; Figure 3.10), I next examined whether addition of RA (0.1 μM and 1 μM) in non-adherent cultures and in the presence of FGF2 and CHIR would be sufficient to promote and maintain an early ENS progenitor transcriptional profile (Figure 4.14A). Gene expression analysis at day 10 revealed non-significant decrease in transcript levels of NC genes (*SOX10*, *SOX9*) in day 10 RA-treated/untreated cultures compared to day 6 (Figure 4.14B). In contrast, *ASCL1* and *PHOX2B* mRNA levels were greatly reduced at day 10 (magenta vs black) and addition of RA was found to maintain the expression, in a dose-dependent fashion (black vs green vs purple; Figure 4.14C). Day 10 cultures also showed reduced levels of PAX6, a result suggesting that RA in the presence of FGF/Wnt does not shift the identity of the cells towards CNS lineage or other PAX6+ entities such as PPE (Figure 4.14D). Addition of RA did not alter the expression of *HOXB1* and *HOXB2* at day 10 of the differentiation but resulted in a dose related increase in the transcript levels of vagal axial identity *HOX* genes (*HOXB4*, *HOXB5*, *HOXB7*) (Figure 4.14E).

Next, to examine the temporal effect of RA on ENS progenitor marker expression, I generated ENS progenitor spheres in the presence/absence of 1 μM RA and performed flow cytometry and RT-qPCR for NC/ENS associated genes in a time course analysis (Figure 4.14F). Flow cytometry analysis showed a significant reduction in the number of SOX10:GFP+ cells over time in both RA-treated and untreated groups (Figure 4.14G), while RT-qPCR analysis revealed that RA treatment had no effect on *SOX10* transcript levels compared to day 6 control, in all the time points examined (Figure 4.14H). Additionally, *PAX6* transcript levels decreased within the four day period and there was no difference between the RA-treated and untreated groups (Figure

4.14H), in line with our previous observations, ruling out the possibility that RA shifted the identity of the cultures towards a CNS fate. RT-qPCR for the expression of *PHOX2B* and *ASCL1* revealed a gradual decrease in their transcript levels during the sphere stage (magenta line; Figure 4.14H) and a significant induction of their expression following day 8 upon RA treatment (black line; Figure 4.14H). Together, these data suggest that RA regulates the expression of *ASCL1* and *PHOX2B* during the sphere stage and in the presence of FGF/Wnt, while it has no effect on SOX10 expression. It also positively regulates the transcription of vagal axial identity *HOX* genes.

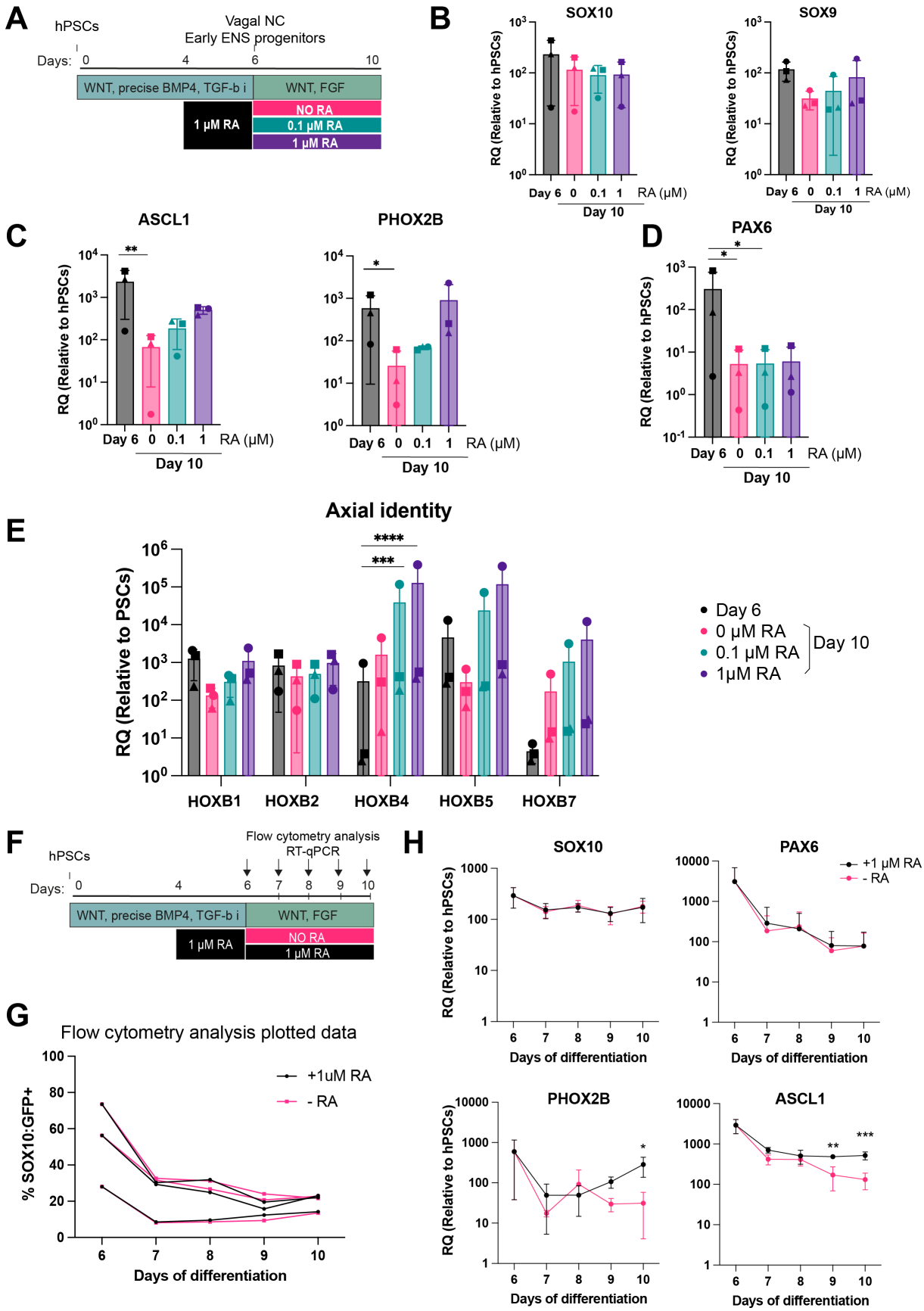

Figure 4.14. Retinoic acid maintains the expression of enteric nervous system progenitor genes upon culture in non-adherent conditions in the presence of Wnt and FGF2 signals. (A) Schematic depicting the differentiation/treatment scheme. (B-E) RT-qPCR analysis of the expression of NC (B), early ENS progenitor (C), PAX6 (D) and *HOX* genes (E) in day 6 NC and day 10 cultures following treatment shown in panel A. Data shown are

the mean of mean values ± SD, n=3 independent experiments with three replicates in each experiment. Each independent experiment is represented by a unique shape,*P <0.05, **P <0.01, ***P <0.001, ****P <0.0001 by one-way ANOVA Dunnett's post-hoc multiple comparisons test with control "Day 6" group. Only statistically significant comparisons are indicated. (F) Diagram depicting RA treatment during differentiation and the time points of analysis. (G) Line graph presenting the percentage of SOX10:GFP+ cells measured by flow cytometry in RA-treated (black) and non-treated (magenta) NC cells in a 4-day time course. Data were acquired using an H9 SOX10:GFP reporter cell line and results from 3 independent experiments are presented as distinct paired lines. (H) RT-qPCR analysis of indicated NC/early ENS progenitor genes (*SOX10*, *PHOX2B*, *ASCL1*) and *PAX6* in RA-treated (black) and non-treated (magenta) cultures between day 6 and 10 of the differentiation. Data state the mean of mean values ± SD, n=3 independent experiments with three replicates in each experiment. Downward error bars in *PAX6* are missing as Y axis is logarithmic and negative values could not be plotted, unpaired t-test; *P <0.05, **P <0.005, ***P ≤0.0005. Only statistically significant comparisons are indicated.

4.4.3. Exploring the role of Notch signalling pathway inhibition in enteric nervous system differentiation

Notch signalling pathway has been shown to modulate cell fate specification in the developing CNS and PNS (reviewed in Louvi and Artavanis-Tsakonas 2006). In particular, studies have shown that Notch exerts diverse functions by promoting: (i) maintenance of neural progenitors, (ii) inhibition of neural differentiation and (iii) induction of gliogenesis (Louvi and Artavanis-Tsakonas 2006). A large body of evidence suggests that the Notch signalling pathway is also implicated in the development of the ENS, as gain or loss of Notch activity in the NC was found to cause defects in the developing mouse ENS and ectopic activation of Notch signalling in pre-migratory NC was shown to disrupt ENS progenitor migration to the gut (Mead and Yutzey 2012; Okamura and Saga 2008). Given the proposed role of Notch in ENS development *in vivo*, I next sought to investigate Notch components expression dynamics in differentiated ENS cultures over time (Figure 4.15D). For this reason, I looked at the transcript levels and at distinct time points of a panel of Notch receptor genes (*NOTCH1*, *NOTCH2*), Jagged family ligands (*JAG1*, *JAG2*) and Delta-like ligands (*DLL1*, *DLL3*, *DLL4*) that were reported to be expressed in the developing or adult ENS (Kuil et al. 2022; Morarach et al. 2021; Okamura and Saga 2008; Sander et al. 2003) (Figure 4.15E). *NOTCH1* and *NOTCH2* receptors were highly expressed in pluripotent and NC state (~CT 24-26). *NOTCH1* mRNA levels increased during the early ENS phase (day 13-22), while *NOTCH2* levels continued to rise at the late ENS phase (day 22-50) (black line; Figure 4.15D). *JAG1* expression showed a similar pattern to *NOTCH1 and JAG2* transcript levels increased after day 22, matching the expression profile of *NOTCH2* (black line; Figure 4.15D). Expression of delta-like ligands was induced at the NC stage and their transcript levels increased during the early ENS phase (day 11-22) before dropping again during late ENS differentiation (black line; Figure 4.15D).

The temporal expression of Notch components at distinct time points further prompted me to examine the function of Notch pathway, and particularly Notch pathway inhibition, on cell fate

specification during ENS differentiation. To this end, I generated early ENS progenitor cells and cultured them in ENS-inducing conditions for 50 days and in the presence of DAPT (Dovey et al. 2001), to indirectly block Notch pathway activity by interfering with γ-secretase mediated Notch receptor cleavage (Figure 4.15A). The solvent DMSO in the same concentration as in the experimental group was used as a control (O'Sullivan et al. 2019; Zhang et al. 2017). Cells grown in the presence/absence of DAPT formed robust neural networks, albeit morphologically different, with small neural clusters emerging in DAPT-treated cultures as opposed to large and dense clusters observed in controls (Figure 4.15B). To test the effect of DAPT treatment, I first looked at the expression of Notch target genes *HES1*, *HES5* (Ohtsuka et al. 1999) and the HES family member *HES6,* which although is not activated from Notch acts as transcriptional repressor of *HES1* (Bae et al. 2000). DAPT (10μM) administration had minimal effect on *HES1* and *HES6*, genes that were expressed in stem cell state and throughout the differentiation (*HES1* ~CT 25 in hPSCs; *HES6* ~CT 28 in hPSCs) but markedly reduced the expression of *HES5,* a gene induced after day 6 of the differentiation, confirming the effective inhibition of Notch signalling (Figure 4.15C). Addition of DAPT in the culture medium, did not significantly affect the expression of *NOTCH1*, even though there was a trend towards a reduction in *NOTCH1* expression, but resulted in a great decrease in the transcript levels of *JAG1* between day 11 and 15 of the differentiation (green vs black line; Figure 4.15D). *NOTCH2* and *JAG2* were slightly upregulated between day 15 and 38 in the DAPT-treated group, whereas delta-like ligands upon Notch inhibition were particularly upregulated at earlier time points compared to control (green vs black line; Figure 4.15D).

Taken together, these data indicate that various Notch signalling pathway components are expressed at different time points during the *in vitro* ENS differentiation and Notch inhibition influences receptor-ligand expression, confirming the presence of a regulatory feedback loop (Manderfield et al. 2012; Ross and Kadesch 2004; Sjoqvist and Andersson 2019). In the case of *JAG1*, Notch inhibition resulted in decrease in ligand expression denoting a positive feedback mechanism controlling its expression, whereas in the case of delta-like ligands and particularly of *DLL3*, transcripts were upregulated upon Notch blockade suggesting that Notch exerts a negative feedback loop by supressing the expression of these ligands. An overview of the Notch receptors-ligands interactions is illustrated in Figure 4.15E (Bray 2006; Guruharsha et al. 2012; Zhou et al. 2022).

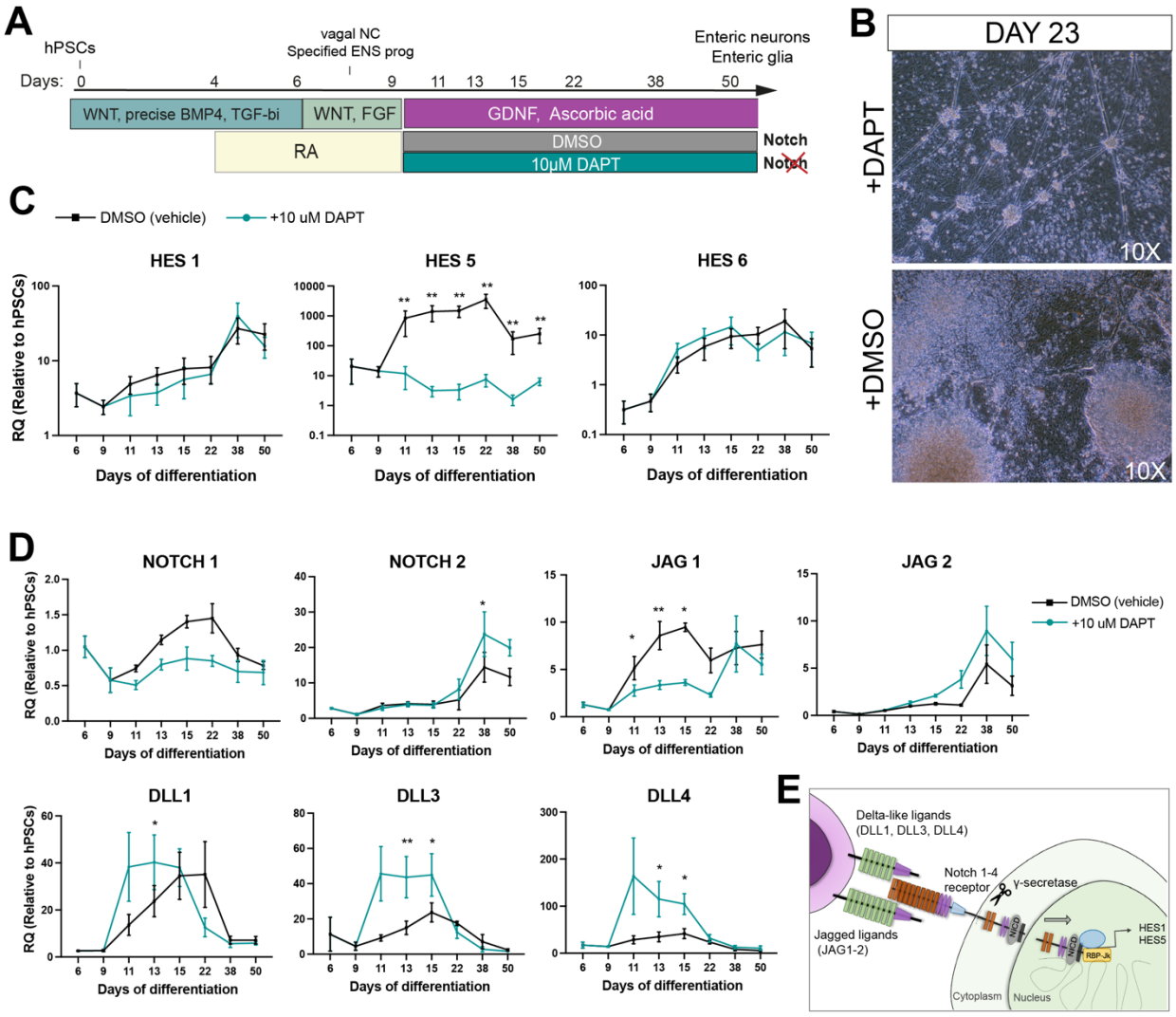

Figure 4.15. Notch signalling pathway dynamics during *in vitro* enteric nervous system differentiation and upon pathway inhibition. (A) Diagram showing differentiation/treatment for Notch pathway inhibition. (B) Representative low-power brightfield images in day 23 ENS cultures upon DAPT (10 μM) treatment and control (DMSO). (C) RT-qPCR analysis of Notch target genes (*HES1*, *HES5*) and *HES6* (negative regulator of *HES1*) in DMSO control and DAPT-treated ENS cultures over time. (D) RT-qPCR analysis of Notch components in DMSO control and DAPT-treated ENS cultures over time. (E) Overview of Notch signalling pathway. Data in all graphs are presented as mean of mean values ± SEM, n=3-4 independent experiments with three replicates in each experiment; **P* <0.05, ***P* <0.005 (paired t-test). Only statistically significant differences are indicated. All data were derived from the hiPS WTC-11 cell line.

I next interrogated the effect of DAPT-mediated Notch inhibition on ENS lineage marker expression by looking at the transcript levels of ENS progenitor/glial and neural genes (Figure 4.16). DAPT treatment resulted in an increase in the levels of the neurogenic gene *ASCL1* between day 13-15 and this coincided with an increase in the neural marker *PRPH* at day 22 (Figure 4.16A). It should be noted that these time points are critical for the enteric neural differentiation *in vitro* as the majority of neurons emerge between day 15 and day 22 in our cultures. *PHOX2B* transcript levels were also slightly elevated upon Notch inhibition and continued to increase over time, while *SOX10* was not greatly affected by DAPT and its

expression decreased over time (Figure 4.16A). On the contrary, *S100* expression slightly increased in the DAPT-treated group and remained to a great extent unchanged, in the control (Figure 4.16A). At days 22 and 38, the expression of ENS-associated neuronal subtype markers showed no difference between the two groups, likely suggesting that Notch inhibition does not influence their expression, at least in these stages (Figure 4.16B).

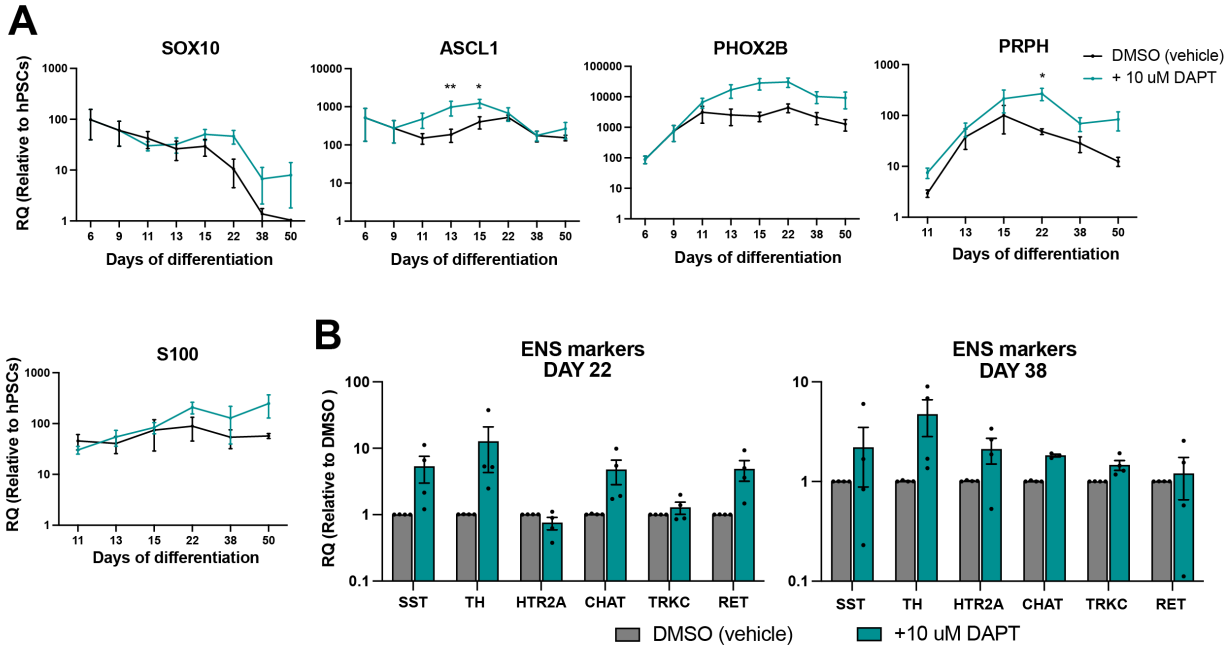

Figure 4.16. Notch pathway inhibition upregulates the expression of neural genes in hPSC-derived enteric nervous system cultures. (A) RT-qPCR expression analysis of indicated ENS genes in DMSO control and DAPT-treated ENS cultures over time. (B) RT-qPCR expression analysis of indicated ENS genes in DMSO control and DAPT-treated ENS cultures at the indicated time points. Data are presented as mean of mean values ± SEM, n=3-4 independent experiments with three replicates in each experiment; **P* <0.05, ***P* <0.005 (paired t-test). Only statistically significant differences are indicated. All data were derived from the hiPS WTC-11 cell line.

Next, I looked at the effect of Notch signalling inhibition at the protein level by quantifying the neural and glial markers in ENS cultures at an early (day 15) and at a late stage (day 22) (Figure 4.17). To ensure the PNS identity of the neurons, PERIPHERIN antibody staining combined with HUCD labelling was carried out and the area covered by HUCD+ cells was measured as a fraction of the total cellular material and used as a proxy to infer neural cell numbers (Figure 4.17Bi-ii; for the quantification please refer to Methods and Materials). This approach was implemented to overcome the difficulty of quantifying total cell numbers as neurons grow in very dense areas and form relatively large clusters. Analysis of HUCD staining at day 15 revealed a significant increase in the HUCD+ area in DAPT-treated cultures compared to DMSO-control (mean value 14.4 ± 2% in DAPT-treated vs 7.6 ± 1% in control; *P* =0.0398) and a similar finding was observed at day 22 of the differentiation (mean value 14.3 ± 2% in DAPT-treated vs 9.8 ± 1% in control; *P* =0.0220), suggesting that more neurons emerge when Notch pathway is blocked

(Figure 4.17Bii). These data also mirror my previous observations regarding the increased expression of neural genes between day 15-22 in DAPT-treated ENS cultures (Figure 4.16A).

Analysis of SOX10 protein expression on day 15 showed a great increase in the SOX10+ area in DAPT-treated group compared to control (mean value 19.3 ± 3% in DAPT-treated vs 13.1 ± 2% in control; *P* =0.0311) and a trend towards an increase, albeit not statistically significant, was also observed at day 22 (mean value 23.9 ± 3% in DAPT-treated vs 17.18 ± 3% in control; *P* =0.2356), consistent with a rise in progenitor and/or glial population upon Notch pathway suppression (Figure 4.17Cii). To discriminate the effect of Notch inhibition on progenitor and glial populations as both are marked by SOX10, I used S100β immunostaining to determine glia occurrence on the basis of SOX10+/S100β+ (Figure 4.17Ci).S100β single-positive cells were disregarded from the analysis as they were considered to be false-positive given the strong nuclear background staining. Quantification on day 15 revealed that DAPT treatment resulted in an increase in the glial population (54 ± 16.7% in DAPT vs 25.9 ± 12.9% in control, *P* =0.0076), while more SOX10+/S100β- progenitors were present in the control group (Figure 4.17Ciii). In contrast, analysis on day 22 demonstrated an overall increase in the glial population compared to day 15, in agreement with the notion that progenitor cells differentiate to their glial derivatives over time and showed no difference in the number of glia between treated and control groups (Figure 4.17Ciii). Collectively, these findings indicate that Notch pathway suppression by the γ-secretase inhibitor, DAPT, promotes neural differentiation and induces the generation of glia at an early stage.

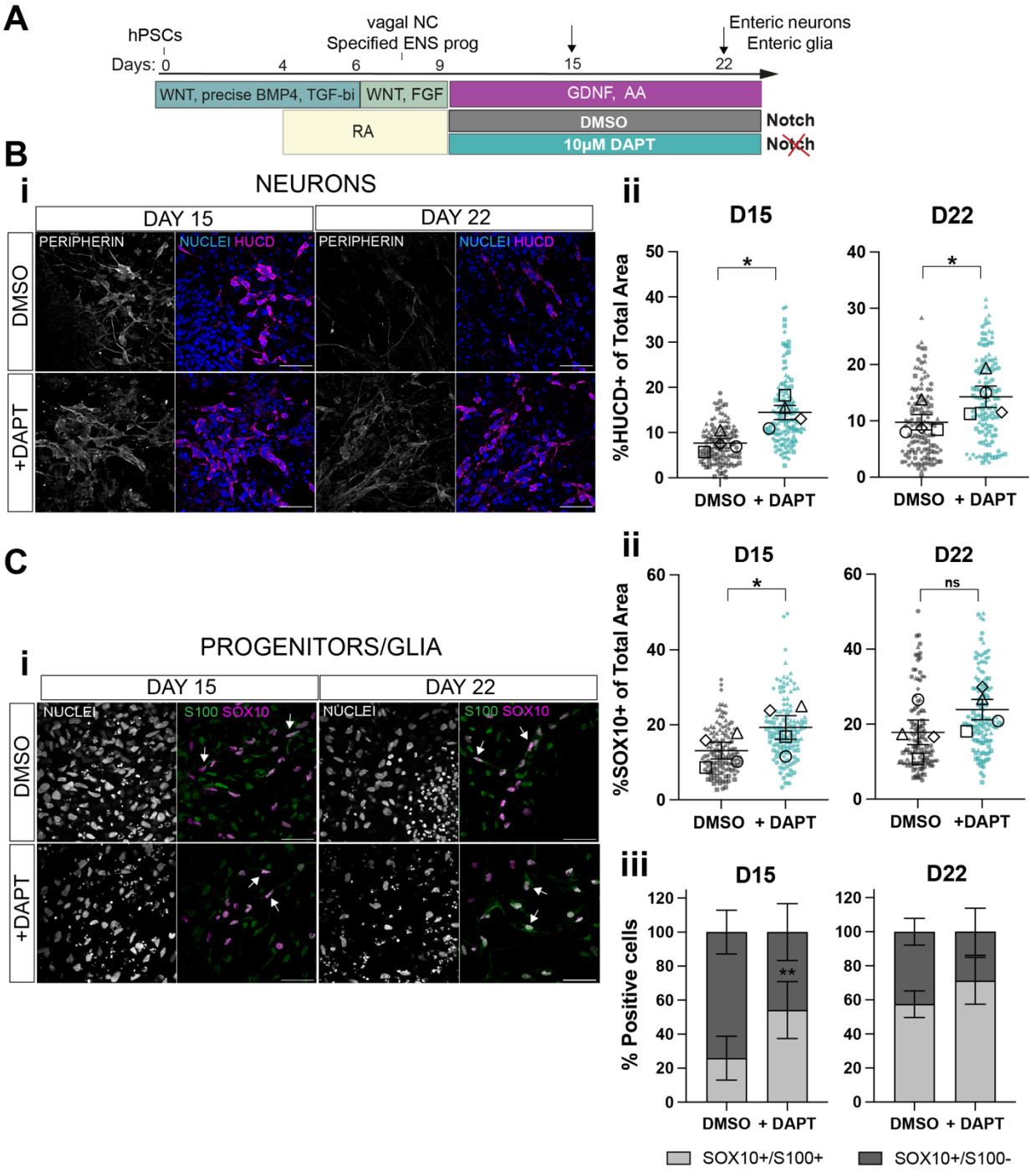

Figure 4.17. Notch pathway inhibition promotes neural and glial differentiation in hPSC-derived enteric nervous system cultures. (A) Schematic showing the differentiation approach/treatment and the time points of analysis. (B) Immunofluorescence analysis of the expression of PERIPHERIN and HUCD in control and DAPT-treated ENS cultures at day 15 and 22 (i) and quantification of the HUCD+ area presented as a ratio over the total area occupied by cellular material for the corresponding time points/conditions (ii). (C) Immunofluorescence analysis of the expression of SOX10 and S100 in control and DAPT-treated ENS cultures at day 15 and 22 (i) and quantification of the SOX10+ area presented as a ratio over the total area occupied by cellular material for the corresponding time points/conditions (ii). Quantification of the double-positive (SOX10+/S100+; glia) and single-positive (SOX10+/S100-; progenitors) cells in control and DAPT-treated cultures at day 15 and 22 of the differentiation (iii). Arrows in the images indicate double-positive cells. All data were derived from the hiPS WTC-11 cell line. SuperPlots show pooled data from 4 independent experiments (30 fields scored/condition for each experiment). Each independent experiment is represented by a unique shape and all values that correspond to every field scored are shown in the superPlot. Large symbols represent the means of different experiments (n=4) and error bars indicate SEM. P value was calculated using the means of 4 experiments. *P <0.05 (paired t-test). Stacked bars represent mean of mean values ± SD (n=4);

**P <0.01 (paired t-test). Only statistically significant changes are indicated. Quantification plots per experiment are included in appendix figure S4 .

4.5. Discussion

4.5.1. Characterisation of the hPSC-derived enteric neurons and glia

In this chapter I showed that our differentiation protocol efficiently generates enteric neurons and glia from hESCs and hiPSCs in a step-wise process that lasts between 3-5 weeks. The *in vitro*-derived ENS cultures originated from a vagal NC intermediate population and consisted of a pool of progenitor and differentiated cells that progressively differentiated into more mature phenotypes as indicated by gene expression analysis, immunocytochemistry and electrical activity in a process that recapitulates, to some degree, the developmental steps occurring *in vivo*. Neurons expressing ChAT, nNOS, TH, CALRETININ representative of various neurochemical subtypes that arise in the developing mouse gastrointestinal tract (Hao and Young 2009; Kang et al. 2021) were observed in ENS cultures and these exhibited electrical activity upon chemical and electrical stimulation. Characterisation of the electrical activity of hPSC-derived enteric neurons revealed the presence of multiple neurotransmitter release sites along the axons (varicosities) instead of a single synaptic knob. The presence of active varicosities is a feature observed in the situ ENS (Bayguinov et al. 2012), proposing that hPSC-derived enteric neurons recapitulate to some extent, their *in vivo* counterparts. However, the absence of later neurochemical markers such as CGRP (Branchek and Gershon 1989), substance P (McCann et al. 2019) and the later glial marker GFAP (Grundmann et al. 2019), suggests that our *in vitro* derived ENS cultures are more likely to resemble a developmentally immature ENS. Moreover, our work in agreement with previous studies (Matsuzawa et al. 1996; Pleasure et al. 1992) demonstrated that the substrate influences neural attachment and projection of axons, and GTX or LAM were the substrates that supported to a great extent neural growth and axonal recovery following replating. This is likely to be due to the interaction of a repertoire of integrins (cell adhesion molecules) expressed by ENS cells (Nagy and Goldstein 2017) with laminins and collagen, components of the basement matrices (Nieuwenhuis et al. 2018).The effect of various substrates on glial survival though was beyond the scope of this study and further research is required to address this question.

My data also revealed that replating of late ENS cultures is a step that holds promise in obtaining “clean”/without debris, purified ENS populations. Cultures following replating appeared more sparse and neurons with the characteristic oval shape (Figure 4.11Aii; day 34 lower panel), reminiscent of enteric neurons, became more visible. This is particularly useful for quantification

analysis of the neural and glial content of these cultures and especially in response of a treatment, given the limitations we previously encountered in microscopy and flow cytometry analysis due to compacted morphology and minimal survival following single cell dissociation, respectively. Therefore, replated cultures could offer a great platform to perform quantitative and functional analysis, to study the effect of gene products in neuron pathophysiology following transfection and are permissive to conduct axonal transport or high-throughput imaging. Nevertheless, these are fairly preliminary findings and further research is required to standardise the process and assess the success rate of replating.

A phenotypic characteristic of our ENS cultures is also the presence of contaminating, flat cells or cell aggregates, with some of them showing immunoreactivity to α-SMA (Barber et al. 2019). These myofibroblasts are likely to represent smooth muscle cells which developmentally arise from cardiac NC, a potential contaminant of the *in vitro*-derived vagal NC cultures as it was mentioned in chapter 3 discussion (see 3.5.1), and contribute to the outflow tract in the developing heart (Kirby et al. 1983). Alternatively, these cells may be derivatives from the recently appreciated vagal NC-derived mesenchymal component (Ling and Sauka-Spengler 2019), which functions in the developing gut and is believed to be critical for stomach patterning and ENS functional integrity (Faure et al. 2015). Interestingly, colonies containing SMA-positive cells, in addition to neural and glial cells, have been previously shown to emerge in clonal cultures derived from NC cells isolated from neural tube explants or fetal peripheral nerve and from ENS progenitors extracted from fetal and postnatal gut (Bondurand et al. 2003; Morrison et al. 1999; Shah et al. 1996), suggesting that our *in vitro* derived vagal NC cells/ENS progenitors may possess a similar developmental potential. The multiple fates towards neurons or smooth muscle could be influenced by external instructive signals (Shah et al. 1996). Whether though the multilineage progeny are clonally derived in our *in vitro* ENS cultures is unclear. Clonal experiments assessing the multipotency of ENS progenitors would be extremely informative to understand their developmental potential and appreciate the progenitor cellular and molecular composition in early ENS cultures.

Notably, our replating experiments demonstrated that SMA-positive cells could be partially eliminated from late ENS cultures. However, the survival of ENS cells long-term (past 2 weeks) following replating was not thoroughly examined. A previous study reported that removal of contaminating cells after multiple replating steps reduced neural survival from 7 months to 10 weeks, possibly due to the lack of soluble factors secreted by non-neuronal cells, consistent with an important role of these cells to neural survival (Pleasure et al. 1992). Whether cells other than neurons and glia, support the ENS maintenance in our *in vitro* system is yet to be defined. My empirical observations of the morphology of the cultures suggest that a uni- or bilateral

communication between contaminating cells and neurons might take place. Flat contaminants in many cases were found to grow in close vicinity or underneath neurons and neural axons, forming track-like structures that potentially stimulated and guided axonal elongation (Figure 4.10A). Axon endings were also found to terminate close to non-neural cells, a result that indicates a functional relationship among different cell types (Figure 4.10B). These observations in combination with preliminary data from time-lapse microscopy showing growth cone driven forward migration of neurons in response to signals coming from neighbouring cells (with non-neural morphology) (Figure 4.4), further outline the importance of cell-cell communication and/or paracrine signalling in neural survival and axonal growth and point to a functional role of these cells in neural differentiation.

4.5.2. Exploring the effect of FGF, Wnt and retinoic acid on enteric nervous system progenitor maintenance

The signals that specify vagal NC to early ENS progenitors as they emigrate from the neural tube and travel to and within the gut to construct a network of neurons and glia are not well understood. Thus, in this chapter I investigated the signalling requirements, particularly that of Wnt/FGF alone or in combination with RA for ENS progenitors' expansion and maintenance. A culture regimen containing FGF2 and CHIR to stimulate FGF and Wnt pathway, respectively, in a process that involved the formation of 3D aggregates/spheres from hPSC-derived vagal NC has been previously used as an intermediate step in the ENS protocol devised by Fattahi and colleagues (Fattahi et al. 2016). Sphere formation under the influence of FGF and Wnt for four days was important to maintain SOX10:GFP expression in vagal NC-derivatives (Fattahi et al. 2016) and served as a purification strategy to enrich particularly for NC/ENS-associated transcripts (*SOX10, ERBB3, GFRA2, EDNRB etc*) (Majd et al. 2022). In our protocol we have adopted this purification step and based on previous studies that demonstrated the long-term maintenance of NC cells in cell suspension as crestospheres (Kerosuo et al. 2015; Mohlin et al. 2019), I next examined whether the early ENS progenitor spheres could be propagated under these conditions for several passages. Prolonged culture in the presence of FGF/Wnt was not sufficient to maintain the NC/early ENS progenitor characteristic gene expression profile, as the transcript levels of *PAX3, PAX7, SOX10* and the fraction of cells with high expression of p75 progressively reduced (Figure 4.13). This contrasts previous findings from Li et al. (2018) who demonstrated that hPSC-derived NC cells could be expanded in cell suspension for up to 15 passages and implies that alternative culture conditions might be more efficient in directing the maintenance and long term culture of SOX10+ ENS progenitors.

Notably, prolonged exposure to FGF2 and CHIR resulted in a reduction in *HOXB5* transcripts and led to an upregulation of more caudal/ trunk *HOX* genes (*HOXB7, HOXC9*), a profile consistent with a shift of the axial identity towards trunk axial levels. The downregulation of *HOXB5* is of particular importance, given the regulatory role of this gene in NC development, gut colonisation (Fu et al. 2003; Kam and Lui 2015) and ENS-associated disease (Lui et al. 2008) and further indicates that these conditions are not suitable to maintain vagal NC/early ENS progenitors over time. On the contrary, supplementing the sphere medium with RA was sufficient to restore the expression of ENS-progenitor genes *ASCL1, PHOX2B,* which were found to be downregulated during the four-day period of 3D culture, and to maintain increased levels of *HOXB5* (Figure 4.14). A requirement for RA during ENS development as it regulates aspects of progenitors' proliferation, migration and gut colonisation has been previously described in the literature (Fu et al. 2010; Gao et al. 2021; Niederreither et al. 2003; Sato and Heuckeroth 2008; Uribe et al. 2018) and a longer exposure to RA (up to 5 days during vagal NC differentiation) has also been used in alternative hPSC-based ENS differentiation protocols (Figure 1.8) (Barber et al. 2019; Fattahi et al. 2016; Lai et al. 2017). Moreover, RA supplied by the paraxial mesoderm was shown to be one of the main drivers of RET expression during quail vagal NC migration towards the gastrointestinal tract and to confer cells with improved enteric colonisation ability (Simkin et al. 2013). Thus, RA is a signal that vagal NC cells naturally encounter *in vivo* and exposure of hPSC-derived vagal NC to RA after the initial RA-mediated posteriorisation potentially specifies cells to ENS lineage. However, thorough characterisation for the expression of later ENS-related genes at day 10 spheres grown in the presence of RA was not performed and examining the expression of RET at the transcript and protein level would be very useful to appreciate whether RA stimulates RET expression similar to its role *in vivo*. Moreover, functional analysis including migration assays and differentiation to enteric neurons and glia downstream of RA-treated spheres would be beneficial to address whether RA influences the ability of cells to migrate or enhances their differentiation potential, respectively.

4.5.3. Examining the effect of Notch signalling pathway inhibition on cell fate specification during enteric nervous system differentiation

Due to its ability to regulate alternative cell-fate decisions between neighbouring cells via a negative feedback loop which results in lateral inhibition (Sjoqvist and Andersson 2019), Notch signalling pathway is a key regulator of cellular diversity in the developing nervous system (Louvi and Artavanis-Tsakonas 2006). Using our hPSC-based ENS system, I showed that Notch signalling pathway is also implicated in ENS specification *in vitro*. Particularly, I demonstrated that Notch inhibition promoted neural differentiation and resulted in an increase in the number of SOX10+ cells, potentially denoting progenitors and glia, at an early and a later stage during

differentiation. While the majority of SOX10-expressing cells appeared negative for S100 at day 15 in the control, the number of SOX10+/S100+ glial cells in DAPT-treated cultures significantly increased, consistent with an early expansion in the glial compartment. At day 22, the effect of Notch inhibition on glial differentiation was less severe but a trend towards an increase in glial numbers upon DAPT treatment in 2/4 biological replicates was noticeable (Figure 4.17- Appendix Figure S4 contains analysis of individual independent experiments). Altogether, these data suggest that Notch inhibition promotes neural differentiation and may influence glial induction in ENS cultures though more repeats are required to determine the effect of Notch inhibition on glial specification. My findings contrast previous work from Theocharatos et al. (2013) which supported a role of Notch inhibition on neural induction in ENS neurospheres while glia remained unaffected and diverge from the notion that Notch actively promotes gliogenesis as it was previously shown in murine PNS/ENS and in NC-derived *in vitro* clonal culture system (Morrison et al. 2000; Ngan et al. 2011; Taylor et al. 2007). Instead, my results are consistent with a function of Notch inhibition in promoting neural and glial differentiation in ENS progenitors. This could be possibly achieved by interfering with the cell cycle machinery, altering the duration of each phase or by inducing cell cycle exit (Borghese et al. 2010). Notch-mediated premature cell cycle exit and onset of differentiation are events coupled with a depletion of the ENS progenitor pool (Ngan et al. 2011; Okamura and Saga 2008). Testing whether this is the case in our system, future analysis would involve examining the effect of Notch inhibition on ENS progenitor population. This was particularly a caveat to our research due to the lack of specific ENS progenitor markers that prevented us from examining thoroughly the effect of DAPT treatment on progenitor numbers and proliferation. Our work relies on SOX10 and S100 co-expression to determine progenitors and glia, however, we cannot rule out the possibility that these generic markers with a relatively broad expression can as well as mark more restricted gliogenic progenitors rather than defined glia (Guyer et al. 2022; Lasrado et al. 2017).

The ability to identify putative hPSC-derived ENS progenitor cells by surface marker expression gives us the exciting advantage of being able to isolate single progenitors cells to further study their developmental potential. In this chapter I showed that CD49d is expressed in hPSC-derived vagal NC and ENS cultures *in vitro*, in line with the reported CD49d expression in migrating NC (Kil et al. 1998) and in the ENS *in vivo* (Nagy and Goldstein 2017). Although CD49d expression was not restricted in SOX10+ NC cells at day 6 of the differentiation (Gogolou et al. 2021), it's expression coincided with SOX10 and S100β at later stages and during ENS differentiation, potentially reflecting ENS progenitors and glial cells (Figure 4.7A, 4.8). The absence of CD49d positivity in neural cells further suggests developmental restriction and raises the intriguing question of whether CD49d is initially ubiquitously expressed in all ENS progenitors and at what stage spatial/temporal restriction takes place. Thus, isolating prospective ENS cells on the basis

of CD49d expression at successive time points to capture progenitors with a broad and progressively more restricted developmental potential and incubation with DAPT would be a more efficient way to address the effect of Notch pathway inhibition on cell fate determination in ENS development and in human context. We envisage that these findings in combination with mathematical modelling, which has been used before in the context of Notch mediated lateral inhibition (Matsuda et al. 2015), would further help us understand the dynamics of lineage segregation in different developmental stages in ENS and shed light to the role of Notch pathway contribution in ENS functional integrity possibly by establishing appropriate numbers of cells with the "right" identity (Mead and Yutzey 2012; Morrison et al. 2000).

Although it is currently unclear how Notch pathway is regulated in ENS progenitor cells and their derivatives, my results demonstrating different expression patterns of Notch receptors, ligands and target genes across different stages of the protocol, propose that direct cell-cell interactions and temporal transcriptional programs might be involved. For instance, the induction of the Notch effector *HES5* coincides with the differentiation of vagal NC progenitors along the ENS lineage (following day 6) and suppression of this gene upon Notch pharmacological inhibition suggests that it might be implicated in ENS specification. Involvement of Hes family members and particularly *Hes1* in ENS development and progenitor maintenance, has been demonstrated previously in the context of Notch inhibition (Okamura and Saga 2008). According to the model, reduction of *Hes1*, a negative regulator of the neurogenic gene *Ascl1* (Chen et al. 1997), following disruption of Notch signalling in NC cells in mice results in upregulation of *Ascl1* and hence excessive neural differentiation which depletes the progenitor pool (Okamura and Saga 2008). The decrease in the levels of *HES5* (Figure 4.15C) and the concomitant increase in *ASCL1* (Figure 4.16A) in DAPT-treated cultures are likely to promote an increase in the neural component in our ENS cultures and potentially reflect a mechanism of neurogenesis that fits well with the proposed model by Okamura and Saga (2008). Notably, the downregulation of Notch target gene *HES5* and not *HES1* in response to DAPT suggests that other mechanisms independent of the canonical Notch guide *HES1* expression (Ingram et al. 2008) and mirrors differences in species as well as between the *in vitro* and *in vivo* given the reported role of Hes1 in mouse ENS development (Okamura and Saga 2008). Similarly, *HES6* was not found to antagonistically influence *HES1* transcription denoting the presence of other mechanisms that might compensate for *HES6*-mediated *HES1* downregulation or simply showing that *HES1* is not a direct target of HES6 in these cultures.

To decipher the molecular mechanism that underpins Notch pathway regulation during ENS differentiation, examining Notch activation upon Notch receptor-ligand binding at single cell level is highly required. Owing to the increased transcripts of *NOTCH1*, *DLL1* and *JAG1* during early

stages of the differentiation (Figure 4.15D), we can speculate that these genes are likely to be involved in Notch signalling fine-tuning. Analysis of the expression of Notch ligands/receptors in combination with cell lineage markers would further illustrate whether Notch signalling functions in a cell-dependent context. My preliminary work and immunofluorescence analysis for NOTCH1 intracellular domain (ICD) on day 15 ENS cultures revealed NOTCH1 ICD nuclear localisation, and hence Notch activation in enteric neurons (Appendix Figure S5). This, together with the findings demonstrating that inhibition of Notch results in increased number of neurons suggests that blocking of Notch, potentially in neurons, might interfere with the cascade of Notch activation which signals from one cell to another, resulting in amended neural and progenitor/glial numbers. Analysis of the nuclear localisation of the rest Notch receptors and the expression of ligands would further illustrate whether Notch acts in the neighbouring cells by supressing or inducing the expression of ligands, reflecting a mechanism of lateral inhibition or induction, respectively. However, a highly sensitive and more specific technique for biomarker analysis, such as RNAscope (an RNA ISH method; Wang et al. 2012), would be beneficial to surpass the lack of reliable Notch antibodies. Moreover, we cannot exclude the possibility that Notch signalling might be controlled indirectly and/or through paracrine signalling in ENS differentiating cultures. Morphogens such as BMP and Wnt family members or receptors such as the auxiliary receptor of Shh, GAS1 have been previously shown to be expressed by ENS progenitors (reviewed in Kang et al. 2021) and some of them were suggested to be involved in Notch signalling pathway regulation (Collu et al. 2012; Irshad et al. 2017; Liu et al. 2013b; Marczenke et al. 2021). Analysis of the expression of these factors and their effect on Notch pathway activity would be an effective way to test this hypothesis and unravel a potential crosstalk given the key role of Shh, BMP and Notch in ENS progenitor's differentiation (Pawolski and Schmidt 2020).

Furthermore, owing to the broad biological functions of γ-secretase (Kopan and Ilagan 2004), the use of DAPT to block γ-secretase and hence NOTCH receptors' proteolytic cleavage, raises questions about whether the observed changes in gene expression are a result of Notch signalling inhibition. To confirm this, knockdown of key components of the canonical Notch signalling pathway such as *JAG1* (Noisa et al. 2014) or RBPjk (Theocharatos et al. 2013) could be additionally performed.

Understanding the contribution of Notch signalling pathway in human ENS specification and whether it could act as a cell-fate controlling switch or as a regulator of progenitors' proliferation would be an exciting avenue to pursue with practical implications in regenerative medicine.

Chapter 5: Defining critical signals/transcription factors for trunk neural crest specification

5.1. Introduction

Until recently the conventional strategy to obtain NC cells of discrete anteroposterior (A-P) levels involved the induction of an anterior NC character which is progressively posteriorized by RA and/or Wnt instructive signals, an approach influenced by classic embryology experiments and the "activation transformation model" (Nieuwkoop and Nigtevecht 1954), which states that an anterior neural identity is first established (activation) before being patterned to more caudal fates in order to form the hindbrain region and spinal cord (transformation). This approach generates NC cells of cranial and cervical axial identity but fails to efficiently induce NC cells of more posterior to vagal NC domains and, thereby a *HOX PG* (*6-9*)+ trunk identity (Barber et al. 2019; Fattahi et al. 2016; Frith et al. 2020; Gogolou et al. 2021; Mica et al. 2013). In particular, as it was demonstrated in chapter 3.3.1, RA treatment was not sufficient to induce *HOX* genes posterior to *HOXB5*, such as *HOXB7* or *HOXC9,* underlying the inefficiency of the culture conditions to specify cells towards trunk and sacral NC and upregulate *HOX* genes that correspond to thoracic and lumbosacral axial levels, in agreement with a previous report (Frith et al. 2018). Moreover, a similar approach via the use of caudalising cues to induce posterior NC and subsequently sympathetic neurons starting from an anterior NC population was shown to yield low numbers of sympathetic neural progenitors (around 5–10% PHOX2B-GFP+ cells), reflecting an inefficiency to properly specify NC towards trunk levels (Oh et al. 2016). However, accumulating recent evidence (Cooper et al. 2022; Frith et al. 2018; Frith and Tsakiridis 2019; Gomez et al. 2019b; Hackland et al. 2019; Kirino et al. 2018) has suggested that the generation of NC cells of a thoracic axial identity (trunk NC) from hPSCs can only be achieved through an initial FGF- and Wnt- induced NMP-like state (Gouti et al. 2014), in line with the role of NMPs to contribute to trunk NC cells in vertebrates *in vivo* (Wymeersch et al. 2016). Nonetheless, the exact links between NMP signalling/transcriptional determinants and posterior NC patterning are undefined. Moreover, it is unclear whether the acquisition of a mesoderm potent progenitor state is an obligatory step toward trunk NC specification.

5.2. Aims

In this chapter I sought to define crucial signals for trunk NC specification *in vitro* and determine the role of the NMP/mesoderm transcriptional modulator TBXT in the acquisition of posterior axial identity by NMP-derived trunk NC cells. Specifically, in this chapter I aimed to:

1. Determine the role of different signals in controlling the acquisition of posterior axial identity and the adoption of a NC fate by hPSC-derived NMPs
2. Examine the role of the NMP/mesodermal transcription factor TBXT in the generation of trunk NC from hPSCs and define a mechanism of its action

5.3. hPSC-derived neuromesodermal progenitor-like cells differentiate into multiple posterior derivatives *in vitro*

To explore the ability to efficiently generate trunk NC cells *in vitro*, I differentiated H9 hESCs into TBXT+/SOX2+ NMP-like cells (Figure 5.1B) following a 3-day treatment of FGF2 (20ng/ml) and CHIR (3μM) and subsequently replated and cultured them in the presence of precise levels of BMP4, lower CHIR concentration and SB 431542 (TGFβ inhibitor) for 5 days to induce a NC identity as described previously (Frith et al. 2018; Frith and Tsakiridis 2019) (Figure 5.1A). To evaluate the differentiation efficiency, I monitored transcript levels of NC markers and posterior *HOX* genes. Gene expression analysis at day 8 revealed a significant increase in mRNA levels of *SOX10* and *PAX3* (Figure 5.1C) and upregulation of *HOX PG (6-9)*, indicative of thoracic axial identity, in all *HOX* gene clusters (Figure 5.1D). The acquisition of a trunk NC identity was also examined at the protein level. Immunofluorescence analysis showed that the majority of day 8 cultures displayed a trunk NC identity mirrored by the co-expression of HOXC9 and SOX10 (45 ± 17%), while a slightly smaller number of cells were positive only for HOXC9 (36 ± 8.5%), potentially reflecting a fraction of early NC cells that have not upregulated SOX10 or other NMP-derived non-NC posterior entities (e.g spinal cord progenitors or paraxial mesoderm). Moreover, a small number of cells was found to be single-positive for SOX10 (7 ± 8.5%), possibly marking NC cells of a non-trunk identity (Figure 5.1E).

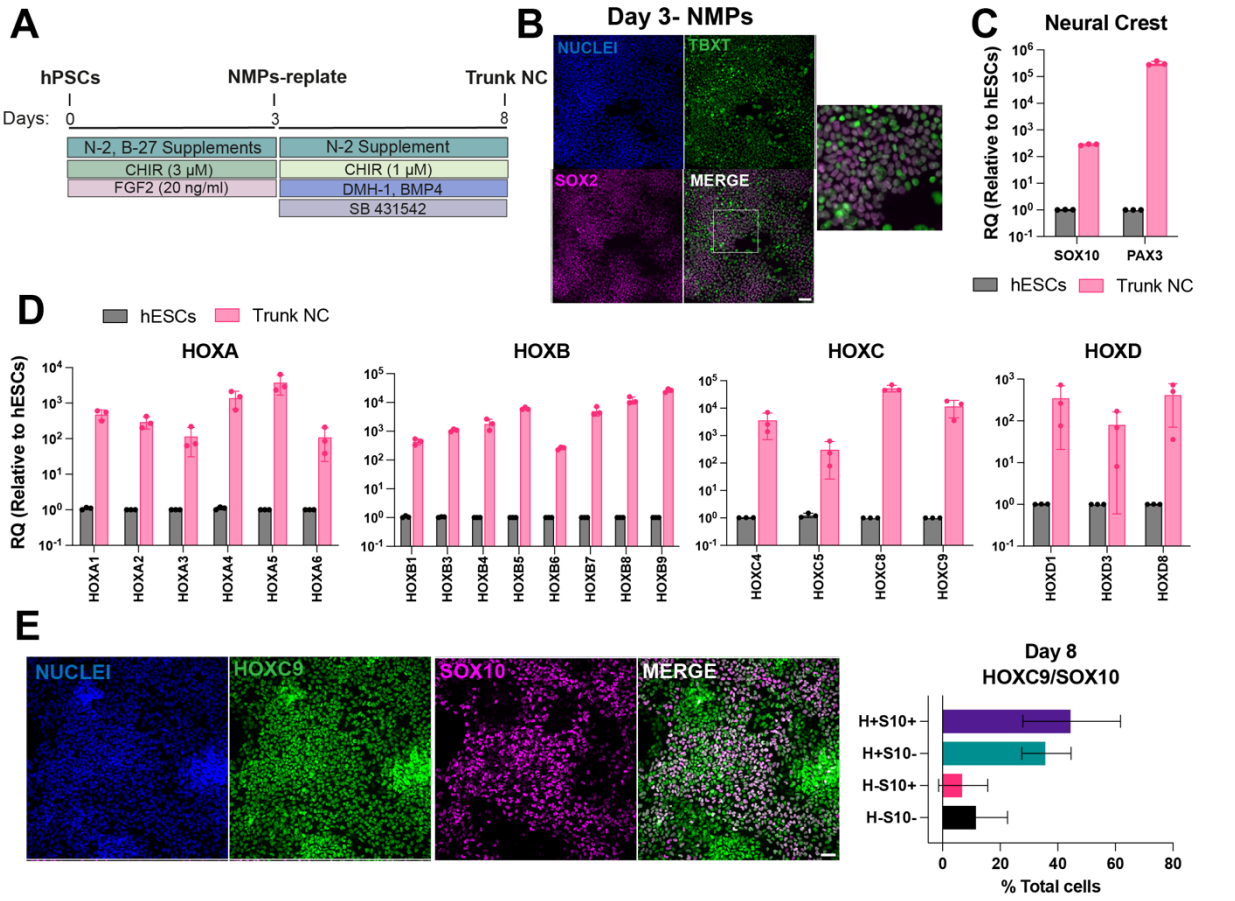

Figure 5.1. Differentiation of neuromesodermal progenitors into trunk neural crest. (A) Schematic depicting the culture regime for the derivation of trunk NC cells. (B) Immunofluorescence images showing the protein expression of TBXT and SOX2 in day 3 hPSC-derived NMPS. (C-D) Gene expression analysis of indicated NC (C) and *HOX* genes (D) in trunk NC cells generated using the protocol described in A. Data shown are the mean of mean values ± SD, n=3 independent experiments with three replicates in each experiment. (E) Immunofluorescence analysis and quantification of the expression of HOXC9 and SOX10 in day 8 trunk NC cultures. Data in the graph were obtained after scoring 30 random fields per experiment. Data are shown as the mean of mean values ± SD (n=3 independent experiments). Scale bars =50 µm. H, HOXC9; S10, SOX10.

To confirm the neuromesodermal potency of NMPs in addition to their ability to generate trunk NC *in vitro*, I also tested their ability to differentiate towards paraxial mesoderm cells and pre-neural spinal cord progenitors following the protocols depicted in Figure 5.2 (Frith et al. 2018; Wind et al. 2021). NMP-like cells generated from hPSCs have been previously shown to differentiate towards paraxial mesoderm and posterior neuroectoderm in response to the same, albeit different in duration and level, prolonged FGF and Wnt signals (Wind et al. 2021). Treatment of NMP-like cells with high levels of CHIR (8 µM) and FGF2 (40ng/ml) for 2 days (Figure 5.2Ai) induced a presomitic/paraxial mesoderm phenotype, marked by the maintained expression of *TBXT*, *CDX2*, *TBX6, MSGN1* transcripts and an increase in *PAX3* (Figure 5.2Aii), while the transcript levels of the NMP-associated neural marker *SOX2* showed no further increase (Figure 5.2Aii). This transcriptional profile was also accompanied by maintained expression of TBXT protein, as the number of cells positive for TBXT remained considerably high

after day 3 (D3: 82 ± 14% vs D5: 73 ± 5%) (Figure 5.2Aiii). In contrast, treatment of hPSC-derived NMPs with high levels of FGF2 (100ng/ml) and lower concentration of CHIR (3 μM) for 4 days (Figure 5.2Bi), resulted in a progressive decrease to almost extinction in the number of cells positive for TBXT (D3: 95 ± 1% vs D7: 1 ± 0.7%), a result consistent with a loss of mesodermal potency (Figure 5.2Bv). Transcriptome analysis for the NMP/early spinal cord-associated markers *CDX1/2* and *NKX1-2* (Gouti et al. 2017) and the neural marker *SOX2* revealed maintained expression in day 7 cultures compared to day 3, and a trend towards an upregulation in the transcript levels of the neural marker *PAX6* (Figure 5.2Bii). Consistent with the RT-qPCR data, immunofluorescence analysis showed that day 7 cultures were primarily comprised of CDX2+ (73 ± 8%; Figure 5.2Biii) and SOX2+ (66 ± 0.3%) cells with the vast majority of the latter being immunoreactive to HOXC9 (60.5 ± 2.3%; Figure 5.2Biv), and thus displaying a pre-neural posterior axial character. Taken together, these data illustrate the ability of hPSC-derived NMPs, similar to their *in vivo* counterparts (Wymeersch et al. 2021), to efficiently generate trunk NC, paraxial mesoderm and early spinal cord cells under the influence of exogenous instructive signals.

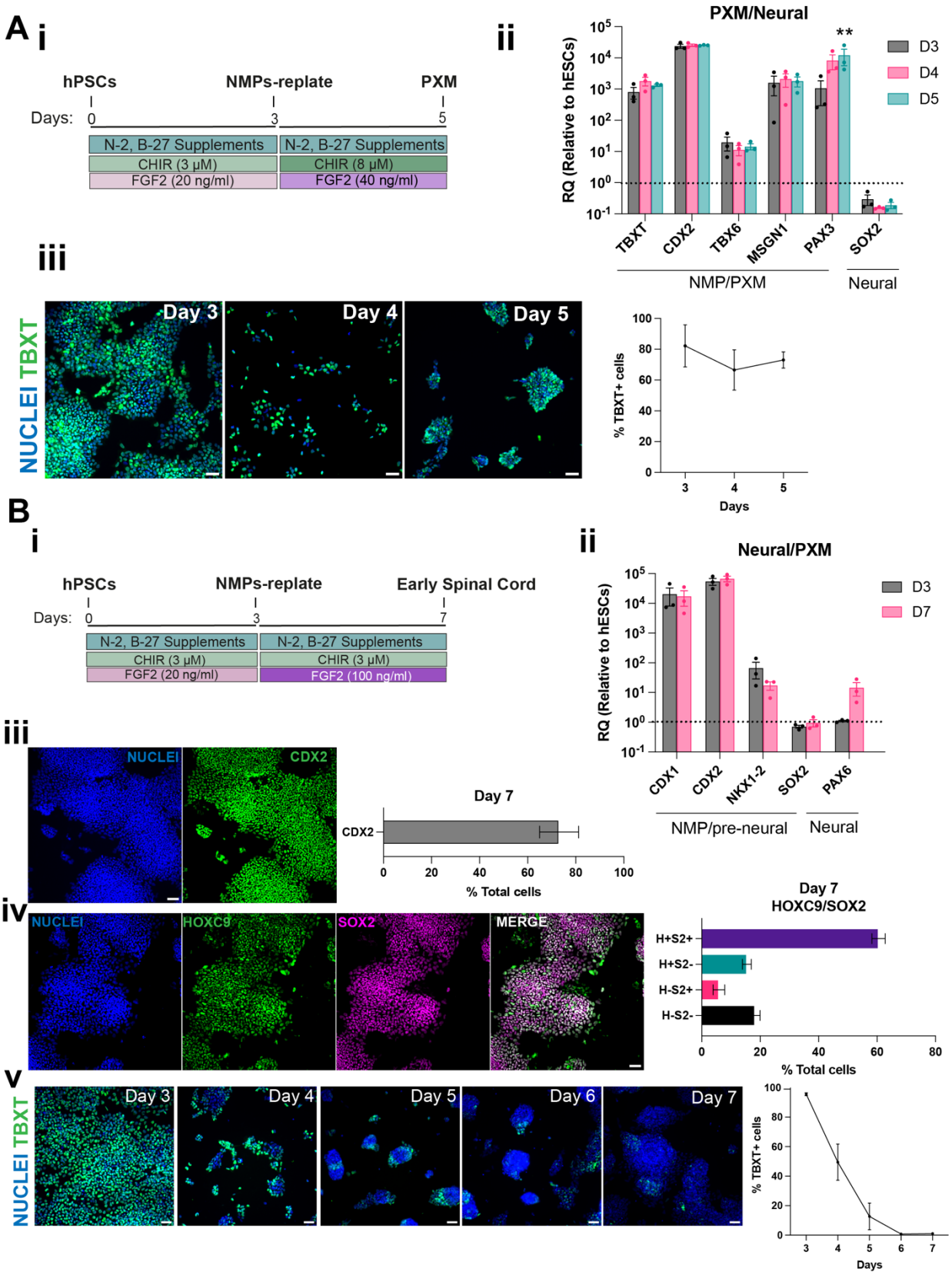

Figure 5.2. Differentiation of neuromesodermal progenitors into paraxial mesoderm and pre-neural spinal cord progenitors. (A.i) Schematic showing the culture conditions for the derivation of presomitic/paraxial mesoderm cells (PXM) from NMPs. (A.ii) RT-qPCR analysis for a panel of NMP/PXM and neural markers in PXM cultures over time. Data shown are the mean of mean values ± SEM, n=3 independent experiments with three replicates in each experiment; ***P* <0.005 by mixed model ANOVA Tukey's post-hoc multiple comparisons test with control "D3" group. Only statistically significant changes are indicated. (A.iii) Immunofluorescence analysis and quantification of TBXT

protein expression in PXM cultures over time. For quantification 10-25 random fields per experiment were scored. Data state the mean of mean values ± SD of independent experiments (n=2). (B.i) Schematic showing the culture conditions for the derivation of pre-neural spinal cord progenitors. (B.ii) RT-qPCR analysis for a panel of NMP/pre-neural and neural markers in pre-neural spinal cord progenitor cultures over time. Data shown are the mean of mean values ± SEM, n=3 independent experiments with three replicates in each experiment. No statistically significant differences were observed (paired t-test). Immunofluorescence analysis and quantification of CDX2 (iii) and HOXC9/SOX2 (iv) protein expression in day 7 pre-neural spinal cord progenitors. Data in the graphs were obtained after scoring 10 random fields per experiment and state the mean of mean values ± SD of independent experiments (n=2). (B.v) Representative fluorescent microscopy images and quantification of TBXT protein expression in pre-neural spinal cord progenitor cultures over time. For quantification 20 random fields per time point and per experiment were scored and data state the mean of mean values ± SD of independent experiments (n=3). Scale bars =50 μm in all images. H, HOXC9; S2, SOX2.

5.4. Deciphering the role of critical posteriorisation signals in the generation of trunk neural crest

5.4.1. Wnt signalling ascribes neuromesodermal progenitors a posterior regional identity

The posterior growth zone, area that NMPs reside *in vivo,* is characterised by an increased activity of Wnt and FGF signals (Wilson et al. 2009; Wymeersch et al. 2021). These signals are implicated in the induction of Brachyury+/Sox2+ axial progenitors and are essential for body axis elongation (Amin et al. 2016b; Gouti et al. 2014; Lippmann et al. 2015; Wilson et al. 2009; Wymeersch et al. 2016; Wymeersch et al. 2021). Wnt and FGF inputs have been shown to promote the upregulation of posterior *HOX PG (5-9)* genes in NMPs and their derivatives (Gouti et al. 2014; Hackland et al. 2019; Lippmann et al. 2015; Mazzoni et al. 2013; Mouilleau et al. 2021; Young et al. 2009) and, thereby stimulate trunk elongation.

Owing to the well-established role of Wnt and FGF as posteriorizing signals (Kudoh et al. 2002), I next sought to examine the effect of their perturbation on the induction of a posterior axial identity during NMP differentiation. I initially explored signal contribution during the transition of hPSCs to NMPs by withdrawing the Wnt or FGF agonist from the NMP induction medium and additionally employing the tankyrase inhibitor XAV939 (XAV; Huang et al. 2009) or the MEK1/2 inhibitor PD 0325901 (PD03; Barrett et al. 2008) to attenuate endogenous Wnt or FGF signals, respectively (Figure 5.3A). Signalling inhibition was confirmed by the downregulation of Wnt (AXIN2, TCF1, LEF1; Lecarpentier et al. 2019) and FGF (SPRY4; Mason et al. 2006) target genes in the presence of XAV and PD03 antagonists, respectively in D3 cultures compared to untreated controls (Figure 5.3B). Gene expression analysis showed that the combined action of FGF and Wnt signals promoted the generation of NMP cells, marked by upregulation of *TBXT*, *CDX2*, *NKX1-2* and *HOX* genes, while loss of either signal severely impaired the induction of all genes (Figure 5.3B-C). Interestingly, loss of *HOX* gene expression was found to be more prevalent upon Wnt pathway inhibition and Wnt stimulation alone (in the absence of FGF) partly

rescued the induction of *TBXT*, *CDX2* and of many *HOX* genes, specifically the ones belonging to *HOXB* cluster (Figure 5.3B-C). In contrast, expression of *HOX* genes of cluster C (*HOXC*) was shown to be severely affected by loss of Wnt or FGF signals (Figure 5.3B-C), suggesting that distinct *HOX* cluster-specific regulatory mechanisms might exist, in line with a previous report (van den Akker et al. 2001). Altogether, these data suggest that during NMP differentiation the induction of major axis extension regulators and *HOX* genes indicative of posterior axial levels predominantly relies on Wnt activity.

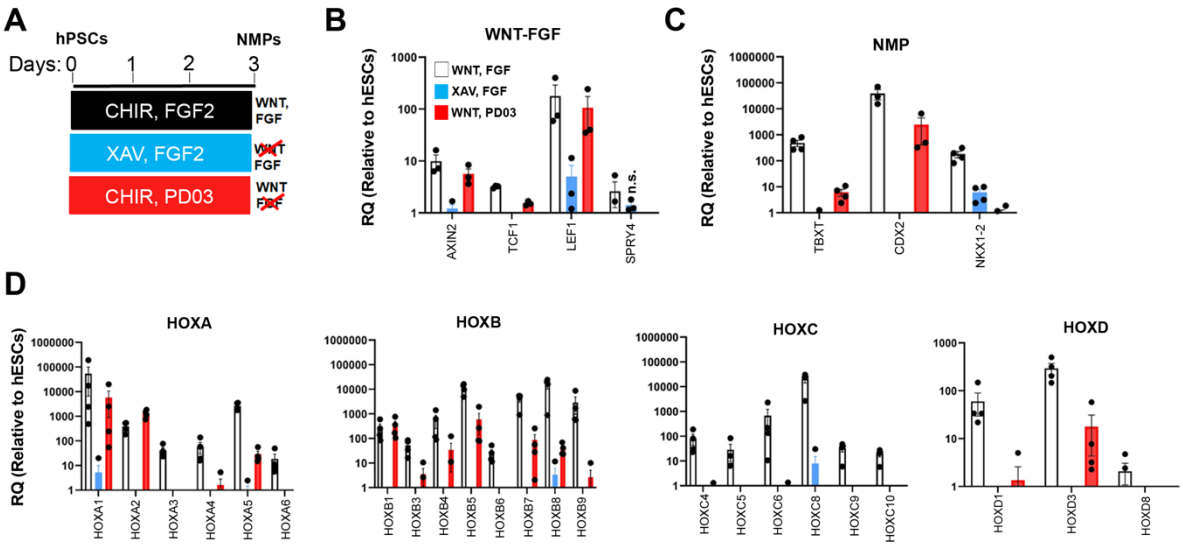

Figure 5.3. Acquisition of posterior axial identity by neuromesodermal progenitors predominantly relies on Wnt signalling. (A) Diagram depicting the protocol followed and agonist/antagonist treatments. (B-C) RT-qPCR analysis of indicated genes involved in WNT-FGF signalling cascade (B) and expressed by NMPs (C) in D3 cultures generated under the treatments indicated in A. (D) RT-qPCR analysis of various *HOX* genes belonging to the four different clusters in D3 cultures upon WNT-FGF agonist/antagonist treatment. Data shown are the mean of mean values ± SD, n=3-4 independent experiments with three replicates in each experiment. All changes were statistically significant unless otherwise stated (ratio paired t-test with WNT,FGF as control). n.s; not significant. Data sourced/modified from Gogolou et al. (2022).

Another caudalising signal that was recently reported to be involved along with Wnt and FGF in *in vitro* NMP induction and concomitant neural differentiation is RA (Gouti et al. 2017). RA has been previously shown to regulate *HOX* gene expression during posterior CNS development (Liu et al. 2001) through its ability to directly activate the transcription of anterior *HOX 1-5* genes (Marshall et al. 1994; Mazzoni et al. 2013) and was reported to act downstream of FGF and Wnt in inducing the expression of posterior neuroectoderm genes (Kudoh et al. 2002). To test the contribution of RA in the induction of NMPs and the interaction between RA, FGF and Wnt signals in the acquisition of a posterior fate by NMPs, I repeated the agonist/antagonist treatments as described previously in combination with exogenously applied RA (0.1 μM) (Figure 5.4A) and monitored the expression of *HOX*, NMP-, neural- associated genes. I found that addition of RA

in the presence/absence of FGF2 could not substitute for the loss of Wnt (green and lilac bars; Figure 5.4D) as *HOX* genes (*HOXA4, HOXA5, HOXB3, HOXB4, HOXB5, HOXB8* and *HOXC*; Figure 5.4D) were severely affected compared to control (Wnt/FGF-treated). Moreover, the combined action of Wnt and RA compared to RA-only (lilac; Figure 5.4D) and Wnt-only (red; Figure 5.3D) resulted in increased and similar to control expression of most cervical *HOX (3-6)* genes in *HOXA* and *HOXB* clusters (purple vs grey; Figure 5.4D), suggesting a synergy between Wnt pathway and RA in the induction of anterior cervical *HOX* domains. Interestingly, addition of RA in the presence of FGF and Wnt resulted in a statistically significant decrease in *HOXC* transcripts (pink vs grey; Figure 5.4D), a finding indicating antagonism between RA and FGF (Diez del Corral et al. 2003; Olivera-Martinez et al. 2012) in controlling the expression of *HOX* genes, particularly of cluster C. Notably, treatment with RA in the absence of FGF and Wnt was sufficient to upregulate most of the hindbrain/cervical *HOX (1-5)* genes, in line with previous reports but not their more posterior counterparts (Mazzoni et al. 2013).

Moreover, cultures treated with RA and different agonist/antagonist combinations had a dramatic and variable decrease in transcript levels of the NMP-associated markers *NKX1-2, TBXT* and *CDX2* (Figure 5.4B) and this coincided with the acquisition of a pre-neural identity exemplified by the upregulation of *SOX2, PAX6 and SOX1* (in the presence of Wnt and RA) in agreement with previous work (Gouti et al. 2017) (Figure 5.4B).

Taken together, these results indicate that while RA can partially promote the expression of *HOX 1-5*, activation of Wnt signalling pathway is required for the transcriptional activation of more caudal cervical/thoracic *HOX* genes. They also confirm that Wnt and FGF signals are required to establish an NMP-like identity and demonstrate that RA promotes a switch towards neural fate.

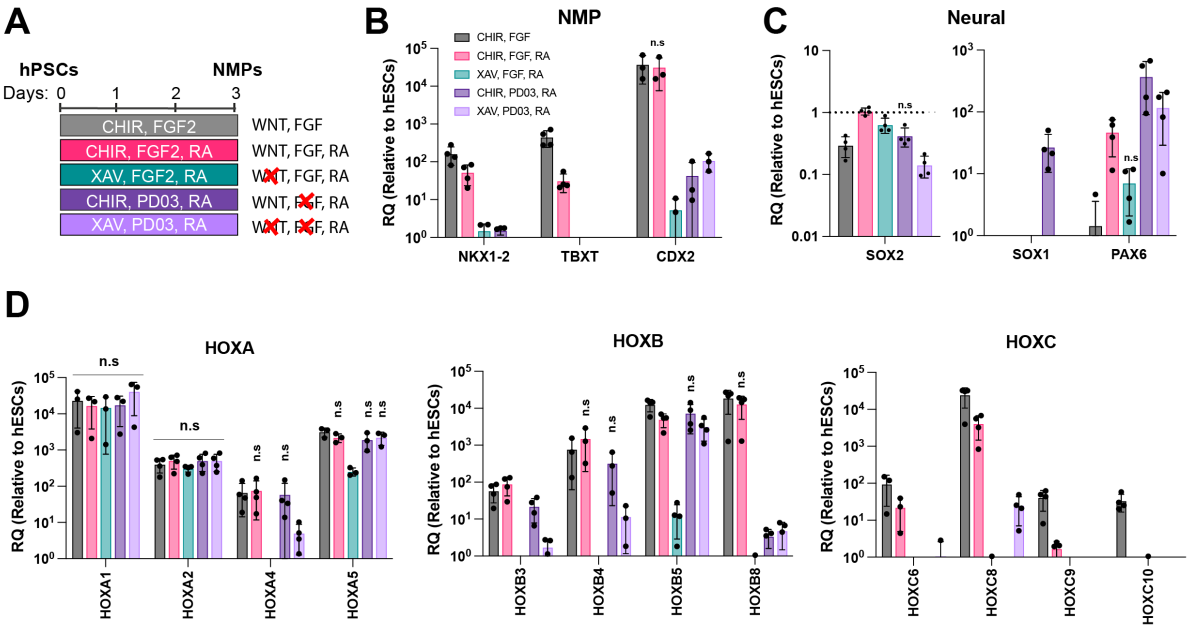

Figure 5.4. Retinoic acid steers neuromesodermal progenitors towards neural fate. (A) Schematic depicting the protocol followed and agonist/antagonist treatments. (B-C) RT-qPCR analysis of indicated NMP (B) and neural (C) genes in NMP cultures generated using the different agonist/antagonist combinations shown in A. (D) RT-qPCR analysis of a battery of HOX genes belonging to *HOXA*, *HOXB* and *HOXC* clusters. Data in all graphs represent the mean of mean values ± SD, n=3-4 independent experiments with three replicates in each experiment. All changes are statistically significant unless otherwise stated (ratio paired t-test with WNT,FGF as control). n.s; not significant.

5.4.2. Wnt and FGF signalling maintain a posterior identity in trunk neural crest

After examining the influence of FGF, Wnt and RA signals during the transition from hPSCs to NMPs, I sought to determine the signalling pathways that are critical for the specification of trunk NC from NMPs. To this end, I generated NMPs as described previously and subjected them in culture conditions in the presence of Wnt and BMP signals to yield trunk NC cells (Figure 5.5). To discern the role of Wnt and BMP signalling pathway activity on trunk NC specification, agonist/antagonist treatments were employed in a similar manner to the experiments carried out from D0-D3. Addition of XAV alongside precise levels of BMP was used to assess the effect of loss of Wnt activity on trunk NC identity, while CHIR in combination with the ALK2/3 inhibitor LDN 193189 (LDN; Cuny et al. 2008) to attenuate BMP was exploited to determine the influence of BMP signalling (Figure 5.5A). Gene expression analysis at day 8 of the differentiation showed that Wnt inhibition did not impede the induction of *SOX10* at transcript (Figure 5.5B) and at the protein level (Figure 5.6) and had no effect on *PAX3* transcripts (Figure 5.5B) as their expression levels appeared similar to the control. However, it promoted an increase in the anterior NC markers *OTX2* (Matsuo et al. 1995) and *ETS1* (Tahtakran and Selleck 2003) and this was accompanied by a decrease in the posterior NC marker *CDX2* (Sanchez-Ferras et al. 2016) (Figure 5.5C). The inability of NMP-derived NC to adopt a posterior axial identity following Wnt inhibition was also confirmed by their inability to activate properly the expression of *HOX* genes compared to Wnt/BMP-treated controls (Figure 5.5D). RT-qPCR analysis showed that XAV treatment alongside BMP, resulted in a statistically significant decrease in transcripts of most *HOX* gene family members, albeit to a lesser degree compared to XAV treatment during day D0-D3 (Figure 5.3D). Interestingly, the total number of cells immunoreactive to HOXC9, showed no significant decrease in the presence of XAV and BMP compared to controls (Figure 5.6).

By contrast, cultures in the absence of BMP failed to upregulate *SOX10* (Figure 5.5B, 5.6), had reduced expression of *PAX3* (Figure 5.5B) and showed a profound increase in *SOX1* at transcript (~1000-fold increase relative to control; Figure 5.5B) and at the protein level (the percentage of SOX1+ cells increased from 0.7 to 45%, $P < 0.05$ paired t-test; Figure 5.6B), a profile consistent with a shift towards a CNS neural fate. Thus, these results provide evidence that BMP activity is highly required for NC induction and suggest a role of BMP in promoting NC identity at the

expense of neuroectoderm, similar to previous observations (Leung et al. 2016). Gene expression analysis for axial regulators upon BMP suppression revealed a significant increase in the levels of *CDX2* and a decrease in *ETS1* transcripts, while *OTX2* expression remained unaffected (Figure 5.5C). This coincided with a global increase in the expression of most *HOX* genes (Figure 5.5D), in line with the established role of *CDX2* in activation of posterior HOX genes (Mazzoni et al. 2013; Neijts et al. 2017). Nevertheless, the total number of cells expressing HOXC9 showed no significant increase (Figure 5.6).

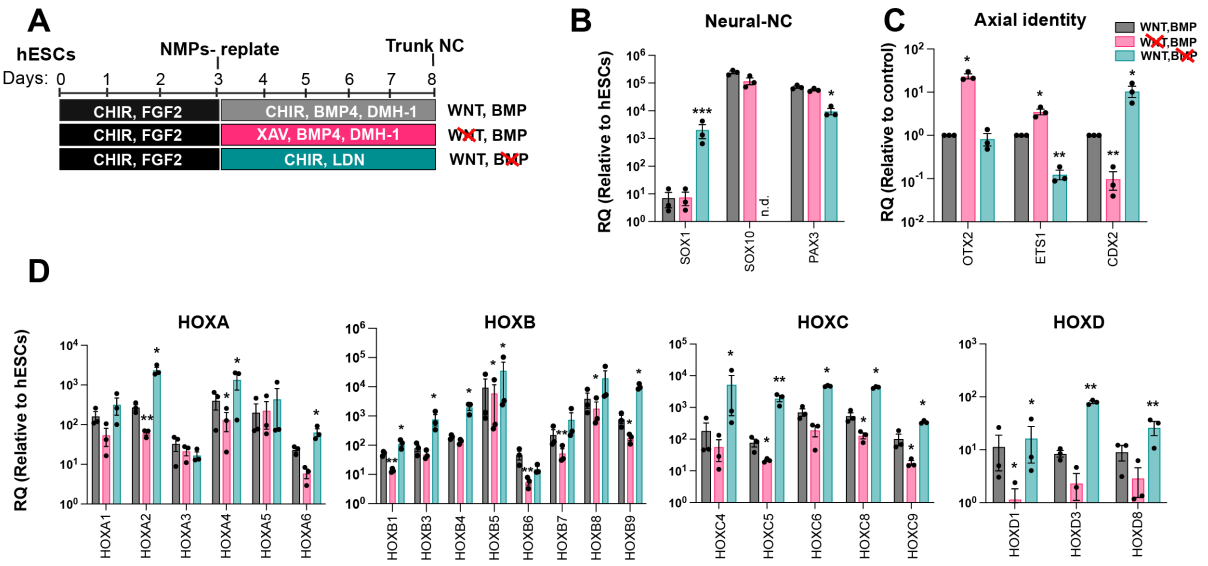

Figure 5.5. Acquisition of posterior axial identity by neuromesodermal progenitor-derived trunk neural crest cells is mainly WNT-dependent. (A) Schematic showing the culture regime and the agonist/antagonist treatments employed for the generation of trunk NC cells via an NMP-intermediate. (B-C) Gene expression analysis of indicated neural-NC (B) and axial identity (C) markers in NMP-derived NC cells generated following WNT-BMP agonists/antagonists combinations depicted in A. (D) Gene expression analysis of various *HOX* genes belonging to the four different clusters in NMP-derived NC cells generated using different treatments. Data in all graphs represent the mean of mean values ± SD, n=3 independent experiments with three replicates in each experiment. Only statistically significant changes are indicated. **P* <0.05, ***P* <0.005 (ratio paired t-test with WNT,BMP as control). n.d; not determined. qPCR data were kindly provided by Celine Souilhol. Data sourced/modified from Gogolou et al. (2022).

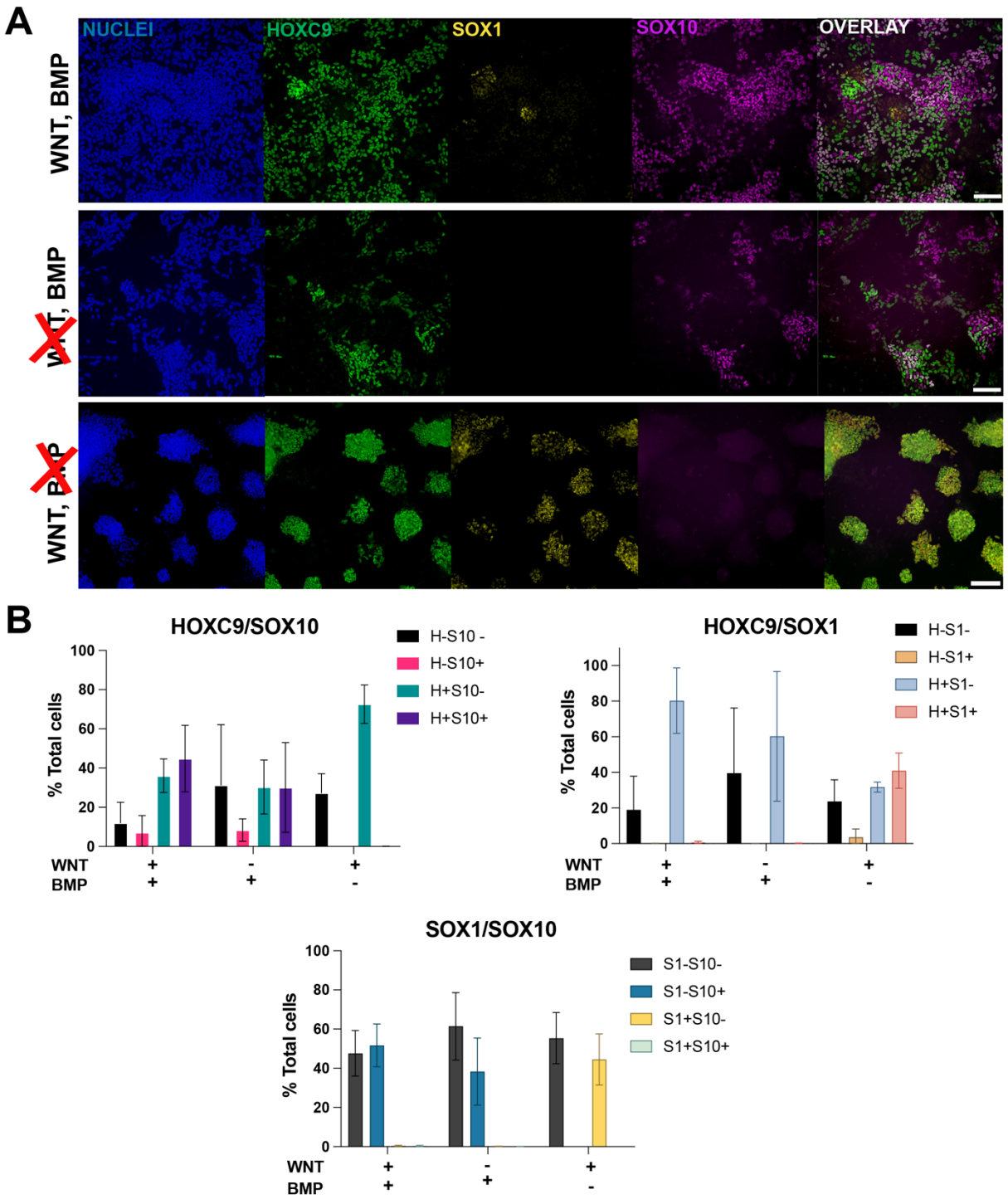

Figure 5.6. Effect of WNT and BMP signalling inhibition on trunk neural crest specification. Immunofluorescence analysis (A) and quantification (B) of the expression of HOXC9, SOX1 and SOX10 in NMP-derived NC cells generated following WNT or BMP signalling pathway perturbation. Data in the graphs were acquired after scoring 30 random fields per condition per experiment and demonstrate the mean of mean values ± SD (n=3 independent experiments). Scale bars=100 μm. H, HOXC9; S10, SOX10; S1, SOX1. Data sourced/modified from Gogolou et al. (2022).

In addition to Wnt and BMP, FGF signalling is reported to play a key role in the induction of NC and coordination of axial identity (Cooper and Tsakiridis 2022a; Gomez et al. 2019b; Hackland et al. 2019; Leung et al. 2016). hPSC cultures differentiating towards trunk NC are considered to have endogenous FGF activity (Hackland et al. 2019). To examine whether inhibition of FGF affects the ability of NMPs to generate trunk NC, I supressed endogenous FGF signalling during the transition of NMPs to posterior NC cells, using the inhibitor PD03 (1μM) (Figure 5.7A). Expression of the FGF target gene *SPRY4* was detected in day 8 Wnt/BMP-treated controls, albeit at lower levels compare to ESCs (Ct 29.5 in D8 vs Ct 26 in ESCs), demonstrating the presence of intrinsic FGF signalling in differentiating trunk NC cultures and in contrast, this was found to be extinct in PD03-treated cultures, verifying the efficacy of the inhibitor treatment (Figure 5.7B). Gene expression analysis revealed that FGF inhibition did not impede the expression of *PAX3* (Figure 5.7C) *a*nd *SOX10* at the transcript (Figure 5.7C) and protein levels (Figure 5.7F-G), in agreement with previous findings (Gomez et al. 2019b; Hackland et al. 2019) and had no effect in *SOX1* expression relative to controls (Figure 5.7C, 5.7F-G). Similarly, *OTX2* and *ETS1* low expression remained unaffected in cultures with attenuated FGF, while a trend towards a decline in *CDX2* expression (2/3 biological repeats) was observed in PD03-treated cultures compared to controls (Figure 5.7D).

Analysis of *HOX* gene transcripts in cultures treated with PD03 showed a slight, although variable between replicates, decrease in their expression and this decline was statistically significant predominantly in *HOX* genes indicative of cervical (*HOX 3-5*) and thoracic (*HOX 6-9*) character (Figure 5.7E). Interestingly, I found that the total number of HOXC9-expressing cells showed a sharp decrease in cultures upon FGF inhibition (the percentage of HOXC9+ cells declined from 80 to 27%, $P < 0.05$ paired t-test; Figure 5.7F-G) and this led to a dramatic reduction in the fraction of cells co-expressing HOXC9/SOX10 (the percentage of HOXC9+/SOX10+ cells declined from 45 to 8%, $P < 0.05$ paired t-test; Figure 5.7F-G), marking a trunk NC entity.

Taken together, these data demonstrate that the activation of *HOX* gene code in hPSC-derived NMPs and that early patterning of a posterior axial identity in NMP-derived NC cells primarily depends on Wnt signalling. They also indicate that as the NMPs differentiate along the NC route, the expression of HOX genes progressively becomes less dependent on Wnt and propose the existence of alternative signalling mechanisms that might modulate *HOX* gene expression, such as FGF signalling through interaction with CDX transcription factors (Amin et al. 2016b) .

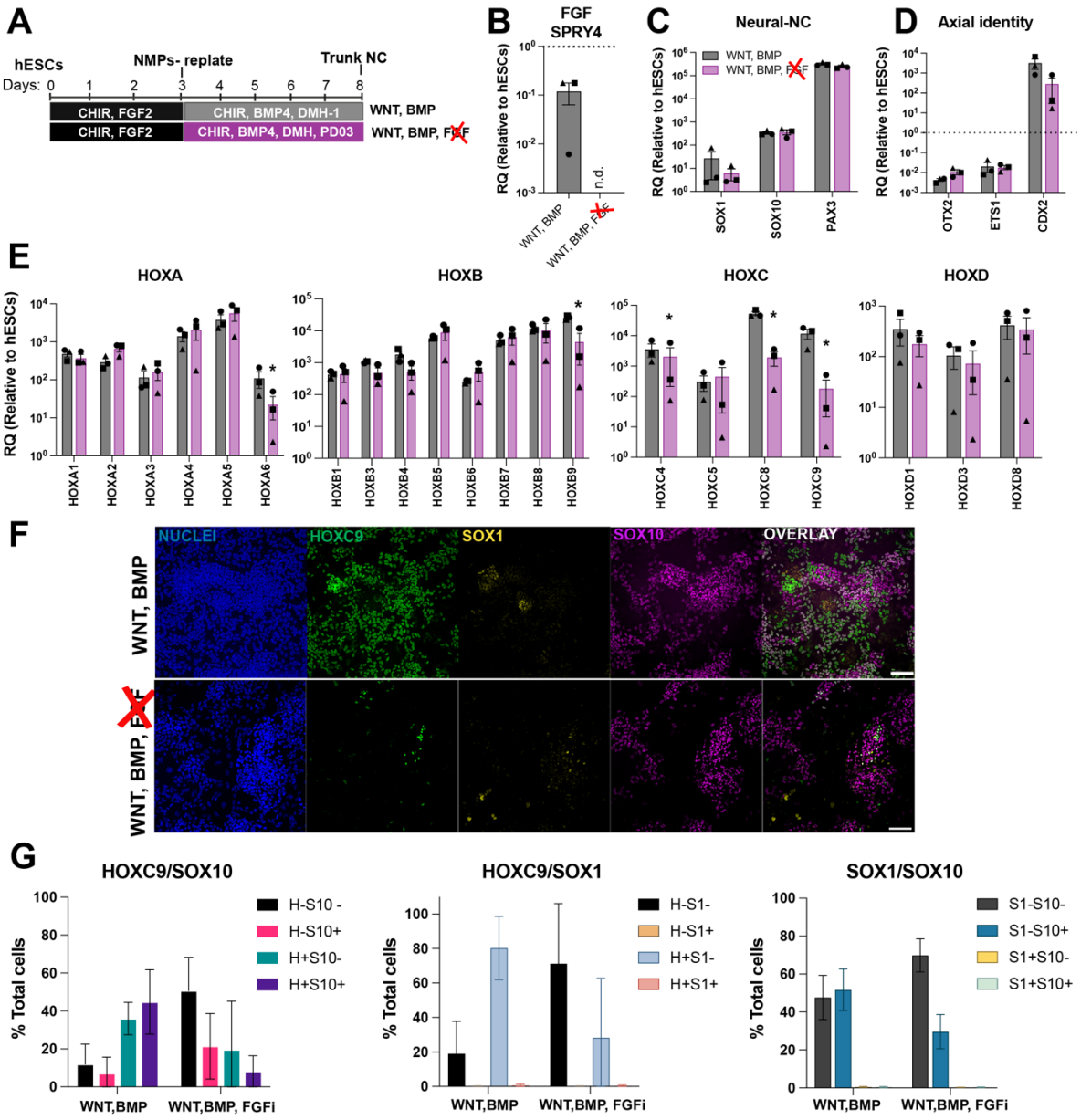

Figure 5.7. Inhibition of FGF signalling impairs the expression of thoracic *HOX* genes in neuromesodermal progenitor-derived trunk neural crest cells. (A) Schematic showing agonists/antagonists treatments. (B-D) RT-qPCR analysis of indicated FGF (B), neural-NC (C) and axial identity (D) markers in NMP-derived NC generated in the presence/absence of FGF inhibition. (E) RT-qPCR analysis of indicated *HOX* genes in NMP-derived NC generated in the presence/absence of FGF inhibition. Data in all graphs state the mean of mean values ± SEM, n=3 independent experiments with three technical replicates in each experiment. Each independent experiment is represented by a unique shape. Only statistically significant changes are indicated. **P* <0.05, (ratio paired t-test). n.d.; not determined. (F-G) Immunofluorescence analysis (F) and quantification (G) of the expression of HOXC9, SOX1 and SOX10 in NMP-derived NC cells generated in control conditions and following FGF signalling pathway perturbation. Data in the graphs were acquired after scoring 30 random fields per condition per experiment and state the mean of mean values ± SD (n=3 independent experiments). Scale bars=100 µm. H, HOXC9; S10, SOX10; S1, SOX1.

5.5. TBXT regulates the acquisition of posterior axial identity by neuromesodermal progenitor-derived neural crest cells

5.5.1. TBXT knockdown impairs neuromesodermal progenitor formation

In section 5.4.1, I showed that the failure of NMPs to induce *HOX* genes in the absence primarily of Wnt was accompanied by a downregulation of the *TBXT*, a core axial progenitor transcriptional regulator (Henrique et al. 2015; Tsakiridis et al. 2014). Previous linage tracing studies have demonstrated that T/Brachyury-expressing neuromesodermal-potent axial progenitor cells contribute to trunk NC within the developing mouse embryo (Mugele et al. 2018; Shaker et al. 2021), however, the role of *TBXT* in the induction of posterior NC has not been examined. In order to understand the function of TBXT in NC specification of hPSC-derived NMPs, I set out to determine the effects of attenuating TBXT during the differentiation of hESCs towards NMPs and subsequently to trunk NC cells. For these experiments, I used a hES cell line containing a tetracycline (Tet)-inducible TBXT shRNA cassette to knockdown the expression of *TBXT* (Bertero et al. 2016). First, I carried out the NMP differentiation in combination with Tet treatment (Figure 5.8A) to deplete the expression of *TBXT* at the NMP stage. A reduction in *TBXT* transcripts in the presence of Tet was confirmed by transcriptome analysis (RNA-seq) (Figure 5.8D) and this was accompanied by a profound decrease at the protein level (protein intensity) compared to untreated controls (Figure 5.8B). As negative control, a hES cell line exhibiting Tet-inducible shRNA targeting the gene *B2M* (Bertero et al. 2016) was utilised and differentiated in a similar manner to TBXT shRNA hESCs. Immunofluorescence analysis and quantification of TBXT expression in D3 NMPs generated from B2M shRNA control cell line upon Tet treatment showed no reduction in TBXT protein, validating the specificity of the method (Figure 5.8C).

To investigate the effect of TBXT depletion during the transition of hESCs towards NMPs, D3 NMPs differentiated in the presence/absence of Tet were harvested for RNA-seq. Analysis of differentially expressed genes showed that 346 and 293 genes were significantly up- and down-regulated, respectively, in TBXT depleted cells compared to untreated controls (padj<0.05, Wald test; log2FC>|0.5|). Gene ontology (GO) biological processes enrichment analysis revealed that the gene families affected were predominantly implicated in A-P patterning, regionalisation and axial specification (Figure 5.8E). Notably, amongst the downregulated genes were genes encoding presomitic mesoderm transcription factors (*MSGN1*, *TBX6*, *FOXC1/2*), FGF (*FGF3/8/17* and *DUSP7*), Wnt (*RSPO3*, *WISP1, WNT5A/B*, *WNT8A*, *LEF1*) and Notch (*HES7, DLL1, DLL3*) signalling pathway components (Figure 5.8F), which have been previously shown to be present in NMPs and their mesodermal derivatives (Gouti et al. 2017; Guillot et al. 2021;

Wymeersch et al. 2019). In contrast, genes associated with anterior visceral endoderm (AVE)/endoderm, anterior neurectoderm, and pluripotency/early post-implantation epiblast were significantly upregulated (*SOX17, LEFTY1/2, OTX2, CER1, HHEX, NANOG, and GDF3*) (Figure 5.8F), further demonstrating an inability of hPSCs to differentiate towards NMPs and their derivatives, presomitic mesoderm progenitor cells.

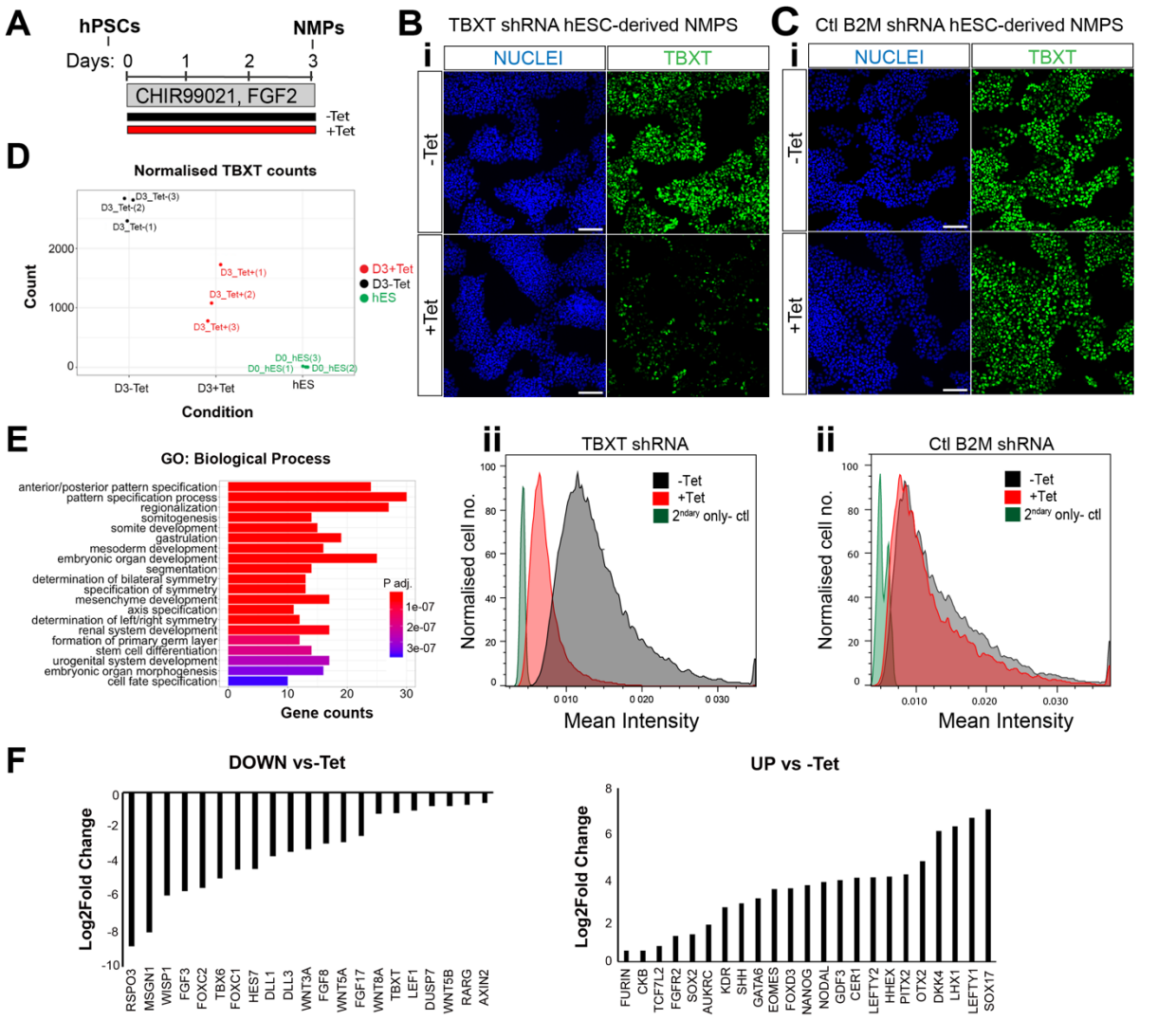

Figure 5.8. TBXT depletion impairs the formation of hPSC-derived neuromesodermal progenitors. (A) Schematic showing tetracycline treatment during NMP differentiation to induce TBXT knockdown. (B) Immunofluorescence analysis of the expression of TBXT protein in TBXT shRNA hESC-derived NMPs in the presence/absence of tetracycline (i) and mean fluorescence intensity of TBXT protein in Tet-treated and control NMP cultures (ii). A representative histogram derived from one biological replicate is shown. (C) Immunofluorescence analysis of the expression of TBXT protein in control B2M shRNA hESC-derived NMPs in the presence/absence of tetracycline (i) and mean fluorescence intensity of TBXT protein in Tet-treated and untreated NMP cultures (ii). A representative histogram derived from one biological replicate is shown. (D) Normalised expression values of TBXT transcripts in control, Tet-treated NMPs and undifferentiated hES cell samples following RNA sequencing (RNA-seq) analysis. Numbers in brackets indicate biological replicates (n=3). (E) Gene ontology (GO) term enrichment analysis for differentially expressed genes in hESC-derived NMPs following TBXT knockdown. (F) Representative significantly

downregulated and upregulated transcripts following TBXT depletion. Scale bars= 100 μm. Data sourced/modified from Gogolou et al. (2022).

I next asked whether TBXT depletion between D0-D3 affected the expression of *HOX* genes and assayed gene expression by performing RT-qPCR (Figure 5.9A). Strikingly, analysis of the *HOX* profile in D3 Tet-treated TBXT shRNA NMPs showed a statistically significant reduction in most *HOX* genes examined, indicative of various axial levels (Figure 5.9B). On the contrary, analysis of the isogenic control B2M shRNA revealed no significant changes in *HOX* gene transcripts following Tet-mediated inducible knockdown (Figure 5.9C), excluding the possibility that the observed results could be due to off target effects of Tet treatment.

Collectively, these findings demonstrate a crucial role of *TBXT* in inducing an NMP transcriptional profile and indicate that TBXT is required for early *HOX* gene activation and A-P patterning, as hPSCs in the absence of TBXT, adopt an identity that resembles the anterior epiblast, despite the constant presence of Wnt and FGF posteriorizing signals.

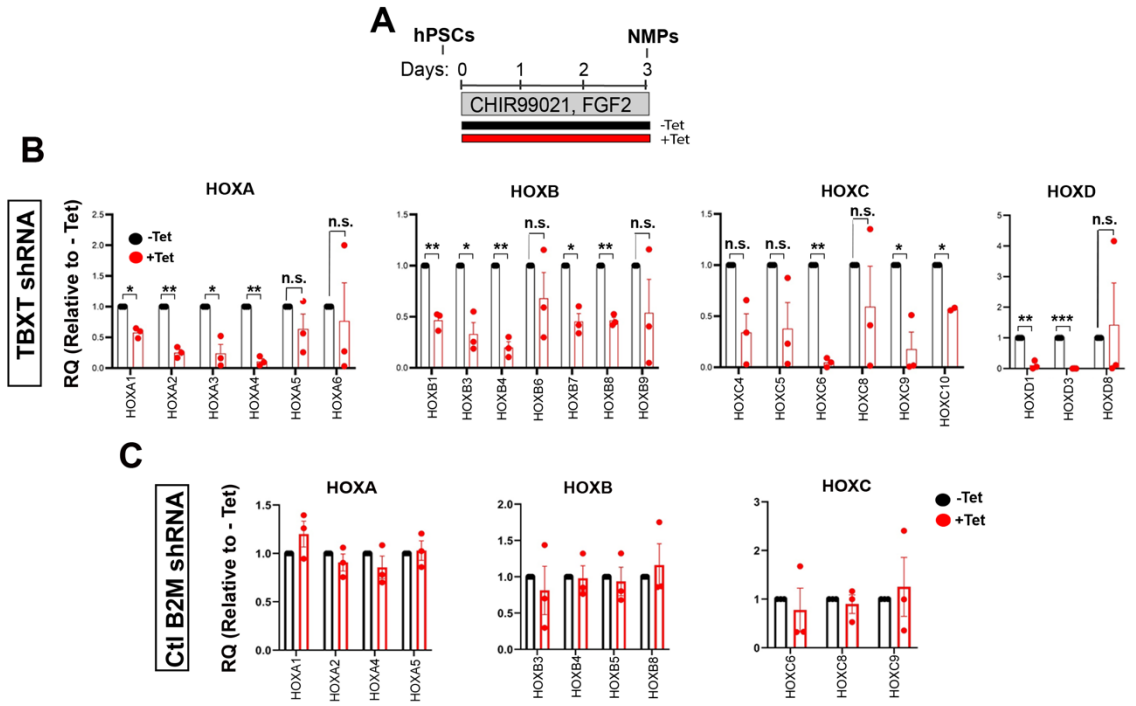

Figure 5.9. Effect of TBXT reduction in the axial identity of neuromesodermal progenitors. (A) Schematic showing NMP differentiation/tetracycline treatment. (B) RT-qPCR analysis of indicated *HOX* genes in TBXT shRNA hESC-derived NMPs in the presence/absence of tetracycline. Data shown are the mean of mean values, n=3 independent experiments with three replicates in each experiment. Error bars indicate SD; **P* <0.05, ***P* <0.005, ****P* <0.0005 (paired t-test). n.s. not significant. (C) RT-qPCR analysis of indicated *HOX* genes in control B2M shRNA hESC-derived NMPs in the presence/absence of tetracycline. Data shown are the mean of mean values, n=3 independent experiments with three replicates in each experiment. Error bars indicate SD. No statistically significant changes were observed. Data sourced/modified from Gogolou et al. (2022).

5.5.2. TBXT knockdown hinders the posterior regionalisation of trunk neural crest

Next, I interrogated the influence of TBXT depletion in trunk NC specification. To investigate this, trunk NC cells were generated under the continuous presence/absence of Tet treatment for Tet-mediated TBXT knockdown from the beginning of the differentiation (Figure 5.10A) and assessed for the expression of a panel of *HOX* genes. Gene expression analysis at day 8 showed a dramatic decrease in *HOX* gene family members in Tet-treated cultures compared to untreated controls (Figure 5.10B), in like manner TBXT knockdown affected *HOX* gene expression in D3 differentiating NMPs, as described above (Figure 5.9B). Additionally, HOXC9 protein levels were found to be severely reduced in the presence of Tet (~50% reduction relative to -Tet, P <0.05; Figure 5.10C). Given the global downregulation observed in *HOX* gene transcripts, expression of the anterior NC markers *OTX2*, *ETS1* was also examined. The analysis showed a slight although not statistically significant increase in the expression of the aforementioned genes (Figure 5.10D).

On the contrary, TBXT depletion resulted in a modest decrease in the transcript levels of *PAX3* and *SOX10* (Figure 5.10D) but this decline was not evident at the SOX10 protein levels (Figure 5.10E). Additionally, no effect in the presence of Tet was observed in *SOX9* mRNA levels (Figure 5.10D). Analysis of neural progenitor genes showed a trend towards an increase in the transcript levels of *SOX1*, while expression of *SOX2* remained unaffected (Figure 5.10D). Quantification of SOX1+ cells (Figure 5.10F-G) showed no significant increase (paired t-test) in the number of SOX1-expressing cells in Tet-treated trunk NC cultures, ruling out the possibility that TBXT depletion promoted a switch towards CNS neuroectoderm.

The transcriptional profile of NMP-derived NC cells following TBXT knockdown and particularly the loss in *HOX* gene expression shared similarities with the gene expression profile observed in trunk NC cells following Wnt inhibition (Figure 5.5). In addition to this, TBXT knockdown resulted in a downregulation in Wnt-signalling components at D3 (Figure 5.8F), supporting the notion that TBXT and Wnt signalling might be linked. To explore this in the context of trunk NC, D8 Tet-treated cultures were assessed for the expression of Wnt target genes (*TCF1*, *LEF1*). TBXT depletion resulted in a significant reduction in all Wnt-associated transcripts examined (Figure 5.10D). Thus, this together with our previous observations indicate the existence of TBXT-Wnt bilateral communication which determines the adoption of a posterior axial signature in hPSC-derived NMPs and their trunk NC derivatives.

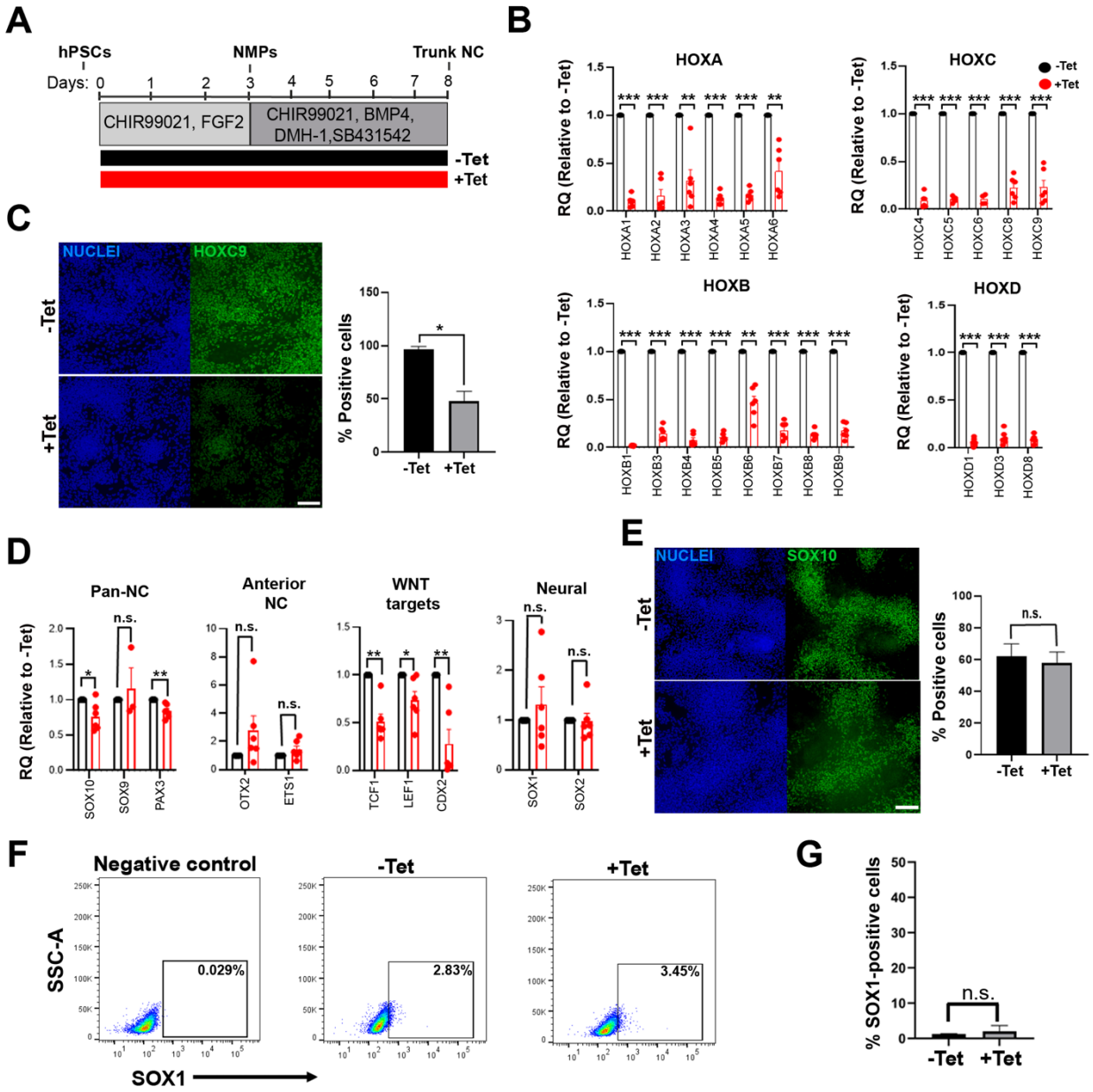

Figure 5.10. Effect of TBXT knockdown in trunk neural crest. (A) Diagram showing culture conditions and Tet treatment during the derivation of trunk NC. (B) RT-qPCR analysis of indicated *HOX* genes in the presence/absence of Tet. Data shown are the mean of mean values, n=4-6 independent experiments with three replicates in each experiment. Error bars indicate SD. **P* <0.05, ***P* <0.005, ****P* <0.0005 (paired t-test). (C) Immunofluorescence analysis and quantification of the expression of HOXC9 in Tet-treated and untreated NMP-derived NC cells. Data state the mean of mean values from 3 independent experiments and error bars indicate SD. **P* <0.05 (paired t-test). Scale bar=100 µm. (D) RT-qPCR analysis of indicated markers in Tet-treated and untreated NMP-derived NC cells. Data denote the mean of mean values, n=6 independent experiments with three replicates in each experiment. Error bars indicate SD; **P* <0.05, ***P* <0.01, n.s. not significant (paired t-test). (E) Immunofluorescence analysis and quantification of the expression of SOX10 protein in Tet-treated and untreated NMP-derived NC cells. Data state the mean of mean values from 3 independent experiments and error bars indicate SD. n.s. not significant (paired t-test). Scale bar=100 µm. (F) Representative flow cytometry analysis plots (n=3) showing the number of SOX1-positive cells in D8 trunk NC following TBXT knockdown (+Tet) and in control (-Tet) cultures. (G) Quantification of the number of SOX1-positive cells assed by immunocytochemistry in D8 trunk NC following TBXT knockdown (+Tet) and in control (-Tet) cultures. Data shown are the mean of mean values from 3 independent experiments and error bars indicate SD. n.s. not significant (paired t-test). Data in A-E panels were obtained by Celine Souilhol. Data sourced/modified from Gogolou et al. (2022).

5.5.3. TBXT establishes a posterior neural crest axial identity early and within uncommitted progenitors

My data so far demonstrate that TBXT regulates *HOX* gene expression in NMPs and their trunk NC derivatives. However, it is not clear whether TBXT acts early, during NMP specification from hPSCs to activate *HOX* genes and establish a posterior identity or at a later stage during differentiation of NMPs toward trunk NC. To clarify the temporal role of TBXT in controlling HOX gene expression dynamics, I set out to attenuate TBXT at distinct time windows during the differentiation of NMPs by introducing Tet in the culture regime at different time points as described in Figure 5.11A. I cultured D3 NMPs in the presence of basal, serum-free and deprived of extrinsic instructive signals media to eliminate their potential influence and assessed gene expression (Figure 5.11A). A previous study has shown that these conditions promote the production of early posterior neural progenitors from hPSC-derived NMPs (Gouti et al. 2014). I found that hPSC-derived NMPs cultured in basal media gave rise to mutually exclusive subpopulations (note the lack of SOX1/SOX10-double positive cells in Figure 5.12B-C) of pre-neural spinal cord progenitors (~15% SOX1+) and NC cells (~25% SOX10+), while a negligible fraction was found to be positive for TBXT+ (~0.27%) (Figure 5.12). Tet treatment at an early (D0-D3) and at a later stage (D3-D7) reduced *TBXT* transcripts, while only early Tet-administration was found to cause a reduction in *CDX2* (Figure 5.11B), suggesting that control of CDX2 via TBXT occurs early and other mechanisms that maintain its expression irrespective of TBXT might exist at a later stage of the differentiation. This is also supported by the findings in 5.4.2, which revealed changes in *CDX2* mRNA levels following Wnt/BMP/FGF signal perturbation.

Furthermore, Tet treatment in all cases did not have an effect on the transcript levels of the early and later neural progenitor marker *SOX2* and *SOX1,* respectively (Figure 5.11B). Nevertheless, Tet administration from D0 resulted in a modest but significant reduction in the percentage of cells co-expressing SOX1/HOXC9, denoting a posterior spinal cord progenitor population (the percentage of SOX1+/HOXC9+ cells dropped from 10 to ~1% in +- and ++ conditions, P <0.05, one-way ANOVA Dunnett's post hoc test relative to -- control) (compare orange bars in the middle graph in Figure 5.12C). Similarly, a slight reduction in *SOX10* transcripts (Figure 5.11B) and a more dramatic decline in the number of SOX10+/HOXC9+ NMP-derived trunk NC cells was observed in cultures grown in the continuous presence of Tet or under Tet treatment during D0-D3 time window (the percentage of SOX10+/HOXC9+ cells dropped from ~20 to ~1% in ++ and ~2 in +- conditions, P <0.005, one-way ANOVA Dunnett's post hoc test relative to -- control) (compare purple bars in the top graph in Figure 5.12C).

I next examined the temporal effect of TBXT knockdown on *HOX* gene dynamics. Depletion of TBXT during the NMP stage (D0-D3), severely impaired the induction of HOX genes (++ and +- ; Figure 5.11C) and this effect persisted even when Tet was withdrawn from the culture regime (+- ; Figure 5.11C). On the contrary, TBXT depletion at a later stage following Tet treatment from D3-D7 had minimal impact on the expression of most HOX genes (-+ ; Figure 5.11C). Analysis of HOXC9 at the protein level revealed a statistically significant reduction in the number of HOXC9-expressing cells when TBXT knockdown was induced at early stage (the percentage of HOXC9+ cells declined from 70 to 6% with Tet added from D0-D7, P <0.005 paired t-test; from 70 to 10% with Tet added from D0-D3 P <0.05 paired t-test; Figure 5.12C), whereas TBXT knockdown at a late stage had no effect on the total number of HOXC9+ cells (the percentage of HOXC9+ cells declined from 70 to 63% with Tet added from D3-D7, paired t-test; Figure 5.12C), results that mirror the changes observed at transcript level.

Altogether, these findings further confirm that TBXT controls a posterior regional signature via regulation of *HOX* genes in NMPs and their immediate derivatives, spinal cord progenitors and NC cells, and furthermore demonstrate that it exerts its effect on A-P regionalisation early, during the transition of hPSC to NMPs. They also indicate that TBXT determines the acquisition of a NC and early spinal cord progenitor fate in the absence of exogenous instructive signals.

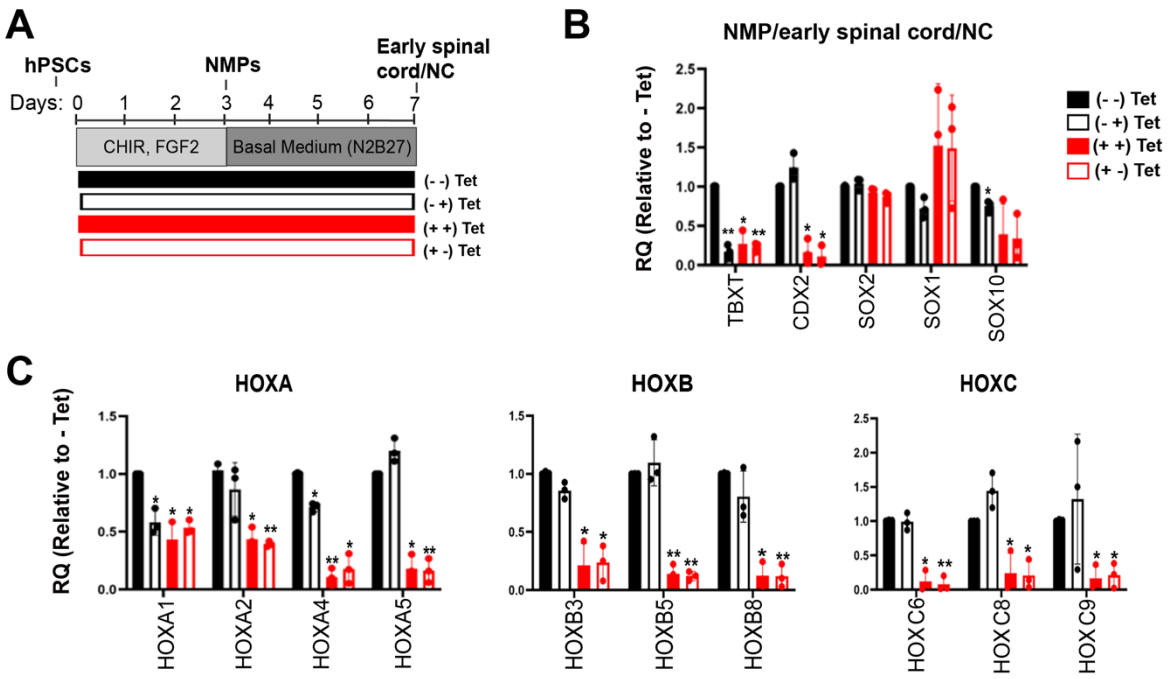

Figure 5.11. TBXT determines the posterior axial identity of neuromesodermal progenitor-derivatives at early stages of the differentiation. (A) Diagram depicting the different time windows that Tet-mediated TBXT knockdown was induced in shRNA hESC-derived NMPs generated upon CHIR, FGF2 treatment and cultured in basal media until day 7 of the differentiation. (B-C) RT-qPCR analysis of indicated NMP, early spinal cord, NC markers (B) and *HOX*

genes (C) in NMP-derived cultures following the different treatments depicted in A. Data shown are the mean of mean values ± SD, n=3 independent experiments with three replicates in each experiment. Only statistically significant changes are indicated. *P <0.05, **P <0.005 (paired t-test). Data sourced/modified from Gogolou et al. (2022).

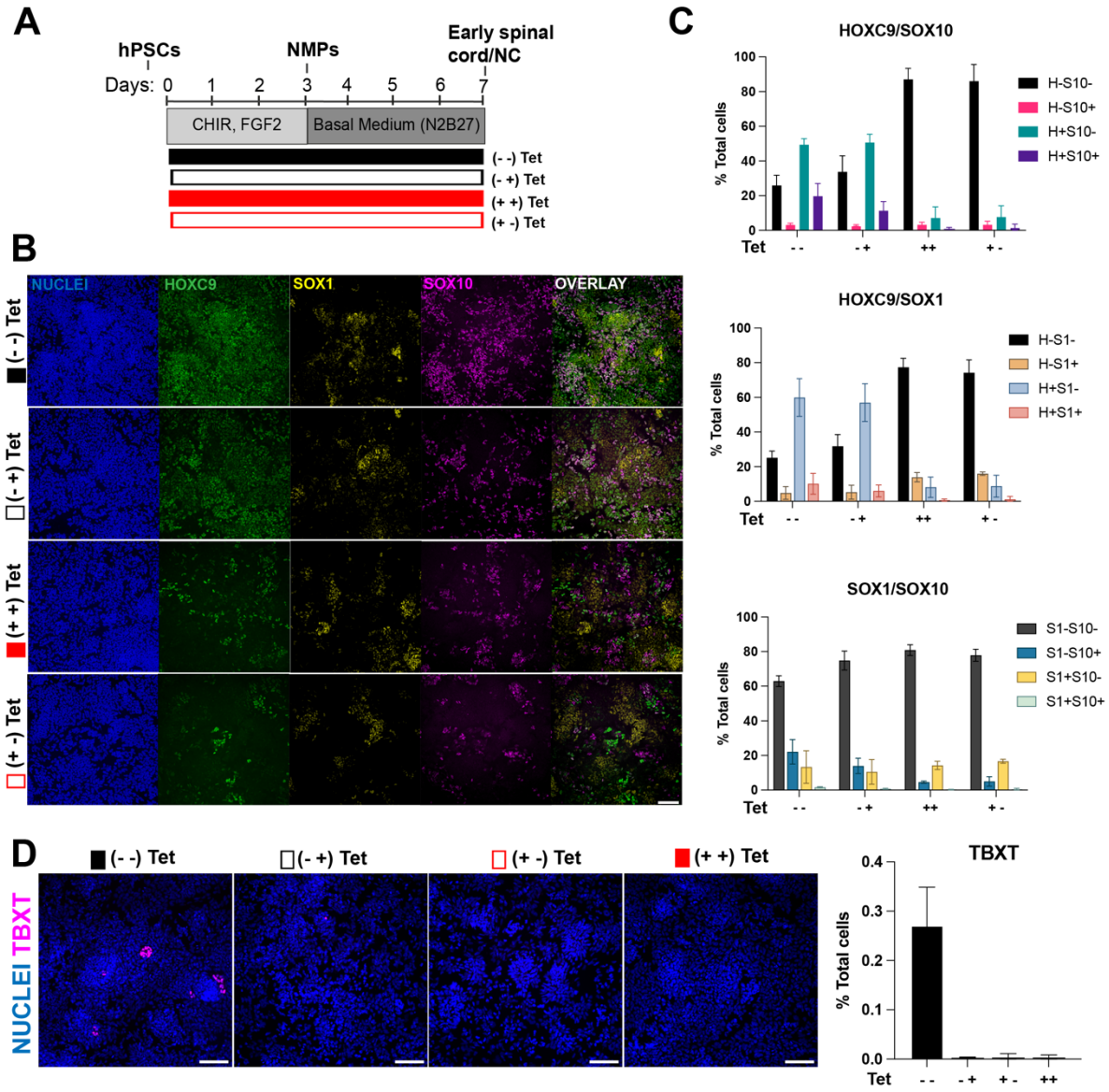

Figure 5.12. TBXT establishes a posterior neural crest axial identity early and within uncommitted progenitors
(A) Diagram depicting the different time points that Tet-mediated TBXT knockdown was induced in shRNA hESC-derived NMPs generated upon CHIR, FGF2 treatment and cultured in basal media until day 7 of the differentiation. (B-C) Immunofluorescence analysis (B) and quantification (C) of the expression of HOXC9, SOX1 and SOX10 proteins in day 7 cultures grown in basal media and following Tet-induced TBXT knockdown at different time windows. Data in the graphs were derived after scoring 25 random fields per experiment per condition and state the mean of mean values from 3 independent experiments. Error bars indicate SD. (D) Immunofluorescence analysis and quantification of TBXT protein expression in day 7 cultures grown in basal media and following Tet-induced TBXT knockdown at different time windows. Data in the graphs were derived after scoring 25 random fields per experiment per condition and state the mean of mean values from 3 independent experiments. Error bars indicate SD. Scale bars= 100 μm. H, HOXC9; S10, SOX10; S1, SOX1. Some data sourced/modified from Gogolou et al. (2022).

5.5.4. TBXT knockdown does not affect the adoption of posterior axial identity by pre-neural spinal cord progenitors in the presence of extrinsic signals

In a previous study we showed that we can also generate early pre-neural progenitors in the presence of Wnt and increased levels of FGF signals (Wind et al. 2021), so next I sought to examine whether TBXT influences *HOX* gene expression under these conditions. To investigate this, I differentiated TBXT shRNA hESCs towards posterior neuroectoderm/pre-neural spinal cord progenitors in the continuous presence/absence of Tet to attenuate the expression of TBXT (Figure 5.13A). Surprisingly, TBXT depletion did not impair the ability of NMPs to differentiate towards their immediate spinal cord descendants, as the levels of NMP/early spinal cord markers (*SOX2*, *CDX2*) in Tet-treated cultures were comparable to untreated controls (Figure 5.13B). Notably, *TBXT* transcript levels in cultures grown in the presence of Tet were similar to their controls (Figure 5.13B), possibly representing a fraction of TBXT+ cells that escaped TBXT knockdown and persisted in D7 early spinal cord progenitor cultures. Interestingly, depletion of TBXT, unlike in D3 NMPs and D8 trunk NC, had no effect on *HOX* gene transcripts, as their expression levels were similar to the untreated controls (Figure 5.13C), suggesting that loss in *HOX* gene expression might be rescued by the exogenous supplementation of high FGF and Wnt.

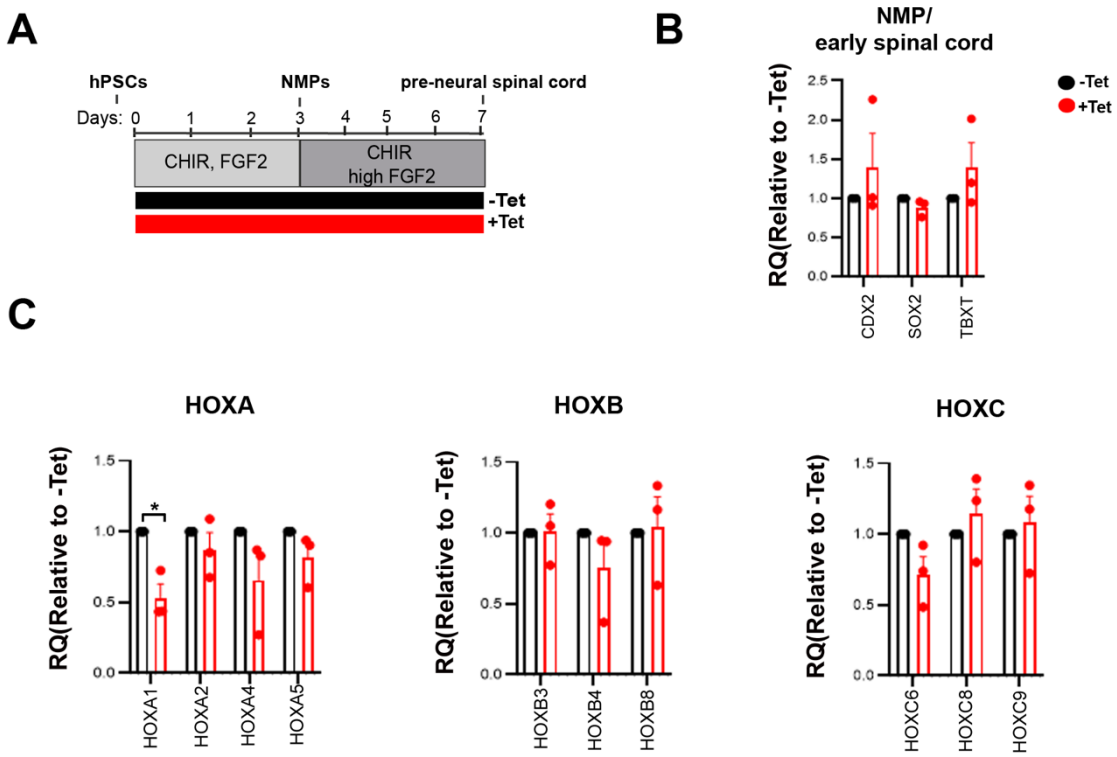

Figure 5.13. TBXT reduction does not affect the acquisition of poster axial identity in pre-neural spinal cord progenitors in the presence of extrinsic signals. (A) Schematic showing culture conditions/tetracycline treatment for the generation of pre-neural spinal cord cells. (B-C) Gene expression analysis of indicated NMP/early spinal cord (B) and Hox (C) genes in day 7 tet-treated and untreated pre-neural spinal cord progenitors. Data shown are the mean of mean values, n=3 independent experiments with three replicates in each experiment. Error bars indicate SD.

Statistically significant changes are indicated. *P <0.05, (paired t-test). Data sourced/modified from Gogolou et al. (2022).

5.5.5. TBXT controls the acquisition of posterior axial identity by influencing chromatin accessibility

Given the key role of TBXT in influencing the positional and cell fate identity in NMPS and trunk NC cells, I next sought to determine its mechanism of action in order to understand whether TBXT activates *HOX* gene family members and stimulates FGF and Wnt signalling pathway components via direct genome binding or regulates their expression indirectly, by influencing the transcription of other signature axial regulators, such as CDX2, located upstream in the transcriptional cascade controlling these genes (Amin et al. 2016b). To identify direct targets of TBXT, I carried out genome-wide binding analysis by performing chromatin immunoprecipitation with parallel sequencing (ChIP-seq; Mikkelsen et al. 2007) using an anti-TBXT antibody in hESC-derived NMPs induced in a 3-day treatment by FGF2 and CHIR and their undifferentiated counterparts (hESCs; control). The analysis identified 24,704 regions that were occupied by TBXT in NMPs (Figure 5.14A), a large fraction of which were located within promoters (~13%), introns (~50%), intergenic and distal intergenic (~38%) regions (Figure 5.14B), reflecting previous findings in the mouse (Beisaw et al. 2018; Tosic et al. 2019). GO analysis of TBXT binding regions around the transcriptional start site (–2000 to +500 bp; 3084 peaks, 2841 genes) demonstrated enrichment of genes involved in processes associated with A-P and pattern specification, regionalisation and embryonic development (Benjamini–Hochberg padj <0.05; Figure 5.14C). Transcription factor motif enrichment analysis revealed that the Brachyury binding consensus sequence together with other T-box binding motifs, such as EOMES and TBX6 (Papaioannou 2014), were among the top enriched motifs in regions bound by TBXT (Figure 5.14D). This is in line with previous observations in the mouse showing that many T-box transcription factor-bound genome regions (e.g. EOMES, TBX6) are also occupied by TBXT (Koch et al. 2017; Tosic et al. 2019). Additionally, our data demonstrated significant enrichment of Wnt signalling cascade components (LEF1, TCF3), CDX factors (CDX2/4) as well as HOX family members motifs (Figure 5.14D), possibly reflecting cooperative binding of these factors and TBXT in human NMPs (Amin et al. 2016b).

I next decided to examine the overlap between TBXT target regions identified by ChIP-seq in NMPs (relative to control hESCs) and differentially expressed genes revealed by RNA-seq in TBXT depleted NMPs (Figure 5.8). I found that ~80% of the downregulated (padj <0.05, log2FC>|1|) and a smaller fraction, ~40% of the upregulated genes contained at least a loci bound by TBXT (Figure 5.14E). Among the TBXT-bound downregulated genes were HOX gene

family members (*HOXA1, HOXA2, HOXB5, HOXC5, HOXD3*), components of the FGF (*FGF9*, *DUSP7*), Wnt (*WNT5B*, *SP8*, *AXIN2*, *WISP1*) and Notch signalling pathway (*DLL3*) as well as genes associated with NMP/presomitic mesoderm (*MSGN1, TBX6, CDX1, FOXF1*) and NC/mesoderm (*MSX1*, *SNAI2*) development (Figure 5.14F; Figure 5.15D-E). These data collectively demonstrate that TBXT predominantly functions as a transcriptional activator of signature NMP/mesoderm specifiers and *HOX* genes in hESC-derived NMPS, in line with previous reports in the mouse (Amin et al. 2016b; Beisaw et al. 2018; Koch et al. 2017).

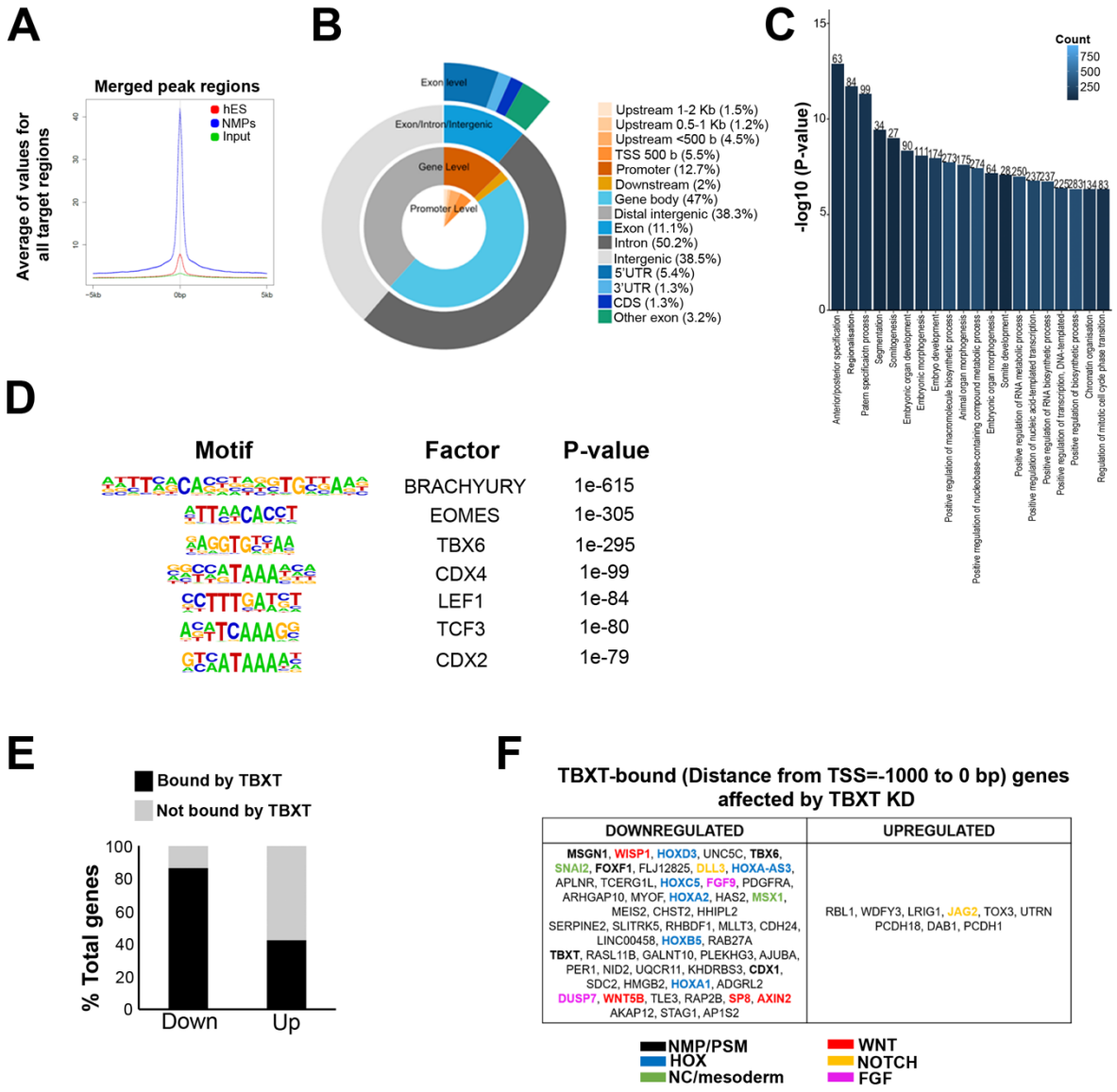

Figure 5.14. TBXT acts as a transcriptional activator of *HOX* genes and Wnt pathway components in hESC-derived neuromesodermal progenitors. (A) Average density plot of tag distributions across peak regions corresponding to the neuromesodermal progenitor (NMP), human embryonic stem cells (hES), and input samples. (B) Genomic distribution of TBXT-bound sites (ChIP-seq). (C) Gene ontology (GO) biological processes enrichment analysis of target genes associated with TXBT binding sites around their transcriptional start site (–2000 to +500 bp), demonstrating overrepresentation of terms associated with A-P patterning. The number of genes within categories is represented as bars and indicated above each bar while P values are indicated on the y axis. (D) Transcription factor-binding motif enrichment in TBXT binding loci. (E) Graph representing the percentage of differentially expressed genes

(padj<0.05, log2FC>|1|) revealed by RNA-seq in hESC-derived NMPs following TBXT depletion that were occupied by TBXT. (F) List of representative down- and up-regulated genes in hESC-derived NMPs following TBXT depletion that are involved in the indicated processes/pathways and are assigned at least a TBXT binding site. Coloured gene names correspond to different groups indicated at the bottom of the table. ChIP-seq analysis was carried out by Active Motif; for more details please refer to Gogolou et al. (2022). Data sourced/modified from Gogolou et al. (2022).

I next investigated the chromatin accessibility profile in TBXT depleted and wild type NMPs by performing assays for transposase-accessible chromatin followed by high-throughput sequencing (ATAC-seq; Buenrostro et al. 2013) to identify putative regulatory regions and active enhancers in differentiated NMPs. Analysis in Tet-treated cultures revealed 4421 and 4027 sites associated with loss and gain of chromatin accessibility, respectively (distance from TSS ranging from –1–1 kb, log2FC cutoff = 2 and p-value<0.05) (Figure 5.15A). Interestingly, the genomic regions characterised by loss of chromatin accessibility were found to be enriched for T-box, CDX and HOX-associated DNA bindings motifs, while sites enriched for POU/OCT, Forkhead and SOX motifs became accessible (annotated using HOMER; Heinz et al. 2010; Benjamini–Hochberg padj<0.05) (Figure 5.15C). Notably, comprehensive analysis of TBXT binding sites aligned with ATAC-seq tracks in Tet-treated and untreated NMPs revealed a loss of “open” chromatin upon Tet administration in loci bound by TBXT (Figure 5.15D,E). Among the genome sites whose chromatin accessibility was reduced were previously identified TBXT targets that were downregulated following TBXT depletion (Figure 5.15B); HOX genes of HOXA (e.g. *HOXA4*), HOXB (e.g. *HOXB4, HOXB5, HOXB8*), HOXC (e.g. *HOXC6*) and HOXD (e.g. *HOXD1, HOXD4, HOXD8*) clusters (Figure 5.15D), Wnt family ligands (e.g. *WNT3A*, *WNT8A;* Figure 5.15Eii) and presomitic mesoderm regulators (e.g. TBX6; Figure 5.15Ei). In contrast, gain of chromatin accessibility in Tet-treated NMPs particularly occurred in genomic regions within/around neural development-associated genes (e.g. SOX3, DLG2; Sanders et al. 2022; Wood and Episkopou 1999) and these sites most importantly, were not occupied by TBXT (Figure 5.15F). Additionally, there was no evident correlation in chromatin changes and upregulated transcripts following TBXT knockdown (Figure 5.15B).

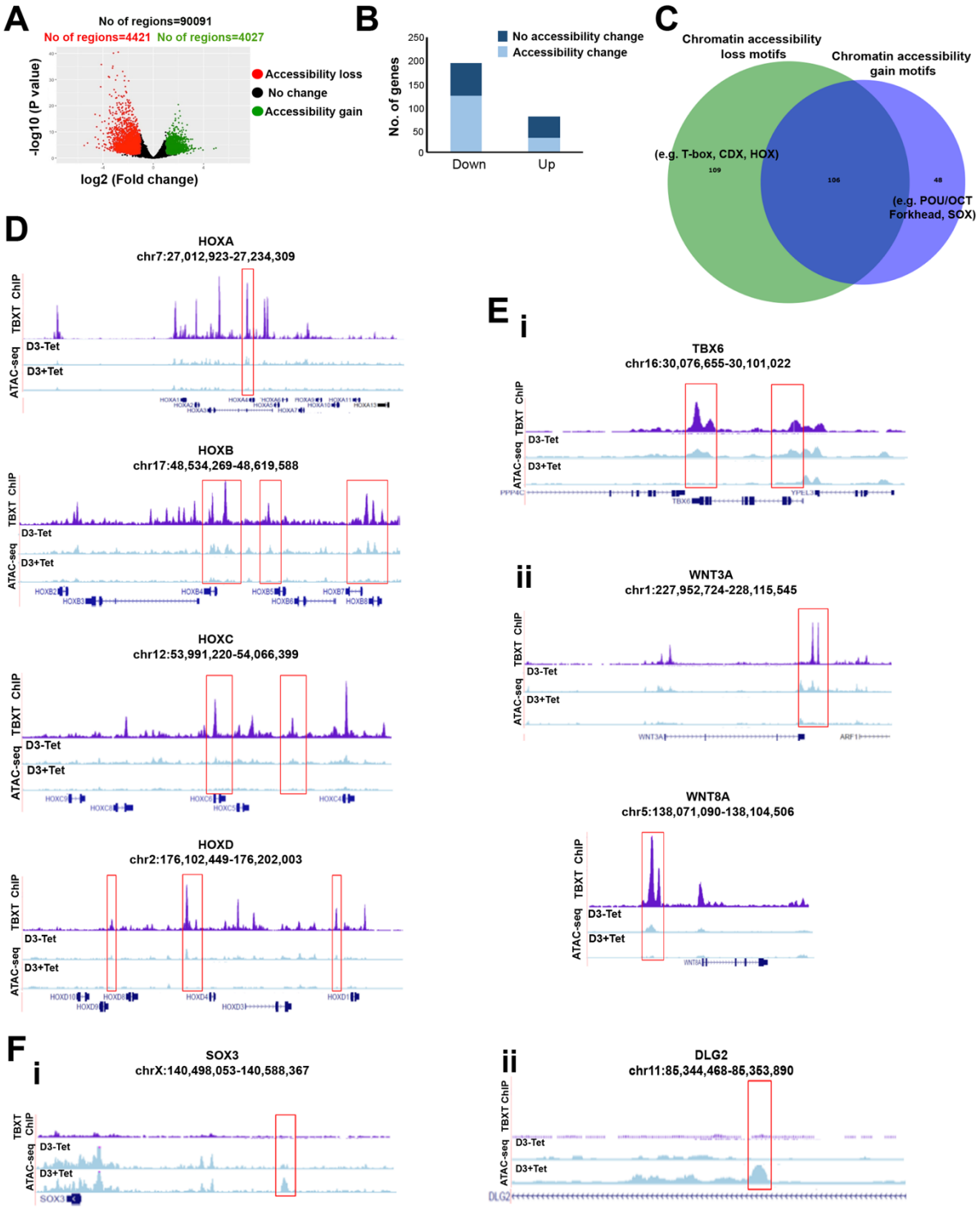

Figure 5.15. TBXT regulates the expression of *HOX* genes and Wnt pathway members in hESC-derived neuromesodermal progenitors by inducing an "open" chromatin landscape. (A) Volcano plot demonstrating the statistically significant number of regions associated with loss (red) and gain (green) of chromatin accessibility from ATAC-seq in D3 Tet-treated and untreated NMPs. (B) Graph representing the number of differentially expressed genes revealed by RNA-seq in hESC-derived NMPs following TBXT depletion in relation to changes in chromatin accessibility. (C) Overlap of top enriched transcription factor binding motifs in genomic loci associated with loss and gain of chromatin accessibility following TBXT knockdown. (D) ChiP-seq and ATAC-seq tracks in D3 NMPs in the presence and absence of Tet for the indicated *HOX* loci. (E) ChiP-seq and ATAC-seq tracks in D3 NMPs in the presence and absence of Tet for *TBX6* (i) and Wnt-associated (ii) loci. (F) ChiP-seq and ATAC-seq tracks in D3 NMPs in the presence and absence of Tet in loci associated with neural-development; SOX3 (i) and DLG2 (ii). Boxed areas

in all panels highlight TBXT-occupied regions marked by loss or gain of chromatin accessibility in the presence of Tet. D3 sample preparation was carried out by Celine Souilhol. ATAC-seq analysis was carried out by the Medical Epigenomics Lab in the research centre for molecular medicine of the Austrian Academy of Sciences; for more details please refer to (Gogolou et al. 2022). Data sourced/modified from Gogolou et al. (2022).

I next interrogated whether TBXT influences the chromatin landscape in addition to NMPs, at a later stage, in their trunk NC derivatives generated under the presence/absence of Tet (D0-D8 Tet treatment). ATAC-seq in combination with ChIP-seq profiling in D8 NC demonstrated that Tet-treatment resulted in loss of "open" chromatin similar to D3, in loci bound by TBXT and associated with reduced transcription following TBXT depletion (e.g. *HOX* family members, *CDX2*, Wnt and BMP pathway components) (Figure 5.16). Some affected components of these pathways, such as *WNT1* and *BMP7*, have been shown to play a crucial role in trunk NC specification and delamination (Burstyn-Cohen et al. 2004; Nguyen et al. 2000). Interestingly, comparison of D3 and D8 peaks revealed an overlap in TBXT-dependent chromatin changes, particularly associated with loss of chromatin accessibility, in *HOX* gene clusters, suggesting that TBXT regulates the chromatin accessibility and transcription of these sites at an earlier and later stage (Figure 5.16A-B). Notably, this analysis uncovered several trunk NC-specific genomic regions with reduced chromatin accessibility following Tet treatment within *CDX2, BMP7* and *HOX* gene clusters (marked with red asterisks; Figure 5.16 A,B,D) that were not bound directly by TBXT at D3 NMPs. This finding suggests a potential indirect role of TBXT in shaping the chromatin landscape indirectly possibly via recruiting alternative chromatin regulators or other NC fate specifiers in the indicated genomic regions, during the TBXT-positive stage of the early transition from NMPs to trunk NC.

In conclusion, TBXT functions as a transcriptional activator of *HOX* genes and other axial regulators including components of the Wnt signalling cascade by binding to enhancers and genomic elements and promoting an "open" chromatin landscape. Depletion of TBXT is linked to loss of chromatin accessibility within regions associated with A-P regionalisation and mesoderm specification, thereby leading to reduced gene expression. Moreover, TBXT controls the acquisition of a NC identity either directly via binding to genes important for NC development and delamination (e.g. *MSX1*, *SNAI2)* or indirectly by influencing chromatin organisation and accessibility in NC signalling specifiers such as BMP7 and WNT1.

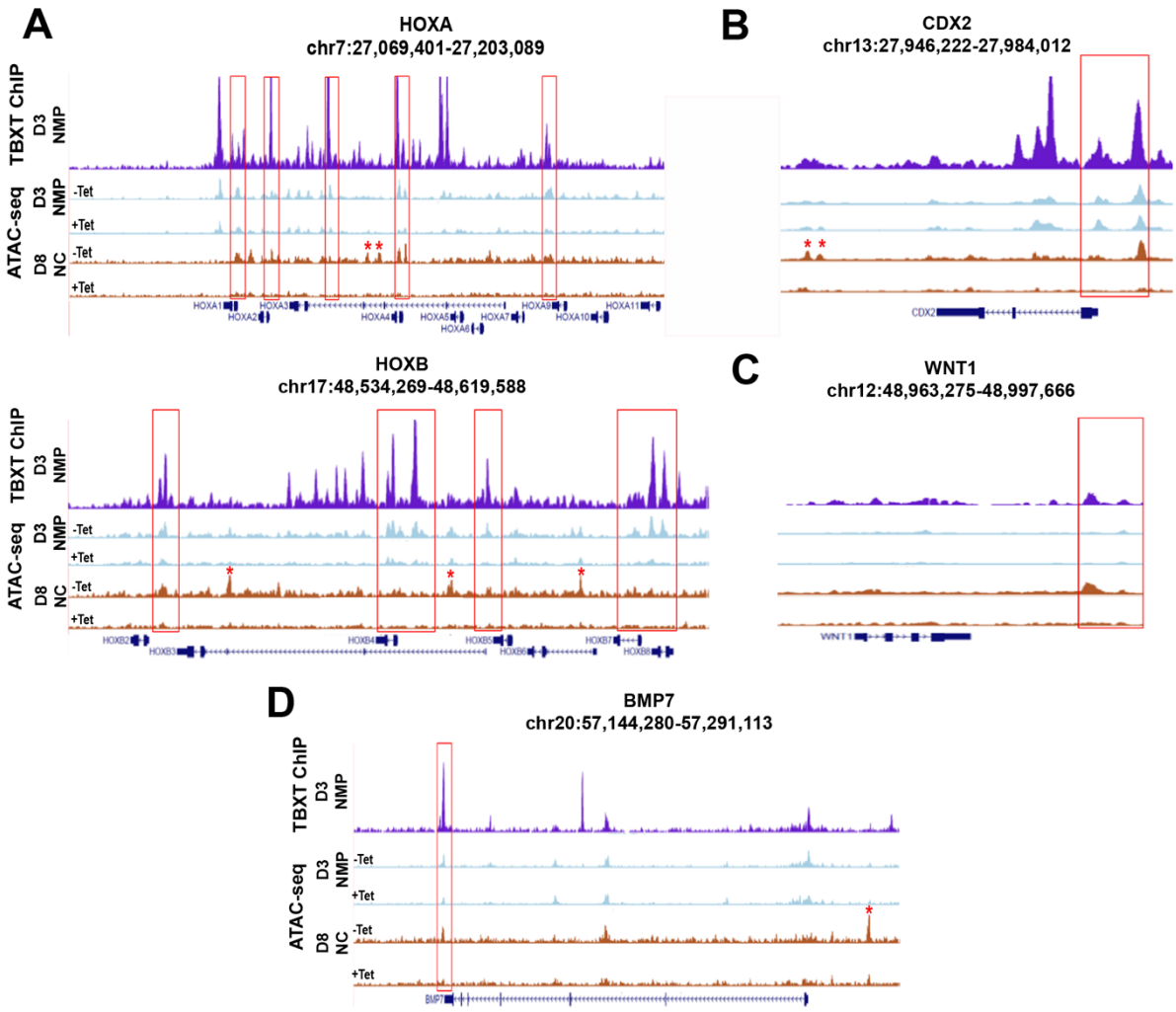

Figure 5.16. Chromatin accessibility dynamics during neuromesodermal progenitor differentiation towards trunk neural crest. ChiP-seq and ATAC-seq tracks in D3 NMPs and D8 trunk NC cells in the presence and absence of Tet for the indicated *HOX* (A), CDX2 (B), Wnt- (C) and BMP- (D) associated loci. Boxed areas highlight TBXT-occupied regions marked by loss of chromatin accessibility in the presence of Tet. Asterisks mark trunk NC-specific regulatory elements that are not bound by TBXT at D3 but exhibit loss of chromatin accessibility at day 8 upon Tet treatment. ATAC-seq analysis was carried out by the Medical Epigenomics Lab in the research centre for molecular medicine of the Austrian Academy of Sciences; for more details please refer to (Gogolou et al. 2022). Data sourced/modified from Gogolou et al. (2022).

5.6. Discussion

5.6.1. Examining the effect of Wnt, FGF, BMP and RA signals on neuromesodermal progenitor and trunk neural crest differentiation

In this chapter, I explored the effect of different established caudalising signals (Wymeersch et al. 2021), in NMP and trunk NC specification *in vitro*. I found that Wnt signalling assigns differentiating cells an early posterior NC/pre-neural spinal cord fate by influencing the expression of axial regulators and *HOX* genes. This predominantly occurs when cells exit the pluripotent state and differentiate to NMPs, as Wnt inhibition during the NC stage did not severely impair the expression of *HOX* genes. On the contrary, suppression of Wnt in NC was accompanied by an increase in the anterior (*OTX2*, *ETS1*) and a decrease in the posterior (*CDX2*) NC markers (Figure 5.5), a finding suggesting a role of Wnt in determining cranial vs trunk NC fate (Gomez et al. 2019b; Hackland et al. 2019). This could possibly occur through negative regulation of anterior genes, as it has been shown in the case of *OtxA* (homolog of human *OTX2*) in *Xenopus* embryo (McGrew et al. 1995) and *Otx2* in the mouse (Satoh et al. 2004), and by promoting the expression of posterior genes such as *CDX2* which could in turn repress a rostral identity (Metzis et al. 2018).

Unlike Wnt, FGF was found to be less important for *HOX* gene activation and axial specification in NMP state and instead, to have a more prominent role in posterior regionalisation and maintenance during trunk NC differentiation. This is supported by the dramatic decrease in the number of HOXC9+/SOX10+ trunk NC cells following FGF inhibition which was also accompanied by a modest, albeit less definite, reduction in some *HOX* gene transcripts, particularly of the ones that correspond to thoracic axial levels. Nevertheless, more biological repeats are highly required to address the role of FGF in controlling *HOX* gene transcription. Additionally, high FGF activity as part of the culture regime was able to rescue the effect of TBXT knockdown on *HOX* genes in pre-neural spinal cord progenitors (Figure 5.13), supporting the role of FGF in mediating *HOX* gene expression. The data provided here are in line with recent reports (Gomez et al. 2019b; Hackland et al. 2019) which demonstrated a loss in the *HOX* gene code in posterior NC following FGF inhibition and suggest a function of FGF in modulating HOX gene expression within the trunk NC compartment without influencing the expression of NC determinants (e.g. SOX10). Since FGF agonists are not part of the NC induction cocktail, we can speculate that endogenous FGF produced by the cells is sufficient to evoke the expression of posterior HOX genes and other axial position markers.

The FGF-dependent regulation of *HOX* gene expression in posterior NMP-derivatives is likely to involve CDX factors such as CDX2 (Bel-Vialar et al. 2002; Mazzoni et al. 2013), which are highly expressed in trunk NC and early spinal cord progenitor cultures and are equally negatively affected by Wnt or FGF suppression. A series of loss/gain of function experiments for CDX2 would further address its role in establishing a posterior axial signature in the context of trunk NC and pre-neural spinal cord progenitors.

One additional signal I examined as a potent trunk NC regulator was BMP4. BMP4 blockade during trunk NC differentiation led to a dramatic loss in SOX10 expression and cells were redirected towards a SOX1+ neuroectodermal fate, a result highlighting a requirement of BMP4 in NC specification (Figure 5.5, 5.6) (Gomez et al. 2019b; Leung et al. 2016). Interestingly, the loss of SOX10 expression in the absence of BMP4 coincided with an increase in *CDX2* and *HOX* gene expression (Figure 5.5), proposing that BMP4 partially restricts *CDX2* and/or *HOX* gene transcripts. This contrasts the findings of Barros et al. (2008) that proposed BMP4 positively regulates CDX2 expression in human gastric carcinoma cell lines and therefore further research is required to address a potential influence of BMP4 in axial specification.

A shift towards a neural fate accompanied by a decrease in *TBXT* expression and upregulation of neural markers was also observed in D3 cultures upon RA treatment (Figure 5.4), in line with the results of a previous report (Gouti et al. 2017). Addition of RA did not severely affect the acquisition of a caudal identity particularly in the presence of Wnt, consistent with the role of RA in *HOX (1-5)* gene activation (Mazzoni et al. 2013), however, resulted in loss of NMP identity. A study published recently by Gouti et al. (2017) suggested an important role of RA signalling in the induction and differentiation of mESC-derived NMPs. According to their model, opposing actions by Wnt and RA signals determine the exit from the pluripotent state and NMPs adopt a mesodermal or neural fate, respectively, based on the levels of each promoting signal. They also propose that low concentration of RA is required for the induction of NMPs, whereas high levels and absence of RA result in neural and mesodermal differentiation, respectively. Our work probably reflects their observations with respect to neural differentiation as our cultures were treated with relatively high levels of RA (100nM RA were used in both studies) and we cannot exclude the possibility that low levels of RA produced endogenously contribute to the induction of NMPs.

5.6.2. TBXT controls A-P regionalisation in neuromesodermal progenitors and their neural crest derivatives by modifying the chromatin architecture

Previous genetic loss of function experiments in combination with genome-wide binding and chromatin accessibility studies in the mouse have demonstrated a role of TBXT in regulating axis elongation and mesoderm specification by direct binding, opening and activating regulatory elements in genes associated with Wnt and FGF signalling pathway and mesoderm development (e.g. *Mesp1*, *Msgn1),* respectively (Amin et al. 2016b; Koch et al. 2017; Tosic et al. 2019). The work included in this chapter supports these observations and expands the role of TBXT in chromatin remodelling and associated axial identity regulation in the human, using a hESC-derived NMP model. It also demonstrates that in addition to WNT/presomitic mesoderm-linked loci, TBXT occupies and activates regulatory elements within all *HOX* gene clusters by introducing an "open" chromatin state, consistent with a previous reported role of TBXT in binding to *HOX* gene genomic regions during hPSC-differentiation (Faial et al. 2015). TBXT functions as transcriptional activator of mesoderm and axial elongation regulators during the transition from pluripotent to NMP-state and depletion of TBXT results in upregulation of genes associated with anterior endoderm, early post-implantation epiblast as well as anterior neuroectoderm, reflecting the acquisition of a transcriptional identity compatible with anterior epiblast. This was further demonstrated by an increase in the chromatin accessibility in genomic regions associated with neural development. The resulted increase in transcriptional activation of neuroectodermal genes following TBXT knockdown is in agreement with previous work from Tosic et al. (2019), which revealed in a series of loss of function experiments during mESC differentiation a crucial role of T/Brachyury in controlling mesoderm specification by actively suppressing the neuroectodermal lineage and promoting a mesoderm identity through chromatin modifications.

On the contrary, our ChIP-seq analysis data diverge from the notion that TBXT directly binds to and represses genes associated with neural development (*SOX3, DLG2*) suggesting that the anti-neural fate role of TBXT may be indirect in human cells. Additionally, our genome-wide binding analysis demonstrated that TBXT binding sites were enriched in Wnt, CDX, HOX and T-box transcription factor binding motifs, suggesting a possible interaction between TBXT and several mesoderm/axial regulators in controlling the expression of common target genes. This hypothesis is also supported by previous studies in mouse NMPs suggesting that cooperative binding between Brachyury and Wnt (β-catenin)(Koch et al. 2017), Cdx (Amin et al. 2016b) and Eomes (Tosic et al. 2019) controls events such as axial elongation, mesoderm formation and pluripotency exit. Therefore we can speculate that additional factors and signals integrate their inputs in the TBXT-WNT-HOX axis to pattern hPSCs towards a posterior axial progenitor fate. A good candidate to explore for a potential TBXT cooperation in A-P patterning in hPSC-derived

NMPs would be CDX2. Cdx2 synergises with T/Brachyury to activate a Wnt and FGF gene regulatory network that drives axial elongation (Amin et al. 2016b) and has a crucial role in the activation of posterior *HOX* genes (Amin et al. 2016b; Mazzoni et al. 2013; Neijts et al. 2017; van den Akker et al. 2002). Thus, given that CDX2 is a direct target of TBXT and potentially affects *HOX* gene expression in a similar way to TBXT, it would be interesting to dissect the exact role of CDX2 in cell fate decision and acquisition of a posterior character through gain/loss of function experiments during hPSC-differentiation. This, would further elucidate the potential cross-talk between TBXT and CDX signalling cascades and contribute to the current model towards understanding axial specification in human NMPs and their posterior derivatives.

5.6.3. TBXT influences the acquisition of a SOX10-positive neural crest identity by hESC-derived axial progenitors

A key finding of this chapter is the previously unknown role of the pro-mesodermal transcription factor TBXT in promoting a SOX10-positive NC identity in hESC-derived NMPs. This became evident by the reduction in the fraction of SOX10-expressing cells in NMP-derived cultures grown under neutral conditions and following the early depletion of TBXT, during the transition from pluripotent towards the NMP-state. The mechanism of action of TBXT in promoting a NC entity is not fully examined, however, our genome-wide binding and chromatin accessibility provide evidence that TBXT influences the acquisition of a SOX10-positive identity through two complementary mechanisms: i) early direct binding in regulatory elements controlling the expression of NC fate determinants *CDX2, BMP7, WNT1* (Burstyn-Cohen et al. 2004; Nguyen et al. 2000; Sanchez-Ferras et al. 2016) present within the NMP compartment and ii) a late indirect activation of trunk NC-specific enhancers by binding to their upstream regulatory elements during the early transition from NMPs to NC (Figure 5.16). The latter is further supported by the experiments showing that media supplementation with Wnt and BMP rescued the negative effect of TBXT knockdown in the number of SOX10-positive cells, suggesting that these extrinsic factors possibly compensate for the loss of TBXT and regulate TBXT-downstream effectors (Figure 5.10, 5.12). Additionally, my experiments demonstrated that depletion of TBXT did not steer NMPs towards a SOX1-positive neuroectodermal identity, consistent with the notion that NC and CNS neuroectoderm arise independently/diverge early in line with previous reports from the avian embryo (Basch et al. 2006) and a hPSC-based model of NC (Leung et al. 2016) (Figure 5.10).

5.6.4. Summary of results and proposed model

The findings in this chapter give an insight into the molecular interactions occurring to ascribe cells a posterior axial identity during the differentiation of hPSCs into NMPs and their posterior derivatives, trunk NC and pre-neural spinal cord cells and propose the existence of two temporally discrete and cell-type dependent modes that control the early posteriorisation events: i) an early TBXT/Wnt-dependent phase at which the primary regionalisation occurs within uncommitted progenitors as hPS cells transit to NMPs and ii) a late FGF-dependent phase at which the refinement and maintenance of posterior axial identity occurs in TBXT-negative/spinal cord progenitors/NC cells (Figure 5.17). During the early phase, TBXT together with Wnt signalling components as part of a positive regulatory loop induce an early posterior NC/spinal cord identity in differentiating cells. This occurs via binding of TBXT in enhancers of *HOX* genes and other key axial regulators including Wnt family members, altering the chromatin state and transcriptionally activating these genes. During the late phase and as cells exit the NMP state, the expression of TBXT diminishes and the control of trunk *HOX* gene expression and maintenance becomes less dependent on Wnt. FGF signals potentially cooperate with CDX2 at this stage and regulate posterior identity maintenance. Moreover, our model proposes that in addition to early posterior regionalisation, TBXT influences trunk NC specification by activating NC fate determinants such as Wnt and BMP effectors during the early transition from NMPs to posterior NC (Figure 5.17).

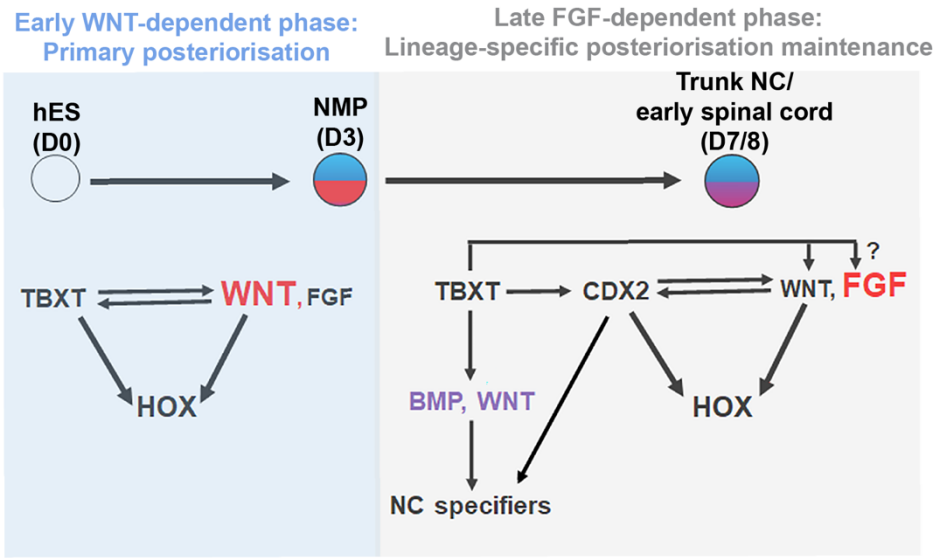

Figure 5.17. Schematic model of the molecular interactions and signalling dynamics that regulate posteriorisation events during the transition of hPSCs to neuromesodermal progenitors and their posterior neural crest and pre-neural spinal cord derivatives. Imaged sourced from Gogolou et al. (2022)

Chapter 6: General discussion and concluding remarks

The early cellular and molecular events that govern ectodermal patterning, NC induction and specification have been a subject of intensive research for quite some time in animal models and hPSC-based studies but little is known about the A-P patterning outside CNS and specifically in NC context. This is also reflected by the lack, until recently, of protocols for the *in vitro* generation of NC with more caudal to cranial axial identity.

The work presented in this thesis built upon our previously published protocols for the derivation of vagal (Frith et al. 2020; Gogolou et al. 2021) and trunk (Frith et al. 2018) NC cells from hPSCs and extended our understanding on the signalling and transcriptional requirements for the posterior patterning of hPSC-derived NC cells. Moreover, it focused on defining critical parameters including signalling cues that would facilitate the derivation and differentiation of NC derivatives that belong to ENS lineage.

In chapter 3, I characterised the *in vitro* differentiation of vagal NC/early ENS progenitors and examined in part the heterogeneity emerging in the culture using immunocytochemistry. I showed that a suboptimal differentiation is accompanied by an increase in the number of cells expressing PAX6. I demonstrated that plating density is critical for NC specification with low densities favouring SOX10 induction and, as a result, NC lineage over PAX6 expression which is associated with PPE or CNS progenitor cells. Interestingly, I found that elevated Wnt activity during NC induction resulted in an upregulation in *PAX6* transcripts, in a similar manner to high plating density, suggesting a link between Wnt signalling and cell density in regulating PAX6. This hypothesis was strengthened by the concomitant increase in the transcript levels of the Wnt target *AXIN2* in cultures initiated with a higher plating density. Therefore, these findings imply that an interplay between cell density and Wnt signalling pathway controls NC differentiation *in vitro* and indicate that precise levels of Wnt in combination with defined density could result in an efficient NC induction limiting the appearance of PAX6. A titration experiment for Wnt activity levels using Wnt agonist and antagonist treatment to overcome any potential discrepancies introduced by the variable endogenous Wnt signalling, in a similar way to that for BMP (Hackland et al. 2017), along with different plating densities would be the next step to define a balance between density and Wnt activity as a means to further optimise the *in vitro* vagal NC differentiation and improve protocol's reproducibility.

Our group's previous work (Frith et al. 2018; Frith et al. 2020) and findings of others (Fattahi et al. 2016; Workman et al. 2017) have shown that patterning of NC to vagal axial identity relies on the initial induction of a default NC character (cranial NC) which is progressively posteriorized

through the action of RA, in a similar mechanism with the activation transformation model (Nieuwkoop and Nigtevecht 1954) proposed by Nieuwkoop to explain embryonic patterning. We also recently demonstrated that in addition to its role in axial patterning, RA specifies vagal NC towards an early ENS progenitor identity (Frith et al. 2020). Based on these, in chapter 4 I generated vagal NC/early ENS progenitors using a hESC and a hiPSC line and explored their ability to form enteric neurons and glia in the presence of neural inducing signals (Frith et al. 2020; Gogolou et al. 2021). Using a panel of progenitor, glial, pan-neural and subtype specific markers I showed that ENS cultures were comprised of progenitors, neurons and glia and progressively acquired a more "mature" phenotype over long term culture. Additionally, the NC-derived enteric-like neurons appeared to be functional as they were able to respond to chemical and electrical stimuli during electrophysiological analysis, an exciting finding that holds great promise for disease modelling of enteric neuropathies and this, to the best of my knowledge, apart from a previous study that performed neuronal activity measurements following co-culture with hPSC-derived intestinal organoids (Workman et al. 2017), has not been shown before in a similar *in vitro* only system.

Treatment of NC-derived ENS progenitor cultures with DAPT, a pharmacological inhibitor of Notch signalling pathway, enhanced neural differentiation and promoted the induction of glia. This finding is particularly interesting given the proposed role of Notch in maintaining ENS progenitors numbers (Okamura and Saga 2008) and it might reflect a mechanism of pre-mature neurogenesis and gliogenesis which could be linked to the aganglionosis observed in HSCR (Ngan et al. 2011). However, a thorough investigation of progenitors' migration and survival at discrete time points is needed to elucidate the exact role of Notch pathway inhibition during ENS differentiation *in vitro*. Following on from this, we next aim to adopt a more targeted approach which entails the use of blocking antibodies against specific Notch receptors (NOTCH1 or NOTCH2) (Wu et al. 2010) and Jagged ligands (JAG1, JAG2) (Lafkas et al. 2015) to interrogate the discrete and temporal function of various Notch components bypassing inhibition of several signalling pathways given the ubiquitous role of Notch in several cellular functions (Hori et al. 2013). The role of Notch signalling pathway on ENS development has not been explored previously in humans and we believe that the proposed experiments in combination with the work described here, will expand our current understanding of its role on cell fate specification in the developing ENS. This knowledge is limited and predominantly derives from clonal assays performed around 2 decades ago in NC stem cells/progenitors isolated from embryonic rat sciatic nerve, gut or postnatal gut (Bixby et al. 2002; Kruger et al. 2002; Morrison et al. 2000).

The *in vitro* generation of trunk NC, as opposed to vagal, is not mediated by the caudalising action of RA but relies on the FGF/Wnt-mediated induction of NMPs which are subsequently steered towards a posterior NC fate (Cooper et al. 2022; Faustino Martins et al. 2020; Frith et al.

2018; Gomez et al. 2019b; Hackland et al. 2019; Kirino et al. 2018). Based on this, in chapter 5 I examined the role of FGF and Wnt signals in controlling the acquisition of posterior axial identity and the adoption of a NC fate by hPSC-derived NMPs. I demonstrated that perturbation of FGF and predominantly Wnt at the NMP stage impairs the posterior axial specification in NMPs and that FGF and Wnt signals are important to maintain the posterior identity in trunk NC. I next showed that the key NMP/mesodermal regulator TBXT plays a critical role in the development of trunk NC as TBXT knockdown disrupted the acquisition of posterior axial identity by NMPs and NMP-derived trunk NC cells, while the axial identity of pre-neural spinal cord progenitors remained unaffected. The inability of NC cells to commit to the right regional identity was linked to a failure of hPSC-derived NMPs to induce and maintain *HOX* genes and critical signalling pathway components, whereas in the case of pre-neural spinal cord progenitors, this phenotype was potentially rescued by the supplementation of media with high FGF. Finally, I demonstrated that TBXT controlled these events by modifying the chromatin landscape in regions associated with *HOX* gene clusters and crucial posterior/NC identity regulators. These findings indicate a previously unknown role for TBXT in influencing trunk NC fate and suggest that the regional identity in NMPs and their derivatives is regulated by temporally discrete mechanisms and in a cell-dependent fashion. They also provide a mechanistic insight into the early action of TBXT within the NMP compartment but further work on identifying the direct targets downstream of TBXT as cells exit from the NMP stage is highly required to complement these findings. Finally, I believe that the work described in this chapter sets the ground to investigate how TBXT cooperates with other transcription factors to establish posterior identities prior to the acquisition of a NC or spinal cord fate. This also is the first time that TBXT, a pro-mesodermal factor, has been implicated in the patterning of NC cells and has been demonstrated to directly bind and regulate *HOX* gene expression in NMPs, the progenitors of spinal cord neurectoderm, presomitic mesoderm and trunk NC. Further, the mechanistic insight provided here may help explain the impairment of NC specification and *HOX* dysregulation in neural tube defects (Anderson et al. 2016; Rochtus et al. 2015; Yu et al. 2019) in which, such as spina bifida, individuals carry mutations in the *TBXT* gene (Agopian et al. 2013; Carter et al. 2011; Shields et al. 2000). Moreover, such disorders characterised as neural tube defects, may as well represent unappreciated cases of neurocristopathies given the proposed link between TBXT and NC patterning.

The work presented in this chapter would benefit from the inclusion of loss of function experiments in the mouse embryo to further investigate/validate the role of TBXT in trunk NC specification *in vivo*. Mouse embryos carrying *Brachyury (T)* mutations fail to develop the A-P axis properly and exhibit truncation posterior to somite 7 (reviewed in Martin 2016). Conditional gene knockout in the CLE to specifically eliminate Brachyury (T) expression in the NMP pool,

would allow to overcome this issue and enable *Brachyury (T)* inactivation in a more controlled manner. This system, in combination with lineage tracing of *Brachyury (T)*-depleted NMP-derived progeny during the formation of trunk NC would reveal whether the *Brachyury (T)-Hox* axis is required to establish a posterior trunk NC identity *in vivo*, in line with my observations from our human *in vitro* model of trunk NC development.

Despite the versatile use and the great number of advantages that hPSC research offers, limitations such as the risk of culture adaptation along with genetic and epigenetic changes that cells may acquire during long term culture and in response to culture conditions (Allegrucci et al. 2007; Baker et al. 2016; Gokhale et al. 2015) can impede differentiation approaches, alter the experimental outcome, through acquisition of misleading results, and most importantly jeopardise the potential use of hPSCs and their derivatives for regenerative medicine. The latter is tightly linked with risk of tumour formation, given that the most commonly acquired cytogenetic abnormalities, which involve gains of chromosome fragments in chromosome 1, 12, 17 and 20, are also commonly reported in embryonal carcinoma cells, the malignant cells that resemble ESCs and are found in teratocarcinomas (Baker et al. 2016). Therefore, screening hPSCs regularly for genetic changes, ensuring that cells are karyotypically normal is a first step towards obtaining reliable data and drawing conclusions about human developmental biology as well as transferring basic research into clinical practice.

Moreover, in spite of the progress made in protocol's refinement, the post-otic NC cultures and their neural progeny continued to be heterogeneous, as they exhibited cells of variable morphology and expression of different lineage-specific genes, with a large subset of them yet to be identified. Increased heterogeneity, a major hallmark of hPSC cultures and particularly of their specialised differentiated derivatives, is predominantly synonymous to poor differentiation outcome. This can occur from asynchronous differentiation due to the fact that hPSCs commonly exist as a continuum of cell states within the stem cell compartment with a subset of cells displaying lineage priming or co-expression of pluripotency and cell fate specific-genes (Allison et al. 2018; Hough et al. 2014; Stavish et al. 2020). Genetic and epigenetic factors assigning cells variable sensitivity to the available small molecules included in the culture regimen as well as changes in the physical forces of the culture environment that cells experience, encompassing mechanical forces, extracellular matrix properties and cell-cell contacts may also, in part, account for the cellular heterogeneity observed in hPSC-derived cultures *in vitro*.

That heterogeneity, which is manifested in our NC cultures by an increase in the expression of PAX6, a marker of CNS, or potentially by the continued presence of cranial or emergence of the cardiac NC subset, given the close and natural relationship of these domains in the developing

embryo and the fact that they also arise in response, to a great extent, to the same developmental cues, requires further investigation. Single cell transcriptome analysis would be highly beneficial and our next step in order to shed light to the cellular heterogeneity exhibited in our *in vitro* cultures. We envisage that this analysis will inform us about differential gene expression among different NC subsets, the presence of specific ligands in various cell clusters and signalling pathway activity. This knowledge could be combined with the findings described here on critical factors and parameters for NC differentiation and implemented in an optimised approach towards eliminating unwanted cellular contaminants and manufacturing “pure” NC populations and their progeny for therapeutic purposes, a long-desired but yet to be achieved goal.

Taken together, this study using an *in vitro* model of human NC development aimed towards understanding the signalling environment experienced by the cells in culture and provided a better insight into the signalling and transcriptional requirements for the specification of post-otic NC (vagal and trunk) *in vitro.* These findings are of particular importance for designing and optimising hPSC-based NC differentiation strategies with potential use in cell therapy for neurocristopathies and NC-related disease. Defining critical parameters that impact vagal NC differentiation yield is beneficial and a prerequisite for protocol’s standardisation and scalability as a first step towards preclinical studies. In line with this, the potential of hPSC-derived vagal NC to generate functional enteric like-neurons *in vitro* along with our groups previous work that demonstrated their ability to integrate into mouse colon *in vivo* (Frith et al. 2020) opens up an exciting opportunity for regenerative medicine and our group is currently working on a periclinal study, developing a strategy for assessing their use in cell therapy for HSCR. Additionally, for future applications it would be very interesting to explore the ability of hiPSCs obtained from patients with HSCR to differentiate along the ENS lineage and to examine whether they exhibit defects in migration, proliferation, survival or specification similar to the impaired functionality *in vivo*. This is of particular importance in order to determine whether the disease phenotype could be recapitulated *in vitro,* and such approach would be advantageous to precision medicine.

References

Adameyko I, Lallemend F, Aquino JB, Pereira JA, Topilko P, Muller T, Fritz N, Beljajeva A, Mochii M, Liste I et al. 2009. Schwann cell precursors from nerve innervation are a cellular origin of melanocytes in skin. Cell. 139(2):366-379.

Aflatoonian B, Ruban L, Shamsuddin S, Baker D, Andrews P, Moore H. 2010. Generation of sheffield (shef) human embryonic stem cell lines using a microdrop culture system. In Vitro Cell Dev Biol Anim. 46(3-4):236-241.

Agopian AJ, Bhalla AD, Boerwinkle E, Finnell RH, Grove ML, Hixson JE, Shimmin LC, Sewda A, Stuart C, Zhong Y et al. 2013. Exon sequencing of pax3 and t (brachyury) in cases with spina bifida. Birth Defects Res A Clin Mol Teratol. 97(9):597-601.

Alkobtawi M, Pla P, Monsoro-Burq AH. 2021. Bmp signaling is enhanced intracellularly by fhl3 controlling wnt-dependent spatiotemporal emergence of the neural crest. Cell Rep. 35(12):109289.

Allegrucci C, Wu YZ, Thurston A, Denning CN, Priddle H, Mummery CL, Ward-van Oostwaard D, Andrews PW, Stojkovic M, Smith N et al. 2007. Restriction landmark genome scanning identifies culture-induced DNA methylation instability in the human embryonic stem cell epigenome. Hum Mol Genet. 16(10):1253-1268.

Allison TF, Smith AJH, Anastassiadis K, Sloane-Stanley J, Biga V, Stavish D, Hackland J, Sabri S, Langerman J, Jones M et al. 2018. Identification and single-cell functional characterization of an endodermally biased pluripotent substate in human embryonic stem cells. Stem Cell Reports. 10(6):1895-1907.

Amemiya HM, Kundaje A, Boyle AP. 2019. The encode blacklist: Identification of problematic regions of the genome. Sci Rep. 9(1):9354.

Amiel J, Sproat-Emison E, Garcia-Barcelo M, Lantieri F, Burzynski G, Borrego S, Pelet A, Arnold S, Miao X, Griseri P et al. 2008. Hirschsprung disease, associated syndromes and genetics: A review. J Med Genet. 45(1):1-14.

Amin H, Maccione A, Marinaro F, Zordan S, Nieus T, Berdondini L. 2016a. Electrical responses and spontaneous activity of human ips-derived neuronal networks characterized for 3-month culture with 4096-electrode arrays. Front Neurosci. 10:121.

Amin S, Neijts R, Simmini S, van Rooijen C, Tan SC, Kester L, van Oudenaarden A, Creyghton MP, Deschamps J. 2016b. Cdx and t brachyury co-activate growth signaling in the embryonic axial progenitor niche. Cell Rep. 17(12):3165-3177.

An WF, Germain AR, Bishop JA, Nag PP, Metkar S, Ketterman J, Walk M, Weiwer M, Liu X, Patnaik D et al. 2010. Discovery of potent and highly selective inhibitors of gsk3b. Probe reports from the nih molecular libraries program. Bethesda (MD).

Anderson MJ, Schimmang T, Lewandoski M. 2016. An fgf3-bmp signaling axis regulates caudal neural tube closure, neural crest specification and anterior-posterior axis extension. PLoS Genet. 12(5):e1006018.

Anderson RM, Stottmann RW, Choi M, Klingensmith J. 2006. Endogenous bone morphogenetic protein antagonists regulate mammalian neural crest generation and survival. Dev Dyn. 235(9):2507-2520.

Angelozzi M, Lefebvre V. 2019. Soxopathies: Growing family of developmental disorders due to sox mutations. Trends Genet. 35(9):658-671.

Aoki Y, Saint-Germain N, Gyda M, Magner-Fink E, Lee YH, Credidio C, Saint-Jeannet JP. 2003. Sox10 regulates the development of neural crest-derived melanocytes in xenopus. Dev Biol. 259(1):19-33.

Bae S, Bessho Y, Hojo M, Kageyama R. 2000. The bhlh gene hes6, an inhibitor of hes1, promotes neuronal differentiation. Development. 127(13):2933-2943.

Baetge G, Gershon MD. 1989. Transient catecholaminergic (tc) cells in the vagus nerves and bowel of fetal mice: Relationship to the development of enteric neurons. Dev Biol. 132(1):189-211.

Baker D, Hirst AJ, Gokhale PJ, Juarez MA, Williams S, Wheeler M, Bean K, Allison TF, Moore HD, Andrews PW et al. 2016. Detecting genetic mosaicism in cultures of human pluripotent stem cells. Stem Cell Reports. 7(5):998-1012.

Baker JC, Beddington RS, Harland RM. 1999. Wnt signaling in xenopus embryos inhibits bmp4 expression and activates neural development. Genes Dev. 13(23):3149-3159.

Barber K, Studer L, Fattahi F. 2019. Derivation of enteric neuron lineages from human pluripotent stem cells. Nature protocols. 14(4):1261-1279.

Barlow AJ, Wallace AS, Thapar N, Burns AJ. 2008. Critical numbers of neural crest cells are required in the pathways from the neural tube to the foregut to ensure complete enteric nervous system formation. Development. 135(9):1681-1691.

Barrell WB, Griffin JN, Harvey JL, HipSci C, Danovi D, Beales P, Grigoriadis AE, Liu KJ. 2019. Induction of neural crest stem cells from bardet-biedl syndrome patient derived hipscs. Front Mol Neurosci. 12:139.

Barrett SD, Bridges AJ, Dudley DT, Saltiel AR, Fergus JH, Flamme CM, Delaney AM, Kaufman M, LePage S, Leopold WR et al. 2008. The discovery of the benzhydroxamate mek inhibitors ci-1040 and pd 0325901. Bioorg Med Chem Lett. 18(24):6501-6504.

Barriga EH, Trainor PA, Bronner M, Mayor R. 2015. Animal models for studying neural crest development: Is the mouse different? Development. 142(9):1555-1560.

Barros R, Pereira B, Duluc I, Azevedo M, Mendes N, Camilo V, Jacobs RJ, Paulo P, Santos-Silva F, van Seuningen I et al. 2008. Key elements of the bmp/smad pathway co-localize with cdx2 in intestinal metaplasia and regulate cdx2 expression in human gastric cell lines. J Pathol. 215(4):411-420.

Basch ML, Bronner-Fraser M, Garcia-Castro MI. 2006. Specification of the neural crest occurs during gastrulation and requires pax7. Nature. 441(7090):218-222.

Bayguinov PO, Broadhead MJ, Okamoto T, Hennig GW, Smith TK. 2012. Activity in varicosities within the myenteric plexus between and during the colonic migrating motor complex in the isolated murine large intestine. Neurogastroenterol Motil. 24(4):e185-201.

Beers J, Gulbranson DR, George N, Siniscalchi LI, Jones J, Thomson JA, Chen G. 2012. Passaging and colony expansion of human pluripotent stem cells by enzyme-free dissociation in chemically defined culture conditions. Nature protocols. 7(11):2029-2040.

Beisaw A, Tsaytler P, Koch F, Schmitz SU, Melissari MT, Senft AD, Wittler L, Pennimpede T, Macura K, Herrmann BG et al. 2018. Brachyury directs histone acetylation to target loci during mesoderm development. EMBO Rep. 19(1):118-134.

Bel-Vialar S, Itasaki N, Krumlauf R. 2002. Initiating hox gene expression: In the early chick neural tube differential sensitivity to fgf and ra signaling subdivides the hoxb genes in two distinct groups. Development. 129(22):5103-5115.

Bertero A, Pawlowski M, Ortmann D, Snijders K, Yiangou L, Cardoso de Brito M, Brown S, Bernard WG, Cooper JD, Giacomelli E et al. 2016. Optimized inducible shrna and crispr/cas9 platforms for in vitro studies of human development using hpscs. Development. 143(23):4405-4418.

Betancur P, Bronner-Fraser M, Sauka-Spengler T. 2010. Genomic code for sox10 activation reveals a key regulatory enhancer for cranial neural crest. Proc Natl Acad Sci U S A. 107(8):3570-3575.

Betters E, Charney RM, Garcia-Castro MI. 2018. Early specification and development of rabbit neural crest cells. Dev Biol. 444 Suppl 1:S181-S192.

Betters E, Liu Y, Kjaeldgaard A, Sundstrom E, Garcia-Castro MI. 2010. Analysis of early human neural crest development. Dev Biol. 344(2):578-592.

Bhave S, Guyer RA, Picard N, Omer M, Hotta R, Goldstein AM. 2022. Ednrb (-/-) mice with hirschsprung disease are missing gad2-expressing enteric neurons in the ganglionated small intestine. Front Cell Dev Biol. 10:917243.

Bier E, De Robertis EM. 2015. Embryo development. Bmp gradients: A paradigm for morphogen-mediated developmental patterning. Science. 348(6242):aaa5838.

Binagui-Casas A, Dias A, Guillot C, Metzis V, Saunders D. 2021. Building consensus in neuromesodermal research: Current advances and future biomedical perspectives. Curr Opin Cell Biol. 73:133-140.

Bixby S, Kruger GM, Mosher JT, Joseph NM, Morrison SJ. 2002. Cell-intrinsic differences between stem cells from different regions of the peripheral nervous system regulate the generation of neural diversity. Neuron. 35(4):643-656.

Blaugrund E, Pham TD, Tennyson VM, Lo L, Sommer L, Anderson DJ, Gershon MD. 1996. Distinct subpopulations of enteric neuronal progenitors defined by time of development, sympathoadrenal lineage markers and mash-1-dependence. Development. 122(1):309-320.

Boesmans W, Hao MM, Fung C, Li Z, Van den Haute C, Tack J, Pachnis V, Vanden Berghe P. 2019. Structurally defined signaling in neuro-glia units in the enteric nervous system. Glia. 67(6):1167-1178.

Bolande RP. 1974. The neurocristopathies: A unifying concept of disease arising in neural crest maldevelopment. Human Pathology. 5:409-429.

Bondurand N, Natarajan D, Thapar N, Atkins C, Pachnis V. 2003. Neuron and glia generating progenitors of the mammalian enteric nervous system isolated from foetal and postnatal gut cultures. Development. 130(25):6387-6400.

Bondurand N, Pingault V, Goerich DE, Lemort N, Sock E, Le Caignec C, Wegner M, Goossens M. 2000. Interaction among sox10, pax3 and mitf, three genes altered in waardenburg syndrome. Hum Mol Genet. 9(13):1907-1917.

Borghese L, Dolezalova D, Opitz T, Haupt S, Leinhaas A, Steinfarz B, Koch P, Edenhofer F, Hampl A, Brustle O. 2010. Inhibition of notch signaling in human embryonic stem cell-derived neural stem cells delays g1/s phase transition and accelerates neuronal differentiation in vitro and in vivo. Stem Cells. 28(5):955-964.

Braak H, Muller CM, Rub U, Ackermann H, Bratzke H, de Vos RA, Del Tredici K. 2006. Pathology associated with sporadic parkinson's disease--where does it end? J Neural Transm Suppl. (70):89-97.

Branchek TA, Gershon MD. 1989. Time course of expression of neuropeptide y, calcitonin gene-related peptide, and nadph diaphorase activity in neurons of the developing murine bowel and the appearance of 5-hydroxytryptamine in mucosal enterochromaffin cells. J Comp Neurol. 285(2):262-273.

Brault V, Moore R, Kutsch S, Ishibashi M, Rowitch DH, McMahon AP, Sommer L, Boussadia O, Kemler R. 2001. Inactivation of the beta-catenin gene by wnt1-cre-mediated deletion results in dramatic brain malformation and failure of craniofacial development. Development. 128(8):1253-1264.

Bray SJ. 2006. Notch signalling: A simple pathway becomes complex. Nat Rev Mol Cell Biol. 7(9):678-689.

Britton G, Heemskerk I, Hodge R, Qutub AA, Warmflash A. 2019. A novel self-organizing embryonic stem cell system reveals signaling logic underlying the patterning of human ectoderm. Development. 146(20).

Bronner ME, LeDouarin NM. 2012. Development and evolution of the neural crest: An overview. Dev Biol. 366(1):2-9.

Buenrostro JD, Giresi PG, Zaba LC, Chang HY, Greenleaf WJ. 2013. Transposition of native chromatin for fast and sensitive epigenomic profiling of open chromatin, DNA-binding proteins and nucleosome position. Nat Methods. 10(12):1213-1218.

Buikema JW, Lee S, Goodyer WR, Maas RG, Chirikian O, Li G, Miao Y, Paige SL, Lee D, Wu H et al. 2020. Wnt activation and reduced cell-cell contact synergistically induce massive expansion of functional human ipsc-derived cardiomyocytes. Cell Stem Cell. 27(1):50-63 e55.

Buitrago-Delgado E, Nordin K, Rao A, Geary L, LaBonne C. 2015. Neurodevelopment. Shared regulatory programs suggest retention of blastula-stage potential in neural crest cells. Science. 348(6241):1332-1335.

Burns AJ, Douarin NM. 1998. The sacral neural crest contributes neurons and glia to the post-umbilical gut: Spatiotemporal analysis of the development of the enteric nervous system. Development. 125(21):4335-4347.

Burns AJ, Le Douarin NM. 2001. Enteric nervous system development: Analysis of the selective developmental potentialities of vagal and sacral neural crest cells using quail-chick chimeras. Anat Rec. 262(1):16-28.

Burns AJ, Thapar N. 2014. Neural stem cell therapies for enteric nervous system disorders. Nat Rev Gastroenterol Hepatol. 11(5):317-328.

Burstyn-Cohen T, Stanleigh J, Sela-Donenfeld D, Kalcheim C. 2004. Canonical wnt activity regulates trunk neural crest delamination linking bmp/noggin signaling with g1/s transition. Development. 131(21):5327-5339.

Carpenter AE, Jones TR, Lamprecht MR, Clarke C, Kang IH, Friman O, Guertin DA, Chang JH, Lindquist RA, Moffat J et al. 2006. Cellprofiler: Image analysis software for identifying and quantifying cell phenotypes. Genome Biol. 7(10):R100.

Carter TC, Pangilinan F, Troendle JF, Molloy AM, VanderMeer J, Mitchell A, Kirke PN, Conley MR, Shane B, Scott JM et al. 2011. Evaluation of 64 candidate single nucleotide polymorphisms as risk factors for neural tube defects in a large irish study population. Am J Med Genet A. 155A(1):14-21.

Catala M, Teillet MA, Le Douarin NM. 1995. Organization and development of the tail bud analyzed with the quail-chick chimaera system. Mech Dev. 51(1):51-65.

Chalazonitis A, Pham TD, Rothman TP, DiStefano PS, Bothwell M, Blair-Flynn J, Tessarollo L, Gershon MD. 2001. Neurotrophin-3 is required for the survival-differentiation of subsets of developing enteric neurons. J Neurosci. 21(15):5620-5636.

Chalazonitis A, Rothman TP, Chen J, Gershon MD. 1998. Age-dependent differences in the effects of gdnf and nt-3 on the development of neurons and glia from neural crest-derived precursors immunoselected from the fetal rat gut: Expression of gfralpha-1 in vitro and in vivo. Dev Biol. 204(2):385-406.

Chalazonitis A, Rothman TP, Chen J, Lamballe F, Barbacid M, Gershon MD. 1994. Neurotrophin-3 induces neural crest-derived cells from fetal rat gut to develop in vitro as neurons or glia. J Neurosci. 14(11 Pt 1):6571-6584.

Chambers SM, Fasano CA, Papapetrou EP, Tomishima M, Sadelain M, Studer L. 2009. Highly efficient neural conversion of human es and ips cells by dual inhibition of smad signaling. Nature Biotechnology. 27(3):275-280.

Chambers SM, Qi Y, Mica Y, Lee G, Zhang XJ, Niu L, Bilsland J, Cao L, Stevens E, Whiting P et al. 2012. Combined small-molecule inhibition accelerates developmental timing and converts human pluripotent stem cells into nociceptors. Nat Biotechnol. 30(7):715-720.

Chen H, Thiagalingam A, Chopra H, Borges MW, Feder JN, Nelkin BD, Baylin SB, Ball DW. 1997. Conservation of the drosophila lateral inhibition pathway in human lung cancer: A hairy-related protein (hes-1) directly represses achaete-scute homolog-1 expression. Proc Natl Acad Sci U S A. 94(10):5355-5360.

Chen S, Zhou Y, Chen Y, Gu J. 2018. Fastp: An ultra-fast all-in-one fastq preprocessor. Bioinformatics. 34(17):i884-i890.

Cheng Y, Cheung M, Abu-Elmagd MM, Orme A, Scotting PJ. 2000. Chick sox10, a transcription factor expressed in both early neural crest cells and central nervous system. Brain Res Dev Brain Res. 121(2):233-241.

Cheung M, Briscoe J. 2003. Neural crest development is regulated by the transcription factor sox9. Development. 130(23):5681-5693.

Cheung M, Chaboissier MC, Mynett A, Hirst E, Schedl A, Briscoe J. 2005. The transcriptional control of trunk neural crest induction, survival, and delamination. Dev Cell. 8(2):179-192.

Chng SH, Pachnis V. 2020. Enteric nervous system: Lessons from neurogenesis for reverse engineering and disease modelling and treatment. Curr Opin Pharmacol. 50:100-106.

Collu GM, Hidalgo-Sastre A, Acar A, Bayston L, Gildea C, Leverentz MK, Mills CG, Owens TW, Meurette O, Dorey K et al. 2012. Dishevelled limits notch signalling through inhibition of csl. Development. 139(23):4405-4415.

Collu GM, Hidalgo-Sastre A, Brennan K. 2014. Wnt-notch signalling crosstalk in development and disease. Cell Mol Life Sci. 71(18):3553-3567.

Conti E, Harschnitz O. 2022. Human stem cell models to study placode development, function and pathology. Development. 149(20).

Cooper F, Gentsch GE, Mitter R, Bouissou C, Healy LE, Rodriguez AH, Smith JC, Bernardo AS. 2022. Rostrocaudal patterning and neural crest differentiation of human pre-neural spinal cord progenitors in vitro. Stem Cell Reports. 17(4):894-910.

Cooper F, Tsakiridis A. 2022a. Shaping axial identity during human pluripotent stem cell differentiation to neural crest cells. Biochem Soc Trans. 50(1):499-511.

Cooper F, Tsakiridis A. 2022b. Towards clinical applications of in vitro-derived axial progenitors. Dev Biol. 489:110-117.

Copeland J, Simoes-Costa M. 2020. Post-transcriptional tuning of fgf signaling mediates neural crest induction. Proc Natl Acad Sci U S A. 117(52):33305-33316.

Cornell RA, Eisen JS. 2000. Delta signaling mediates segregation of neural crest and spinal sensory neurons from zebrafish lateral neural plate. Development. 127(13):2873-2882.

Couly GF, Coltey PM, Le Douarin NM. 1993. The triple origin of skull in higher vertebrates: A study in quail-chick chimeras. Development. 117(2):409-429.

Cuny GD, Yu PB, Laha JK, Xing X, Liu JF, Lai CS, Deng DY, Sachidanandan C, Bloch KD, Peterson RT. 2008. Structure-activity relationship study of bone morphogenetic protein (bmp) signaling inhibitors. Bioorg Med Chem Lett. 18(15):4388-4392.

D'Amico-Martel A, Noden DM. 1983. Contributions of placodal and neural crest cells to avian cranial peripheral ganglia. Am J Anat. 166(4):445-468.

de Croze N, Maczkowiak F, Monsoro-Burq AH. 2011. Reiterative ap2a activity controls sequential steps in the neural crest gene regulatory network. Proc Natl Acad Sci U S A. 108(1):155-160.

De Giorgio R, Bovara M, Barbara G, Canossa M, Sarnelli G, De Ponti F, Stanghellini V, Tonini M, Cappello S, Pagnotta E et al. 2003. Anti-hud-induced neuronal apoptosis underlying paraneoplastic gut dysmotility. Gastroenterology. 125(1):70-79.

Deardorff MA, Tan C, Saint-Jeannet JP, Klein PS. 2001. A role for frizzled 3 in neural crest development. Development. 128(19):3655-3663.

Denham M, Hasegawa K, Menheniott T, Rollo B, Zhang D, Hough S, Alshawaf A, Febbraro F, Ighaniyan S, Leung J et al. 2015. Multipotent caudal neural progenitors derived from human pluripotent stem cells that give rise to lineages of the central and peripheral nervous system. Stem Cells. 33(6):1759-1770.

Diez del Corral R, Olivera-Martinez I, Goriely A, Gale E, Maden M, Storey K. 2003. Opposing fgf and retinoid pathways control ventral neural pattern, neuronal differentiation, and segmentation during body axis extension. Neuron. 40(1):65-79.

Dobin A, Davis CA, Schlesinger F, Drenkow J, Zaleski C, Jha S, Batut P, Chaisson M, Gingeras TR. 2013. Star: Ultrafast universal rna-seq aligner. Bioinformatics. 29(1):15-21.

Dottori M, Gross MK, Labosky P, Goulding M. 2001. The winged-helix transcription factor foxd3 suppresses interneuron differentiation and promotes neural crest cell fate. Development. 128(21):4127-4138.

Doufexi AE, Mina M. 2008. Signaling pathways regulating the expression of prx1 and prx2 in the chick mandibular mesenchyme. Dev Dyn. 237(11):3115-3127.

Dovey HF, John V, Anderson JP, Chen LZ, de Saint Andrieu P, Fang LY, Freedman SB, Folmer B, Goldbach E, Holsztynska EJ et al. 2001. Functional gamma-secretase inhibitors reduce beta-amyloid peptide levels in brain. J Neurochem. 76(1):173-181.

Drokhlyansky E, Smillie CS, Van Wittenberghe N, Ericsson M, Griffin GK, Eraslan G, Dionne D, Cuoco MS, Goder-Reiser MN, Sharova T et al. 2020. The human and mouse enteric nervous system at single-cell resolution. Cell. 182(6):1606-1622 e1623.

Dupin E, Calloni GW, Coelho-Aguiar JM, Le Douarin NM. 2018. The issue of the multipotency of the neural crest cells. Dev Biol. 444 Suppl 1:S47-S59.

Dupin E, Creuzet S, Le Douarin NM. 2006. The contribution of the neural crest to the vertebrate body. Adv Exp Med Biol. 589:96-119.

Dyachuk V, Furlan A, Shahidi MK, Giovenco M, Kaukua N, Konstantinidou C, Pachnis V, Memic F, Marklund U, Muller T et al. 2014. Neurodevelopment. Parasympathetic neurons originate from nerve-associated peripheral glial progenitors. Science. 345(6192):82-87.

El-Nachef D, Shi K, Beussman KM, Martinez R, Regier MC, Everett GW, Murry CE, Stevens KR, Young JE, Sniadecki NJ et al. 2020. A rainbow reporter tracks single cells and reveals heterogeneous cellular dynamics among pluripotent stem cells and their differentiated derivatives. Stem Cell Reports. 15(1):226-241.

El-Nachef WN, Bronner ME. 2020. De novo enteric neurogenesis in post-embryonic zebrafish from schwann cell precursors rather than resident cell types. Development. 147(13).

Elmentaite R, Kumasaka N, Roberts K, Fleming A, Dann E, King HW, Kleshchevnikov V, Dabrowska M, Pritchard S, Bolt L et al. 2021. Cells of the human intestinal tract mapped across space and time. Nature. 597(7875):250-255.

Endo Y, Osumi N, Wakamatsu Y. 2002. Bimodal functions of notch-mediated signaling are involved in neural crest formation during avian ectoderm development. Development. 129(4):863-873.

Enomoto H, Araki T, Jackman A, Heuckeroth RO, Snider WD, Johnson EM, Jr., Milbrandt J. 1998. Gfr alpha1-deficient mice have deficits in the enteric nervous system and kidneys. Neuron. 21(2):317-324.

Escurat M, Djabali K, Gumpel M, Gros F, Portier MM. 1990. Differential expression of two neuronal intermediate-filament proteins, peripherin and the low-molecular-mass neurofilament protein (nf-l), during the development of the rat. J Neurosci. 10(3):764-784.

Espinosa-Medina I, Jevans B, Boismoreau F, Chettouh Z, Enomoto H, Muller T, Birchmeier C, Burns AJ, Brunet JF. 2017. Dual origin of enteric neurons in vagal schwann cell precursors and the sympathetic neural crest. Proc Natl Acad Sci U S A. 114(45):11980-11985.

Etchevers HC, Dupin E, Le Douarin NM. 2019. The diverse neural crest: From embryology to human pathology. Development. 146(5).

Faial T, Bernardo AS, Mendjan S, Diamanti E, Ortmann D, Gentsch GE, Mascetti VL, Trotter MW, Smith JC, Pedersen RA. 2015. Brachyury and smad signalling collaboratively orchestrate distinct mesoderm and endoderm gene regulatory networks in differentiating human embryonic stem cells. Development. 142(12):2121-2135.

Fattahi F, Steinbeck JA, Kriks S, Tchieu J, Zimmer B, Kishinevsky S, Zeltner N, Mica Y, El-Nachef W, Zhao H et al. 2016. Deriving human ens lineages for cell therapy and drug discovery in hirschsprung disease. Nature. 531(7592):105-109.

Faure L, Wang Y, Kastriti ME, Fontanet P, Cheung KKY, Petitpre C, Wu H, Sun LL, Runge K, Croci L et al. 2020. Single cell rna sequencing identifies early diversity of sensory neurons forming via bi-potential intermediates. Nat Commun. 11(1):4175.

Faure S, McKey J, Sagnol S, de Santa Barbara P. 2015. Enteric neural crest cells regulate vertebrate stomach patterning and differentiation. Development. 142(2):331-342.

Faust GG, Hall IM. 2014. Samblaster: Fast duplicate marking and structural variant read extraction. Bioinformatics. 30(17):2503-2505.

Faustino Martins JM, Fischer C, Urzi A, Vidal R, Kunz S, Ruffault PL, Kabuss L, Hube I, Gazzerro E, Birchmeier C et al. 2020. Self-organizing 3d human trunk neuromuscular organoids. Cell Stem Cell. 26(2):172-186 e176.

Foong JP, Hirst CS, Hao MM, McKeown SJ, Boesmans W, Young HM, Bornstein JC, Vanden Berghe P. 2015. Changes in nicotinic neurotransmission during enteric nervous system development. J Neurosci. 35(18):7106-7115.

Freter S, Fleenor SJ, Freter R, Liu KJ, Begbie J. 2013. Cranial neural crest cells form corridors prefiguring sensory neuroblast migration. Development. 140(17):3595-3600.

Frith TJ, Granata I, Wind M, Stout E, Thompson O, Neumann K, Stavish D, Heath PR, Ortmann D, Hackland JO et al. 2018. Human axial progenitors generate trunk neural crest cells in vitro. Elife. 7.

Frith TJR, Gogolou A, Hackland JOS, Hewitt ZA, Moore HD, Barbaric I, Thapar N, Burns AJ, Andrews PW, Tsakiridis A et al. 2020. Retinoic acid accelerates the specification of enteric neural progenitors from in-vitro-derived neural crest. Stem Cell Reports. 15(3):557-565.

Frith TJR, Tsakiridis A. 2019. Efficient generation of trunk neural crest and sympathetic neurons from human pluripotent stem cells via a neuromesodermal axial progenitor intermediate. Curr Protoc Stem Cell Biol. 49(1):e81.

Fu M, Lui VC, Sham MH, Cheung AN, Tam PK. 2003. Hoxb5 expression is spatially and temporarily regulated in human embryonic gut during neural crest cell colonization and differentiation of enteric neuroblasts. Dev Dyn. 228(1):1-10.

Fu M, Sato Y, Lyons-Warren A, Zhang B, Kane MA, Napoli JL, Heuckeroth RO. 2010. Vitamin a facilitates enteric nervous system precursor migration by reducing pten accumulation. Development. 137(4):631-640.

Fung C, Vanden Berghe P. 2020. Functional circuits and signal processing in the enteric nervous system. Cell Mol Life Sci. 77(22):4505-4522.

Furlan A, Adameyko I. 2018. Schwann cell precursor: A neural crest cell in disguise? Dev Biol. 444 Suppl 1:S25-S35.
Furlan A, Dyachuk V, Kastriti ME, Calvo-Enrique L, Abdo H, Hadjab S, Chontorotzea T, Akkuratova N, Usoskin D, Kamenev D et al. 2017. Multipotent peripheral glial cells generate neuroendocrine cells of the adrenal medulla. Science. 357(6346).
Furness JB. 2006. The enteric nervous system. Malden, Mass.: Blackwell Pub.
Furness JB. 2012. The enteric nervous system and neurogastroenterology. Nat Rev Gastroenterol Hepatol. 9(5):286-294.
Galligan JJ, LePard KJ, Schneider DA, Zhou X. 2000. Multiple mechanisms of fast excitatory synaptic transmission in the enteric nervous system. J Auton Nerv Syst. 81(1-3):97-103.
Gandhi S, Ezin M, Bronner ME. 2020. Reprogramming axial level identity to rescue neural-crest-related congenital heart defects. Dev Cell. 53(3):300-315 e304.
Gans C, Northcutt RG. 1983. Neural crest and the origin of vertebrates: A new head. Science. 220(4594):268-273.
Gao T, Wright-Jin EC, Sengupta R, Anderson JB, Heuckeroth RO. 2021. Cell-autonomous retinoic acid receptor signaling has stage-specific effects on mouse enteric nervous system. JCI Insight. 6(10).
Garcia-Castro MI, Marcelle C, Bronner-Fraser M. 2002. Ectodermal wnt function as a neural crest inducer. Science. 297(5582):848-851.
Gariepy CE, Cass DT, Yanagisawa M. 1996. Null mutation of endothelin receptor type b gene in spotting lethal rats causes aganglionic megacolon and white coat color. Proc Natl Acad Sci U S A. 93(2):867-872.
George RM, Maldonado-Velez G, Firulli AB. 2020. The heart of the neural crest: Cardiac neural crest cells in development and regeneration. Development. 147(20).
Gerrard L, Rodgers L, Cui W. 2005. Differentiation of human embryonic stem cells to neural lineages in adherent culture by blocking bone morphogenetic protein signaling. Stem Cells. 23(9):1234-1241.
Glavic A, Silva F, Aybar MJ, Bastidas F, Mayor R. 2004. Interplay between notch signaling and the homeoprotein xiro1 is required for neural crest induction in xenopus embryos. Development. 131(2):347-359.
Gogolou A, Frith TJR, Tsakiridis A. 2021. Generating enteric nervous system progenitors from human pluripotent stem cells. Curr Protoc. 1(6):e137.
Gogolou A, Souilhol C, Granata I, Wymeersch FJ, Manipur I, Wind M, Frith TJR, Guarini M, Bertero A, Bock C et al. 2022. Early anteroposterior regionalisation of human neural crest is shaped by a pro-mesodermal factor. Elife. 11.
Gokhale PJ, Au-Young JK, Dadi S, Keys DN, Harrison NJ, Jones M, Soneji S, Enver T, Sherlock JK, Andrews PW. 2015. Culture adaptation alters transcriptional hierarchies among single human embryonic stem cells reflecting altered patterns of differentiation. PLoS One. 10(4):e0123467.
Gomez GA, Prasad MS, Sandhu N, Shelar PB, Leung AW, Garcia-Castro MI. 2019a. Human neural crest induction by temporal modulation of wnt activation. Dev Biol. 449(2):99-106.
Gomez GA, Prasad MS, Wong M, Charney RM, Shelar PB, Sandhu N, Hackland JOS, Hernandez JC, Leung AW, Garcia-Castro MI. 2019b. Wnt/beta-catenin modulates the axial identity of embryonic stem cell-derived human neural crest. Development. 146(16).
Gonzalez Malagon SG, Liu KJ. 2022. Linking neural crest development to neuroblastoma pathology. Development. 149(15).

Gonzalez Malagon SG, Lopez Munoz AM, Doro D, Bolger TG, Poon E, Tucker ER, Adel Al-Lami H, Krause M, Phiel CJ, Chesler L et al. 2018. Glycogen synthase kinase 3 controls migration of the neural crest lineage in mouse and xenopus. Nat Commun. 9(1):1126.

Gould DB, Walter MA. 2000. Cloning, characterization, localization, and mutational screening of the human barx1 gene. Genomics. 68(3):336-342.

Gouti M, Delile J, Stamataki D, Wymeersch FJ, Huang Y, Kleinjung J, Wilson V, Briscoe J. 2017. A gene regulatory network balances neural and mesoderm specification during vertebrate trunk development. Dev Cell. 41(3):243-261 e247.

Gouti M, Tsakiridis A, Wymeersch FJ, Huang Y, Kleinjung J, Wilson V, Briscoe J. 2014. In vitro generation of neuromesodermal progenitors reveals distinct roles for wnt signalling in the specification of spinal cord and paraxial mesoderm identity. PLoS Biol. 12(8):e1001937.

Grundmann D, Loris E, Maas-Omlor S, Huang W, Scheller A, Kirchhoff F, Schafer KH. 2019. Enteric glia: S100, gfap, and beyond. Anat Rec (Hoboken). 302(8):1333-1344.

Guillaud L, El-Agamy SE, Otsuki M, Terenzio M. 2020. Anterograde axonal transport in neuronal homeostasis and disease. Front Mol Neurosci. 13:556175.

Guillot C, Djeffal Y, Michaut A, Rabe B, Pourquie O. 2021. Dynamics of primitive streak regression controls the fate of neuromesodermal progenitors in the chicken embryo. Elife. 10.

Guruharsha KG, Kankel MW, Artavanis-Tsakonas S. 2012. The notch signalling system: Recent insights into the complexity of a conserved pathway. Nat Rev Genet. 13(9):654-666.

Guyer RA, Stavely RS, Robertson K, Bhave S, Hotta R, Kaltschmidt JA, Goldstein AM. 2022. Single-cell multiome sequencing clarifies enteric glial cell diversity and identifies an intraganglionic population poised for neurogenesis. bioRxiv.2021.2008.2024.457368.

Hackland JOS, Frith TJR, Thompson O, Marin Navarro A, Garcia-Castro MI, Unger C, Andrews PW. 2017. Top-down inhibition of bmp signaling enables robust induction of hpscs into neural crest in fully defined, xeno-free conditions. Stem Cell Reports. 9(4):1043-1052.

Hackland JOS, Shelar PB, Sandhu N, Prasad MS, Charney RM, Gomez GA, Frith TJR, Garcia-Castro MI. 2019. Fgf modulates the axial identity of trunk hpsc-derived neural crest but not the cranial-trunk decision. Stem Cell Reports. 12(5):920-933.

Hall BK. 2000. The neural crest as a fourth germ layer and vertebrates as quadroblastic not triploblastic. Evol Dev. 2(1):3-5.

Hao MM, Bornstein JC, Young HM. 2013. Development of myenteric cholinergic neurons in chat-cre;r26r-yfp mice. J Comp Neurol. 521(14):3358-3370.

Hao MM, Young HM. 2009. Development of enteric neuron diversity. J Cell Mol Med. 13(7):1193-1210.

Heanue TA, Pachnis V. 2006. Expression profiling the developing mammalian enteric nervous system identifies marker and candidate hirschsprung disease genes. Proc Natl Acad Sci U S A. 103(18):6919-6924.

Heanue TA, Pachnis V. 2007. Enteric nervous system development and hirschsprung's disease: Advances in genetic and stem cell studies. Nat Rev Neurosci. 8(6):466-479.

Heanue TA, Pachnis V. 2008. Ret isoform function and marker gene expression in the enteric nervous system is conserved across diverse vertebrate species. Mech Dev. 125(8):687-699.

Hearn CJ, Murphy M, Newgreen D. 1998. Gdnf and et-3 differentially modulate the numbers of avian enteric neural crest cells and enteric neurons in vitro. Dev Biol. 197(1):93-105.

Heinz S, Benner C, Spann N, Bertolino E, Lin YC, Laslo P, Cheng JX, Murre C, Singh H, Glass CK. 2010. Simple combinations of lineage-determining transcription factors prime cis-

regulatory elements required for macrophage and b cell identities. Mol Cell. 38(4):576-589.
Heldin CH, Miyazono K, ten Dijke P. 1997. Tgf-beta signalling from cell membrane to nucleus through smad proteins. Nature. 390(6659):465-471.
Henrique D, Abranches E, Verrier L, Storey KG. 2015. Neuromesodermal progenitors and the making of the spinal cord. Development. 142(17):2864-2875.
Hernandez-Lagunas L, Powell DR, Law J, Grant KA, Artinger KB. 2011. Prdm1a and olig4 act downstream of notch signaling to regulate cell fate at the neural plate border. Dev Biol. 356(2):496-505.
Heuckeroth RO, Lampe PA, Johnson EM, Milbrandt J. 1998. Neurturin and gdnf promote proliferation and survival of enteric neuron and glial progenitors in vitro. Dev Biol. 200(1):116-129.
His W. 1868. Untersuchungen über die erste anlage des wirbelthierleibes : Die erste entwickelung des hühnchens im ei. Leipzig: F.C.W. Vogel.
Hoffman TL, Javier AL, Campeau SA, Knight RD, Schilling TF. 2007. Tfap2 transcription factors in zebrafish neural crest development and ectodermal evolution. J Exp Zool B Mol Dev Evol. 308(5):679-691.
Hong CS, Saint-Jeannet JP. 2005. Sox proteins and neural crest development. Semin Cell Dev Biol. 16(6):694-703.
Hong CS, Saint-Jeannet JP. 2007. The activity of pax3 and zic1 regulates three distinct cell fates at the neural plate border. Mol Biol Cell. 18(6):2192-2202.
Hosoda K, Hammer RE, Richardson JA, Baynash AG, Cheung JC, Giaid A, Yanagisawa M. 1994. Targeted and natural (piebald-lethal) mutations of endothelin-b receptor gene produce megacolon associated with spotted coat color in mice. Cell. 79(7):1267-1276.
Hough SR, Thornton M, Mason E, Mar JC, Wells CA, Pera MF. 2014. Single-cell gene expression profiles define self-renewing, pluripotent, and lineage primed states of human pluripotent stem cells. Stem Cell Reports. 2(6):881-895.
Huang M, Miller ML, McHenry LK, Zheng T, Zhen Q, Ilkhanizadeh S, Conklin BR, Bronner ME, Weiss WA. 2016. Generating trunk neural crest from human pluripotent stem cells. Sci Rep. 6:19727.
Huang SM, Mishina YM, Liu S, Cheung A, Stegmeier F, Michaud GA, Charlat O, Wiellette E, Zhang Y, Wiessner S et al. 2009. Tankyrase inhibition stabilizes axin and antagonizes wnt signalling. Nature. 461(7264):614-620.
Hunt P, Gulisano M, Cook M, Sham MH, Faiella A, Wilkinson D, Boncinelli E, Krumlauf R. 1991. A distinct hox code for the branchial region of the vertebrate head. Nature. 353(6347):861-864.
Hutchins EJ, Kunttas E, Piacentino ML, Howard AGAt, Bronner ME, Uribe RA. 2018. Migration and diversification of the vagal neural crest. Dev Biol. 444 Suppl 1(Suppl 1):S98-S109.
Ikeya M, Lee SM, Johnson JE, McMahon AP, Takada S. 1997. Wnt signalling required for expansion of neural crest and cns progenitors. Nature. 389(6654):966-970.
Ingram WJ, McCue KI, Tran TH, Hallahan AR, Wainwright BJ. 2008. Sonic hedgehog regulates hes1 through a novel mechanism that is independent of canonical notch pathway signalling. Oncogene. 27(10):1489-1500.
Irshad S, Bansal M, Guarnieri P, Davis H, Al Haj Zen A, Baran B, Pinna CMA, Rahman H, Biswas S, Bardella C et al. 2017. Bone morphogenetic protein and notch signalling crosstalk in poor-prognosis, mesenchymal-subtype colorectal cancer. J Pathol. 242(2):178-192.

Isern J, Garcia-Garcia A, Martin AM, Arranz L, Martin-Perez D, Torroja C, Sanchez-Cabo F, Mendez-Ferrer S. 2014. The neural crest is a source of mesenchymal stem cells with specialized hematopoietic stem cell niche function. Elife. 3:e03696.

Iyyanar PPR, Wu Z, Lan Y, Hu YC, Jiang R. 2022. Alx1 deficient mice recapitulate craniofacial phenotype and reveal developmental basis of alx1-related frontonasal dysplasia. Front Cell Dev Biol. 10:777887.

Javali A, Misra A, Leonavicius K, Acharyya D, Vyas B, Sambasivan R. 2017. Co-expression of tbx6 and sox2 identifies a novel transient neuromesoderm progenitor cell state. Development. 144(24):4522-4529.

Jho EH, Zhang T, Domon C, Joo CK, Freund JN, Costantini F. 2002. Wnt/beta-catenin/tcf signaling induces the transcription of axin2, a negative regulator of the signaling pathway. Mol Cell Biol. 22(4):1172-1183.

Johnsen JI, Dyberg C, Wickstrom M. 2019. Neuroblastoma-a neural crest derived embryonal malignancy. Front Mol Neurosci. 12:9.

Joseph NM, Mukouyama YS, Mosher JT, Jaegle M, Crone SA, Dormand EL, Lee KF, Meijer D, Anderson DJ, Morrison SJ. 2004. Neural crest stem cells undergo multilineage differentiation in developing peripheral nerves to generate endoneurial fibroblasts in addition to schwann cells. Development. 131(22):5599-5612.

Kam MK, Lui VC. 2015. Roles of hoxb5 in the development of vagal and trunk neural crest cells. Dev Growth Differ. 57(2):158-168.

Kang YN, Fung C, Vanden Berghe P. 2021. Gut innervation and enteric nervous system development: A spatial, temporal and molecular tour de force. Development. 148(3).

Kapur RP. 2000. Colonization of the murine hindgut by sacral crest-derived neural precursors: Experimental support for an evolutionarily conserved model. Dev Biol. 227(1):146-155.

Kastriti ME, Faure L, Von Ahsen D, Bouderlique TG, Bostrom J, Solovieva T, Jackson C, Bronner M, Meijer D, Hadjab S et al. 2022. Schwann cell precursors represent a neural crest-like state with biased multipotency. EMBO J. 41(17):e108780.

Kastriti ME, Kameneva P, Kamenev D, Dyachuk V, Furlan A, Hampl M, Memic F, Marklund U, Lallemend F, Hadjab S et al. 2019. Schwann cell precursors generate the majority of chromaffin cells in zuckerkandl organ and some sympathetic neurons in paraganglia. Front Mol Neurosci. 12:6.

Kempf H, Olmer R, Haase A, Franke A, Bolesani E, Schwanke K, Robles-Diaz D, Coffee M, Gohring G, Drager G et al. 2016. Bulk cell density and wnt/tgfbeta signalling regulate mesendodermal patterning of human pluripotent stem cells. Nat Commun. 7:13602.

Kerosuo L, Nie S, Bajpai R, Bronner ME. 2015. Crestospheres: Long-term maintenance of multipotent, premigratory neural crest stem cells. Stem Cell Reports. 5(4):499-507.

Kil SH, Krull CE, Cann G, Clegg D, Bronner-Fraser M. 1998. The alpha4 subunit of integrin is important for neural crest cell migration. Dev Biol. 202(1):29-42.

Kim J, Lo L, Dormand E, Anderson DJ. 2003. Sox10 maintains multipotency and inhibits neuronal differentiation of neural crest stem cells. Neuron. 38(1):17-31.

Kim WK, Kwon Y, Jang M, Park M, Kim J, Cho S, Jang DG, Lee WB, Jung SH, Choi HJ et al. 2019. Beta-catenin activation down-regulates cell-cell junction-related genes and induces epithelial-to-mesenchymal transition in colorectal cancers. Sci Rep. 9(1):18440.

Kim YJ, Lim H, Li Z, Oh Y, Kovlyagina I, Choi IY, Dong X, Lee G. 2014. Generation of multipotent induced neural crest by direct reprogramming of human postnatal fibroblasts with a single transcription factor. Cell Stem Cell. 15(4):497-506.

Kirby ML, Gale TF, Stewart DE. 1983. Neural crest cells contribute to normal aorticopulmonary septation. Science. 220(4601):1059-1061.

Kirino K, Nakahata T, Taguchi T, Saito MK. 2018. Efficient derivation of sympathetic neurons from human pluripotent stem cells with a defined condition. Sci Rep. 8(1):12865.
Koch F, Scholze M, Wittler L, Schifferl D, Sudheer S, Grote P, Timmermann B, Macura K, Herrmann BG. 2017. Antagonistic activities of sox2 and brachyury control the fate choice of neuro-mesodermal progenitors. Dev Cell. 42(5):514-526 e517.
Kohler G, Milstein C. 1975. Continuous cultures of fused cells secreting antibody of predefined specificity. Nature. 256(5517):495-497.
Kontges G, Lumsden A. 1996. Rhombencephalic neural crest segmentation is preserved throughout craniofacial ontogeny. Development. 122(10):3229-3242.
Kopan R, Ilagan MX. 2004. Gamma-secretase: Proteasome of the membrane? Nat Rev Mol Cell Biol. 5(6):499-504.
Korinek V, Barker N, Morin PJ, van Wichen D, de Weger R, Kinzler KW, Vogelstein B, Clevers H. 1997. Constitutive transcriptional activation by a beta-catenin-tcf complex in apc-/- colon carcinoma. Science. 275(5307):1784-1787.
Kos R, Reedy MV, Johnson RL, Erickson CA. 2001. The winged-helix transcription factor foxd3 is important for establishing the neural crest lineage and repressing melanogenesis in avian embryos. Development. 128(8):1467-1479.
Kreitzer FR, Salomonis N, Sheehan A, Huang M, Park JS, Spindler MJ, Lizarraga P, Weiss WA, So PL, Conklin BR. 2013. A robust method to derive functional neural crest cells from human pluripotent stem cells. Am J Stem Cells. 2(2):119-131.
Kruger GM, Mosher JT, Bixby S, Joseph N, Iwashita T, Morrison SJ. 2002. Neural crest stem cells persist in the adult gut but undergo changes in self-renewal, neuronal subtype potential, and factor responsiveness. Neuron. 35(4):657-669.
Kudoh T, Wilson SW, Dawid IB. 2002. Distinct roles for fgf, wnt and retinoic acid in posteriorizing the neural ectoderm. Development. 129(18):4335-4346.
Kuil LE, Kakiailatu N, Windster JD, Bindels E, Zink JTM, van der Zee G, Hofstra RMW, Shepherd IT, Melotte V, Alves MM. 2022. Unbiased intestinal single cell transcriptomics reveals previously uncharacterized enteric nervous system populations in larval zebrafish. bioRxiv.2022.2008.2011.503619.
Kuo BR, Erickson CA. 2010. Regional differences in neural crest morphogenesis. Cell Adh Migr. 4(4):567-585.
Kuo BR, Erickson CA. 2011. Vagal neural crest cell migratory behavior: A transition between the cranial and trunk crest. Dev Dyn. 240(9):2084-2100.
Kustermann A, Neuhuber W, Brehmer A. 2011. Calretinin and somatostatin immunoreactivities label different human submucosal neuron populations. Anat Rec (Hoboken). 294(5):858-869.
Kwon HJ, Bhat N, Sweet EM, Cornell RA, Riley BB. 2010. Identification of early requirements for preplacodal ectoderm and sensory organ development. PLoS Genet. 6(9):e1001133.
LaBonne C, Bronner-Fraser M. 1998. Neural crest induction in xenopus: Evidence for a two-signal model. Development. 125(13):2403-2414.
Laddach A, Chng SH, Lasrado R, Progatzky F, Shapiro M, Artemov A, Castaneda MS, Erickson A, Bon-Frauches AC, Kleinjung J et al. 2022. A branching model of cell fate decisions in the enteric nervous system. bioRxiv.2022.2007.2012.499640.
Lai FP, Lau ST, Wong JK, Gui H, Wang RX, Zhou T, Lai WH, Tse HF, Tam PK, Garcia-Barcelo MM et al. 2017. Correction of hirschsprung-associated mutations in human induced pluripotent stem cells via clustered regularly interspaced short palindromic repeats/cas9, restores neural crest cell function. Gastroenterology. 153(1):139-153 e138.

Laing O, Halliwell J, Barbaric I. 2019. Rapid pcr assay for detecting common genetic variants arising in human pluripotent stem cell cultures. Curr Protoc Stem Cell Biol. 49(1):e83.
Lake JI, Heuckeroth RO. 2013. Enteric nervous system development: Migration, differentiation, and disease. Am J Physiol Gastrointest Liver Physiol. 305(1):G1-24.
Lang D, Chen F, Milewski R, Li J, Lu MM, Epstein JA. 2000. Pax3 is required for enteric ganglia formation and functions with sox10 to modulate expression of c-ret. J Clin Invest. 106(8):963-971.
Lang D, Epstein JA. 2003. Sox10 and pax3 physically interact to mediate activation of a conserved c-ret enhancer. Hum Mol Genet. 12(8):937-945.
Langmead B, Salzberg SL. 2012. Fast gapped-read alignment with bowtie 2. Nat Methods. 9(4):357-359.
Lasrado R, Boesmans W, Kleinjung J, Pin C, Bell D, Bhaw L, McCallum S, Zong H, Luo L, Clevers H et al. 2017. Lineage-dependent spatial and functional organization of the mammalian enteric nervous system. Science. 356(6339):722-726.
Lau ST, Li Z, Pui-Ling Lai F, Nga-Chu Lui K, Li P, Munera JO, Pan G, Mahe MM, Hui CC, Wells JM et al. 2019. Activation of hedgehog signaling promotes development of mouse and human enteric neural crest cells, based on single-cell transcriptome analyses. Gastroenterology. 157(6):1556-1571 e1555.
Le Douarin N. 1973. A biological cell labeling technique and its use in expermental embryology. Dev Biol. 30(1):217-222.
Le Douarin NM, Creuzet S, Couly G, Dupin E. 2004. Neural crest cell plasticity and its limits. Development. 131(19):4637-4650.
Le Douarin NM, Teillet MA. 1973. The migration of neural crest cells to the wall of the digestive tract in avian embryo. J Embryol Exp Morphol. 30(1):31-48.
Le Douarin NM, Teillet MA. 1974. Experimental analysis of the migration and differentiation of neuroblasts of the autonomic nervous system and of neurectodermal mesenchymal derivatives, using a biological cell marking technique. Dev Biol. 41(1):162-184.
Le Lievre CS. 1978. Participation of neural crest-derived cells in the genesis of the skull in birds. J Embryol Exp Morphol. 47:17-37.
Le Lievre CS, Le Douarin NM. 1975. Mesenchymal derivatives of the neural crest: Analysis of chimaeric quail and chick embryos. J Embryol Exp Morphol. 34(1):125-154.
Le MNT, Takahi M, Ohnuma K. 2021. Auto/paracrine factors and early wnt inhibition promote cardiomyocyte differentiation from human induced pluripotent stem cells at initial low cell density. Sci Rep. 11(1):21426.
LeBlanc L, Kim M, Kambhampati A, Son AJ, Ramirez N, Kim J. 2022. Beta-catenin links cell seeding density to global gene expression during mouse embryonic stem cell differentiation. iScience. 25(1):103541.
Lecarpentier Y, Schussler O, Hebert JL, Vallee A. 2019. Multiple targets of the canonical wnt/beta-catenin signaling in cancers. Front Oncol. 9:1248.
Lee G, Chambers SM, Tomishima MJ, Studer L. 2010. Derivation of neural crest cells from human pluripotent stem cells. Nature protocols. 5(4):688-701.
Lee G, Kim H, Elkabetz Y, Al Shamy G, Panagiotakos G, Barberi T, Tabar V, Studer L. 2007. Isolation and directed differentiation of neural crest stem cells derived from human embryonic stem cells. Nat Biotechnol. 25(12):1468-1475.
Leibl MA, Ota T, Woodward MN, Kenny SE, Lloyd DA, Vaillant CR, Edgar DH. 1999. Expression of endothelin 3 by mesenchymal cells of embryonic mouse caecum. Gut. 44(2):246-252.

Leung AW, Kent Morest D, Li JY. 2013. Differential bmp signaling controls formation and differentiation of multipotent preplacodal ectoderm progenitors from human embryonic stem cells. Dev Biol. 379(2):208-220.

Leung AW, Murdoch B, Salem AF, Prasad MS, Gomez GA, Garcia-Castro MI. 2016. Wnt/beta-catenin signaling mediates human neural crest induction via a pre-neural border intermediate. Development. 143(3):398-410.

Leussink B, Brouwer A, el Khattabi M, Poelmann RE, Gittenberger-de Groot AC, Meijlink F. 1995. Expression patterns of the paired-related homeobox genes mhox/prx1 and s8/prx2 suggest roles in development of the heart and the forebrain. Mech Dev. 52(1):51-64.

Lewis JL, Bonner J, Modrell M, Ragland JW, Moon RT, Dorsky RI, Raible DW. 2004. Reiterated wnt signaling during zebrafish neural crest development. Development. 131(6):1299-1308.

Li B, Dewey CN. 2011. Rsem: Accurate transcript quantification from rna-seq data with or without a reference genome. BMC Bioinformatics. 12:323.

Li H, Durbin R. 2009. Fast and accurate short read alignment with burrows-wheeler transform. Bioinformatics. 25(14):1754-1760.

Li W, Huang L, Zeng J, Lin W, Li K, Sun J, Huang W, Chen J, Wang G, Ke Q et al. 2018. Characterization and transplantation of enteric neural crest cells from human induced pluripotent stem cells. Mol Psychiatry. 23(3):499-508.

Li Z, Chalazonitis A, Huang YY, Mann JJ, Margolis KG, Yang QM, Kim DO, Cote F, Mallet J, Gershon MD. 2011. Essential roles of enteric neuronal serotonin in gastrointestinal motility and the development/survival of enteric dopaminergic neurons. J Neurosci. 31(24):8998-9009.

Li ZS, Pham TD, Tamir H, Chen JJ, Gershon MD. 2004. Enteric dopaminergic neurons: Definition, developmental lineage, and effects of extrinsic denervation. J Neurosci. 24(6):1330-1339.

Lignell A, Kerosuo L, Streichan SJ, Cai L, Bronner ME. 2017. Identification of a neural crest stem cell niche by spatial genomic analysis. Nat Commun. 8(1):1830.

Ling ITC, Sauka-Spengler T. 2019. Early chromatin shaping predetermines multipotent vagal neural crest into neural, neuronal and mesenchymal lineages. Nat Cell Biol. 21(12):1504-1517.

Linville A, Gumusaneli E, Chandraratna RA, Schilling TF. 2004. Independent roles for retinoic acid in segmentation and neuronal differentiation in the zebrafish hindbrain. Dev Biol. 270(1):186-199.

Lippmann ES, Estevez-Silva MC, Ashton RS. 2014. Defined human pluripotent stem cell culture enables highly efficient neuroepithelium derivation without small molecule inhibitors. Stem Cells. 32(4):1032-1042.

Lippmann ES, Williams CE, Ruhl DA, Estevez-Silva MC, Chapman ER, Coon JJ, Ashton RS. 2015. Deterministic hox patterning in human pluripotent stem cell-derived neuroectoderm. Stem Cell Reports. 4(4):632-644.

Liu JA, Wu MH, Yan CH, Chau BK, So H, Ng A, Chan A, Cheah KS, Briscoe J, Cheung M. 2013a. Phosphorylation of sox9 is required for neural crest delamination and is regulated downstream of bmp and canonical wnt signaling. Proc Natl Acad Sci U S A. 110(8):2882-2887.

Liu JP, Laufer E, Jessell TM. 2001. Assigning the positional identity of spinal motor neurons: Rostrocaudal patterning of hox-c expression by fgfs, gdf11, and retinoids. Neuron. 32(6):997-1012.

Liu KJ, Arron JR, Stankunas K, Crabtree GR, Longaker MT. 2007. Chemical rescue of cleft palate and midline defects in conditional gsk-3beta mice. Nature. 446(7131):79-82.

Liu XH, Wu Y, Yao S, Levine AC, Kirschenbaum A, Collier L, Bauman WA, Cardozo CP. 2013b. Androgens up-regulate transcription of the notch inhibitor numb in c2c12 myoblasts via wnt/beta-catenin signaling to t cell factor elements in the numb promoter. J Biol Chem. 288(25):17990-17998.

Livak KJ, Schmittgen TD. 2001. Analysis of relative gene expression data using real-time quantitative pcr and the 2(-delta delta c(t)) method. Methods. 25(4):402-408.

Lo LC, Johnson JE, Wuenschell CW, Saito T, Anderson DJ. 1991. Mammalian achaete-scute homolog 1 is transiently expressed by spatially restricted subsets of early neuroepithelial and neural crest cells. Genes Dev. 5(9):1524-1537.

Louvi A, Artavanis-Tsakonas S. 2006. Notch signalling in vertebrate neural development. Nat Rev Neurosci. 7(2):93-102.

Love MI, Huber W, Anders S. 2014. Moderated estimation of fold change and dispersion for rna-seq data with deseq2. Genome Biol. 15(12):550.

Ludwig TE, Bergendahl V, Levenstein ME, Yu J, Probasco MD, Thomson JA. 2006. Feeder-independent culture of human embryonic stem cells. Nat Methods. 3(8):637-646.

Lui VC, Cheng WW, Leon TY, Lau DK, Garcia-Barcelo MM, Miao XP, Kam MK, So MT, Chen Y, Wall NA et al. 2008. Perturbation of hoxb5 signaling in vagal neural crests down-regulates ret leading to intestinal hypoganglionosis in mice. Gastroenterology. 134(4):1104-1115.

Lukoseviciute M, Mayes S, Sauka-Spengler T. 2021. Neuromesodermal progenitor origin of trunk neural crest in vivo. bioRxiv.2021.2002.2010.430513.

Lumsden A, Guthrie S. 1991. Alternating patterns of cell surface properties and neural crest cell migration during segmentation of the chick hindbrain. Dev Suppl. Suppl 2:9-15.

Luo T, Matsuo-Takasaki M, Thomas ML, Weeks DL, Sargent TD. 2002. Transcription factor ap-2 is an essential and direct regulator of epidermal development in xenopus. Dev Biol. 245(1):136-144.

Lustig B, Jerchow B, Sachs M, Weiler S, Pietsch T, Karsten U, van de Wetering M, Clevers H, Schlag PM, Birchmeier W et al. 2002. Negative feedback loop of wnt signaling through upregulation of conductin/axin2 in colorectal and liver tumors. Mol Cell Biol. 22(4):1184-1193.

MacDonald BT, Tamai K, He X. 2009. Wnt/beta-catenin signaling: Components, mechanisms, and diseases. Dev Cell. 17(1):9-26.

Maczkowiak F, Mateos S, Wang E, Roche D, Harland R, Monsoro-Burq AH. 2010. The pax3 and pax7 paralogs cooperate in neural and neural crest patterning using distinct molecular mechanisms, in xenopus laevis embryos. Dev Biol. 340(2):381-396.

Maguire LH, Thomas AR, Goldstein AM. 2015. Tumors of the neural crest: Common themes in development and cancer. Dev Dyn. 244(3):311-322.

Majd H, Samuel RM, Ramirez JT, Kalantari A, Barber K, Ghazizadeh Z, Chemel AK, Cesiulis A, Richter MN, Das S et al. 2022. Hpsc-derived enteric ganglioids model human ens development and function. bioRxiv.2022.2001.2004.474746.

Maltman DJ, Christie VB, Collings JC, Barnard JH, Fenyk S, Marder TB, Whiting A, Przyborski SA. 2009. Proteomic profiling of the stem cell response to retinoic acid and synthetic retinoid analogues: Identification of major retinoid-inducible proteins. Mol Biosyst. 5(5):458-471.

Manderfield LJ, High FA, Engleka KA, Liu F, Li L, Rentschler S, Epstein JA. 2012. Notch activation of jagged1 contributes to the assembly of the arterial wall. Circulation. 125(2):314-323.

Mansouri A, Stoykova A, Torres M, Gruss P. 1996. Dysgenesis of cephalic neural crest derivatives in pax7-/- mutant mice. Development. 122(3):831-838.

Manthorpe M, Engvall E, Ruoslahti E, Longo FM, Davis GE, Varon S. 1983. Laminin promotes neuritic regeneration from cultured peripheral and central neurons. J Cell Biol. 97(6):1882-1890.

Marchant L, Linker C, Ruiz P, Guerrero N, Mayor R. 1998. The inductive properties of mesoderm suggest that the neural crest cells are specified by a bmp gradient. Dev Biol. 198(2):319-329.

Marczenke M, Sunaga-Franze DY, Popp O, Althaus IW, Sauer S, Mertins P, Christ A, Allen BL, Willnow TE. 2021. Gas1 is required for notch-dependent facilitation of shh signaling in the ventral forebrain neuroepithelium. Development. 148(21).

Marshall H, Studer M, Popperl H, Aparicio S, Kuroiwa A, Brenner S, Krumlauf R. 1994. A conserved retinoic acid response element required for early expression of the homeobox gene hoxb-1. Nature. 370(6490):567-571.

Martin BL. 2016. Factors that coordinate mesoderm specification from neuromesodermal progenitors with segmentation during vertebrate axial extension. Semin Cell Dev Biol. 49:59-67.

Mason JM, Morrison DJ, Basson MA, Licht JD. 2006. Sprouty proteins: Multifaceted negative-feedback regulators of receptor tyrosine kinase signaling. Trends Cell Biol. 16(1):45-54.

Massey J, Liu Y, Alvarenga O, Saez T, Schmerer M, Warmflash A. 2019. Synergy with tgfbeta ligands switches wnt pathway dynamics from transient to sustained during human pluripotent cell differentiation. Proc Natl Acad Sci U S A. 116(11):4989-4998.

Matsuda M, Koga M, Woltjen K, Nishida E, Ebisuya M. 2015. Synthetic lateral inhibition governs cell-type bifurcation with robust ratios. Nat Commun. 6:6195.

Matsuo I, Kuratani S, Kimura C, Takeda N, Aizawa S. 1995. Mouse otx2 functions in the formation and patterning of rostral head. Genes Dev. 9(21):2646-2658.

Matsuzawa M, Weight FF, Potember RS, Liesi P. 1996. Directional neurite outgrowth and axonal differentiation of embryonic hippocampal neurons are promoted by a neurite outgrowth domain of the b2-chain of laminin. Int J Dev Neurosci. 14(3):283-295.

Mayor R, Guerrero N, Martinez C. 1997. Role of fgf and noggin in neural crest induction. Dev Biol. 189(1):1-12.

Mazzoni EO, Mahony S, Peljto M, Patel T, Thornton SR, McCuine S, Reeder C, Boyer LA, Young RA, Gifford DK et al. 2013. Saltatory remodeling of hox chromatin in response to rostrocaudal patterning signals. Nat Neurosci. 16(9):1191-1198.

McCann CJ, Alves MM, Brosens E, Natarajan D, Perin S, Chapman C, Hofstra RM, Burns AJ, Thapar N. 2019. Neuronal development and onset of electrical activity in the human enteric nervous system. Gastroenterology. 156(5):1483-1495 e1486.

McDonald-McGinn DM, Sullivan KE. 2011. Chromosome 22q11.2 deletion syndrome (digeorge syndrome/velocardiofacial syndrome). Medicine (Baltimore). 90(1):1-18.

McGonnell IM, Graham A. 2002. Trunk neural crest has skeletogenic potential. Curr Biol. 12(9):767-771.

McGrew LL, Lai CJ, Moon RT. 1995. Specification of the anteroposterior neural axis through synergistic interaction of the wnt signaling cascade with noggin and follistatin. Dev Biol. 172(1):337-342.

McKeown SJ, Lee VM, Bronner-Fraser M, Newgreen DF, Farlie PG. 2005. Sox10 overexpression induces neural crest-like cells from all dorsoventral levels of the neural tube but inhibits differentiation. Dev Dyn. 233(2):430-444.

Mead TJ, Yutzey KE. 2012. Notch pathway regulation of neural crest cell development in vivo. Dev Dyn. 241(2):376-389.

Menendez L, Yatskievych TA, Antin PB, Dalton S. 2011. Wnt signaling and a smad pathway blockade direct the differentiation of human pluripotent stem cells to multipotent neural crest cells. Proc Natl Acad Sci U S A. 108(48):19240-19245.

Metzis V, Steinhauser S, Pakanavicius E, Gouti M, Stamataki D, Ivanovitch K, Watson T, Rayon T, Mousavy Gharavy SN, Lovell-Badge R et al. 2018. Nervous system regionalization entails axial allocation before neural differentiation. Cell. 175(4):1105-1118 e1117.

Meyers EN, Lewandoski M, Martin GR. 1998. An fgf8 mutant allelic series generated by cre- and flp-mediated recombination. Nat Genet. 18(2):136-141.

Mica Y, Lee G, Chambers SM, Tomishima MJ, Studer L. 2013. Modeling neural crest induction, melanocyte specification, and disease-related pigmentation defects in hescs and patient-specific ipscs. Cell Rep. 3(4):1140-1152.

Mikkelsen TS, Ku M, Jaffe DB, Issac B, Lieberman E, Giannoukos G, Alvarez P, Brockman W, Kim TK, Koche RP et al. 2007. Genome-wide maps of chromatin state in pluripotent and lineage-committed cells. Nature. 448(7153):553-560.

Mikkola I, Bruun JA, Holm T, Johansen T. 2001. Superactivation of pax6-mediated transactivation from paired domain-binding sites by dna-independent recruitment of different homeodomain proteins. J Biol Chem. 276(6):4109-4118.

Minoux M, Rijli FM. 2010. Molecular mechanisms of cranial neural crest cell migration and patterning in craniofacial development. Development. 137(16):2605-2621.

Mitchell PJ, Timmons PM, Hebert JM, Rigby PW, Tjian R. 1991. Transcription factor ap-2 is expressed in neural crest cell lineages during mouse embryogenesis. Genes Dev. 5(1):105-119.

Mohlin S, Kunttas E, Persson CU, Abdel-Haq R, Castillo A, Murko C, Bronner ME, Kerosuo L. 2019. Maintaining multipotent trunk neural crest stem cells as self-renewing crestospheres. Dev Biol. 447(2):137-146.

Monsoro-Burq AH, Fletcher RB, Harland RM. 2003. Neural crest induction by paraxial mesoderm in xenopus embryos requires fgf signals. Development. 130(14):3111-3124.

Monsoro-Burq AH, Wang E, Harland R. 2005. Msx1 and pax3 cooperate to mediate fgf8 and wnt signals during xenopus neural crest induction. Dev Cell. 8(2):167-178.

Montero JA, Giron B, Arrechedera H, Cheng YC, Scotting P, Chimal-Monroy J, Garcia-Porrero JA, Hurle JM. 2002. Expression of sox8, sox9 and sox10 in the developing valves and autonomic nerves of the embryonic heart. Mech Dev. 118(1-2):199-202.

Morarach K, Mikhailova A, Knoflach V, Memic F, Kumar R, Li W, Ernfors P, Marklund U. 2021. Diversification of molecularly defined myenteric neuron classes revealed by single-cell rna sequencing. Nat Neurosci. 24(1):34-46.

Morrison SJ, Perez SE, Qiao Z, Verdi JM, Hicks C, Weinmaster G, Anderson DJ. 2000. Transient notch activation initiates an irreversible switch from neurogenesis to gliogenesis by neural crest stem cells. Cell. 101(5):499-510.

Morrison SJ, White PM, Zock C, Anderson DJ. 1999. Prospective identification, isolation by flow cytometry, and in vivo self-renewal of multipotent mammalian neural crest stem cells. Cell. 96(5):737-749.

Motohashi T, Watanabe N, Nishioka M, Nakatake Y, Yulan P, Mochizuki H, Kawamura Y, Ko MS, Goshima N, Kunisada T. 2016. Gene array analysis of neural crest cells identifies transcription factors necessary for direct conversion of embryonic fibroblasts into neural crest cells. Biol Open. 5(3):311-322.

Mouilleau V, Vaslin C, Robert R, Gribaudo S, Nicolas N, Jarrige M, Terray A, Lesueur L, Mathis MW, Croft G et al. 2021. Dynamic extrinsic pacing of the hox clock in human axial progenitors controls motor neuron subtype specification. Development. 148(6).

Mugele D, Moulding DA, Savery D, Molè MA, Greene NDE, Martinez-Barbera JP, Copp AJ. 2018. Genetic approaches in mice demonstrate that neuro-mesodermal progenitors express t/brachyury but not sox2. bioRxiv.503854.

Muncie JM, Ayad NME, Lakins JN, Xue X, Fu J, Weaver VM. 2020. Mechanical tension promotes formation of gastrulation-like nodes and patterns mesoderm specification in human embryonic stem cells. Dev Cell. 55(6):679-694 e611.

Murko C, Bronner ME. 2017. Tissue specific regulation of the chick sox10e1 enhancer by different sox family members. Dev Biol. 422(1):47-57.

Murphy EM, Defontgalland D, Costa M, Brookes SJ, Wattchow DA. 2007. Quantification of subclasses of human colonic myenteric neurons by immunoreactivity to hu, choline acetyltransferase and nitric oxide synthase. Neurogastroenterol Motil. 19(2):126-134.

Nagy N, Goldstein AM. 2006. Endothelin-3 regulates neural crest cell proliferation and differentiation in the hindgut enteric nervous system. Dev Biol. 293(1):203-217.

Nagy N, Goldstein AM. 2017. Enteric nervous system development: A crest cell's journey from neural tube to colon. Semin Cell Dev Biol. 66:94-106.

Nataf V, Lecoin L, Eichmann A, Le Douarin NM. 1996. Endothelin-b receptor is expressed by neural crest cells in the avian embryo. Proceedings of the National Academy of Sciences. 93(18):9645-9650.

Natarajan D, Marcos-Gutierrez C, Pachnis V, de Graaff E. 2002. Requirement of signalling by receptor tyrosine kinase ret for the directed migration of enteric nervous system progenitor cells during mammalian embryogenesis. Development. 129(22):5151-5160.

Neijts R, Amin S, van Rooijen C, Deschamps J. 2017. Cdx is crucial for the timing mechanism driving colinear hox activation and defines a trunk segment in the hox cluster topology. Dev Biol. 422(2):146-154.

Ngan ES, Garcia-Barcelo MM, Yip BH, Poon HC, Lau ST, Kwok CK, Sat E, Sham MH, Wong KK, Wainwright BJ et al. 2011. Hedgehog/notch-induced premature gliogenesis represents a new disease mechanism for hirschsprung disease in mice and humans. J Clin Invest. 121(9):3467-3478.

Nguyen VH, Schmid B, Trout J, Connors SA, Ekker M, Mullins MC. 1998. Ventral and lateral regions of the zebrafish gastrula, including the neural crest progenitors, are established by a bmp2b/swirl pathway of genes. Dev Biol. 199(1):93-110.

Nguyen VH, Trout J, Connors SA, Andermann P, Weinberg E, Mullins MC. 2000. Dorsal and intermediate neuronal cell types of the spinal cord are established by a bmp signaling pathway. Development. 127(6):1209-1220.

Niederreither K, Vermot J, Le Roux I, Schuhbaur B, Chambon P, Dolle P. 2003. The regional pattern of retinoic acid synthesis by raldh2 is essential for the development of posterior pharyngeal arches and the enteric nervous system. Development. 130(11):2525-2534.

Nieuwenhuis B, Haenzi B, Andrews MR, Verhaagen J, Fawcett JW. 2018. Integrins promote axonal regeneration after injury of the nervous system. Biol Rev Camb Philos Soc. 93(3):1339-1362.

Nieuwkoop PD, Nigtevecht Gv. 1954. Neural activation and transformation in explants of competent ectoderm under the influence of fragments of anterior notochord in urodeles. Development. 2(3):175-193.

Nikitina N, Sauka-Spengler T, Bronner-Fraser M. 2008. Dissecting early regulatory relationships in the lamprey neural crest gene network. Proc Natl Acad Sci U S A. 105(51):20083-20088.

Noisa P, Lund C, Kanduri K, Lund R, Lahdesmaki H, Lahesmaa R, Lundin K, Chokechuwattanalert H, Otonkoski T, Tuuri T et al. 2014. Notch signaling regulates the differentiation of neural crest from human pluripotent stem cells. J Cell Sci. 127(Pt 9):2083-2094.

O'Sullivan A, Lange S, Rotheneichner P, Bieler L, Aigner L, Rivera FJ, Couillard-Despres S. 2019. Dimethylsulfoxide inhibits oligodendrocyte fate choice of adult neural stem and progenitor cells. Front Neurosci. 13:1242.

Oh Y, Cho GS, Li Z, Hong I, Zhu R, Kim MJ, Kim YJ, Tampakakis E, Tung L, Huganir R et al. 2016. Functional coupling with cardiac muscle promotes maturation of hpsc-derived sympathetic neurons. Cell Stem Cell. 19(1):95-106.

Ohtsuka T, Ishibashi M, Gradwohl G, Nakanishi S, Guillemot F, Kageyama R. 1999. Hes1 and hes5 as notch effectors in mammalian neuronal differentiation. EMBO J. 18(8):2196-2207.

Okamura Y, Saga Y. 2008. Notch signaling is required for the maintenance of enteric neural crest progenitors. Development. 135(21):3555-3565.

Olivera-Martinez I, Harada H, Halley PA, Storey KG. 2012. Loss of fgf-dependent mesoderm identity and rise of endogenous retinoid signalling determine cessation of body axis elongation. PLoS Biol. 10(10):e1001415.

Osumi N, Hirota A, Ohuchi H, Nakafuku M, Iimura T, Kuratani S, Fujiwara M, Noji S, Eto K. 1997. Pax-6 is involved in the specification of hindbrain motor neuron subtype. Development. 124(15):2961-2972.

Osumi-Yamashita N, Ninomiya Y, Doi H, Eto K. 1994. The contribution of both forebrain and midbrain crest cells to the mesenchyme in the frontonasal mass of mouse embryos. Dev Biol. 164(2):409-419.

Pachnis V, Mankoo B, Costantini F. 1993. Expression of the c-ret proto-oncogene during mouse embryogenesis. Development. 119(4):1005-1017.

Papaioannou VE. 2014. The t-box gene family: Emerging roles in development, stem cells and cancer. Development. 141(20):3819-3833.

Patthey C, Edlund T, Gunhaga L. 2009. Wnt-regulated temporal control of bmp exposure directs the choice between neural plate border and epidermal fate. Development. 136(1):73-83.

Patthey C, Gunhaga L, Edlund T. 2008. Early development of the central and peripheral nervous systems is coordinated by wnt and bmp signals. PLoS One. 3(2):e1625.

Pattyn A, Hirsch M, Goridis C, Brunet JF. 2000. Control of hindbrain motor neuron differentiation by the homeobox gene phox2b. Development. 127(7):1349-1358.

Pattyn A, Morin X, Cremer H, Goridis C, Brunet JF. 1999. The homeobox gene phox2b is essential for the development of autonomic neural crest derivatives. Nature. 399(6734):366-370.

Pawolski V, Schmidt MHH. 2020. Neuron-glia interaction in the developing and adult enteric nervous system. Cells. 10(1).

Pfaff SL, Mendelsohn M, Stewart CL, Edlund T, Jessell TM. 1996. Requirement for lim homeobox gene isl1 in motor neuron generation reveals a motor neuron-dependent step in interneuron differentiation. Cell. 84(2):309-320.

Phillips BT, Kwon HJ, Melton C, Houghtaling P, Fritz A, Riley BB. 2006. Zebrafish msxb, msxc and msxe function together to refine the neural-nonneural border and regulate cranial placodes and neural crest development. Dev Biol. 294(2):376-390.

Piacentino ML, Bronner ME. 2018. Intracellular attenuation of bmp signaling via ckip-1/smurf1 is essential during neural crest induction. PLoS Biol. 16(6):e2004425.

Piacentino ML, Hutchins EJ, Bronner ME. 2021. Essential function and targets of bmp signaling during midbrain neural crest delamination. Dev Biol. 477:251-261.

Pichel JG, Shen L, Sheng HZ, Granholm AC, Drago J, Grinberg A, Lee EJ, Huang SP, Saarma M, Hoffer BJ et al. 1996. Defects in enteric innervation and kidney development in mice lacking gdnf. Nature. 382(6586):73-76.

Pieper M, Ahrens K, Rink E, Peter A, Schlosser G. 2012. Differential distribution of competence for panplacodal and neural crest induction to non-neural and neural ectoderm. Development. 139(6):1175-1187.
Pilon N. 2021. Treatment and prevention of neurocristopathies. Trends Mol Med. 27(5):451-468.
Pini J, Kueper J, Hu YD, Kawasaki K, Yeung P, Tsimbal C, Yoon B, Carmichael N, Maas RL, Cotney J et al. 2022. Alx1-related frontonasal dysplasia results from defective neural crest cell development and migration. EMBO Mol Med. 14(7):e16289.
Pla P, Hirsch MR, Le Crom S, Reiprich S, Harley VR, Goridis C. 2008. Identification of phox2b-regulated genes by expression profiling of cranial motoneuron precursors. Neural Dev. 3:14.
Platt JB. 1893. Ectodermic origin of the cartilages of the head. Anat Anz. 8:506-509.
Pleasure SJ, Page C, Lee VM. 1992. Pure, postmitotic, polarized human neurons derived from ntera 2 cells provide a system for expressing exogenous proteins in terminally differentiated neurons. J Neurosci. 12(5):1802-1815.
Plouhinec JL, Roche DD, Pegoraro C, Figueiredo AL, Maczkowiak F, Brunet LJ, Milet C, Vert JP, Pollet N, Harland RM et al. 2014. Pax3 and zic1 trigger the early neural crest gene regulatory network by the direct activation of multiple key neural crest specifiers. Dev Biol. 386(2):461-472.
Polak JM, Rost FW, Pearse AG. 1971. Fluorogenic amine tracing of neural crest derivatives forming the adrenal medulla. Gen Comp Endocrinol. 16(1):132-136.
Prasad MS, Charney RM, Garcia-Castro MI. 2019. Specification and formation of the neural crest: Perspectives on lineage segregation. Genesis. 57(1):e23276.
Przybyla L, Lakins JN, Weaver VM. 2016. Tissue mechanics orchestrate wnt-dependent human embryonic stem cell differentiation. Cell Stem Cell. 19(4):462-475.
Qu ZD, Thacker M, Castelucci P, Bagyanszki M, Epstein ML, Furness JB. 2008. Immunohistochemical analysis of neuron types in the mouse small intestine. Cell Tissue Res. 334(2):147-161.
Rada-Iglesias A, Bajpai R, Prescott S, Brugmann SA, Swigut T, Wysocka J. 2012. Epigenomic annotation of enhancers predicts transcriptional regulators of human neural crest. Cell Stem Cell. 11(5):633-648.
Rao M, Gershon MD. 2016. The bowel and beyond: The enteric nervous system in neurological disorders. Nat Rev Gastroenterol Hepatol. 13(9):517-528.
Rauch U, Klotz M, Maas-Omlor S, Wink E, Hansgen A, Hagl C, Holland-Cunz S, Schafer KH. 2006. Expression of intermediate filament proteins and neuronal markers in the human fetal gut. J Histochem Cytochem. 54(1):39-46.
Reedy MV, Faraco CD, Erickson CA. 1998. Specification and migration of melanoblasts at the vagal level and in hyperpigmented silkie chickens. Dev Dyn. 213(4):476-485.
Rharass T, Lantow M, Gbankoto A, Weiss DG, Panakova D, Lucas S. 2017. Ascorbic acid alters cell fate commitment of human neural progenitors in a wnt/beta-catenin/ros signaling dependent manner. J Biomed Sci. 24(1):78.
Rocha M, Beiriger A, Kushkowski EE, Miyashita T, Singh N, Venkataraman V, Prince VE. 2020. From head to tail: Regionalization of the neural crest. Development. 147(20).
Rochtus A, Izzi B, Vangeel E, Louwette S, Wittevrongel C, Lambrechts D, Moreau Y, Winand R, Verpoorten C, Jansen K et al. 2015. DNA methylation analysis of homeobox genes implicates hoxb7 hypomethylation as risk factor for neural tube defects. Epigenetics. 10(1):92-101.
Rodrigo Albors A, Halley PA, Storey KG. 2018. Lineage tracing of axial progenitors using nkx1-2creer(t2) mice defines their trunk and tail contributions. Development. 145(19).

Roellig D, Tan-Cabugao J, Esaian S, Bronner ME. 2017. Dynamic transcriptional signature and cell fate analysis reveals plasticity of individual neural plate border cells. Elife. 6.

Ross AH, Grob P, Bothwell M, Elder DE, Ernst CS, Marano N, Ghrist BF, Slemp CC, Herlyn M, Atkinson B et al. 1984. Characterization of nerve growth factor receptor in neural crest tumors using monoclonal antibodies. Proc Natl Acad Sci U S A. 81(21):6681-6685.

Ross DA, Kadesch T. 2004. Consequences of notch-mediated induction of jagged1. Exp Cell Res. 296(2):173-182.

Rothstein M, Bhattacharya D, Simoes-Costa M. 2018. The molecular basis of neural crest axial identity. Dev Biol. 444 Suppl 1:S170-S180.

Saint-Jeannet JP, He X, Varmus HE, Dawid IB. 1997. Regulation of dorsal fate in the neuraxis by wnt-1 and wnt-3a. Proc Natl Acad Sci U S A. 94(25):13713-13718.

Saldana-Guerrero IM, Montano-Gutierrez LF, Hafemeister C, Stavish D, Shaw LE, Fetahu IS, Wenninger-Weinzierl A, Sturtzel C, Souilhol C, Tarelli S et al. 2022. Neuroblastoma-associated chromosomal aberrations drive cell identity loss in human neural crest via disruption of developmental regulators. bioRxiv.2022.2011.2021.515753.

Sanchez-Ferras O, Bernas G, Farnos O, Toure AM, Souchkova O, Pilon N. 2016. A direct role for murine cdx proteins in the trunk neural crest gene regulatory network. Development. 143(8):1363-1374.

Sander GR, Brookes SJ, Powell BC. 2003. Expression of notch1 and jagged2 in the enteric nervous system. J Histochem Cytochem. 51(7):969-972.

Sanders B, D'Andrea D, Collins MO, Rees E, Steward TGJ, Zhu Y, Chapman G, Legge SE, Pardinas AF, Harwood AJ et al. 2022. Transcriptional programs regulating neuronal differentiation are disrupted in dlg2 knockout human embryonic stem cells and enriched for schizophrenia and related disorders risk variants. Nat Commun. 13(1):27.

Sasai N, Kutejova E, Briscoe J. 2014. Integration of signals along orthogonal axes of the vertebrate neural tube controls progenitor competence and increases cell diversity. PLoS Biol. 12(7):e1001907.

Sasai N, Mizuseki K, Sasai Y. 2001. Requirement of foxd3-class signaling for neural crest determination in xenopus. Development. 128(13):2525-2536.

Sasselli V, Pachnis V, Burns AJ. 2012. The enteric nervous system. Dev Biol. 366(1):64-73.

Sato T, Sasai N, Sasai Y. 2005. Neural crest determination by co-activation of pax3 and zic1 genes in xenopus ectoderm. Development. 132(10):2355-2363.

Sato TS, Handa A, Priya S, Watal P, Becker RM, Sato Y. 2019. Neurocristopathies: Enigmatic appearances of neural crest cell-derived abnormalities. Radiographics. 39(7):2085-2102.

Sato Y, Heuckeroth RO. 2008. Retinoic acid regulates murine enteric nervous system precursor proliferation, enhances neuronal precursor differentiation, and reduces neurite growth in vitro. Dev Biol. 320(1):185-198.

Satoh K, Kasai M, Ishidao T, Tago K, Ohwada S, Hasegawa Y, Senda T, Takada S, Nada S, Nakamura T et al. 2004. Anteriorization of neural fate by inhibitor of beta-catenin and t cell factor (icat), a negative regulator of wnt signaling. Proc Natl Acad Sci U S A. 101(21):8017-8021.

Satokata I, Ma L, Ohshima H, Bei M, Woo I, Nishizawa K, Maeda T, Takano Y, Uchiyama M, Heaney S et al. 2000. Msx2 deficiency in mice causes pleiotropic defects in bone growth and ectodermal organ formation. Nat Genet. 24(4):391-395.

Sauka-Spengler T, Bronner-Fraser M. 2008. A gene regulatory network orchestrates neural crest formation. Nat Rev Mol Cell Biol. 9(7):557-568.

Sauka-Spengler T, Meulemans D, Jones M, Bronner-Fraser M. 2007. Ancient evolutionary origin of the neural crest gene regulatory network. Dev Cell. 13(3):405-420.

Schindelin J, Arganda-Carreras I, Frise E, Kaynig V, Longair M, Pietzsch T, Preibisch S, Rueden C, Saalfeld S, Schmid B et al. 2012. Fiji: An open-source platform for biological-image analysis. Nat Methods. 9(7):676-682.

Schlieve CR, Fowler KL, Thornton M, Huang S, Hajjali I, Hou X, Grubbs B, Spence JR, Grikscheit TC. 2017. Neural crest cell implantation restores enteric nervous system function and alters the gastrointestinal transcriptome in human tissue-engineered small intestine. Stem Cell Reports. 9(3):883-896.

Schlosser G, Ahrens K. 2004. Molecular anatomy of placode development in xenopus laevis. Dev Biol. 271(2):439-466.

Schoenwolf GC. 1977. Tail (end) bud contributions to the posterior region of the chick embryo. Journal of Experimental Zoology. 201(2):227-245.

Schoenwolf GC, Chandler NB, Smith JL. 1985. Analysis of the origins and early fates of neural crest cells in caudal regions of avian embryos. Dev Biol. 110(2):467-479.

Schorle H, Meier P, Buchert M, Jaenisch R, Mitchell PJ. 1996. Transcription factor ap-2 essential for cranial closure and craniofacial development. Nature. 381(6579):235-238.

Schuchardt A, D'Agati V, Larsson-Blomberg L, Costantini F, Pachnis V. 1994. Defects in the kidney and enteric nervous system of mice lacking the tyrosine kinase receptor ret. Nature. 367(6461):380-383.

Schumacher JA, Hashiguchi M, Nguyen VH, Mullins MC. 2011. An intermediate level of bmp signaling directly specifies cranial neural crest progenitor cells in zebrafish. PLoS One. 6(11):e27403.

Serbedzija GN, Bronner-Fraser M, Fraser SE. 1994. Developmental potential of trunk neural crest cells in the mouse. Development. 120(7):1709-1718.

Sergi CM, Caluseriu O, McColl H, Eisenstat DD. 2017. Hirschsprung's disease: Clinical dysmorphology, genes, micro-rnas, and future perspectives. Pediatr Res. 81(1-2):177-191.

Shah NM, Groves AK, Anderson DJ. 1996. Alternative neural crest cell fates are instructively promoted by tgfbeta superfamily members. Cell. 85(3):331-343.

Shaker MR, Lee JH, Kim KH, Ban S, Kim VJ, Kim JY, Lee JY, Sun W. 2021. Spatiotemporal contribution of neuromesodermal progenitor-derived neural cells in the elongation of developing mouse spinal cord. Life Sci. 282:119393.

Sheng G, Stern CD. 1999. Gata2 and gata3: Novel markers for early embryonic polarity and for non-neural ectoderm in the chick embryo. Mech Dev. 87(1-2):213-216.

Shields DC, Ramsbottom D, Donoghue C, Pinjon E, Kirke PN, Molloy AM, Edwards YH, Mills JL, Mynett-Johnson L, Weir DG et al. 2000. Association between historically high frequencies of neural tube defects and the human t homologue of mouse t (brachyury). Am J Med Genet. 92(3):206-211.

Simkin JE, Zhang D, Rollo BN, Newgreen DF. 2013. Retinoic acid upregulates ret and induces chain migration and population expansion in vagal neural crest cells to colonise the embryonic gut. PLoS One. 8(5):e64077.

Simoes-Costa M, Bronner ME. 2015. Establishing neural crest identity: A gene regulatory recipe. Development. 142(2):242-257.

Simoes-Costa M, Bronner ME. 2016. Reprogramming of avian neural crest axial identity and cell fate. Science. 352(6293):1570-1573.

Simoes-Costa MS, McKeown SJ, Tan-Cabugao J, Sauka-Spengler T, Bronner ME. 2012. Dynamic and differential regulation of stem cell factor foxd3 in the neural crest is encrypted in the genome. PLoS Genet. 8(12):e1003142.

Sjoqvist M, Andersson ER. 2019. Do as i say, not(ch) as i do: Lateral control of cell fate. Dev Biol. 447(1):58-70.
Soldatov R, Kaucka M, Kastriti ME, Petersen J, Chontorotzea T, Englmaier L, Akkuratova N, Yang Y, Haring M, Dyachuk V et al. 2019. Spatiotemporal structure of cell fate decisions in murine neural crest. Science. 364(6444).
Southard-Smith EM, Kos L, Pavan WJ. 1998. Sox10 mutation disrupts neural crest development in dom hirschsprung mouse model. Nat Genet. 18(1):60-64.
Spokony RF, Aoki Y, Saint-Germain N, Magner-Fink E, Saint-Jeannet JP. 2002. The transcription factor sox9 is required for cranial neural crest development in xenopus. Development. 129(2):421-432.
Stamp LA. 2017. Cell therapy for gi motility disorders: Comparison of cell sources and proposed steps for treating hirschsprung disease. Am J Physiol Gastrointest Liver Physiol. 312(4):G348-G354.
Stavish D, Boiers C, Price C, Frith TJR, Halliwell J, Saldana-Guerrero I, Wray J, Brown J, Carr J, James C et al. 2020. Generation and trapping of a mesoderm biased state of human pluripotency. Nat Commun. 11(1):4989.
Steventon B, Araya C, Linker C, Kuriyama S, Mayor R. 2009. Differential requirements of bmp and wnt signalling during gastrulation and neurulation define two steps in neural crest induction. Development. 136(5):771-779.
Stottmann RW, Klingensmith J. 2011. Bone morphogenetic protein signaling is required in the dorsal neural folds before neurulation for the induction of spinal neural crest cells and dorsal neurons. Dev Dyn. 240(4):755-765.
Streit A, Stern CD. 1999. Neural induction. A bird's eye view. Trends Genet. 15(1):20-24.
Stuhlmiller TJ, Garcia-Castro MI. 2012a. Current perspectives of the signaling pathways directing neural crest induction. Cell Mol Life Sci. 69(22):3715-3737.
Stuhlmiller TJ, Garcia-Castro MI. 2012b. Fgf/mapk signaling is required in the gastrula epiblast for avian neural crest induction. Development. 139(2):289-300.
Tahtakran SA, Selleck MA. 2003. Ets-1 expression is associated with cranial neural crest migration and vasculogenesis in the chick embryo. Gene Expr Patterns. 3(4):455-458.
Tam PK. 2016. Hirschsprung's disease: A bridge for science and surgery. J Pediatr Surg. 51(1):18-22.
Tang W, Bronner ME. 2020. Neural crest lineage analysis: From past to future trajectory. Development. 147(20).
Tang W, Jacobs-Li J, Li C, Bronner ME. 2022. Single-cell profiling coupled with lineage analysis reveals distinct sacral neural crest contributions to the developing enteric nervous system. bioRxiv.2022.2005.2009.491197.
Tapper EJ, Lewand DL. 1981. Actions of a nicotinic agonist, dmpp, on intestinal ion transport in vitro. Life Sci. 28(2):155-162.
Taraviras S, Marcos-Gutierrez CV, Durbec P, Jani H, Grigoriou M, Sukumaran M, Wang LC, Hynes M, Raisman G, Pachnis V. 1999. Signalling by the ret receptor tyrosine kinase and its role in the development of the mammalian enteric nervous system. Development. 126(12):2785-2797.
Taylor MK, Yeager K, Morrison SJ. 2007. Physiological notch signaling promotes gliogenesis in the developing peripheral and central nervous systems. Development. 134(13):2435-2447.
Teillet MA, Kalcheim C, Le Douarin NM. 1987. Formation of the dorsal root ganglia in the avian embryo: Segmental origin and migratory behavior of neural crest progenitor cells. Dev Biol. 120(2):329-347.

Teng L, Mundell NA, Frist AY, Wang Q, Labosky PA. 2008. Requirement for foxd3 in the maintenance of neural crest progenitors. Development. 135(9):1615-1624.
Thawani A, Groves AK. 2020. Building the border: Development of the chordate neural plate border region and its derivatives. Front Physiol. 11:608880.
Theocharatos S, Wilkinson DJ, Darling S, Wilm B, Kenny SE, Edgar D. 2013. Regulation of progenitor cell proliferation and neuronal differentiation in enteric nervous system neurospheres. PLoS One. 8(1):e54809.
Theveneau E, Duband JL, Altabef M. 2007. Ets-1 confers cranial features on neural crest delamination. PLoS One. 2(11):e1142.
Thiery A, Buzzi AL, Hamrud E, Cheshire C, Luscombe N, Briscoe J, Streit A. 2022. A gradient border model for cell fate decisions at the neural plate border. bioRxiv.2022.2002.2015.480567.
Thomson JA, Itskovitz-Eldor J, Shapiro SS, Waknitz MA, Swiergiel JJ, Marshall VS, Jones JM. 1998. Embryonic stem cell lines derived from human blastocysts. Science. 282(5391):1145-1147.
Tissier-Seta JP, Mucchielli ML, Mark M, Mattei MG, Goridis C, Brunet JF. 1995. Barx1, a new mouse homeodomain transcription factor expressed in cranio-facial ectomesenchyme and the stomach. Mech Dev. 51(1):3-15.
Tonge DA, de Burgh HT, Docherty R, Humphries MJ, Craig SE, Pizzey J. 2012. Fibronectin supports neurite outgrowth and axonal regeneration of adult brain neurons in vitro. Brain Res. 1453:8-16.
Tosic J, Kim GJ, Pavlovic M, Schroder CM, Mersiowsky SL, Barg M, Hofherr A, Probst S, Kottgen M, Hein L et al. 2019. Eomes and brachyury control pluripotency exit and germ-layer segregation by changing the chromatin state. Nat Cell Biol. 21(12):1518-1531.
Trainor PA. 2010. Craniofacial birth defects: The role of neural crest cells in the etiology and pathogenesis of treacher collins syndrome and the potential for prevention. Am J Med Genet A. 152A(12):2984-2994.
Treanor JJ, Goodman L, de Sauvage F, Stone DM, Poulsen KT, Beck CD, Gray C, Armanini MP, Pollock RA, Hefti F et al. 1996. Characterization of a multicomponent receptor for gdnf. Nature. 382(6586):80-83.
Tribulo C, Aybar MJ, Nguyen VH, Mullins MC, Mayor R. 2003. Regulation of msx genes by a bmp gradient is essential for neural crest specification. Development. 130(26):6441-6452.
Tsakiridis A, Huang Y, Blin G, Skylaki S, Wymeersch F, Osorno R, Economou C, Karagianni E, Zhao S, Lowell S et al. 2014. Distinct wnt-driven primitive streak-like populations reflect in vivo lineage precursors. Development. 141(6):1209-1221.
Tzouanacou E, Wegener A, Wymeersch FJ, Wilson V, Nicolas JF. 2009. Redefining the progression of lineage segregations during mammalian embryogenesis by clonal analysis. Dev Cell. 17(3):365-376.
Uesaka T, Nagashimada M, Enomoto H. 2013. Gdnf signaling levels control migration and neuronal differentiation of enteric ganglion precursors. J Neurosci. 33(41):16372-16382.
Uesaka T, Nagashimada M, Enomoto H. 2015. Neuronal differentiation in schwann cell lineage underlies postnatal neurogenesis in the enteric nervous system. J Neurosci. 35(27):9879-9888.
Uribe RA, Hong SS, Bronner ME. 2018. Retinoic acid temporally orchestrates colonization of the gut by vagal neural crest cells. Dev Biol. 433(1):17-32.
van de Wetering M, Cavallo R, Dooijes D, van Beest M, van Es J, Loureiro J, Ypma A, Hursh D, Jones T, Bejsovec A et al. 1997. Armadillo coactivates transcription driven by the product of the drosophila segment polarity gene dtcf. Cell. 88(6):789-799.

van den Akker E, Forlani S, Chawengsaksophak K, de Graaff W, Beck F, Meyer BI, Deschamps J. 2002. Cdx1 and cdx2 have overlapping functions in anteroposterior patterning and posterior axis elongation. Development. 129(9):2181-2193.

van den Akker E, Fromental-Ramain C, de Graaff W, Le Mouellic H, Brulet P, Chambon P, Deschamps J. 2001. Axial skeletal patterning in mice lacking all paralogous group 8 hox genes. Development. 128(10):1911-1921.

Veeman MT, Slusarski DC, Kaykas A, Louie SH, Moon RT. 2003. Zebrafish prickle, a modulator of noncanonical wnt/fz signaling, regulates gastrulation movements. Curr Biol. 13(8):680-685.

Vega-Lopez GA, Cerrizuela S, Aybar MJ. 2017. Trunk neural crest cells: Formation, migration and beyond. Int J Dev Biol. 61(1-2):5-15.

Vega-Lopez GA, Cerrizuela S, Tribulo C, Aybar MJ. 2018. Neurocristopathies: New insights 150 years after the neural crest discovery. Dev Biol. 444 Suppl 1:S110-S143.

Walters JR, Bishop AE, Facer P, Lawson EM, Rogers JH, Polak JM. 1993. Calretinin and calbindin-d28k immunoreactivity in the human gastrointestinal tract. Gastroenterology. 104(5):1381-1389.

Wang F, Flanagan J, Su N, Wang LC, Bui S, Nielson A, Wu X, Vo HT, Ma XJ, Luo Y. 2012. Rnascope: A novel in situ rna analysis platform for formalin-fixed, paraffin-embedded tissues. J Mol Diagn. 14(1):22-29.

Wang RN, Green J, Wang Z, Deng Y, Qiao M, Peabody M, Zhang Q, Ye J, Yan Z, Denduluri S et al. 2014. Bone morphogenetic protein (bmp) signaling in development and human diseases. Genes Dis. 1(1):87-105.

Wattchow DA, Furness JB, Costa M. 1988. Distribution and coexistence of peptides in nerve fibers of the external muscle of the human gastrointestinal tract. Gastroenterology. 95(1):32-41.

Wei S, Xu G, Bridges LC, Williams P, White JM, DeSimone DW. 2010. Adam13 induces cranial neural crest by cleaving class b ephrins and regulating wnt signaling. Dev Cell. 19(2):345-352.

Williams BP, Daniels GL, Pym B, Sheer D, Povey S, Okubo Y, Andrews PW, Goodfellow PN. 1988. Biochemical and genetic analysis of the oka blood group antigen. Immunogenetics. 27(5):322-329.

Williams RM, Candido-Ferreira I, Repapi E, Gavriouchkina D, Senanayake U, Ling ITC, Telenius J, Taylor S, Hughes J, Sauka-Spengler T. 2019. Reconstruction of the global neural crest gene regulatory network in vivo. Dev Cell. 51(2):255-276 e257.

Wilson PA, Hemmati-Brivanlou A. 1995. Induction of epidermis and inhibition of neural fate by bmp-4. Nature. 376(6538):331-333.

Wilson SI, Rydstrom A, Trimborn T, Willert K, Nusse R, Jessell TM, Edlund T. 2001. The status of wnt signalling regulates neural and epidermal fates in the chick embryo. Nature. 411(6835):325-330.

Wilson V, Olivera-Martinez I, Storey KG. 2009. Stem cells, signals and vertebrate body axis extension. Development. 136(10):1591-1604.

Wind M, Gogolou A, Manipur I, Granata I, Butler L, Andrews PW, Barbaric I, Ning K, Guarracino MR, Placzek M et al. 2021. Defining the signalling determinants of a posterior ventral spinal cord identity in human neuromesodermal progenitor derivatives. Development. 148(6).

Wood HB, Episkopou V. 1999. Comparative expression of the mouse sox1, sox2 and sox3 genes from pre-gastrulation to early somite stages. Mech Dev. 86(1-2):197-201.

Workman MJ, Mahe MM, Trisno S, Poling HM, Watson CL, Sundaram N, Chang CF, Schiesser J, Aubert P, Stanley EG et al. 2017. Engineered human pluripotent-stem-cell-derived intestinal tissues with a functional enteric nervous system. Nat Med. 23(1):49-59.

Wrana JL, Attisano L, Wieser R, Ventura F, Massague J. 1994. Mechanism of activation of the tgf-beta receptor. Nature. 370(6488):341-347.

Wu J, Yang J, Klein PS. 2005. Neural crest induction by the canonical wnt pathway can be dissociated from anterior-posterior neural patterning in xenopus. Dev Biol. 279(1):220-232.

Wymeersch FJ, Huang Y, Blin G, Cambray N, Wilkie R, Wong FC, Wilson V. 2016. Position-dependent plasticity of distinct progenitor types in the primitive streak. Elife. 5:e10042.

Wymeersch FJ, Skylaki S, Huang Y, Watson JA, Economou C, Marek-Johnston C, Tomlinson SR, Wilson V. 2019. Transcriptionally dynamic progenitor populations organised around a stable niche drive axial patterning. Development. 146(1).

Wymeersch FJ, Wilson V, Tsakiridis A. 2021. Understanding axial progenitor biology in vivo and in vitro. Development. 148(4).

Xie Y, Su N, Yang J, Tan Q, Huang S, Jin M, Ni Z, Zhang B, Zhang D, Luo F et al. 2020. Fgf/fgfr signaling in health and disease. Signal Transduct Target Ther. 5(1):181.

Xue X, Sun Y, Resto-Irizarry AM, Yuan Y, Aw Yong KM, Zheng Y, Weng S, Shao Y, Chai Y, Studer L et al. 2018. Mechanics-guided embryonic patterning of neuroectoderm tissue from human pluripotent stem cells. Nat Mater. 17(7):633-641.

Yamaguchi K, Zhu C, Ohsugi T, Yamaguchi Y, Ikenoue T, Furukawa Y. 2017. Bidirectional reporter assay using hal promoter and topflash improves specificity in high-throughput screening of wnt inhibitors. Biotechnol Bioeng. 114(12):2868-2882.

Yardley N, Garcia-Castro MI. 2012. Fgf signaling transforms non-neural ectoderm into neural crest. Dev Biol. 372(2):166-177.

Yntema CL, Hammond WS. 1954. The origin of intrinsic ganglia of trunk viscera from vagal neural crest in the chick embryo. J Comp Neurol. 101(2):515-541.

Young HM, Bergner AJ, Anderson RB, Enomoto H, Milbrandt J, Newgreen DF, Whitington PM. 2004. Dynamics of neural crest-derived cell migration in the embryonic mouse gut. Dev Biol. 270(2):455-473.

Young HM, Bergner AJ, Muller T. 2003. Acquisition of neuronal and glial markers by neural crest-derived cells in the mouse intestine. J Comp Neurol. 456(1):1-11.

Young HM, Ciampoli D, Hsuan J, Canty AJ. 1999. Expression of ret-, p75(ntr)-, phox2a-, phox2b-, and tyrosine hydroxylase-immunoreactivity by undifferentiated neural crest-derived cells and different classes of enteric neurons in the embryonic mouse gut. Dev Dyn. 216(2):137-152.

Young HM, Hearn CJ, Farlie PG, Canty AJ, Thomas PQ, Newgreen DF. 2001. Gdnf is a chemoattractant for enteric neural cells. Dev Biol. 229(2):503-516.

Young HM, Turner KN, Bergner AJ. 2005. The location and phenotype of proliferating neural-crest-derived cells in the developing mouse gut. Cell Tissue Res. 320(1):1-9.

Young T, Rowland JE, van de Ven C, Bialecka M, Novoa A, Carapuco M, van Nes J, de Graaff W, Duluc I, Freund JN et al. 2009. Cdx and hox genes differentially regulate posterior axial growth in mammalian embryos. Dev Cell. 17(4):516-526.

Yu J, Wang L, Pei P, Li X, Wu J, Qiu Z, Zhang J, Ao R, Wang S, Zhang T et al. 2019. Reduced h3k27me3 leads to abnormal hox gene expression in neural tube defects. Epigenetics Chromatin. 12(1):76.

Yuan F, Fang KH, Cao SY, Qu ZY, Li Q, Krencik R, Xu M, Bhattacharyya A, Su YW, Zhu DY et al. 2015. Efficient generation of region-specific forebrain neurons from human pluripotent stem cells under highly defined condition. Sci Rep. 5:18550.

Zhang C, Deng Y, Dai H, Zhou W, Tian J, Bing G, Zhao L. 2017. Effects of dimethyl sulfoxide on the morphology and viability of primary cultured neurons and astrocytes. Brain Res Bull. 128:34-39.

Zhang J, Hagopian-Donaldson S, Serbedzija G, Elsemore J, Plehn-Dujowich D, McMahon AP, Flavell RA, Williams T. 1996. Neural tube, skeletal and body wall defects in mice lacking transcription factor ap-2. Nature. 381(6579):238-241.

Zhang X, Huang CT, Chen J, Pankratz MT, Xi J, Li J, Yang Y, Lavaute TM, Li XJ, Ayala M et al. 2010. Pax6 is a human neuroectoderm cell fate determinant. Cell Stem Cell. 7(1):90-100.

Zhang Y, Liu T, Meyer CA, Eeckhoute J, Johnson DS, Bernstein BE, Nusbaum C, Myers RM, Brown M, Li W et al. 2008. Model-based analysis of chip-seq (macs). Genome Biol. 9(9):R137.

Zhou B, Lin W, Long Y, Yang Y, Zhang H, Wu K, Chu Q. 2022. Notch signaling pathway: Architecture, disease, and therapeutics. Signal Transduct Target Ther. 7(1):95.

Appendix

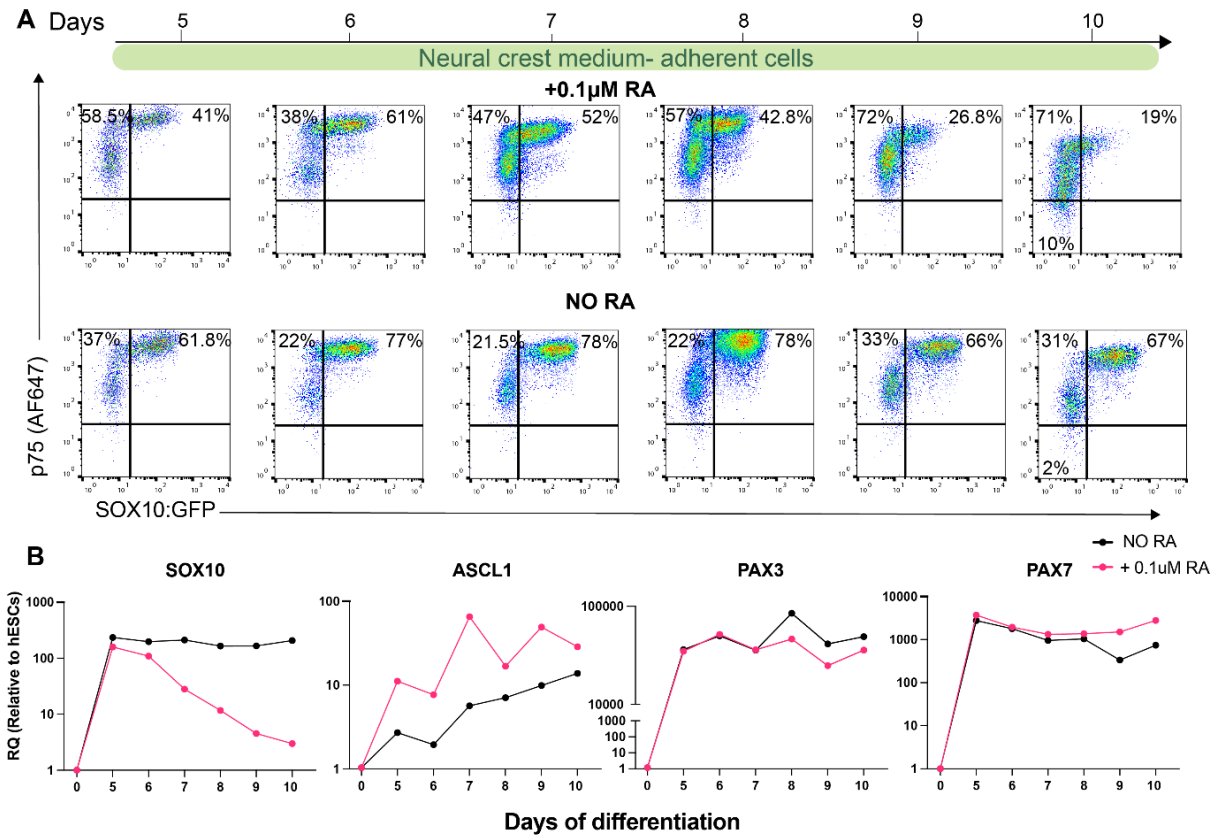

Figure S1. Characterisation of p75 surface marker expression and SOX10:GFP in hESC-derived neural crest cells cultured for prolonged period in neural crest media in the presence/absence of retinoic acid treatment. (A) FACS scatter plots showing co-expression of p75 and SOX10:GFP in NC cultures treated with 0.1μM RA (upper panel) and without RA (lower panel) at 6 successive time points during prolonged NC treatment. In the presence or RA, the number of +/+ cells reaches a peak at day 6 and drops in the following days, while in untreated cultures the +/+ population is maintained considerably high throughout the time course. Moreover, the number of +/+ is higher in untreated sample compare to RA-treated. (B) Relative gene expression of NC/ENS progenitor associated transcripts in NC line (n=1). RA, retinoic acid.

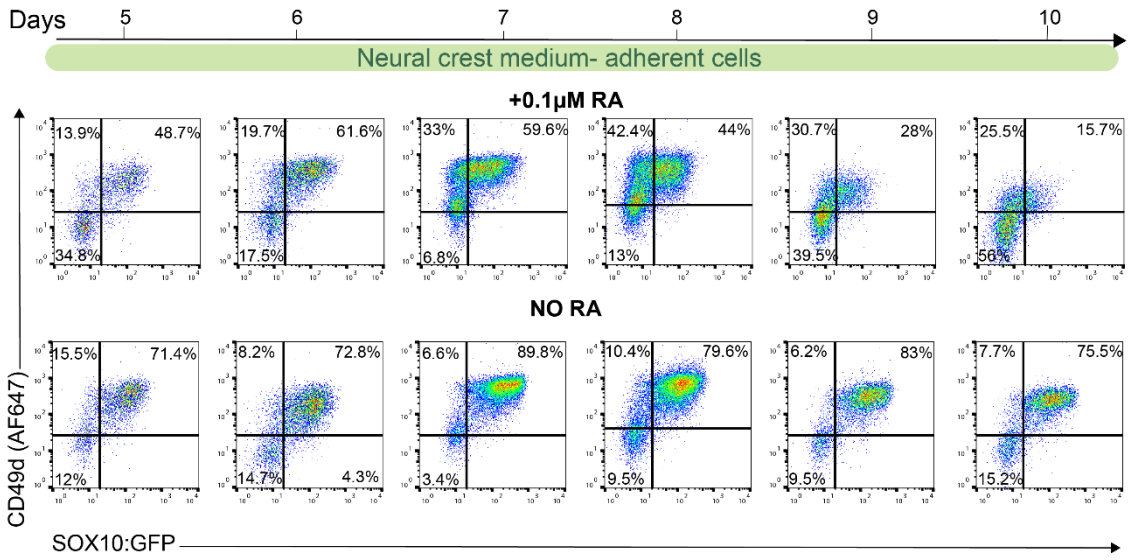

Figure S2. Time course of CD49d surface epitope expression and SOX10:GFP in hESC-derived neural crest cells grown for prolonged period in neural crest media in the presence/absence of retinoic acid treatment. FACS plots showing co-expression of CD49d and SOX10:GFP in NC cultures treated with 0.1μM RA (upper panel) or without RA (lower panel) at 6 successive time points during prolonged NC treatment. The number of +/+ cells is considerably higher in the control compared to RA-treated cultures and it is maintained throughout the culture period. On the other hand, the number of +/+ cells in treated cultures increases between day 6-7 before it drops at day 8 onwards (n=1). RA, retinoic acid.

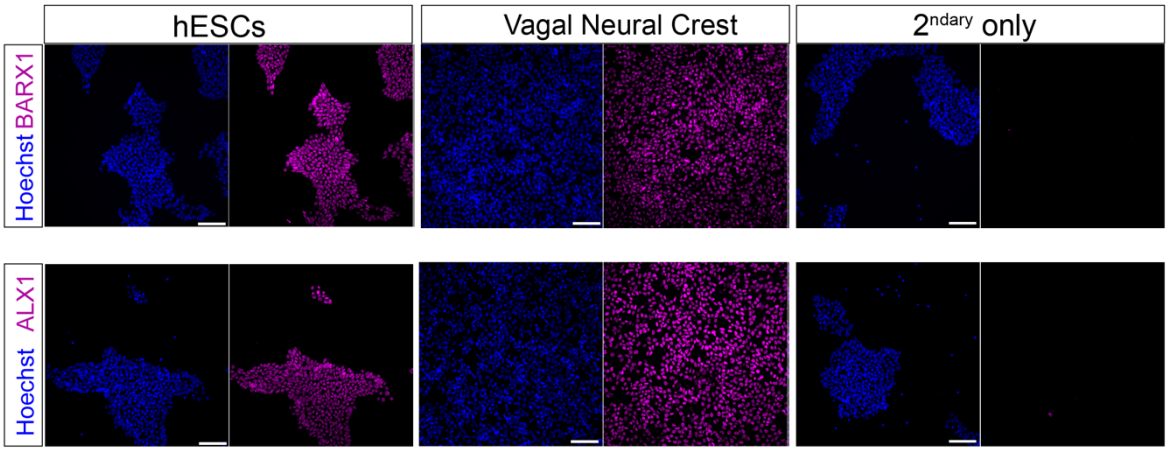

Figure S3. Non-specific binding of antibodies against BARX1 and ALX1 used to identify cardiac and cranial neural crest contaminants in day 6 cultures. Left panel shows stained pluripotent stem cells expected to show minimal reactivity to the antibodies but deceptively appear positive. Middle panel shows stained day 6 vagal NC cultures while left panel shows cells incubated with secondary antibody in the absence of primary antibody staining. All images were acquired and processed with identical settings. (anti-BARX1; Merck, Cat No: HPA055858; anti-ALX1; ThermoFisher, Cat No: PA5-51608).

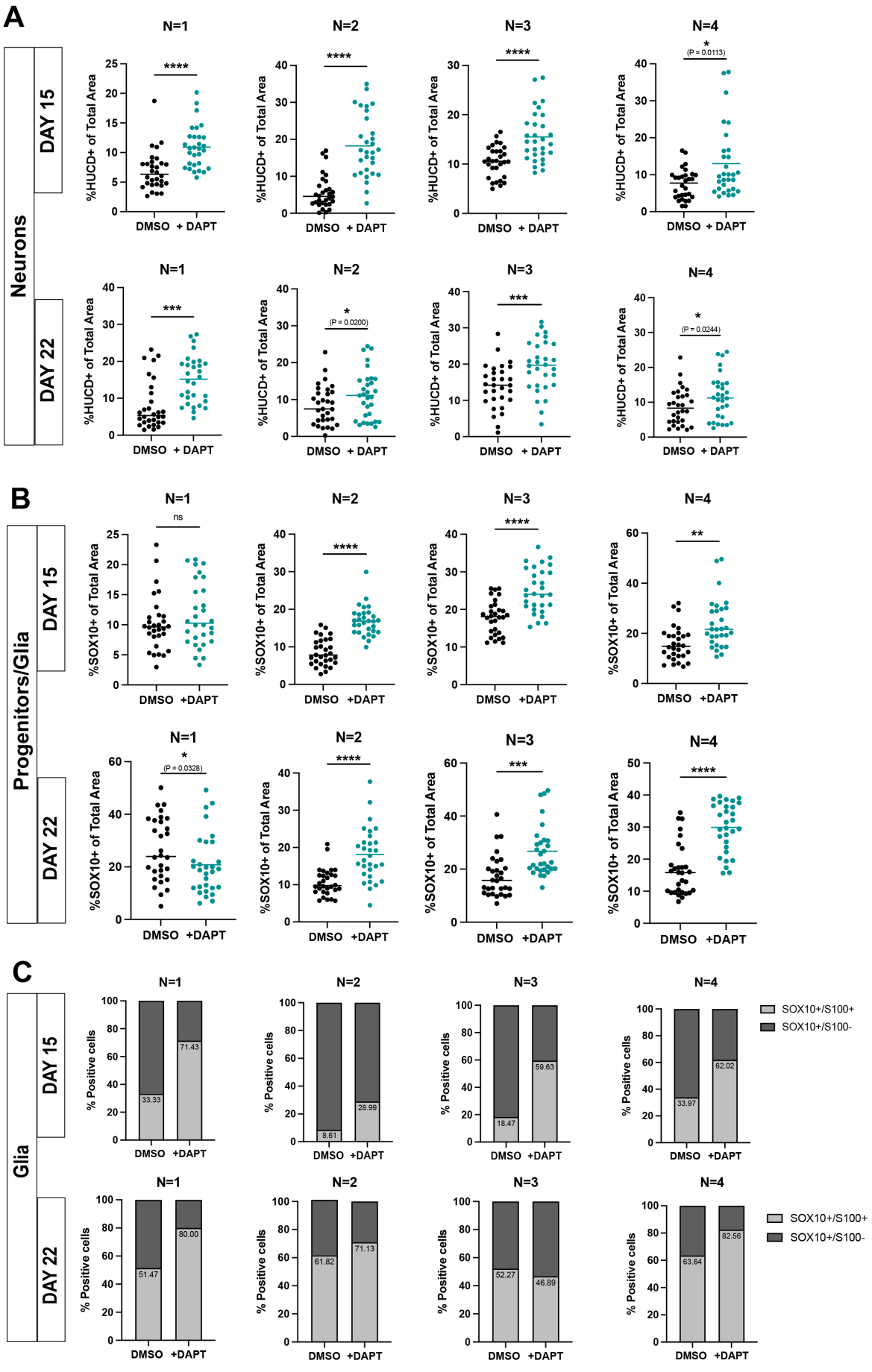
A
Neurons
DAY 15
DAY 22
N=1
N=2
N=3
N=4
%HUCD+ of Total Area
DMSO + DAPT
****
***
*
(P = 0.0113)
(P = 0.0200)
(P = 0.0244)
B
Progenitors/Glia
%SOX10+ of Total Area
DMSO +DAPT
ns
**
(P = 0.0328)
C
Glia
% Positive cells
SOX10+/S100+
SOX10+/S100-
33.33
71.43
8.61
28.99
18.47
59.63
33.97
62.02
51.47
80.00
61.82
71.13
52.27
46.89
63.64
82.56

Figure S4. Quantification of DAPT-treated and untreated cultures presented per biological experiment. (A) Quantification of neural content based on HUCD+ area at day 15 and day 22 of the differentiation. Discrete values correspond to the fields quantified (30 fields/condition). (B) Quantification of progenitors/glia based on SOX10+ area at day 15 and day 22 of the differentiation. Discrete values correspond to the fields quantified (30 fields/condition). (C) Quantification of glial content based on the co-expression of SOX10 and S100 at day 15 and day 22 of the differentiation. Values within bars indicate the median for the double positive population (30 fields/condition). **P* <0.05, ***P* <0.01, ****P* <0.001, *****P* <0.0001(Paired t-test); ns= not significant.

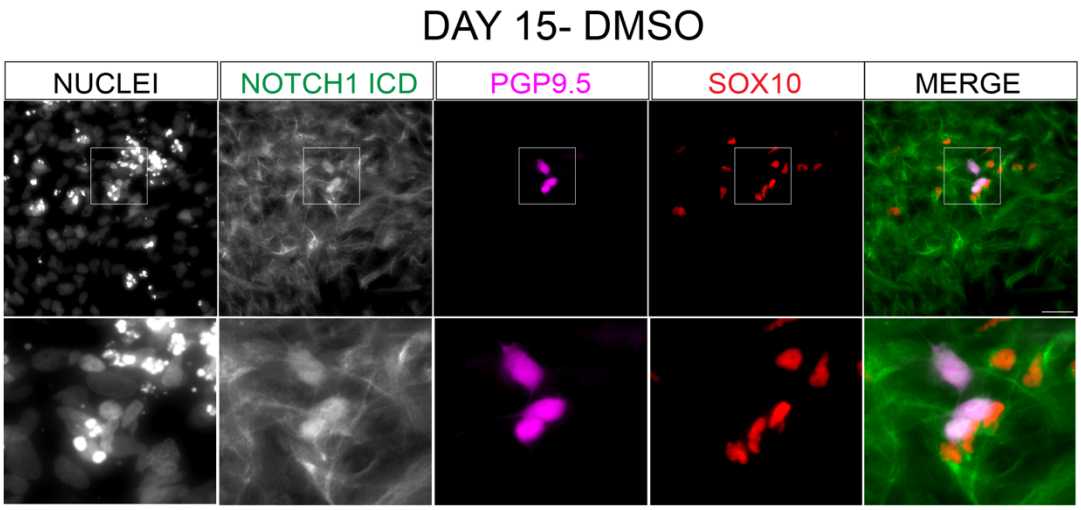

Figure S5. Immunofluorescence analysis of the expression of Notch1 intracellular domain (ICD), PGP9.5 and SOX10 in control day 15 (without DAPT) enteric nervous system cultures. Notch1-ICD has nuclear localisation in PGP9.5+ neurons. Scale bars=50 µm.

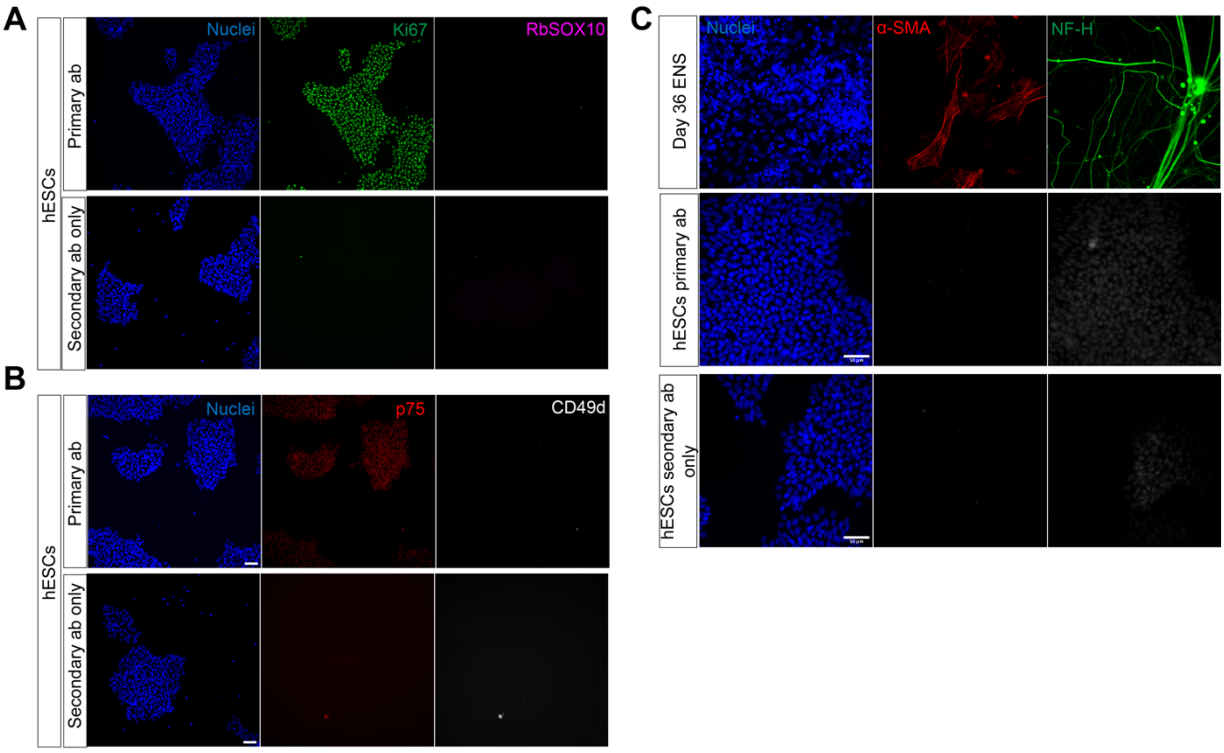

Figure S6. Representative immunofluorescence analysis images demonstrating the specificity of the antibodies employed based on negative controls or samples incubated with secondary antibodies only. Scale bars=50 μm.

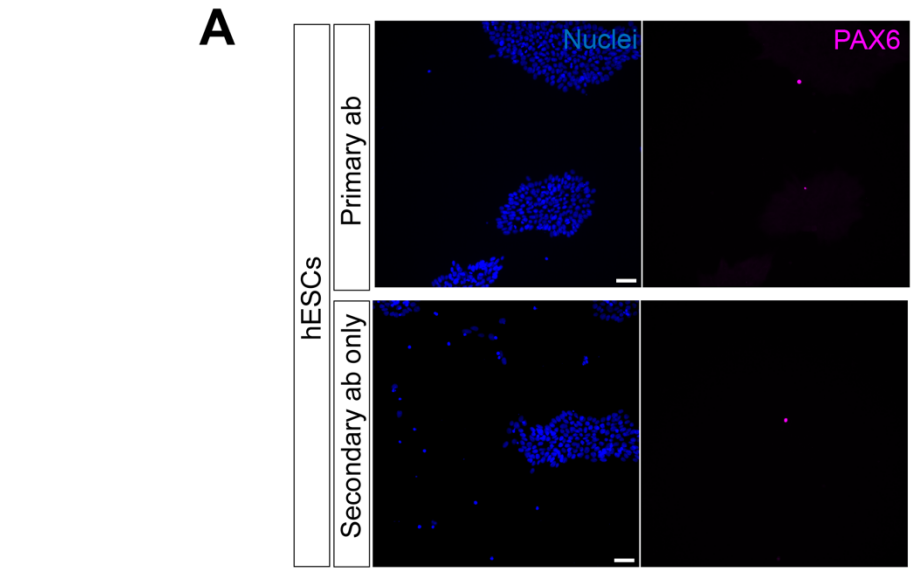

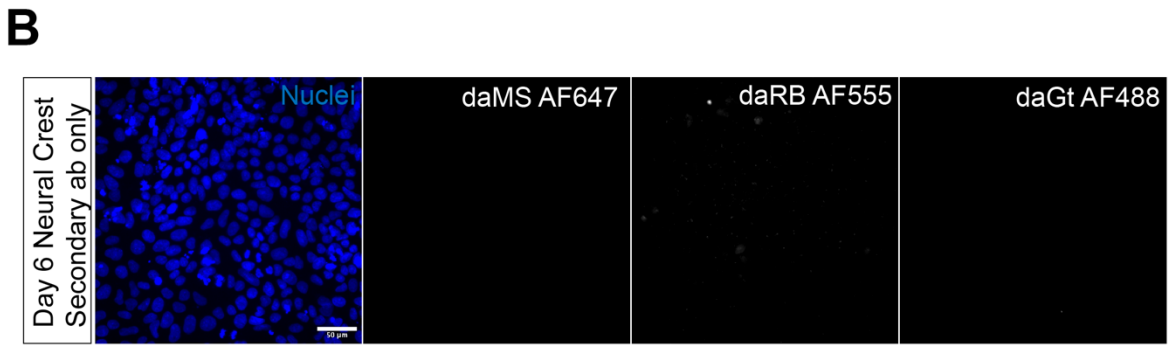

Figure S7. Representative immunofluorescence analysis images in negative controls or samples incubated with secondary antibodies only. Scale bars=50 μm.

Image analysis macros for measuring HUCD+ and SOX10+ area in Fiji

HUCD

```
//Create arrays for storing area data
setOption("ExpandableArrays", true);
BlueData = newArray();
GreenData = newArray();
SumData = newArray();
PcData = newArray();

//Get Directory from user and get list of files
dir = getDirectory("Please choose a directory containing images...");
filelist = getFileList(dir)
for (i=0; i<filelist.length; i++) {
	run("Bio-Formats Importer", "open=[" + dir + filelist[i] + "] autoscale color_mode=Default
view=Hyperstack stack_order=XYCZT");
	img = getTitle();
	run("Split Channels");

	//Process DAPI image
	selectWindow("C1-"+img);
	setAutoThreshold("Li dark no-reset");
	setOption("BlackBackground", true);
	run("Convert to Mask");
	rename("Blue");
	setAutoThreshold("Li dark no-reset");
	run("Create Selection");
	run("Set Measurements...", "area redirect=None decimal=3");
	run("Measure");
	BlueData[i] = Table.get("Area", 0);
	close("Results");

	//Process Green Image
	selectWindow("C2-"+img);
	setAutoThreshold("Otsu dark no-reset");
	setOption("BlackBackground", true);
```

```
        run("Convert to Mask");
        rename("Green");
        setAutoThreshold("Li dark no-reset");
        run("Create Selection");
        run("Set Measurements...", "area redirect=None decimal=3");
        run("Measure");
        GreenData[i] = Table.get("Area", 0);
        close("Results");

        //Merge Blue and Green areas to determine total area of cellular material
        imageCalculator("Add create", "Blue","Green");
        selectWindow("Result of Blue");
        setAutoThreshold("Li dark no-reset");
        run("Create Selection");
        run("Set Measurements...", "area redirect=None decimal=3");
        run("Measure");
        SumData[i] = Table.get("Area", 0);
        close("Results");

        //Calculate green area as a fraction of total cellular area
        PcData[i] = (GreenData[i]/SumData[i])*100;
        close("*");
}

//Generate final results table
Table.create("Results");
Table.setColumn("Image", filelist);
Table.setColumn("Blue Area", BlueData);
Table.setColumn("Green Area", GreenData);
Table.setColumn("Total Cell Area", SumData);
Table.setColumn("Green% of Total Area", PcData);
saveAs("Results", dir + "Results.csv");
close("Results");
```

SOX10/S100

```
//Create final results tables
Table.create("Positive Red Cell Green Data");
Table.create("%Red Cell Area");
setBatchMode(true);

//Create Array for final result table
setOption("ExpandableArrays", true);
ImageFile = newArray();
GrCells = newArray();
GrArea = newArray();
GrMean = newArray();
GrMin = newArray();
GrMax = newArray();
GrMedian = newArray();
RedCellArea = newArray();
Im = newArray();
ImageNames = newArray();

//Get Directory information from user
dir1 = getDirectory("Please select a directory containing images to be processed");
filelist = getFileList(dir1);

for (j=0; j<filelist.length; j++) {
        run("Bio-Formats Importer", "open=[" + dir1 + filelist[j] + "] autoscale color_mode=Default
view=Hyperstack stack_order=XYCZT");

        //Get image name, plit channels and measure area occupied by blue signal
        roiManager("reset");
        Img = getTitle();
        Im[j] = Img;
        run("Split Channels");
        selectWindow("C1-"+Img);
        setAutoThreshold("Li dark");
        run("Create Selection");
        run("Set Measurements...", "area mean redirect=None decimal=3");
```

```
	run("Measure");
	AreaBlue = Table.get("Area", 0);
	close("Results");

	//Detect red cells, determine area occupied by red, count number
	selectWindow("C3-"+Img);
	setAutoThreshold("Li dark");
	run("Analyze Particles...", "size=30.00-280.00 show=Nothing summarize");
	selectWindow("Summary");
	CellCount = Table.get("Count", 0);
	if(CellCount==0){
		AreaRed = 0;
		RedCells = 0;
	}
	else{
		close("Summary");
		run("Analyze Particles...", "size=30.00-280.00 show=Nothing display summarize
add");
		selectWindow("Summary");
		AreaRed = Table.get("Total Area", 0);
		close("Summary");
		RedCells = roiManager("count");
		close("Results");

		//Loop each red cell selection, enlarge band into cytoplasm and measre green
signl
		run("Set Measurements...", "area mean min centroid median redirect=C2-"+Img+"
decimal=3");
		n = roiManager("count");
		cell = newArray();
		for (i = 0; i < n; i++) {
		   roiManager('select', i);
		   run("Make Band...", "band=1.98");
			roiManager("Update");
			roiManager("Measure");
			cell[i] = i+1;
			ImageNames[i] = Img;
```

```
            }

            CellArea = Table.getColumn("Area");
            CellMean = Table.getColumn("Mean");
            CellMin= Table.getColumn("Min");
            CellMax = Table.getColumn("Max");
            CellMedian = Table.getColumn("Median");
            close("Results");

            GrCells = Array.concat(GrCells, cell);
            GrArea = Array.concat(GrArea,CellArea);
            GrMean = Array.concat(GrMean,CellMean);
            GrMin = Array.concat(GrMin,CellMin);
            GrMax = Array.concat(GrMax,CellMax);
            GrMedian = Array.concat(GrMedian,CellMedian);

            ImageFile = Array.concat(ImageFile,ImageNames);
            ImageNames = newArray();

            close("*");
            PcRed = (AreaRed/AreaBlue)*100;
            RedCellArea = Array.concat(RedCellArea,PcRed);
        }
}

selectWindow("Positive Red Cell Green Data");
Table.setColumn("File", ImageFile);
Table.setColumn("Cell", GrCells);
Table.setColumn("Area", GrArea);
Table.setColumn("Mean", GrMean);
Table.setColumn("Min", GrMin);
Table.setColumn("Max", GrMax);
Table.setColumn("Median", GrMedian);
saveAs("Results", dir1+"CellData.txt");
run("Close");

selectWindow("%Red Cell Area");
```

```
Table.setColumn("File", Im);
Table.setColumn("%Red Cell Area", RedCellArea);
saveAs("Results", dir1+"CellAreaData.txt");
run("Close");
```

All macros were created by Dr Darren Robinson, Facility Manager of the Wolfson Light Microscopy Facility at the University of Sheffield.